“IMAGE COMPRESSION”

BY

GAJANAN KASHIRAM KHARATE

FOR THE DEGREE OF

DOCTOR OF PHILOSOPHY
IN ELECTRONICS ENGINEERING

SUBMITTED TO

UNIVERSITY OF PUNE

NAME OF THE RESEARCH CENTRE

DEPARTMENT OF ELECTRONICS ENGINEERING
PIET’s COLLEGE OF ENGINEERING,
PUNE

JUNE 2006

CERTIFICATE

This is to certify that the thesis entitled ***"IMAGE COMPRESSION"***, being submitted by ***Shri Gajanan Kashiram Kharate*** to University of Pune, (Maharashtra) for award of Doctor of Philosophy in Electronics Engineering and is a record of bonafied research work carried out by him. He has worked under our supervision and guidance and has fulfilled the requirement of submission of the thesis. The matter embodied in this thesis has not been submitted elsewhere in part or full for the award of any degree or diploma.

Prof. Dr. P. P. Rege
(Co-Guide)
Professor,
Department of Electronics and Telecommunication Engineering,
PIET's College of Engineering, Pune.

Prof. Dr. A. A. Ghatol
(Guide)
Vice Chancellor,
Dr. Babasaheb Ambedkar Technological University, Lonere
Dist. Raigad, Maharashtra.

Prof. Dr. M. A. Joshi
Professor and Head,
Department of Electronics and Telecommunication Engineering,
PIET's College of Engineering, Pune.

Prof. V. K. Kokate
Director,
PIET's College of Engineering, Pune

TABLE OF CONTENTS

LIST OF TABLES

LIST OF FIGURES

ACKNOWLEDGEMENT

I take this opportunity to express my deep sense of gratitude to my research guide Dr. A. A. Ghatol, Vice Chanceller Dr. Babasaheb Ambedkar Technological University, Lonere, Dist. Raigad, Maharashtra, and co-guide Dr. P. P. Rege, Professor, Department of Electronics and Telecommunication Engineering, PIET's College of Engineering, Pune, for their inspiring and stimulating guidance, invaluable thought provoking suggestions, constant encouragement and unceasing enthusiasm at every stage of this research work. I am deeply indebted to Prof. M. A. Joshi, Head, Department of Electronics and Telecommunication Engineering, PIET's College of Engineering, Pune from whom I received continual encouragement and advice. I express my sincere thanks to him. I express my indentedness to Prof. V. K. Kokate, Director, PIET's College of Engineering, Pune for providing necessary assistance during this research work.

I thank Hon. Shri Balasaleb Wagh, Vice Chairman, all trustees K. K. Wagh Education Society, Nashik, and Principal Dr. K. N. Nandurkar for allowing me to complete my research work and providing continual encouragement. I am thankful to all staff members and technical staff of Department Electronics and Telecommunication Engineering, PIET's College of Engineering, Pune, and Department of Information Technology, K. K. Wagh Institute of Engineering Education and research, Nashik. I wish to thank Prof. V. H. Patil, Prof. N. L. Bhale, Prof. J. A. Bhardwaj, Prof Vishal Wankhede, Mr. H. D. Deshpande who helped me during the progress of my research work. Thanks are due to all my friends, relatives and colleagues who have contributed directly or indirectly to the completion of this work. Above all I am extremely grateful to my Mother, Father, Brothers, Wife Sangeeta, daughter Pooja and son Pushkaraj for their sacrifice and excellent co-operation during the entire period of this research work. Their loving, caring and sacrificing attitude has been the driving force in this endeavor and no words of thanks are enough.

(Gajanan Kashiram Kharate)

ABSTRACT

Data compression has wide range of applications in the areas of data transmission and data storage. Many data processing applications require storage of voluminous images, and the numbers of such applications are constantly increasing as the use of computers extends to new disciplines. At the same time, the proliferation of computer communication networks is resulting in massive transfer of data over communication links. Compressing data to be transmitted or stored reduces communication and/or storage costs. When the amount of data to be transmitted is reduced, the effect is that of increasing the capacity of the communication channel. Similarly, compressing a file to half of its original size is doubling the capacity of the storage medium. It may then become feasible to store and transmit the data at a higher rate.

There are two basic approaches to improve the speed viz,

1. By increasing the capacity of the channel
2. By using efficient data compression techniques

Data compression techniques represent some pictorial information in more compact form by removing the redundancies. In essence, compression techniques represent image data using fewer bits than what is required for original image. These types of techniques may also improve features such as extraction and selection procedures.

Image compression techniques through which image information can be represented by less number of bits are very useful for image transmission from one point to another and for image archival purpose. For many image compression techniques incur losses such that some errors are introduced in the image reconstruction from its compressed representation. These kinds of techniques are called lossy compression. There are some techniques that provide lossless compression. Thus the compression ratio and the amount of error introduced will be considered during the selection/development of compression methods.

A lot of research is currently being in progress on following data compression techniques viz,

1. Wavelet transform, and
2. Fractal block coding

Both are lossy compression techniques. Wavelet transforms compression technique is very much similar to dictionary based compression techniques. In wavelet

transform, as compression ratio increases the quality of image becomes poor, and in case of fractal block coding, compression ratio is high but the encoding and decoding process requires more processing time.

The scope of this research work is to study data compression methods spanning over almost forty years of research, from the work of Shannon, Fano, and Huffman in the late 40's to a technique developed in 1986, and suggest a novel technique to achieve the maximum compression ratio by retaining the visual quality of images with lesser encoding/decoding processing time so as to support real time image processing. The focus of this research is to develop the algorithms for digital image data compression.

In this thesis, the work starts with the proper selection of the mother wavelet from the known wavelets. As per the literature survey, it is found that wavelet image compression techniques are not suitable for high frequency images, and hence the results of wavelet packets and wavelet are compared in this thesis. By considering the merits of wavelet packets, this technique is selected for transformation. To select the best basis function, the algorithms are developed, which uses threshold entropy; log entropy, and Shannon entropy. The results are compared with new suggested technique, ***"The Best Basis Selection Based On Energy Contain"***.

In the compression process, threshold selection plays crucial role. In the present work, adaptive thresholding is introduced, where the threshold is calculated on the basis of the nature of the image. Lossy RLE technique is introduced for encoding during the last phase of compression. The algorithm is developed, implemented, and tested over the range of natural and synthetic images, and conclusions are drawn. The results revealed that the performance of the presented method is better than the existing known compression methods.

NOTATION AND ABBREVIATIONS

SYMBOL	DESCRIPTION
ω	Angular frequency
⊗	Correlations operations
*	Convolution operator
2D	Two-dimensional
a	Scaling parameter
AD	Average Difference
ADPCM	Adaptive differential pulse code modulation
b	Shift parameter
CMY	Cyan, Magenta, Yellow
CMYK	Cyan, Magenta, Yellow, Black
CSF	Constant Sensitivity Function
CT	Computer Tomography
CWT	Continuous Wavelet Transform
da/a^2	Differential change in frequency
DCT	Discrete Cosine Transform
DFT	Discrete Fourier Transform
DWT	Discrete Wavelet Transform
EBCOT	Embedded Block Coding with Optimized Truncation
EZW	Embedded Zerotree Wavelet
FEC	Forward Error Correction
FIR	Finite impulse response
f_{max}	Maximum frequency
$h(t)$	Mother wavelet
H.261	Video codec for audiovisual Group
h_{ab}	Daughter wavelet
HDTV	High Definition Television
HHT	Hadamard-Haar Transform
HSI	Hue, Saturation and Intensity
HVS	Human Visual System
IIF	Image Interchange Facility
ISO	International Standards Organization
IWT	Integer Wavelet Transform
JPEG	Joint Photographic Expert Group

KLT	Karhune-Loeve Transforms
KLT	Karhunen-Loeve Transform
LOCO-I	Low Complexity Lossless Compression for Images
LZW	Lempel-Ziv-Welch
MD	Maximum Difference
MDA	Monochrome Display Adaptors
MOS	Mean Option Score
MPEG	Motion Picture Expert Group
MRI	Magnetic Resonance Imaging
MSE	Mean Square Error
MSVQ	Multistage Vector Quantization
NAE	Normalized Absolute Error
NK	Normalized Cross-correlation
NTSC	United States National Television Systems Committee
PR	Perfect Reconstruction
PSNR	Peak Signal to Noise Ration
PWL	Piecewise Linear Transform
PZW	Packetizable zerotree wavelet
QMF	Quadrature mirror filter
QT	Quadtree Decomposition
RGB	Red, Green, and Blue
RLE	Run-Length Encoding
ROI	Region of Interest
$S(\omega)$	Fourier transform
$s(t)$	Time domain signal
s(t)	Rectangular function
SAR	Synthetic Aperture Radar
SC	Structural Content
SFT	Short Fourier Transforms
SHT	Slant-Haar Transform
SNR	Signal to Noise Ratio
SPIHT	Set Partitioning In Hierarchical Trees
STFT	Short-Time Fourier Transform
TIFF	Tagged Interchanged File Format
T_s	Time variable
TT	TRI-TREE decomposition

VQ	Vector Quantization
WHT	Walsh-Hadamard Transform
W_s	Wavelet coefficients
WT	Wavelet Transforms

CHAPTER 1
INTRODUCTION

1.1.0 PREAMBLE

In today's modern era, multimedia has tremendous impact on human lives. It becomes inseparable part of our day-to-day activities. Image is one of the most important media contributing to multimedia. The unprocessed image heavily consumes very important resources of the system. And hence it is highly desirable that the image be processed, so that efficient storage, representation and transmission of it can be worked out. The processes involve one of the important processes- "*Image Compression*". Methods for digital image compression have been the subject of research over the past decade. Advances in Wavelet Transforms and Quantization methods have produced algorithms capable of surpassing image compression standards, like the Joint Photographic Expert Group (JPEG) algorithm. The recent growth of data intensive multimedia based applications have not only sustained the need for more efficient ways to encode the signals and images but also have made compression of such signals central to storage and communication technology. The research confined to this thesis is to aim at improving the compression ratio by maintaining the quality of image. This chapter includes the motivation for the research, current techniques in use for the image compression and objectives of research work.

1.2.0 MOTIVATION

In Information Technology, multimedia plays an important role. The image is one of the media of information. Thousands of words of information can be replaced by a single image. It is always said that, " a picture worth thousands of words". This is true in the modern era where information has become one of the most important values of the assets. Uncompressed image requires large memory to store the image and large bandwidth to transmit the image data. At the present state of technology, the only solution is to compress the multimedia data before its storage and transmission, and decompress it at the receiver. For example, with compression ratio of 30:1, the space, bandwidth and transmission time requirement can be reduced by the factor of 30, with acceptable quality.

The table 1.2.1 shows the parameters: disk space, transmission bandwidth and transmission time needed to store and transmit various types of unprocessed data from text to full motion video [1].

Table 1.2.1 Uncompressed Multimedia data and required storage space, transmission bandwidth, and transmission time

Multimedia Data	*Size/Duration*	*Bits/Pixel or Bits/Sample*	*Uncompressed Size (B for bytes)*	*Transmission Bandwidth (b for bits)*	*Transmission Time (using a 28.8K Modem)*
A page of text	*11" × 8.5"*	*Varying resolution*	*4-8 KB*	*32 – 64 KB/page*	*1.1 – 2.2 sec*
Telephone quality speech	*10 sec*	*8 bps*	*80 KB*	*64 KB/sec*	*22.2 sec*
Grayscale Image	*512 × 512*	*8 bps*	*262 KB*	*2.11 MB/image*	*1 min 13 sec*
Color Image	*512 × 512*	*24 bps*	*786 KB*	*6.29 MB/image*	*3 min 39 sec*
Medical Image	*2048 × 1680*	*12 bps*	*5.16 MB*	*41.3 MB/image*	*23 min 54 sec*
Full-motion video	*640 × 480, 1 min (30 frames/sec)*	*24 bps*	*1.66 GB*	*221 MB/sec*	*5 days 8 hrs*

The table1.2.1 clearly illustrates the need of large storage space, large transmission bandwidth and more transmission time for images and other data. While the advancements of the computer storage technology and communication technology continue at the rapid rate, the means for reduction in storage requirement of an image is still needed for most of the applications. Image compression is concerned with minimizing the number of bits required to represent the image, which reduces the storage space, requirements of bandwidth, and transmission time. Thus the science of digital image compression has emerged. Current methods of image compression, such as the popular Joint Photographic Experts Group (JPEG) standard can provide good performance in terms of retaining image quality while reducing storage requirements. But even the popular standards like JPEG have limitations. Research for new and better methods of image compression is ongoing. This thesis discusses the previous work, and present status of image compression, and presents new method of Image Compression to improve the compression ratio by retaining the quality of image. The thesis also includes, the potential of proposed method for inclusion in new compression applications, and standards.

1.3.0 RECENT METHODS IN USE

By understanding the need of the image compression, a number of methods have been presented over the years for performing image compression. They all have one common goal, to alter the representation of the information contained in an image, so that it can be represented sufficiently well with less amount of memory. It is always desired that the image representation is acceptable, in which the content of an image can be approximated using a small number of parameters. The Discrete Cosine Transform

(DCT) developed by Ahmed, Natrajan, and Rao[1974] is one of the transforms used in image compression application. Its application to image compression was pioneered by Chen and Pratt [1984] [2].

During the 1980's and 1990's, Discrete Cosine Transform (DCT) based compression algorithms, and international standards were developed to alleviate storage, and bandwidth limitations imposed by digital still images, and motion video applications [3, 89]. Today there are three DCT-based standards, widely used and accepted worldwide:

- JPEG (Joint Photographic Expert Group)
- H.261 (Video codec for audiovisual Group)
- MPEG (Motion Picture Expert Group)

Each of these standards is well suited for particular applications: JPEG for still image compression, H.261 for video conferencing, and MPEG for high-quality, multimedia systems. The basic compression scheme for all three standards can be summarized as follows: divide the picture into 8 × 8 blocks, determine the relevant picture information, discard redundant or insignificant information, and encode relevant information with least number of bits. Common stages in all three standards are:

- Discrete Cosine Transform (DCT)
- Zig-Zag Scanning
- Quantization
- Entropy Coding
- Motion Estimation

The International Standards Organization (ISO) has proposed the JPEG standard [2, 4, 5] for image compression. Each color component of still image is treated as a separate gray scale picture by JPEG. Although JPEG allows any color component separation, images are usually separated into Red, Green, and Blue (RGB) or Luminance (Y), with Blue and Red color differences (U = B – Y, V = R – Y). Separation into YUV color components allows the algorithm to take the advantages of human eyes' lower sensitivity to color information. For quantization, JPEG uses quantization matrices. JPEG allows a different quantization matrix to be specified for each color component [3].

Though the JPEG provides good results previously, it is not perfectly suited for modern multimedia applications because of blocking artifacts. JEPG can only work with 8 × 8 blocks one at a time. This causes the artifact in compressed images-small squares all over the images, known as blocking artifacts [9] when compression ratio is high.

Wavelet theory and its application in image compression had been well developed over the past decade. The field of wavelets is still sufficiently new and further advancements will continue to be reported in many areas. Many authors have contributed to the field to make it what it is today, with the most well known pioneer probably being Ingrid Daubechies. Other researchers whose contribution directly influence this work include Stephane Mallat for the pyramid filtering algorithm, and the team of R. R. Coifman, Y. Meyer, and M. V. Wickerhauser for their introduction of wavelet packet [6].

Although the JPEG methods are the efficient, the block noise (artifact) appears in the resulting image. The block noise in an image makes the picture quality poor especially for our human eyes [9]. Further research has been done on still image compression and JPEG-2000 standard is established in 1992 and work on JPEG-2000 for coding of still images has been completed at end of year 2000. The upcoming JPEG-2000 standard employs wavelet for compression due to its merits in terms of scalability, localization and energy concentration [6, 7]. It also provides the user with many options to choose to achieve further compression. JPEG-2000 standard supports decomposition of all the sub-bands at each level and hence requires full decomposition at a certain level.

The basic compression scheme in JPEG-2000 can be summarized as: the source image is first transformed using Discrete Wavelet Transform (DWT); then quantization of transformed image is carried out; the quantized image is then encoded by using the entropy encoders. Even though the JPEG-2000 is widely used, it suffers from blurring and artifacts.

1.4.0 OBJECTIVES OF RESEARCH WORK

Wavelet is used to compress the image in standard JPEG 2000. JPEG-2000 operates in spectral domain, trying to represent the image as a sum of smooth oscillating waves. Spectral domain is appropriate for capturing relatively smooth color gradients, but not particularly appropriate for capturing the edges [9]. Therefore, the wavelet packet and wavelet packet best tree based on Log entropy, Shannon entropy, and Threshold entropy are being used for image compression to avoid the loss of high frequency components. As per the survey, a thorough investigation with the intention of determining whether the wavelet packet best tree on the basis of energy contain with the adaptive thresholding can be a better choice for image compression. The thesis presents an innovating state-of-the-art image compression technique based on wavelet packet

best tree on the basis of energy contain with adaptive thresholding and lossy encoding. The images used in this work include many popular images like Aishwarya, Cheetah, Lena, Woman, Barbara, Mandrill, Donkey, Butterfly, and Bird. Additionally 'Synthetic' Computer generated images have been chosen for having characteristics different from natural images. This research work includes the following objectives:

1. Comparative analysis of the well known, Daubechies, Biorthogonal and Coiflets wavelet is presented. Both quantitative and qualitative measures of performance are examined for each of the several natural and synthetic images.
2. Comparative analysis of the wavelet and wavelet packet tree is presented. Both quantitative and qualitative measures of performance are examined for each of the several natural and synthetic images.
3. The Comparative analysis of new wavelet packet tree on the basis of energy contain is presented with known wavelet packet best tree on the basis of Log entropy, Shannon entropy, Threshold entropy. Both quantitative and qualitative measures of performance are examined for each of the several natural and synthetic images.
4. The use of wavelet packet best tree on the basis of energy contain with adaptive threshold for thresholding is proposed as a new technique for the image compression. Both quantitative and qualitative measures of performance are examined for each of the several natural and synthetic images.
5. The lossy encoding technique is implemented. Both quantitative and qualitative measures of performance are examined for each of the several natural and synthetic images.

1.5.0 ORGANIZATION OF REPORT

The research work reported in this thesis has been focused on Image Compression with the review of current existing techniques. The highlights of the research work presented are,

- The quantitative and qualitative measures of known, Daubechies, Biorthogonal and Coiflets wavelet performance are examined for each of the several natural, and synthetic images, and the analyses of the same are presented.
- The quantitative and qualitative measures of the wavelet and wavelet packet tree performance are examined for each of the several natural and synthetic images, and the analyses of the same are presented.

- The quantitative and qualitative measures of new wavelet packet tree on the basis of energy contain performance are examined for each of the several natural and synthetic images, and the comparative analysis of new wavelet packet tree on the basis of energy contain is presented with known wavelet packet best tree on the basis of Log, Shannon, Threshold Entropy.

The work reported in this thesis has been organized into six chapters. The content of each chapter is presented briefly in following paragraphs.

In chapter one, the Image Compression is elaborated and motivation behind the work is presented, the recent methods used for Image Compression are surveyed, and the objectives and methodology of the proposed research work are defined.

In chapter two, the fundamentals of Image Compression and the literature survey is presented, various ways of image representation are considered; explicit definition of compression ratio is provided; various redundancies and irrelevancy occurring in an image are mentioned. Classification of the compression techniques and methods used are explained. The criteria for image quality measurements are mentioned in detail such as Mean Option Score (MOS), Peak Signal to Noise Ration (PSNR), Mean Square Error (MSE), Normalized Absolute Error (NAE), Maximum Difference (MD) and Average Difference (AD). The design criteria for compressing graphical data are discussed. In chapter two, the Image Compression methodology is discussed thoroughly and current trends and techniques are surveyed. Wavelet packet tree and multi-wavelets are the thirst areas of research in this regard. The shortcoming and discrepancies among the methods are identified.

In chapter three, the basic theory of wavelet and many popular wavelets with characteristics are discussed in details. The wavelet tree, wavelet packet tree and well-known techniques of entropy are discussed such as log entropy, threshold entropy and Shannon entropy.

In chapter four, the implementation of proposed algorithm is presented. This chapter includes comparative analysis of the known wavelets, comparative analysis of the wavelet, and wavelet packet tree. Then the comparative analysis of new wavelet packet best tree on the basis of energy contain with the known entropy and proposed methods of image compression for natural images and synthetic images are presented. The new technique of Image Compression, 'Wavelet packet best tree on the basis of energy contain with adaptive thresholding and lossy encoding technique for image compression' is presented.

In chapter five, the results of proposed algorithm are presented as compressed images. The image includes the wide variety of natural and synthetic colored and gray images. The test images are - viz Aishwarya, Cheetah, Lena, Barbara, Bird, Donkey, Mandrill, Butterfly, Horizontal, and Vertical line based images. Alongwith the compressed images the resultant percentage of compression, compression ratio, and peak signal to noise ratio for the different values of P are presented. Here P is a quality factor defined in the algorithm for the additional flexibility as per the demand of the application.

Chapter six concludes with summary of results and throws light on future developments in the same area.

CHAPTER 2
LITERATURE SURVEY

Chapter one included the discussion of motivation for the research work, current techniques in use, and objectives of research work. This chapter discusses basics of image representations, and image compression. In Image Compression, the researchers' aim is to reduce the number of bits needed to represent an image by removing the spatial and spectral redundancies. Image Compression method used may be Lossy or Lossless. As lossless image compression focuses on the quality of compressed image, the compression ratio achieved is very low. Hence, one cannot save the resources significantly by using lossless image compression. The image compression technique with compromising resultant image quality, without much notice of the viewer is the lossy image compression. The loss in the image quality is adding to the percentage compression, hence results in saving the resources. Many modern image compression techniques are based on lossy methods. In lossy image compression Mean Square Error (MSE) and Peak Signal to Noise Ratio (PSNR) are most commonly used objective measures of image quality. Applications of image compression are primarily in representation, transmission, and storage of information [104].

This chapter also includes the principle of image compression, and various color models used for colored image representation, and review of current techniques used for image compression.

2.1.0 IMAGE REPRESENTATION

The digital image is represented as two-dimensional array of picture elements having M rows and N columns. M × N defines the resolution of the image. Every sampled picture element is known as pixel in digital image processing. Each pixel is identified with unique positional tuple (x, y). In other words, image is stored as a two dimensional signal. It is represented by function f (x, y), where x and y are spatial co-ordinates of a pixel and the value of function f at any pair of co-ordinate (x, y) is called as intensity of a pixel or gray level of a pixel of the image at that point in gray images [11]. For color images the function f maps the color information associated with the pixel at (x, y).

Different techniques are used to represent the digital image. The basic techniques used to represent the digital images are:

- Indexed image
- Binary image
- Intensity image
- Color image

2.1.1 INDEXED IMAGE

An indexed image representation consists of two matrices: i) data matrix (X) and ii) color matrix (map). Map is an L × 3 array of class double containing floating-point values in the range of 0 to 1, where L is the maximum intensity of the pixel. For example, if eight binary bits are used for representation of intensity of a pixel, then value of L is 256. Each row of the map specifies the red, green, and blue components of a single color. Matrix X is M × N array of class integer, containing integer value in the range of 0 to 255. Each element of array X is an index to the map [12], to retrieve the color components red, green and, blue from the map. This entry defines the true colors of corresponding pixel. For example, if the value of the pixel is 100, the value 100 acts as a pointer to the color map and selects the row number 101, the red, green, and blue value corresponding the row, define the true colors of the pixel of intensity 100. The value '0' point to the first row in a map and value '1' points to the second row in a map, and value 255 point to the row number 256 in a map. Matlab supports the usage of indexed image representation. There are various color maps supported by Matlab, but it is tested and proved that the usage of these color maps result in total change in color complexion of the resultant image. That's why the true color image processing is not recommended with indexed image file format.

2.1.2 BINARY IMAGE

Binary image representation is the primitive type of image representation. It is represented by a single matrix (B) of size M × N, where M is the width, and N is the height of the digital image in terms of pixels. Larger the values of M and N, better the resolution of an image, but it takes more storage space. The number of bits required to store the digital image is M × N × 1. The value of each pixel assumes to be one of the two discrete (binary) values; these two values correspond to ON (1) or OFF (0). A binary image is stored in terms of 0's and 1's. It is special kind of intensity image containing only black and white colors [13]. Where value 0 represents black color and value 1 represents white color. It requires very less storage space, but due to only two

color options it is impossible to represents real gray and color images. That's why it is not recommended for image representation and processing. It is only used for pure black and white images. It can be considered as indexed image with only two colors. It was previously used to display the images using Monochrome Display Adaptors (MDA).

2.1.3 INTENSITY IMAGE

Intensity image representation is one of the simplest and elementary types of image representation. It is represented by a single matrix (I) of size M × N, where M is the width, and N is the height of the digital image in terms of pixels. Larger the values of M and N, better the resolution of an image, but it takes more storage space. The number of bits required to store the digital image is M × N × number of bits used for intensity representation. Each element of the image matrix represents the intensity of a corresponding pixel of image. The elements in the intensity matrix represent various intensities or gray levels [13]. If N bits are used to represent the intensity or gray scale of every pixel, then 2^N various intensities are possible. The minimum intensity value is zero and the maximum intensity value 2^N–1. If 8 bits are used for representation of gray scale, then the minimum intensity 0 represents black color and maximum intensity 255 represents white color. If 16 bits are used for representation of gray scale, then the intensity 0 represents black color and maximum intensity 65535 represents white color. As the intensity value changes from minimum to maximum, different gray shades are generated from full black color to full white color.

2.1.4 COLOR IMAGE

In today's multimedia era color images have significant impact on human lives. There are various techniques of representation of color in color images have been developed and used in various applications. The color associated with a single picture element is constituted by the intermixes of various color components. The color models are developed to support the idea of color image representation. Color model is a specification of a co-ordinate system and a sub space within that system, where a single point represents each color. Most color models in use today, are oriented either towards hardware or towards applications, where color manipulation is goal. In terms of digital image processing the hardware oriented models most commonly used in practice are RGB (Red, Green, Blue); the CMY (Cyan, Magenta, Yellow); the CMYK (Cyan, Magenta, Yellow, Black); and the HSI (Hue, Saturation and Intensity) [13, 14].

2.1.4.1 RED, GREEN, BLUE COLOR MODEL

In the RGB model, each color appears in its primitive spectral component of red, green, and blue. These are the primary colors of light. This model is based on Cartesian coordinate system. The RGB is referred as 'true color' or "full color" image. The number of bits used to represent each pixel in RGB space is called the pixel depth. In color image representation each pixel has three-color values red, green, and blue. The color of each pixel is determined by the triplet (R, G, B). In graphical file formats, RGB images are stored as 24-bit images; where 8 bits represent the red, green, and blue components of every pixel [13]. This yields a potential of sixteen million different colors. The actual numbers of colors in a 24-bit RGB image are 2^{24} = 16,777,216.

When the color value of basic color components is zero, then the corresponding color component is absent, and when the color value of basic color components is 255, then the corresponding color component is fully present in the corresponding pixel. The pixel whose components are (0, 0, 0) displayed as black, and pixel whose color components are (255, 255, 255) displayed as a white. Generally RGB model is preferred to process the color images due to rich range of color shades and it gives the true color perceptions. RGB image is stored in MATLAB as an M × N × 3 data array. The three-color components for each pixel are stored along the third dimension of the data array. For example the red, green, and blue color components of the pixel (x, y) are stored in MATLAB as RGB (x, y, 1), RGB (x, y, 2) and RGB (x, y, 3) respectively. The RGB color model, use predominantly for light emitting systems (for example Televisions and Computer monitors).

2.1.4.2 CMY AND CMYK COLOR MODELS

Cyan, Magenta, and Yellow are the secondary colors of light but are primary colors of color pigments. Since these colors of the pigments the original colors of light are not reflected. For example when a surface is coated with Cyan pigment is illuminated with white light, red light is not reflected from the surface. That is Cyan subtract from red light from reflected white light, which it self is composed of equal red, green, and blue light. CMY color values are computed from the primary colors values. Equal amount of pigment primaries Cyan, Magenta, and Yellow should produced black and it gives rise to CMYK color model. The CMY color model, use for light-absorbing systems (for example printing) [14].

2.1.4.3 HSI COLOR MODEL

Hue, Saturation and Intensity are calculated from the primary colors (RGB). Hue is the color attribute that describes the pure color (pure Yellow, Orange, or Red), where saturation gives a measure of the degree to which the pure color is diluted by white light. The intensity is the most useful descriptor of monochromatic images. HIS color model; decouple the intensity components from the color carrying information in color image [14].

2.2.0 COLOR SPACE AND HUMAN PERCEPTION

The use of color in image processing algorithm is motivated due to two-principle factors [13]

i) The color is powerful component, that often simplifies object identification and extraction of the scenes;

ii) The human visual perception can identify thousands of color shades and intensities, compared to about only few shades of gray color.

The color image processing is divided into two major areas: full color and pseudo color image processing. Basically the colors that humans and some other animals perceive an object are determined by the nature of the light reflected from the object. The human eye has two types of cells playing major role in object perception; Rod cell and Cone cell. Detail experimental evidence has established that the six to seven million cone cells in the human eye can be divided into three principle sensing categories corresponding roughly to red, green and blue. Approximately sixty-five percent of all cones are sensitive to red light, thirty-three percent are sensitive to green light and two percent are sensitive to blue light. Wavelength of red light is 700 nm, green light is 546.1 nm and blue light is 435.8 nm. The characteristics used to distinguish one color from another are brightness, hue, and saturation. Brightness embodies chromatic notation of intensity. Hue is an attribute associated with the dominant wavelength by an observer. Saturation refers to the relative purity or the amount of the white light mixed with a hue. Degree of saturation is inversely proportional to the amount of white light added. Hue and saturation taken together are called chromaticity and therefore a color may be characterized by its brightness and chromaticity.

RGB color model is ideal for image color generation, but when it is used for color description, its scope is much limited. The HSI model is an ideal tool for

developing image-processing algorithm based on color descriptions that are natural and intuitive to human eye.

Image is a two-dimension signal, it is represented by the positive function $I = f(x, y)$, where x and y are the co-ordinates of pixel and I is value corresponding to the pixel. The digital color image is constituted by the three primary color values, (that is RGB); such an image is referred as RGB color image. RGB color image is represented by a three dimensional array, where the first plane in the third dimension, represents the red pixel intensities, the second plane represents the green pixel intensities and the third plane represents the blue pixel intensities. Human visual perception is very sensitive to small change in the value of one of the colors when the remaining colors are fixed, and therefore the individual components of RGB color image cannot be analyzed independently.

For color image compression techniques, the selection of proper color model is extremely crucial because in lossy image compression technique data cannot be recovered exactly. Red, green and blue color components of pixel are correlated with visual appearance, therefore even though RGB is most common storage format for images; it is not used for image compression. If it is used, high visual distortion is introduced. It necessitates the conversion of RGB colors into another colors representation, which doesn't have the correlation among the components.

2.2.1 YUV AND YC_rC_b COLOR REPRESENTATION

NTSC (United States National Television Systems Committee) mandated color encoding for color televisions. It uses YUV color encoding, where Y is luminance, U is the difference (R – Y), and V is difference (B – Y). U and V represent color information (chrominance) [14].

YCrCb is subset of YUV. The luminance Y and chrominance U (R – Y) and V (V – Y) are calculated with the equations

$$Y = 0.299 \times Red + 0.587 \times Green + 0.114 \times Blue \quad \text{--- 2.2.1}$$

$$R - Y = 0.701 \times Red - 0.587 \times Green - 0.114 \times Blue \quad \text{--- 2.2.2}$$

$$B - Y = -0.299 \times Red - 0.587 \times Green + 0.886 \times Blue \quad \text{--- 2.2.3}$$

The Red, Green and Blue values are assumed to be the fractions in the range of 0.0 to 1.0. Notice that the luminance equation will always produce a value of Y in the range of 0.0 to 1.0. However, the value of color difference (R – Y) produces values in the range from – 0.701 to +0.701, and the value of color difference (B – Y) produces values in the range from – 0.886 to +0.886. These ranges are not ideal for digital

representation, so they are both remapped into the range of values –0.5 to +0.5 [14]. This gives

$$Cr = 0.500 \times Red - 0.419 \times Green - 0.081 \times Blue \quad \text{--- 2.2.4}$$

$$Cb = -0.169 \times Red - 0.331 \times Green - 0.5 \times Blue \quad \text{--- 2.2.5}$$

These values are converted to an 8-bit binary encoding using the equations:

$$Y = \text{round}(219 \times Y + 16)$$

$$Cr = \text{round}(224 \times 0.713 \times (R - Y) + 128)$$

$$Cb = \text{round}(224 \times 0.564 \times (B - Y) + 128)$$

The Red, Green and Blue values are assumed to be in the range of 0 to 255 the luminance equation will produce a value of Y in the range of 0 to 255. Human eyes are more sensitive to the change of brightness of color. It is proved that YCrCb color space do not have correlation among the spaces hence this is correct choice of color space for the color image compression. The equations used to convert the basic colors RGB into YCrCb are given by

$$Y = 0.299 \times Red + 0.587 \times Green + 0.114 \times Blue \quad \text{--- 2.2.6}$$

$$Cr = 0.701 \times Red - 0.587 \times Green - 0.114 \times Blue \quad \text{--- 2.2.7}$$

$$Cb = -0.299 \times Red - 0.587 \times Green + 0.886 \times Blue \quad \text{--- 2.2.8}$$

After the color image processing, the components YCrCb are remapped to RGB color components to display the image, using the equations

$$Xr = Y + Cr \quad \text{--- 2.2.9}$$

$$Xg = Y - 0.509 \times Cr - 0.194 \times Cb \quad \text{--- 2.2.10}$$

$$Xb = Y + Cb \quad \text{--- 2.2.11}$$

Many graphic file formats use YCrCb color encoding method such as IIF (Image Interchange Facility), JEPG (Joint Photograph Expert Group), MPEG (Motion Picture Expert Group), and TIFF (Tagged Interchanged File Format).

2.3.0 PRINCIPLE OF IMAGE COMPRESSION

In today's multimedia era, images are one of the important media of information representation. We have already discussed the importance of image compression to use the resources efficiently. Image compression reduces the number of bits required to represent the image, therefore the amount of memory required to store the data set is reduced. It also reduces the amount of time required to transmit a data set over a communication link at a given rate. Different methods are developed to perform the image compression. The compression ratio is one of the quantitative parameters to

measure the performance of compression methods. Compression ratio is defined as *ratio of the size of original data set to the size of the compressed data set* [14].

$$Compression\ ratio = \frac{Number\ of\ bytes\ in\ the\ original\ data\ set}{Number\ of\ bytes\ in\ the\ compressed\ data\ set} \quad \text{--- 2.3.1}$$

The compression ratio is expressed as a single number or as two numbers with the second number typically being one. For example 10:1 means 10 bytes of the original data are represented by one byte.

The percentage of compression is also one of the alternative parameter to measure the performance of the compression. It is *the ratio of difference of number of bytes of original image and compress image to number of bytes of original image into hundred.*

$$Compression\ Percentage = \frac{No.\ of\ bytes\ in\ the\ original\ data\ set - No.\ of\ bytes\ in\ the\ compressed\ data\ set}{No.\ of\ bytes\ in\ the\ original\ data\ set} \times 100 \quad \text{--- 2.3.2}$$

Bits/pixel is another standard method of specifying a compression ratio. The average number of bits required to represent the data value for the single pixel of an image is referred as bits/pixel [14].

The common characteristic of most of the images is that, the neighboring pixels are correlated, and image contains redundant information [1]. Therefore the most important task in image compression is to find a less correlated representation of the image. The fundamental component of image compression is reduction of redundancy and irrelevancy. Redundancy reduction aims at removing duplication from image, and irrelevancy reduction omits parts of the signal that will not be noticed by Human Visual System (HVS) [96]. The redundancies in an image can be identified as spatial redundancy, spectral redundancy and temporal redundancy.

- **Spatial redundancy**

  It is the correlation between neighboring pixel values.

- **Spectral redundancy**

  It is correlation between different color planes or spectral band.

- **Temporal Redundancy**

  It is correlation between adjacent frames in a sequence of images.

Image compression research aims at reducing the number of bits needed to represent an image by removing the spatial and spectral redundancies as much as possible. Since the focus is only on still natural image compression, the temporal redundancy is not considered as it is used in motion picture compression (video) [1].

2.4.0 COMPRESSION TECHNIQUES

Various applications demand various degrees of compression with/without compromising the quality of image. The compression techniques are classified into two groups:

- Lossless compression
- Lossy compression

2.4.1 LOSSLESS COMPRESSION

In lossless compression schemes the reconstructed image, after compression, is identical to the original image. Lossless compression can achieve modest compression but the information of all pixels is preserved after the compression and the original image may be perfectly reconstructed. The small error is introduced due to rounding during the calculations, and it is insignificant, and cannot be noticed by human eye. Lossless methods rely on elimination of coding redundancy; it finds probability distribution of the data stream to reduce the data volume by using a customized representation of the information content. This technique of compression often has low compression ratio, but retains the quality of an image. And hence this technique is suitable for application, which do not allow loss in image information. An example application is: media includes a program file or text and media where the data must be preserved exactly for legal or other reasons. The Run-Length coding, Huffman coding and Arithmetic coding, bit plain coding, lossless predictive coding and Lempel-Ziv-Welch (LZW) coding are the few examples of lossless image compression coding technique [14, 99]. Though reconstructed image quality is extremely good in lossless compression, this technique fails to save the resources significantly. Hence, there is need to develop the compression technique, which can save the considerable amount of resources in multimedia applications.

2.4.2 LOSSY COMPRESSION

To save the resources significantly another technique known as lossy compression was developed. In lossy compression technique, the information of all pixels is not preserved after the compression. These methods rely on elimination of coding redundancy; inter pixel redundancy, and psycho-visual redundancy. In lossy compression technique, methods are applied which extract the essential information from the original image and discard irrelevant information. The extracted information is coded compactly to improve the further compression ratio.

The extraction of the information from the original image is based on Human Visual System. By exploring Human Visual interaction characteristics carefully, the compression algorithm can discard information, which is irrelevant to human eye. This technique of compression has high compression ratio and compromised image quality. This technique is suitable in applications that require more compression ratio, and can accept the compromise image quality. Based on lossy compression technique algorithms were suggested by few researchers. The popular techniques are used in JPEG and JPEG 2000 [1]. Basic goal of researcher is to improve the compression ratio by maintaining the quality of image.

2.5.0 MEASURES OF IMAGE QUALITY

In lossless image compression techniques, the reconstructed image is identical to the original image and hence quality is not an issue. But in lossy compression technique, quality is one of the issues because decoded image is an approximation of the original image. There are different quality measure criteria, available for quality assessments. These measure criteria are classified as [15]:

- Subjective measures
- Objective measures

2.5.1 SUBJECTIVE MEASURES

The subjective criteria are based on group of human examiners, assessing the image quality. In subjective criteria the group of human examines original image, and reconstructed image; the examiners assign grades. On the basis of the grade, quality of reconstructed image is assessed. Mean Opinion Score (MOS) is one of the subjective evaluations of image quality measure. The MOS values were obtained from an experiment involving the group of persons; the testing methodology was the double stimulus impairment scale method. The double stimulus impairment scale method uses references and test conditions, which are arranged in pairs such that the first in the pair is unimpaired reference, the second is the same sequence impaired. The original source image without compression was used as the reference condition. The assessor is asked to note on the second, keeping in mind the first and five-grade impairment scales described in ITU-BT Rec. 500 [15,16]. Five grade impairment with proper description for each grade: 5-imperceptible, 4-perceptible, 3-slightly annoying, 2-annoying, 1-very annoying. MOS for each test condition and test image are calculated

$$MOS = \sum_{i=1}^{5} ip(i) \qquad \text{--- 2.5.1}$$

Where ‘i’ is the grade and p (i) is the grade probability. Another method for evaluation of the quality based is Double Stimulus Continuous Quality Scale (DSCQS) [17], which was presented to the viewers for two images, one original image, and other was processed image. Viewers evaluated image quality of both images using grading scale of five intervals (1=Excellent, 2=Good, 3=Fair, 4=Poor, 5=Bad) [15]. However subjective evaluation is usually too convenient, but it is more expensive, and measurements should be processed very carefully [17,18,19,20]. This method has some difficulties:

- Human judgment vary from time to time and person to person
- Human judgment may be significantly affected by the presence of the system, which introduce errors or artifacts.

With due consideration of discrepancies in subjective criteria for compressed image assessment, objective criteria for quality assessment were recommended.

2.5.2 OBJECTIVE MEASURES

In the process of image compression, the noise is introduced due to thresholding/quantization. The noise is referred as an error in image processing, and it degrades the quality of image. To measure the quality of compressed image, the different objectives measures are recommended. As Human Intervention is involved in subjective criteria of image quality assessment, it is prone to improper interpretation. Hence objective criteria are preferred over the subjective criteria for quality of image assessment. These criteria involved computations to calculate various parameters contributing to quality assessment of an image. There are many objective quality-measuring methods that have been developed for image quality evaluation in last few years. And they are based on numerical measures of image quality and computable distortion measures [17]. These criteria can be divided into two categories: Image differencing, and Feature Extraction.

i) Image differencing

Image differencing usually uses matrix-based operations to derive important parameters of an image.

ii) Feature Extraction.

In feature extraction category, the important features of image quality are extracted.

The few common objective quality measures are discussed here, which are evaluated in work [15, 20, 21]. They are discrete and provide some degree of closeness between the digital images by exploiting the differences in the statistical distributions of

pixels. The objective criteria considered for the discussion which are commonly used to measure the quality of an image are [20, 21]:

i) Mean Square Error (MSE)
ii) Signal to Noise Ratio (SNR)
iii) Peak Signal to Noise Ratio (PSNR)
iv) Normalized Cross-correlation (NK)
v) Average Difference (AD)
vi) Maximum Difference (MD)
vii) Structural Content (SC)
viii) Normalized Absolute Error (NAE)

i) Mean Square Error (MSE)

It is measured as the average of square of error introduced in a compressed image. It is defined by the equation

$$MSE = \left[\frac{1}{MN} \sum_{r=0}^{M-1} \sum_{c=0}^{N-1} \left\{ f(r,c) - \hat{f}(r,c) \right\}^2 \right] \quad \text{--- 2.5.2.1}$$

Where M × N s size of image $f(r,c)$ and $\hat{f}(r,c)$ denotes the row element r, and column element c of original image and the reconstructed image respectively.

The root mean square error is calculated from MSE and some times RMSE is used as one of the objective quality measures. It is given by the equation-

$$RMSE = \left[\frac{1}{MN} \sum_{r=0}^{M-1} \sum_{c=0}^{N-1} \left\{ f(r,c) - \hat{f}(r,c) \right\}^2 \right]^{\frac{1}{2}} \quad \text{--- 2.5.2.2}$$

ii) Signal to Noise Ratio (SNR)

Signal to Noise Ratio is defined as ratio of signal power to noise power. It is given by the equation

$$S.N.R. = 10 \log \left(\frac{\sum_{r=0}^{M-1} \sum_{c=0}^{N-1} \left\{ f^2(r,c) \right\}}{\sum_{r=0}^{M-1} \sum_{c=0}^{N-1} \left\{ f(r,c) - \hat{f}(r,c) \right\}^2} \right) \quad \text{--- 2.5.2.3}$$

iii) Peak Signal to Noise Ratio (PSNR)

Peak Signal to Noise Ratio is defined as ratio of maximum signal power to noise power. It is given by the equation

$$PSNR = 20 \log \left(\frac{2^n - 1}{RMSE} \right) \quad \text{--- 2.5.2.4}$$

Where n is number of bits used for the intensity of pixel. For n = 8

$$PSNR = 20\log\left(\frac{255}{RMSE}\right) \quad \text{--- 2.5.2.5}$$

iv) Normalized Cross-correlation (NK)

Normalized Cross-correlation is obtained by the given equation

$$NK = \left(\frac{\sum_{r=0}^{M-1}\sum_{c=0}^{N-1} f(r,c)\,.\,\hat{f}(r,c)}{\sum_{r=0}^{M-1}\sum_{c=0}^{N-1} f^{2}(r,c)}\right) \quad \text{--- 2.5.2.6}$$

v) Average Difference (AD)

Average Difference is obtained by the given equation

$$AD. = \sum_{r=0}^{M-1}\sum_{c=0}^{N-1} f(r,c) - \hat{f}(r,c) / MN \quad \text{--- 2.5.2.7}$$

vi) Maximum Difference (MD)

Maximum Difference is obtained by the given equation

$$MD = max\left(\left| f(r,c) - \hat{f}(r,c)\right|\right) \quad \text{--- 2.5.2.8}$$

vii) Structural Content (SC)

Structural Content is obtained by the given equation

$$SC = \left(\frac{\sum_{r=0}^{M-1}\sum_{c=0}^{N-1} f^{2}(r,c)}{\sum_{r=0}^{M-1}\sum_{c=0}^{N-1} \hat{f}^{2}(r,c)}\right) \quad \text{--- 2.5.2.9}$$

viii) Normalized Absolute Error (NAE)

Normalized Absolute Error is obtained by the given equation

$$NAE = \sum_{r=0}^{M-1}\sum_{c=0}^{N-1}\left| f(r,c) - \hat{f}(r,c)\right| / \sum_{r=0}^{M-1}\sum_{c=0}^{N-1}\left| f(r,c)\right| \quad \text{--- 2.5.2.10}$$

The Mean Square Error and Peak Signal to Noise Ratio are most commonly used objective quality measures in image quality evaluation. Because they are simple to calculate, have clear physical meanings and mathematically convenient in the context of optimization. For color images the Mean Square Error is calculated for the reconstruction of each space and their average is used to generate the Peak Signal to Noise Ratio of the reconstructed RGB images. If the calculated value of MSE is low, it indicates that noise introduced due to processing is low; it is desirable as it results in good quality of processed image. If the calculated value of PSNR is high, it indicates that noise introduced due to processing is low; it is desirable as it results in good quality of processed image.

2.6.0 COMPRESSION DESIGN CRITERIA

The compression of graphical data is useful for a variety of applications and each application imposes different design criteria and constraints on the compression schemes. There are many design constraints, few of them are: time, cost, information loss, and compression ratio [14]. These constraints vary according to application demands. For example, real time applications impose stiff constraints regarding time. If special purpose hardware is required for the application then it adds to the expenses. Some applications can tolerate loss of information, but in applications like bio-medical the loss of information cannot be tolerated. Many multimedia applications demand high compression ratio with compromising quality of information. As with almost any design task, tradeoff must be made between design constraints to meet cost and performance criteria.

2.7.0 APPLICATIONS OF IMAGE COMPRESSION

In today's modern era multimedia play an important role. As image is one of the important media of information it captures major focus in processing. For efficient/optimum utilization of storages-space and bandwidth, the image compression is desired. Applications of image compression are primarily in transmission and storage of information. Image transmission applications are in broadcast television, streaming videos, remote information sensing via satellite, and military communications via aircraft, radar and sonar, teleconferencing, video conferencing, remote medical consultation, desk-top publishing, computer communication and facsimile transmission. Image storage is required for educational and business documents, medical images that arise in Computer Tomography (CT), Magnetic Resonance Imaging (MRI) and digital radiology, motion pictures, satellite images, weather maps, geological surveys, and astronomy [14].

2.8.0 IMAGE COMPRESSION METHODOLOGY

There are various methods of compressing still images, but every method has three basic steps involved in any of the data compression scheme: Transformation, reduced precision (quantization or thresholding), and minimization of number of bits to represent the image (encoding). The basic block diagram of compression scheme is shown in figure 2.8.1.

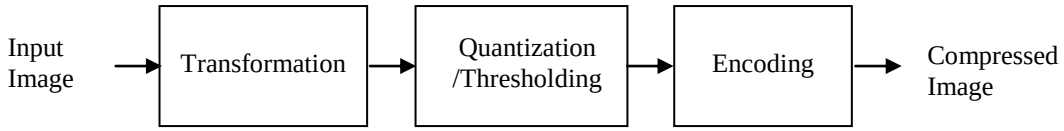

Figure 2.8.1: The block diagram of compression scheme

2.8.1 TRANSFORMATION

The transformation block transforms the data set into another equivalent data set. For image compression, it is desirable that the selection of transform should reduce the size of resultant data set as compared to source data set. Few transformations reduce the number of data items in the data set. Few transformations reduce the numerical size of the data items that allows them to represent by the fewer binary bits. Many mathematical transformations exist that transform a data set from one system of measurement into another in such a way that the data can be represented by the small number of bits. In data compression, transform is intended to decorelate the input signals by transforming. The data represented in the new system has properties that facilitate the compression. Some mathematical transformations have been invented for the sole purpose of data compression; selection of proper transform is one of the important factors in data compression scheme. It still remains an active field of research. The technical name given to these processes of transformation is mapping [14]. Some mathematical transformations have been invented for the sole purpose of data compression, other have been borrowed from various applications and applied to data compression. The partial list includes:

- Discrete Fourier Transform (DFT)
- Discrete Cosine Transform (DCT)
- Hadamard-Haar Transform (HHT)
- Karhune-Loeve Transforms (KLT)
- Slant-Haar Transform (SHT)
- Walsh-Hadamard Transform (WHT)
- Short Fourier Transforms (SFT)
- Wavelet Transforms (WT)

2.8.2 QUANTIZATION/THRESHOLDING

There have been numerous methods proposed to perform quantization of the transformed coefficients. In the process of quantization each sample is scaled by the quantization factor. Where as in the process of thresholding the samples are eliminated

if the value of sample is less than the defined threshold value. These two methods are responsible for introduction of error and it degrades the quality. In image compression, introduction of the error degrades the visual quality of an image. The degradation is based on selection of quantization factor and threshold value. For the high value of threshold the loss of information is more, and for low value of threshold the loss of information is less. By considering the resultant loss of information, the selection of threshold should be low, but for the low value of the threshold there is negligible compression of data. Hence quantization factor, or threshold value should be selected in such a way that it should satisfy the constraints of human visual system for better visual quality, and high compression ratio. Human Visual System is less sensitive to high frequency signal and more sensitive to low frequency signal [22]. By considering this phenomenon, the threshold value or quantization factor is selected and thresholding / quantization take place in image compression.

In image compression technique two types of thresholding are used as:

- Hard Thresholding
- Soft Thresholding.

In hard thresholding technique, if the value of the coefficient is less than defined value of threshold, then the coefficient is scaled to zero, otherwise the value of the coefficient is maintained as it is. This process is repeated until all the pixels in the image are exhausted.

In soft thresholding technique, if the value of the coefficient is less than defined value of threshold, then the coefficient value is scaled to zero and otherwise the value of coefficient is reduced by the amount of defined value of threshold. This process is repeated until all the pixels in the image are exhausted.

Quantization/thresholding remains an active field of research. Prime objective of the research is to develop novel technique of image compression, wavelet packet best tree on the basis of energy contain with *adaptive thresholding* and lossy encoding. Details of proposed Image Compression techniques are covered in chapter 4.

2.8.3 ENCODING

This phase of compression reduces the overall number of bits needed to represent the data set. An entropy encoder further compresses the quantized values to give better overall compression. This process removes the redundancy in the form of repetitive bit pattern in the output of quantizer. It uses a model to accurately determine the probabilities for each quantized value and produces an appropriate code based on

these probabilities so that the resultant output code stream will be smaller than the input stream. The most commonly used entropy encoders are Huffman encoder and the Arithmetic encoder.

Huffman Encoder

Huffman codes assign a variable length code to each possible data item, such that the values that occur most often in the data set have smaller length codes while the values that occur less frequently have longer length codes. Given the probability of occurrence of each individual data value, the Huffman algorithm can automatically create an appropriate code assignment for each data value. This method of encoding works, but in many cases it wastes coding capacity [23]. The other problem with Huffman encoding is that when a Huffman code exceeds the size of target data type there is a problem of overflow.

Arithmetic Encoding

Arithmetic codes are based on sequences of data values. Instead of assigning a unique code to each individual data value, this scheme outputs a series of values that corresponds to unique sequence of data. The probability of occurrence of each individual data value is used to create the output codes. This scheme works well for incrementally encoding data. But there is potential for a loss of precision under certain circumstances [23].

Run Length Encoding (RLE)

The Run Length encoding is used in a process of compression to encode the data before the coding. Run-Length Encoding is a simple technique used to compressed runs of identical components in a data stream. RLE is a pattern recognition scheme that searches for the repetition of identical data values in the component array. The data set is compressed by replacing the repetitive sequence with a single data value and a count of the value. The compression ratio obtained from run-length encoding schemes, vary depending on the type of data to be encoded, and repetitions present within any given data set. Some data sets can be highly compressed by run-length encoding, whereas other data sets can actually grow larger due to the compression.

The Huffman algorithm requires each code to have an integral number of bits, while arithmetic coding methods allow for fractional numbers of bits per code by grouping two or more such codes together into a block composed of an integral number of bits. This allows arithmetic codes to outperform Huffman codes, and consequently arithmetic codes are more commonly used in wavelet-based algorithm.

2.9.0 LITERATURE SURVEY

The rapid growth of digital image applications including desktop publishing, multimedia, teleconferencing, and High Definition Television (HDTV) has increased the need, for effective and standardized image compression techniques. Numbers of Image Compression methodologies have been presented over the years for performing image compression. These methods have one common goal to alter the representation of the information contained in an image, so that it can be represented sufficiently well with less amount of memory. Still active research is going on for the perfection to match the technological advancements. The research of data compression started from the work of Shannon, Fano and Huffman in the late 1940, and technique is developed in 1986 [24]. Shannon, Fano technique has an advantage of its simplicity. The source data and their probabilities are listed in order of non-increasing probability. This list is then divided in such way as to form two groups of as nearly equal total probability as possible. Each data in the first group receives zero as the first digit of its codeword; the data in the second half have codeword beginning with one. Each of these groups is then divided according to the same criterion and additional code digits are appended. The process is continued until each subset contains only one datum.

The Discrete Cosine Transform (DCT) developed by Ahmed, Natrajan, and Rao [1974] was one of the transform used in image compression application; the DCT is a close relative of the Discrete Fourier Transform (DFT). Its application to image compression was pioneered by Chen and Pratt [1984] [2]. The Discrete Cosine Transform is a technique for converting a signal into elementary frequency components. It is widely used in image compression. During the 1980's and 1990's, Discrete Cosine Transform (DCT) based compression algorithm and international standard were developed to alleviate storage and bandwidth limitation imposed by digital still images and motion video applications [3]. Today there are three DCT-based standards that are widely used and accepted worldwide

- JPEG (Joint Photographic Expert Group)
- H.261 (Video codes for audiovisual Group)
- MPEG (Motion Picture Expert Group)

Each of these standards is well suited for particular applications: JPEG is for still image compression, H.261 is for video conferencing, and MPEG is for high-quality, multimedia systems [3].

The International Standard Organization (ISO) has proposed the JPEG standard for image compression. The JPEG standard defines a suite of data encoding for full

color and continuous-tone raster images. The JPEG standard includes four distinct modes of operation: [14]

- Lossless JPEG
- Sequential JPEG
- Progressive JPEG
- Hierarchical JPEG

Lossless JEPG

Lossless JPEG mode uses predictive (a form of differencing) compression scheme, and in the image reconstruction each row (scan line) is decoded, and is sequential displayed in full resolution.

Sequential JEPG

Sequential JPEG mode uses Discrete Cosine Transform (DCT) compression scheme, and in the image reconstruction each row (blocks of 8 × 8 pixels) is decoded, and is sequential displayed in full accuracy and resolution.

Progressive JEPG

Progressive JPEG mode uses Discrete Cosine Transform (DCT) compression scheme, and in the image reconstruction the entire image is decoded and displayed at the certain accuracy; and further decodings of the entire image add to this accuracy.

Hierarchical JEPG

Hierarchical JPEG mode uses Discrete Cosine Transform (DCT) or predictive compression scheme, and in the image reconstruction image is decoded at a certain resolution, and further decodings at higher resolutions are added into the previous decodings to increase the resolution.

The Discrete Cosine Transform is closely related to the Discrete Fourier Transform (DFT), and allows data to be represented in terms of its frequency components. Similarly in image processing applications the two-dimensional DCT maps a picture or picture segment into its two dimensional frequency components [3]. The DCT transforms transfer a data set into the cosine-frequency domain. The values in the upper-left corner of the transformed data represent the lower-order frequencies while the values in the lower-right corner represent the higher-order frequencies. The low-order frequency terms capture the essence of the data while the higher-frequency terms capture the fine details and noise. The DCT component at coordinates (0,0) is referred to as the DC bin, and all other components are referred to as AC bins. In JPEG method the original image is divided into square blocks of size M × M, where M is an integer of

size 8, 16, 32 etc. Generally M = 8 is preferred for image compression. Each block of size M × M is transformed to frequency domain using discrete cosine transform. The mappings of the DCT components are from lower to higher frequencies along the horizontal and vertical directions. To transform two dimensional frequency bins clusters packets of picture information is scanned using zigzag scanning, so that it includes the frequency components in increasing order as a one dimensional stream of bins [102].

The resulting matrix is then processed in a quantization stage in which a user specified quality factor, usually between 1 and 100, is utilized to define quality matrix. The precision is reduced during encoding (i.e., the quantization process) by dividing each data value in the 8 x 8 block by a unique divisor that is stored in an 8 x 8 table. Mathematically the quantization step is simply a division operation. In the JPEG image compression standard, compression ratios can be adjusted by uniformly scaling the quantization matrix by a multiplicative factor, called the Q-factor. A higher Q-factor gives better compression but increased blockiness; a lower Q-factor gives better image quality but worse compression. The quantization matrix, however, is not defined by the standard but it is supplied by the user and stored or transmitted with the compressed image. Previous research on improving the visual quality of JPEG coded images for a given bit rate has concentrated on optimizing the quantization matrices for optimal visual quality [25]. However, the quantization matrix must be optimized for each individual image, which is very computationally intensive. Moreover, this technique does not consider the different activity levels across the image. Quantization is the primary source of data loss in DCT based image compression algorithms. Quantization reduces the amount of information required to represent the frequency bins. For simplicity, all the standard image compression algorithms use linear quantization, where the step size quantization levels are constant [3]. Quantization in the frequency domain has many advantages over directly quantizing the pixel values. This takes advantages of the fact that the human eye is less sensitive to high frequency visual noise, but is more sensitive to lower frequency noise. Therefore, the quantization factors are usually chosen to be larger for the higher frequencies as compared to the lower frequencies [3]. It is in this stage that loss occurs as high frequency components of the matrix are in effect zeroed out. This stage is significant component of this compression technique, in that the user has the trade off the decision between file size and data loss. If quality factor is high then the compression ratio is high but it results in high image degradation, and if quality factor is low then the compression ratio is low but it results in better image quality [26].

Entropy coding is a lossless compression scheme based on statistical properties of the picture or the stream of information to be compressed. Although entropy coding is implemented slightly different in each of the standards, the basic entropy-coding scheme consists of encoding the most frequently occurring patterns with the least number of bits. In, this manner, data can be compressed by an additional factor of three or four [3]. In JPEG standard the coding process is performed after the quantization. The quantized data is encoded by run-length encoding, which reduces repetition redundancy then it is coded using Huffman coding. To summarize JPEG image compression algorithm includes the following steps [3].

1. Divide the image into the M × M blocks.
2. Discrete Cosine Transform of each block
3. Quantization
4. Zigzag scanning
5. Encoding
6. Coding

Each color component of still image is treated as separate gray-scale picture by JPEG. Although JPEG allows any color components separations; images are usually separated into Red, Green, Blue (RGB) or Luminance (Y), with Blue and Red color differences (U=B – Y, V=R – Y). Separation into YUV color components allows the algorithm to take an advantage of the human eye, which is lower sensitivity to color information. The U and V color components are recorded at lower bandwidth and sub-sampled to one-half in horizontal dimensions (called 4:2:2), or one-half in both the horizontal and vertical (called 4:2:0) [3]. JPEG partitions each color components picture into 8 × 8 pixel blocks of image samples, and DCT is applied to each block .For quantization, JPEG uses quantization matrices. JPEG allows a different quantization matrix to be specified for each color component. Using quantization matrices allows each frequency bin to be quantized in different step size [3].

Debra A. Lelewer and Daniel S. Hirschberg [24] presented the *Surveys Of Variety of Data Compression Methods*, spanning almost forty years of research from the work Shannon-Fano and Huffman in the late 1940's to a technique developed in 1986. They discussed the concept of information theory, as related to the goals of evaluation of data compression methods. The framework for the evaluation and comparison of method was constructed and applied to the algorithm presented. Comparisons of both theoretical and empirical natures were reported related to both Shannon-Fano and Huffman mapping.

GuoCan Feng and Jianmin Jiang [25] presented *Image Segmentation In Compressed Domain*. They proposed a direct segmentation image algorithm in JPEG compressed domain. The algorithm featured in extracting statistical parameters from DCT coefficients without its inversed transform, and growing regions in line with JPEG compression seamlessly in blocks of 8 × 8 pixels. They claimed that, in comparison with latest research efforts in region based image segmentation, the proposed algorithm achieved significant advantages including: a) no iteration was involved; b) no full decompression was needed; and c) segmentation performance was competitive. Image segmentation can be mainly divided into two categories edge based approaches and region based approaches and all the segmentation techniques were developed in pixel domain, these techniques used for image compression were time consuming and insufficient to overcome this problem. Researcher proposed direct segmentation in DCT domain for JPEG compressed images would have the advantage that any necessity of decompression could be eliminated. This property would greatly reduce the computational cost. Authors concluded that their algorithm had additional advantages over the existing one due to the fact that the proposed segmentation was directly carried out in compressed domain rather than in pixel domain, and no iteration was involved in the process of segmentation.

David Jeff Jackson and Sidney Joel Hannah [26] presented the *Comparative Analysis of Image Compression Techniques*. This paper addressed the area of data compression as it was applicable to image processing. Analyses of several image compression strategies were examined for their relative effectiveness. Several topics concerning image compression were examined in this study including generic data compression algorithms, file format schemes, and fractal image compression. An overview of the popular LZW compression algorithm and its subsequent variations was also given. A survey of several common image file formats was presented with respect to the differing approaches to image compression. Fractal compression was examined in depth to reveal how an interactive approach to image compression was implemented. While both the GIF and JPEG techniques were standardized, the potential for further research in the fractal compression area was great. They concluded that it was possible to take the advantage of large compression ratio achieved from fractal compression and produced trade-off of compression ratio for information loss.

Lena Chang, Ching-Min Cheng and Ting-Chung Chen [27] presented *An Adaptive KLT Algorithm For Multi-Spectral Image Compression*. The KLT (Karhunen-Loeve Transform) converted discrete signals into a sequence of uncorrelated

coefficients. The transformation was developed on the basis of statistical properties of the signal. It was also known as Hotelling transform, and it was widely used in data compression. KLT minimized the MSE for any input image, and any number of retained coefficients. In their paper authors proposed the algorithm, which was fully exploiting the spectral and spatial correlation in the data. KLT algorithm could divide the original image into some proper regions and transform each region image data set by corresponding transformation function. The algorithm was suited for hardware implementation. They claimed that more the small region size, the more efficient was the spectrally decorrelation process. But the drawback with the selection of small region size was reselecting increase in the overhead bit rate due to an increase in the number of regions. The proposed Adaptive Variable Region KLT algorithm could determine a proper region for different local terrain characteristics of image, and corresponding KLT transformation was adapted for each extracted terrain region.

Salih Burak Gokturk, Carlo Tomasi, Bernd Girod and Chris Beaulieu [28] presented *Medical Image Compression Based on Region of Interest, With Application to Colon CT Images.* They discussed a hybrid model of lossless compression in the region of interest with high rate lossy compression in other regions. In this method the image was segmented through a sequence of two dimension morphological image processing techniques. Then motion vectors were coded for each block of the image. Finally the error between the real image and the motion predicted image was coded for Region of Interest (ROI) blocks. With the experiment on CT abdomen images with the colon wall as ROI, researchers claimed that a compression rate of 2.5% could be obtained.

Jeffrey C. Wehnes, Hung-Ta Pai and Alan C. Bovik [29] presented *Fast Lossless Compression*. This paper presented a simple algorithm for fast lossless compression of gray scale images. It consisted of differential pulse code modulation followed by Huffman coding of the most likely residual magnitudes. The authors claimed that this algorithm gave higher compression with less computation than the lossless JPEG method. They further claimed that for the large dynamic ranges possible with pixel sizes greater than eight-bits, it required significantly less computation than any peer compression schemes.

Marcelo J. Wienberger, Gadiel Seroussi and Guillermo Sapiro [30] presented *The LOCO-I Lossless Image Compression Algorithm: Principles and Standardization into JPEG-LS.* Low Complexity Lossless Compression for Images (LOCO-I) was algorithm at the core of ISO/ITU standard for lossless and near lossless compression of continuous tone images, JPEG – LS. It was based on simple fixed context model, which

approaches the capability of the more complex universal techniques for capturing high order dependency. Lossless data compression scheme often consisted of two distinct and independent components modeling and coding. Modeling part could be formulated as an inductive inference problem, in which the data (image) was observed sample by sample in some predefined order. LOCO-I was systematically projecting the image modeling principles outlined and further developed into a low complexity plane both from a modeling and coding perspective.

Marcia G. Ramos and Shelia S. Hemami [31] presented *Edge Adaptive JPEG Image Compression*. The quantization was one of the important phases in the method of image compression. The quantization factor changed with step with respect to spectral distribution in an image. The quantization step sizes were adapted to the active level of the block, and the activity selection was based on edge driven quad tree decomposition of the image. It was claimed that the proposed technique achieved higher visual quality than standard JPEG compression at the same bit rate and reduced the mosquito noise in the frames. Mosquito noise was the high frequency temporal noise that appeared in the low bit rate videos. The proposed method required a very small over-head (an average of 0.0035 bpp for 512 × 512) compared to JPEG data string by coding the quad tree efficiently.

Hiroshi Kondo and Yuriko Oishi [32] presented *Digital Image Compression Using Directional Sub-Block DCT*. The proposed technique gave reconstruction image with lower block artifact (noise), even if a low bit rate coding was applied. In this technique, signs and amplitudes of DCT coefficients were processed separately. Amplitude of DCT coefficients belonging to one of the sub-block, which was predicted from those of one the former four neighbors' sub-blocks and the prediction errors were coded. The one of four neighbor sub-blocks was chosen by a minimum mean square error technique. The indications of the chosen sub-block and DCT signs were coded by an arithmetic coding. The picture quality of the reconstructed image was always better than that received by an ordinary JPEG method. The authors concluded that the proposed method came from JPEG one but the resulting coded image was always superior to the ordinary JPEG one. It meant that the correlation direction index was effective for one step vector prediction. The sequence of the index numbers was coded by an arithmetic coding method, which was well known as the best entropy coding one.

Mitchell A. Golner, Wasfy B. Mikhaei, Arun Ramaswamy and Venkatesh Krishnan [33] presented *Region Based Variable Quantization For Jpeg Image Compression*. This paper was based on region based variable quantization JPEG

software codec that was developed, tested, and compared with other image compression techniques. They proposed, the quantization matrix was global to the entire image, scaling factors was chosen on block-to-block basis to achieve varied degrees of quantization for different regions of the image. This method was implemented for DCT coefficients. The region selection could be performed manually or automatically according to predetermined requirements. The authors concluded that pattern recognition techniques could be used to identify areas containing color and geometry that meet certain criteria. They indicated that future might also focused on the development of an objective perceptual measurement that could provide effective feedback for achieving high compression and maximum overall perceptual quality.

The number of researchers pursued the research based on DCT technique in the domain of image compression. Few researchers noticed shortcomings of DCT technique. As DCT is one of the phases in JPEG compression it affects the overall compression. Although the JPEG methods are efficient, the blocking noise (artifact) appears in the resulting image. The blocking noise on an image makes the picture quality degenerate especially for our human eyes [9]. Further research work has been done on still image compression and JPEG-2000 standard is established in 1992 and work on JPEG-2000 for coding of still images had been completed at end of year 2000 [1].

The upcoming JPEG-2000 standard employs wavelet for compression due to its merits in terms of scalability, localization and energy concentration [1, 34]. It also provides the user with many options to choose to achieve further compression. A JPEG-2000 standard support decomposition of all the sub-bands at each level and is hence requires full decomposition at a certain level even though that may not be necessary.

G. F. Fahmy, J. Bhalod and S. Panchanathan [34] presented *A Joint Compression and Indexing Technique in Wavelet-Compressed Domain*. The authors proposed a new technique for joint compression and indexing in the wavelet domain. In the proposed technique, the wavelet-decomposed image was first preprocessed to extract features, which were then used for compressing the image as well as for deriving the indices. The wavelet decomposition structure is the regular dynamic tree. The low level features are extracted from the wavelet-decomposed image. Typically these features include shape, texture and color. The extracted features are used for compressing the image as well as for deriving the indices. A dominant channel profile based on the relative energy of each band is used as feature for indexing. The results

demonstrated significant coding gains using the proposed approach at a similar retrieval performance.

E. Yeung [35] presented *Image Compression Using Wavelets*. The author first introduced the theory behind the wavelet transform and overviewed the implementation of the wavelet image compression. Both quantitative and subjective evaluations were performed on images compressed with the wavelet compressor. The author concluded that wavelet compression was better choice over JPEG compression.

Sonja Grgic, Kresimir Kers, Mislav Grgic [36] presented *Image Compression Using Wavelets*. This paper provided the fundamentals of wavelet based image compression. The options for wavelet image representation were tested. The results of image quality measurements for different wavelet function, image contents, compression ratio and resolutions were given. They discussed in detail the selection of wavelet family depended on application. In image compression application the choice of wavelet selection depended on image content. They concluded that, although JPEG processing speed and compression ratio were good, there were noticeable blocking artifacts at high compression ratios. However there were no blocking effects at all in reconstructed images by wavelet-based methods. They further mentioned that the proposed simple and fast compression scheme based in Discrete Wavelet Transform (DWT) provided better results than standard JPEG especially for higher compression ratio and predicted the progress in research for years to come.

Tao Yu, Anthony Tung-Shuen Ho, Siu-Chung Tam, Siong-Chai Tan and Lian-Teck Yap [37] presented *A Novel Hybrid Bi-Orthogonal Wavelets / ADPCM Algorithm For Very Low Bit Rate Satellite Image Compression*. The paper discussed an overview of remote sensing image compression using wavelet transform. The authors first described the wavelet properties that were most important for image compression. The method of constructing by orthogonal wavelet and their finite impulse response (FIR) filter bands was presented. Then the adaptive differential pulse code modulation (ADPCM) algorithm was presented for very low bit rate satellite image compression. They discussed that ADPCM technique could achieve high compression ratio for only at low bit-rate satellite image compression. They claimed that by using wavelet transform and combination of vector quantization and ADPCM, they could achieve very low bit rate compression and blocking efforts in satellite images were also minimized. The authors concluded that by using this method high compression ratio could be achieved by maintaining high degree image quality.

Christos Chrysafis and Antonio Ortega [38] presented *Line-Based, Reduced Memory, Wavelet Image Compression*. The authors presented a complete system to perform the low memory wavelet image coding. Their approach was line based, in that the images were read line by line, and only the minimum required number of lines were kept in memory. The main contribution of their work was, firstly they introduced a line based approach for the implementation of the wavelet transform, and then they proposed a novel context based encoder which require no global information, and stored only a local set of wavelet coefficients. This low memory coder achieved performance comparable to state-of-the-art coders at a fraction of their memory utilization. They claimed that the method offered the significant advantage by making a wavelet coder attractive both in terms of speed and memory needs.

Y. Li and C. Moloney [39] presented *SAR Image Compression using wavelet Transform and Soft Thresholding Synthetic*. The authors mentioned that Synthetic Aperture Radar (SAR) Image Compression is important in image transmission and archiving. Their studies showed that the speckle noise which is inherent in SAR imaging system, is also an obstacle to image compression. In order to improve the reconstructed image quality, and to increase the compression efficiency, the wavelet domain soft-thresholding technique was implemented to reduce the speckle noise before compression was performed. The authors concluded that the proposed algorithm could remove most of the speckle noise, and improved the compression performance.

V. N. Ramaswamy, K.R. Namuduri and N. Rangnathan [40] presented *Lossless Image Compression Using Wavelet Decomposition.* The authors proposed lossless image compression scheme using wavelet decomposition. In the first scheme the approximated wavelet coefficient were encoded using variable block size segmentation algorithm, and the detail signals were encoded using directional predication and categorization. The residual error due to the finite precision arithmetic was significant, and was encoded using adaptive arithmetic encoding technique. In the second scheme authors proposed a new concept of multi-resolution, which avoided the finite precision arithmetic errors. The approximated image, in the scheme was a decimated version of the original image instead of the image being convolved with low pass filter and then decimated (along x and y direction). The performance of the proposed scheme was comparable to that exhibited by JPEG lossless schemes, and out perform the Huffman, the Lempel-Ziw, and the Arithmetic. The authors concluded that they have found that the wavelet filter should increase smoothness in the image and yet posses the perfect reconstructed property with compact support.

Julien Reichel, Gloria Menegaz, Marcus J. Nadenau, Murat Kunt [41] presented *Integer Wavelet Transform For Embedded Lossy To Lossless Image Compression.* This topic was investigated in a theoretical framework. The authors proposed a model of the degradations caused by the use of Integer Wavelet Transform (IWT) instead of the Discrete Wavelet Transform (DWT) for lossy compression. The rounding operations were modeled as additive noise. The noises were then propagated through the lifting scheme structure to measure their impact on the reconstructed pixels. This methodology was verified using simulation with random noise as input. It predicted accurately the results obtained using images compressed by the well-known algorithm like Embedded Zerotree Wavelet (EZW). Experiments were also performed to measure the difference in terms of bitrate and visual quality. The use of Mean Square Error (MSE) showed significant difference between the two approaches. The IWT could lead too much larger degradation than the DWT, especially for small quantization steps, that is small compression factor. It was noticed that IWT and DWT were equivalent for large compression ratio in both MSE and visual quality point of view.

Chrostos Chrysafis and Antonio Ortega [42] presented *Efficient Context-Based Entropy Coding For Lossy Wavelet Image Compression.* The authors presented an adaptive image-coding algorithm based on novel backward adaptive quantization/classification techniques. They used a simple uniform scalar quantizer to quantize image sub-bands. Their algorithm put each coefficient into one of the several classes depending on the values of neighboring, previously quantized coefficients. These previously quantized coefficients formed context, which were used to characterize the sub-band data. To each context type, corresponded a different probability model, and thus each sub-band coefficient was compressed with an arithmetic coder, having the appropriate model depending on that coefficient's neighborhood. They showed the context selection could be driven by rate distortion criteria, by choosing the context in a way that the total distortion by given bit rate was minimized. They concluded the potential benefits of this method compared to then existing methods with respect to speed and simplicity. Also by choosing fine enough quantization, they expected the same algorithm could be used for lossless compression.

Jiaming Li and Jesse S. Jin [43] *presented An Image Coding Method of High Compression Rate And Clarity Preserving*. The authors presented an image compression scheme based on wavelet transform and the Human Visual System (HVS) was proposed. They discussed the evaluation criteria of the image quality. It is clear that Human eyes are more sensitive to noise in low frequency than to noise in high

frequency. So they suggested that they should give smaller quantization step to low frequency WT coefficients, and bigger quantization step to high frequency WT coefficients. It would give the minimum annoying effects over the reconstructed effects for human observer. The main purpose of their research was to design a quantizer for WT coefficients, which took into account the relative importance of different coefficients to the human visual perception, and minimized noise introduced in quantization. In the proposed method, authors developed an efficient perceptual quantization method by minimizing a specially selected quantization noise function, which was perceptually weighted, based on experimental research on the special–frequency response of the human visual system. Compared with pervious human visual perception based image compression methods, the proposed method showed improved image quality for the same compression ratio.

Maria Grazia Albanesi [44] presented *Wavelets and Human Visual Perception in Image Compression.* The author described a new adaptive coding technique for still, gray level images. The proposed algorithm was based on a multi-resolution decomposition on bi-orthogonal wavelet basis, and it included different non-linear models of the human visual perception in the compression task. Quantization was adaptive, and it was based on both global and local considerations about the contrast sensitivity. The author applied a non-linear filtering F(u) to the intensity image, three expressions of F(u) were tested. F(u) = u, F(u) = log (u) and F(u) = $u^{0.33}$ and then the wavelet decomposition was applied. The author concluded that for high contrast images, introduction of the non-linear part of the Human Visual System (HVS) model improved the performance. The performance of the algorithm for high contrast image was better for the case F(u) = $u^{0.33}$, but for high compression ratio the case F(u) = log (u) performed better.

Dorota Biela-Wiraszka [45] presented *Two-Stage Approach To Image Compression Using Wavelet And Piecewise Linear Transforms.* The author presented, the new approach to image compression, using wavelet and piecewise linear wavelet transforms. For effective compression performance, an image of given class was first modeled by the compression algorithm, to generate some intermediate representation of image depending on the chosen method of compression. The attention has been concentrated on the step of modeling, where the two-stage transformation was used to generate the intermediate representation of the image. Firstly the original image was the wavelet transform to obtained a pre-intermediate representation, consisting of four sub-images, being the result of spatial low pass and high pass filter. At this stage the zonal

sampling was performed and only the low pass filtered sub-image was kept. During the second stage the pre-compressed image was transformed by using the periodic walsh Piecewise Linear Transform (PWL). It produced the PWL spectrum of the former representation, then compressed by the threshold compression scheme and the final intermediate representation of the image was obtained. Reconstruction of the original image required similar two-stage decompression processed, first the inverse PWL transform was calculated and then the intermediate reconstruction was transformed by the inverse wavelet transform. This technique provides a better compression ratio but high frequency components are lost.

A. P. Beegan, L. R. Iyer, A. E. Bell, V. R. Maher, and M. A. Ross [46] presented *Design And Evaluation Of Perceptual Masks For Wavelet Image Compression*. The authors presented, a new HVS technique in the form of perceptual weighting masks derived from the luminance contrast sensitivity function and illustrates their performance for gray scale, and color images using bi-orthogonal wavelet transforms. In this paper, authors described, and evaluated four new methods for generating perceptual weighting mask using Constant Sensitivity Function (CSF), and its Discrete Wavelet Transform (DWT). The masks were based on the luminance and not on the thresholds. They suggested that peak Constant Sensitivity Function (CSF) mask with six unique weights (1, 4.6, 6.54, 6.54, 5.22, 2.20). They further developed a subjective image quality testing procedure for expert and non-expert observers; a comparison of qualitative and quantitative result was presented. They claimed that their algorithm improved both peak signal to noise ratio and subjective quality for color images, and grayscale images. A model of the contrast sensitivity function for luminance images originally proposed by Mannos and Sakrison is given by

$$H(f) = 2.6\,(0.00192 + 0.114f)\,.\,e^{\,[-(\,0.114f)^{1.1}\,]} \qquad \text{--- 2.9.1}$$

Where spatial frequency $f = (f_x^2 \times f_y^2)^{1/2}$

The proposed method when used on gray scale images resulted in decrease in PSNR, however it increased in PSNR for color images.

Olivier Rioul [47] presented *On The Choice of Wavelet Filters For Still Image Compression.* The author presented simple compression scheme using orthogonal separable wavelet transforms, scalar quantization, rate/distortion optimization, various coding criteria, and large number of wavelet filters with balanced regularity, frequency selectivity and phase. The paper investigated the usefulness of several filter properties in a simple image compression scheme using DWT implemented as an octave band tree

filter bank allowing perfect reconstruction. In order to provide a fare comparison of compression result for different filters, author used an optimization procedure based on wavelet packets, which selected the best set of quantizer for each sub image and the based number decomposition levels, which minimized the overall distortion at the reconstruction.

S. Phimoltares, K. Chamnongthai and C. Lursinsap [48] presented *Hybrid Binary Image Compression*. The authors proposed new lossless binary image compression-processing scheme, which increased local redundancy for more compression efficiency. The algorithm consisted of reordering rows and columns of image data for assembling data that has some values 0 or 1, merging the data to reduce the redundancy, encoding data to bit stream, then the encoded data would be compressed by other image compression algorithms. They claimed that, this hybrid algorithm produced smaller compressed images than other algorithms by compromising the execution time. The extra time overhead was due to the reordering process.

Amir Averbuch, Danny Lazar, Moshe Israen [49] presented *Image Compression Using Wavelet Transform And Multi-resolution Decomposition*. The authors presented the compression method, which was based on Vector Quantization (VQ) applied on the wavelet coefficients resulting from the wavelet transform of the trend images, using the pyramidal multi-resolution architectures. Vector quantization uses a dictionary (code book) of pixel patterns. The wavelet coefficients were partitioned into small pixel block and each block was encoded as reference to the dictionary pattern, which most resembled the block. The authors used vector quantization using the LGB algorithm. They claimed that the compression using vector bit allocation yielded the high compression ratio and good PSNR.

Surya Peramraju, Sunanda Mitra [50] presented *Efficient Image Coding Using Multiresolution Wavelet Transform And Vector Quantization.* The authors presented the compression method, which was based on adaptive Vector Quantization (VQ) applied on the wavelet coefficients resulting from the wavelet transform of the trend images, using the pyramidal multi-resolution architectures. The adaptive vector quantization algorithm proposed used wavelet decomposition as a preprocessing stage for quantization as this mapping put the image in the form of a smooth image, which was much smaller in size than the original image, and several error sub-images that could be represented by lesser number of bits. The adaptive vector algorithm used a neuro-fuzzy clustering technique for optimizing the distortion measure. The fuzzy approach formed

the basis for accurately optimizing each code vector. They claimed that adaptive vector quantization algorithm outperformed LGB vector quantization.

Mohamad A. El-Sharkawy, Christian A. White, Harry Gundrum [51] presented *Sub-band Image Compression Using Wavelet Transform And Vector Quantization.* The authors proposed an algorithm, which incorporated a fast tree structure quantization scheme, and partial search vector quantization. The algorithm described in this paper was that a novel quantization thresholding scheme, which used the DWT to decompose an image into octave wide frequency bands, then quantized the coefficients using a "look ahead" measurement of the image based on the low frequency sub-image inherent in the DWT. This algorithm then used vector quantization to code the thresholded coefficient of the decomposed image. Using sorted table of the energy content of the code vector used the partial search vector quantization algorithm to increase the speed of the quantization. The authors claimed that the results obtained by implementing this algorithm were comparable to the results obtained by those in literature using sub-band coding.

Olga Kosheleva, Vladik Kreinovich, and Hung T. Nguyen [52] presented *On the Optimal Choice of Quality Metric In Image Compression*. The authors presented, the metrics describing the distance between the two images; original image and compressed image, was known as quality metrics. They discussed the general class of quality metrics and selection of best value of the parameter p, depending on the image. The authors suggested that the value of this suggested quality metrics for the compression method should be as small as possible. In this paper they showed that under certain reasonable symmetry conditions, L^p metrics $d(I,\tilde{I}) = \int \left| I(x) - \tilde{I}(x) \right|^p dx$ were the best, and that the optimal value of p could be selected depending on the expected, related size r of the informative part of the image. They claimed that the natural way to select an optimal scheme was to select the scheme for which the average value of the quality metrics should be the smallest possible one.

Armando J. Pinho [53] *On The Impact of Histogram Sparseness on Some Lossless Image Compression Techniques.* The author presented, the problem of degradation of the compression performance that was verified in state-of-the-are lossless compression technique, such as JPEG-LS, and JPEG-2000, when handling images having spars histograms. He presented result, showing that histogram packing could provide important improvement in compression ratios. Finally he proposed a

simple procedure for online histogram packing, which held nearly the same improvement as offline histogram packing.

Armando J. Pinho, and Antonio J. R. Nevws [54] presented *Improvement Of The Lossless Compression Of Images With Quasi-Sparse Histograms.* The authors first addressed the problem with offline histogram packing. In offline histogram packing, even if most of the intensity values occurred only ones or just a few number of times in the image, they would be considered by the offline histogram packing technique as having equal importance as those that occurred most frequently. In other words, images having quasi-spars histograms could not benefit from this method. The proposed method was also offline, but work using a reduced set of symbols. The authors claimed that the proposed method provided globally better method than the normal offline packing.

Paulo J. S. G. Ferreira and Armando J. Pinho [55] presented *Histogram Packing, Total Variation And Lossless Image Compression*. The authors presented, the preprocessing technique for image compression. The state-of-the-art lossless image compression methods, such as JPEG–LS, and lossless JPEG-2000 performed considerably better on images with spars histogram, when preprocessing technique was used. In this paper authors addressed the preprocessing issue, and attempted to explain how, the preprocessing stage, which basically packed the histogram of the images, affected the image's total variation, and as a result the ability of the compression algorithms to work more efficiently. The graphical textual images do not use the complete set of available intensities (of color tones of gray) that is the histogram of the intensities is sparse. For such image this preprocessing technique was proposed. In this technique before coding, the image was subjected to transformation T, which packs its histograms. To recover the original image, the inverse transformation T^{-1} was applied to the decoded image. The packing transformation reduces the total variation of the image, yielding an image of smaller total variation, easier to compress.

Jinwen Tian, Su Kang, Jian Liu and Qian Gao [56] presented *A novel Image Compression Encoding*. The authors presented the new adaptive image compression method based on wavelet transform, bit image compression, fractal iteration, and Huffman code. And suggested a novel technique of image compression, which included bit image compression, wavelet transform, fractal iteration and Huffman code. In the first stage, segmentation of the original image to bit image was carried out, different bit image in different bit digit was obtained, then the entropy of each bit image was calculated, and it was determined whether to compress the bit image by some criterion,

after that the image of bit compression was preserved. In the second stage, wavelet transform was applied. In next stage fractal was used, and lastly Huffman coding was used for coding. The authors claimed that the proposed method was better than the bitmap wavelet and fractal image compression methods.

Miroslav Galabow [57] presented *Fractal Image Compression*. The author presented the new technique of image compression using fractal. A fractal is a structure that is made up of similar forms and pattern, which occur in many different sizes. Fractal encoding is a mathematical process used to encode the bitmaps containing a real world images as a set of mathematical data. The fractal encoding is largely used to convert bitmap images to fractal codes. Fractal decoding is just the reverse in which a set of fractal codes is converted to a bitmap. The encoding process is extremely computational intensive, millions or billions of iterations are required to find the fractal patterns in an image, but decoding a fractal image is a much simpler process. This has the ability to scale any fractal image up/down in size without the introduction of the image artifacts, or a loss in details, that occurs in bitmap images. Images with high fractal content, result in much higher compression ratio than images with low fractal content. Because of the variation in time of encoding and decoding the image, fractal compression technique is suited and only used in image databases and CD-ROM applications.

I. Andreopoulos, Y.A. Karayiannis and T. Stouraitis [58] presented *A Hybrid Image Compression Algorithm Based on Fractal Coding and Wavelet Transform*. The authors presented, a novel algorithm for very high compression of images. First of all the image was decomposed through a wavelet transform. Then the low frequency part of the decomposed image was coded by using a near lossless method, while the rest of image was coded by using a fractal coding techniques. In addition, two classification methods were applied sequentially: geometric classification and luminance classifications. The authors claimed that this fast novel algorithm achieved good image compression quality at very high compression ratios. At these levels of compression it outperformed the JPEG standard.

Geoffrey M. Davis [59] presented *A Wavelet-Based Analysis of Fractal Image Compression.* The author presented the new wavelet based framework for analyzing block based fractal compression scheme. Within this framework authors were able to draw upon insides from the well established, transform coder paradigm in order to address the issue of “why fractal coders work?” The author examined the generalization of the scheme to smooth wavelets with additional vanishing moments. This framework

gave new insight into the conversions properties of fractal block coders, and led them to develop an unconditionally convergent scheme with the fast decoding algorithm. The algorithm with fractal block coders had drawbacks, that the coders possessed no control over the code book, code words are too densely clustered around the very common all zero sub-tree and too sparsely distributed elsewhere, this dense clustering of near zero trees increased code word cost, but contributed very little to image fidelity. The main advantage enjoyed by using this algorithm was the ability to efficiently represent the zero trees.

Vania Cordeiro Da Silva and Joao Marques De Carvalho [60] presented *Image Compression Via TRITREE Decomposition*. The authors presented the new method of image compression, using TRI-TREE decomposition (TT). TT decomposition was similar to the Quadtree Decomposition (QT), which had been broadly used by image processing algorithms, mainly for segmentation and compression. However, while QT subdivided the image into progressively smaller quadratic regions, TT decomposition subdivided the image in triangular region. The goal was to segment the image into a set of triangular homogeneous regions, where the differences among the pixel values didn't exceed the certain threshold. A tree was built to represent the decomposition. Each triangle would be the node of the tree TT. The initial triangle, that contained the whole image, was the root of the tree. The final triangle represented in the compressed image, where the leaves of the tree. Reconstruction of the image was accomplished by planer interpolation among the vertices of each triangle leaf. The authors claimed that the TT could produce higher PSNR and compression rate in comparison with QT.

Axel Van De Walle [61] presented *Merging Fractal Image Compression And Wavelet Transform Methods.* The author presented, the method with the advantage of the approach, was to significantly reduce the tiling artifacts: operating in wavelet space allowed range blocks to overlap without introducing redundant coding. Fractal image compression and wavelet transform methods could be combined into a single compression scheme by using an iterated function system, to generate the wavelet coefficient. The scheme also permitted reconstruction in a finite numbers of iterations, and let to relax conversion criteria. The author concluded by mentioning the properties of new developed scheme such as: tiling effect was overcome; reconstruction was achieved in a finite number of steps; efficient indices of the domain blocks could be easily computed from the low frequency wavelet coefficients; it simply reduced to conventional fractal compression.

Sunanda Mitra, Rodney Long, Surya Pemmaraju, Richard Muyshondt, and George Thoma [62] presented *Color Image Coding Using Wavelet Pyramid Codes*. The authors presented the suitability and requirement of further development of wavelet pyramid coding in compressing color images, specifically the color visible human digital photographic data set. The distinct advantages of the newly developed adaptive Vector Quantization (VQ) over commonly used scalar quantization, and conventional VQ of the wavelet-decomposed error pyramids were also discussed. The paper demonstrated the feasibility of applying wavelet pyramid coding using adaptive vector quantization for visible human color data set, and thus showed the possibility of the compression, and other large color data set such as satellite images for easy and cost effective storage and transmission.

Armando Manduca, and Amir Said [63] presented *Wavelet Compression Of Medical Images With Set Portioning In Hierarchical Trees.* The authors presented, a novel scheme for encoding wavelet coefficients, termed Set Partitioning In Hierarchical Trees (SPIHT). The SPIHT technique is also based on a wavelet transform, and differs from conventional wavelet compression only in how it encodes the wavelet coefficients. SPIHT is based on the three principles i) exploitation of hierarchical structure of the wavelet transforms by using a tree-based organization of the coefficient ii) partial ordering of the transformed coefficients by magnitude and iii) ordered bit plane transmission of refinements bits for the coefficients values. The SPIHT algorithm maintains the lists of insignificant sets, insignificant pixel, and significant pixel, and is initialized with list of insignificant sets being the sets of the sub-tree descendant of the each such node. In a sorting pass, the algorithm works its way down the list of insignificant pixels first, testing their magnitude against the current threshold, outputting their significance, and when one is significant, outputting its sign and moving it to the list of significant pixels. Then it moves through the list of insignificant list of the sets, performing the magnitude test to all the coefficients in the current sets. This algorithm SPIHT can be used with any wavelet on sub-band transform. The authors claimed that the result of proposed algorithm was of highest quality and the differences were quite significant compared to JPEG, and standard wavelets.

Fredrick W. Wheeler, and William A. Pearlman [64] presented *Low-Memory Packetized SPHIT Image Compression.* The authors presented the SPIHT image compression algorithm with modification for applications to the large images with limited processor memory. The sub-band decomposition coefficients were partitioned into a small tree-preserving spatial block, which were each independently coded using

the SPIHT algorithm. The bits streams for each spatial block were assembled into a single final bit stream through the packetization scheme. The authors concluded that the SPIHT encoding and decoding of the special blocks could be done parallel for real time video compression saving the resources.

Jerome M. Shapiro [65] presented *Embedded Image Coding Using Zerotrees of wavelet Coefficients.* The author presented embedded Zerotree Wavelet Algorithm (EZW) as a simple, yet remarkably effective, having the property that the bits in the bit stream were generated in the order of importance, yielding a fully embedded code. The embedded code presented a sequence of binary decisions that distinguish an image from the null image. Using an embedded coding algorithm, an encoder could terminate the encoding at any point their by alloying the target arte or target distortion metric to be made exactly. Also, given a bit stream, the decoder could cease a decoding at any point in the bit stream and still produced exactly the same image that would have been encoded at the bit rate corresponding to the truncated bit stream. The EZW algorithm was based on four key concepts: i) a discrete wavelet transform or hierarchical sub-band decomposition ii) prediction of the absence of significant information across scales by exploiting the self-similarity inherent in images, iii) entropy coded successesive approximation quantization, and iv) universal lossless data compression, which was achieved via adaptive arithmetic coding. The zerotree data structure works on the following principle.

A wavelet coefficient x is said to be insignificant with respect to a given threshold T, if $|x| < T$. The zerotree is based on hypothesis that, if a wavelet coefficient at a coarse scale is insignificant with respect to a given threshold T, then all wavelet coefficient of the same orientation in the same spatial location at finer scales are likely to be insignificant with respect to T. Empirical evidence suggests that this hypothesis is often true. The authors claimed that the compression performance of this algorithm was competitive with virtually all known techniques. The precise rate control that was achieved with this algorithm was a distinct advantage.

Jayshree Karlekar, P. G. Poonacha, and U. B. Desai [66] presented *Image Compression Using Zerotree and Multistage Vector Quantization.* The authors presented, new algorithm that provided good quality of reconstructed images at very low bit rates. The algorithm used successive approximations quantization of both scalars, and vectors on wavelet coefficients of the image. The successive-approximation quantization of scalars and vectors was done using EZW and MSVQ algorithms respectively. EZW algorithm was applied to wavelet coefficients belonging to coarser

level sub-bands, and MSVQ was applied to vectors of wavelet coefficients belonging to finer level sub-bands. The proposed method further used static Huffman coding to achieve more compression. The basic idea of multistage vector quantization (MSVQ) was to divide the encoding task into successive stages, where the first stage performed relatively crude quantization of the input vector using a small codebook. Then, a second stage quantizer operated on the error vector between the original, and quantized first stage output. The quantized error vector thereby provided a second approximation to the input original vector hence leading to the more accurate representation of the input vector. A third stage quantizer might then be used to quantize the second stage error vector to provide further refinement. The authors observed that, the penalty they were paying for using MSVQ was that of a marginally reduced PSNR for the encoded image at the cost of reduced complexity and memory requirements of MSVQ.

David Taubman [67] presented *High Performance Scalable Image Compression With EBCOT*. The author presented, a new image compression algorithm based on independent Embedded Block Coding With Optimized Truncation of the embedded bit stream (EBCOT). The algorithm exhibited the state-of-the-art compression performance while producing a bit stream with a rich set of features, including resolution, and SNR scalability together with a "random access" property. The algorithm had modest complexity, and was suitable for applications involving remote browsing of large compressed images. The algorithm lended, itself to explicit application with respect to MSE as well as more realistic psycho-visual metrics capable of modeling the spatially varying visual masking phenomenon.

Jon K. Rogers and Pamela C. Cosman [68] presented T*he Wavelet ZeroTree Image Compression With Packetization*. The authors presented, an algorithm that was a combined wavelet zerotree coding, and packetization method that provided excellent image compression and graceful degradation against packet eraser. The wavelet zerotree compression and packetization method described in this paper was resilient to packet erasures without the use of forward error correction or retransmission protocols. The authors used four levels of wavelet decomposition, and each head coefficient in the low-low band had three children. For 512 × 512 image, there were 1024 head coefficients in the low-low band, each had 2 × (1 + 4 + 16 + 64) = 255 descendents in its tree. If one of the trees were lost then lost coefficients were obtained by interpolation with its neighbours. Four bits of header defined, how many trees were fit in a packet. The authors claimed that PZW was more suitable for the case of burst errors and packet

erasures. In conjunction with Forward Error Correction (FEC), PZW might prove to be robust against high levels of both random noise and burst errors.

Jon K. Rogers, and Pamela C. Cosman [69] presented *Robust Wavelet Zerotree Image Compression With Fixed-Length Packetization.* The authors presented, a novel robust image compression algorithm, in which the output of a wavelet zerotree-style coder was manipulated into fixed length segments. The segments were independently decodable, and errors occurring in one segment did not propagate into any other segments. The method provided both excellent compression performance and graceful degradation under increasing packet losses. The authors extended the basic scheme to perform the region-based compression, in which specified portion of the image were coded to higher quality with little or no side information required by the decoder. This algorithm might be useful for channels with long round trip delays, or for real time interactive system.

Zixiang Xiong, Kannan Ramchandran, and Michael T. Orchard [70] presented *Joint Optimization of Scalar And Tree-Structured Quantization of Wavelet Image Decomposition.* The authors proposed an image compression algorithm based on optimal bit rate allocation between scalar and tree structure quantizers, a predictive approach to representing the pruned tree structure was presented, and the entropy of this representation was included in the optimal allocation problem. The algorithm coupled Lagrangian optimization of the scalar quantizers with a marginal analysis approach for optimizing the tree structure, and achieved excellent coding efficiency in the rate-distortion sense. The algorithm was constituted by four major steps i) zero tree pruning algorithm ii) predicting the tree iii) optimizing the scalar quantizers and iv) joint optimization of the scalar and the tree structure quantizers. The authors claimed that the proposed algorithm offered substantially improved signal to noise ratio at matching bit rates, compared with similarly structured compression algorithms.

Marcus J. Nadcnau, Julien Reichel, and Murat Kunt [71] presented *Wavelet-Based Color Images Compression: Exploiting The Contrast Sensitivity Function*. The authors presented, the algorithm focused on the implementation of the masking phenomenon that was parameterized by the Contrast Sensitivity Function (CSF), into a codec. The discussion concerned codecs based on Discrete Wavelet Transformation (DWT), chosen for its similarity to the Human Visual System (HVS). The best compression performance was typically achieved in color spaces that were composed of one luminance, and two chrominance channels. Using this concept, a specific opponent color space based on a linear transformation with optimal color-pattern-separability

properties were developed and corresponding CFS's measured. This separability was valid not strictly, but in approximate manner. However, experiment had shown that for compression proposes the property to de-correlate the color channels was more important than the color pattern separability. Therefore compression in a color space like YcrCb was still preferable.

Lakshmi R. Iyer, and Amy E. Bell [72] presented *Improving Image Compression Performance With Balanced Multiwavelets.* The authors analyzed the effect of many multiwavelets properties on image compression. The properties like shift variance, and magnitude response influence PSNR, and perceived image quality. The multiwavelets transform unlike the scalar wavelet transform allows orthogonality and symmetry to co-exists. Multiwavelets are very similar to wavelets, but have some important differences. In particular, where as wavelets have an associated scaling function, and wavelet function, multiwavelets have two or more scaling, and wavelet function. The authors concluded that balancing order was essential for good compression performance, but balancing did not automatically ensure good performance. The analysis indicate that shift invariance, and desirable magnitude response characteristic where also significant determinants of image compression performance.

S. Rout and A. E. Bell [73] presented *Color Image Compression: Multiwavelets Vs. Scalar Wavelets.* The authors presented, the property, perfect reconstruction (PR) used for explaining the performance differences. This paper compared the compression performance of three scalar wavelets and five balanced multiwavelets on seven color images. The authors observed that SA_4 depicted the best performance amongst the multiwavelets in terms of both subjective quality, and peak signal to noise ratio; and only the SA_4 balanced multiwavelets satisfied the perfect reconstruction conditions. The errors for four remaining balanced multiwavelets were significant. The authors also claimed that there was 0.01 – 0.47 dB performance gap between the best scalar wavelets and the best-balanced multiwavelets. For most of the images with same compression ratio, the signal to noise ratio was more for scalar wavelets than multiwavelets.

Deepti Gupta, and Shital Mutha [74] presented *Image Compression Using Wavelet Packets.* The authors presented, new wavelet packets algorithms for image compression. Despite of wavelet transform's general success, the wavelet transform often fails to accurately capture high frequency information, especially at lower bit rate, where such information is lost in quantization noise. A technique has been developed called wavelet packets that is better able to represent high frequency information. Wavelet packets are the conventional wavelet transforms in which the details are

iteratively filtered. A multilevel wavelet filter bank involves iterating the low-pass and high-pass filtering, and down sampling procedure on the output of low-pass branch, and high-pass branch of previous stage to form full tree decomposition. The authors concluded that, their techniques exhibited performance equal to, or in several cases superior to, the current wavelet filter.

A. Majid Awam, Nasir M. Rajpoot, and S. Afaq Husain [75] presented *Stack-Run Adaptive Wavelet Image Compression.* The authors presented, the compression method on the development of an adaptive image coder based on stack-run image representation of the quntaized coefficients. The results from various image-coding methods based on wavelet packets showed that they were particularly good in coding images with oscillatory pattern. There had been much less research on wavelet packet image. The authors presented an adaptive wavelet transform based image coder, which employ a stack run representation for quantized transforms coefficients in order to benefit from the infra sub-band redundancies. They discussed on the adaptive wavelet packet basis scheme best wavelet packet quantization with optimal scalar quantization and representation of the quantized coefficients with stack-run coding. The authors claimed that their coder was relatively simple and did not need to maintain any list of coefficients, as is the case with EZW, and SPIHT. For future development they suggested the development of the cost function for selection of best wavelet packet tree.

Francois G. Meyar, Amir Averbuch, Jan-Olvo Stromberg, and Ronald R. Coifman [76] presented *Fast Wavelet Packet Image Compression*. The authors presented, a new fast wavelet packet compression algorithm, which encoded very efficiently textured images. This fast wavelet packet compression technique relied on four stages: i) Fast convolution and decimation of the image with factorized non-separable very fast filters. ii) Selection of a best basis in the large wavelet packet library by using the cost function. The cost function was first order entropy for each node. It was also refereed as Threshold Entropy. The authors discussed the best basis algorithm, on the basis of cost function, best basis were selected and cost was calculated on the basis of threshold, scanning of the world packet coefficient by increased the frequency for encoding. iii) Scanning of the wavelet packet coefficients by increasing the frequency. This organization resulted in sequences of coefficients with rapid decay. iv) successive approximation quantization and entropy coding of the coefficients. This quantization technique encoded the coefficients according to their significance, and generated long sequence of zeros. This method achieved very good quality image compression even at low bit rate. The authors claimed that, the results achieved by this

method were better than those achieved by standard techniques such as JPEG or wavelet coders.

Francois G. Meyer, Jan-Olvo Stromberg, and Amir Z. Averbuch [77] presented *Fast Adaptive Wavelet Packet Image Compression*. The authors discussed that wavelets were ill suited to represent oscillatory patterns: rapid variation of intensity could only be described by the small scale wavelet coefficients, which were often quantized to zero, even at high bit rate, therefore wavelet packet was used for image compression. The authors presented an algorithm, in order to demonstrate that the advantage could be gained by constructing a basis adapted to a target image. Emphasis in this paper had been placed on developing algorithms that were computationally efficient. The authors developed a new fast two-dimensional (2D) convolution decimation algorithm with factorized non-separable two-dimensional filters. The algorithm was four times faster than standard convolution decimation. An extensive evaluation of the algorithm was on a large class of textured image. The authors claimed that the algorithm had an ability to reproduced textures so well, the wavelet packet coder significantly outperformed one of the best wavelet coder on images such as Barbara, and Fingerprints, both visually and in terms of PSNR. The authors concluded that when coding images that contain a mixture of smooth texture features, the best basis algorithm was always trying to find a compromise between the conflicting goals.

G. Hong, G. Hall, and T. J. Terrell [78] presented *Joint Entropy And Multiband Prediction For Lossless Compression.* The authors explained that correlation redundancy was first exploited within each band of the multi-band image. The new stage exploiting inter-band redundancy was then introduced. The final stage was the reduction of statistical redundancy. Inter-band redundancy had previously attracted little research interest. In this paper, the authors had quantitatively analyzed this form of redundancy, and two schemes had been developed to exploit it. During inter-band redundancy reduction phase joint entropy coding had been carried out. The joint entropy was calculated by using a cost function, which depended on log calculations. It was also referred as log entropy. The authors claimed that the results had shown an average compression ratio of 2.80 bits/pixels was achieved, which was about 35% of the original eight bit/pixels. The results had shown that the inter-band correlation among different spectral bands could be exploited, achieving about 5 – 10% better compression than was achieved by compression then individually.

Andreas Uhl [79] presented *Wavelet Packed Best Basis Selection on Moderate Parallel MIMD Architectures*. The author introduced a sub-band based parallelization,

which over comes most of the difficulties of a straightforward parallel version of the sequential algorithm. Beside the higher efficiency algorithm was easier to implement. The author further discussed the best basis selection based on Shannon entropy. The experimental result showed higher speedup compared to traditional block based parallel implementation of the sequential algorithm. The author claimed that the sub-band parallelization is much easier to implement due to less communication, and synchronization demand.

Michel B. Martin, and Amy E. Bell [80] presented *New Image Compression Techniques Using Multiwavelets And Multi-wavelet Packets.* The authors presented, new multi-wavelet transform and quantization methods, and introduced multi-wavelet packets. The authors discussed shuffling of coefficients in each 2 × 2 block. The computational complexity for multi-wavelet packets was higher than for wavelet packets and benefit of shuffling was not realized for image with more high frequency content. The authors claimed that SA_4 and ORT_4 multiwavelets tend to perform best on synthetic images and bi-orthogonal scalar wavelets performed best on smooth images. Further they discussed the comparative study with results, and claimed that the multi-wavelet packets typically gave the best results for the synthetic images while wavelet packets gave the best results for the natural images.

2.10.0 LIMITATIONS OF CURRENT TECHNIQUES

The well-known JPEG standard was established for image compression. It supports gray as well as colored image. There are various allied techniques available for JPEG standard. Discrete Cosine Transform (DCT) is one of the important phases in the image compression process for JPEG standard. In DCT the compression process is confined to the block of pixels of size M × M, where M = 8 is accepted for image compression by most of the JPEG based methods [2, 32]. In the process of image compression the JPEG standard firstly the two dimensional image is divided into square blocks, DCT is carried out, quantization takes place, and the quantized information is encoded. During the reconstruction process, the reverse operations are carried out. This division of the image into the blocks, and reconstruction later causes the errors introduced, known as blocking artifacts [9].

The new transform, discrete wavelet transform (DWT) was invented in 1996. The image compression techniques developed later used DWT as one of the important phase. Then the new standard for the image compression, JPEG-2000 was established in 2000. As no subdivision of the image is carried out in the compression processed based

on DWT, no blocking artifacts are generated or observed in reconstructed image. The wavelet transforms in JPEG-2000 are no longer limited to fixed-size blocks. Although JPEG-2000 supports optional tiles (but for a different purpose-handling very large images), they're rarely used, as they too cause noticeable blocking artifacts [9].

As human eyes are not as sensitive to color as to brightness, much of the detailed color (chrominance) information is disposed, while luminance is retained. This process is called chroma sub-sampling, and it means that a color image is split into a brightness image and two color images. The brightness (luma) image is stored at the original resolution, whereas the two color (chroma) images are stored at a lower resolution. The compressed images look slightly washed-out, with less brilliant color. This problem appears to be worse in JPEG than in JPEG-2000 [9].

Both JPEG-2000 and JPEG operate in spectral domain, trying to represent the image as a sum of smooth oscillating waves. Spectral domain is appropriate for capturing relatively smooth color gradients, but not particularly appropriate for capturing edges. So, instead of capturing an edge as such, both methods attempt to fit a wave function to it. The main effects are the distributing short vertical and horizontal ridges in the image, and it is known as ringing artifacts. Baseline JPEG suffers from a similar problem, worsened by serious blocking artifacts. [9]

Blurring means that the image is smoother than that of the original image. Note that JPEG-2000 has many problems with such artifacts. Although the shape information is correctly retained, the texture is lost. In such cases, JPEG-2000 does not function well, it is perhaps worse than JPEG. People are quite good at spotting smoothness in the image [9], and this effect is known as blurring artifacts.

2.11.0 OVERVIEW OF LITERATURE SURVEY

A number of methods have been presented over the years for performing image compression. The Discrete Cosine Transform (DCT) developed by Ahmed, Natrajan and Rao in 1974 is one of the transforms used in image compression application, JPEG. There are three DCT-based standards those are widely used and accepted worldwide: JPEG (Joint Photographic Expert Group), H.261 (Video codes for audiovisual Group) and MPEG (Motion Picture Expert Group). Each of these standards is well suited for particular applications: JPEG is for still image compression, H.261 is for video conferencing, and MPEG is for high-quality, multimedia systems [3]. The International Standard Organization (ISO) has proposed the JPEG standard [14] for image compression. The JPEG standard includes four distinct modes of operation: lossless,

sequential, progressive, and hierarchical. Lossless JPEG uses predictive compression scheme and other method uses DCT. JPEG's baseline sequential scheme is a combination of the Discrete Cosine Transform (DCT), reduced precision of the DCT coefficients (quantization), run-length encoding and Huffman or arithmetic encoding [26, 57, 71].

Although the JPEG methods are the efficient, the block noise (artifact) appears in the resulting image. The block noise in an image makes the picture quality poor especially for human eyes [9]. Further research work has been done on still image compression and JPEG-2000 standard is established in 1992 and work on JPEG-2000 for coding of still images had been completed at end of year 2000. The upcoming JPEG-2000 standard employs wavelet for compression due to its merits in terms of scalability, localization and energy concentration [6, 7]. It also provides the user with many options to choose for achieving further compression. JPEG-2000 standard supports decomposition of all the sub-bands at each level and hence requires full decomposition at a certain level.

A wide variety of wavelet-based image compression schemes have been represented in literature ranging from simple entropy coding [KLT] [27] to more complex techniques such as vector quantization, adaptive transform, tree encoding, multi-wavelet, multi wavelet packet [74, 78, 79], and edge based coding [31]. Wavelets however are ill suited to represent oscillatory patterns or the wavelet transform, often fails to accurately capture high frequency information [38, 76, 78, 80]. Therefore, the JPEG-2000 is suffering bluring effects [9]. The current literature presents the Image Compression using wavelet packet tree and multi wavelet. In a wavelet packet area the little work has reported as far as Image Compression is concerned. It is observed that there is a scope to develop the efficient techniques of Image Compression using wavelet packet tree and also a necessity to develop such an efficient technique in multimedia.

CHAPTER 3
WAVELET AND WAVELET PACKETS TREE

3.1.0 INTRODUCTION

The information is represented by the signal. This signal representation may be uni-dimensional or multidimensional. For example audio information is represented by single dimensional signal and image information is represented by two-dimensional signal. Signal can be represented in time domain or in frequency domain. Different mathematical tools are available to convert the signal from time domain to frequency domain and vice versa. Various operations are carried out over the signal, such that, the signal information becomes appropriate for the particular application. Signal processing is based on transforming a signal in the manner that it is more useful to the application. For example, it is easy to measure the time (period) of a signal in time domain representation, but it is difficult to find frequency of a complex signal. It is easy to measure the frequency of a signal in frequency domain representation but it is difficult to find time of a signal. The wavelet transform is one of the transforms used for signal transformation. This chapter includes the detail discussion on wavelet and wavelet packets tree.

3.2.0 SIGNAL REPRESENTATION AND TRANSFORMS

The common representations for one-dimensional signal are: the temporal representation (i.e. the time signal) and spectral representation (frequency signal). Unfortunately, these two representations are orthogonal to each other, the meaning, that it is not easy to extract the frequency information from the time signal and the time information from frequency signal [81]. For this reason, the top two representations in figure 3.2.1 belong to opposite corners of the time resolution time plane, as the high accuracy in one domain is traded-off for a complete uncertainty in the other. Few signal representations are available in which this trade-off is not so extreme. The different choices of the time-frequency resolution will result in a different signal representation. The choice of the proper signal processing technique is based on the signal that needs to be analyzed.

The Short-Time Fourier Transform (STFT), and the Continuous Wavelet Transform (CWT) are used to represent a signal with finite resolution in time as well as in frequency domains. By adding the constraints to transformation used, the new Discrete Wavelet

Transform (DWT) or the Wavelet Series Sub-band Transforms are developed. This will result in more compact representations of the signals suited to a specific application, at the cost of reduced versatility [81]. The key principles used to move from one representation to another are shown in figure3.2.1.

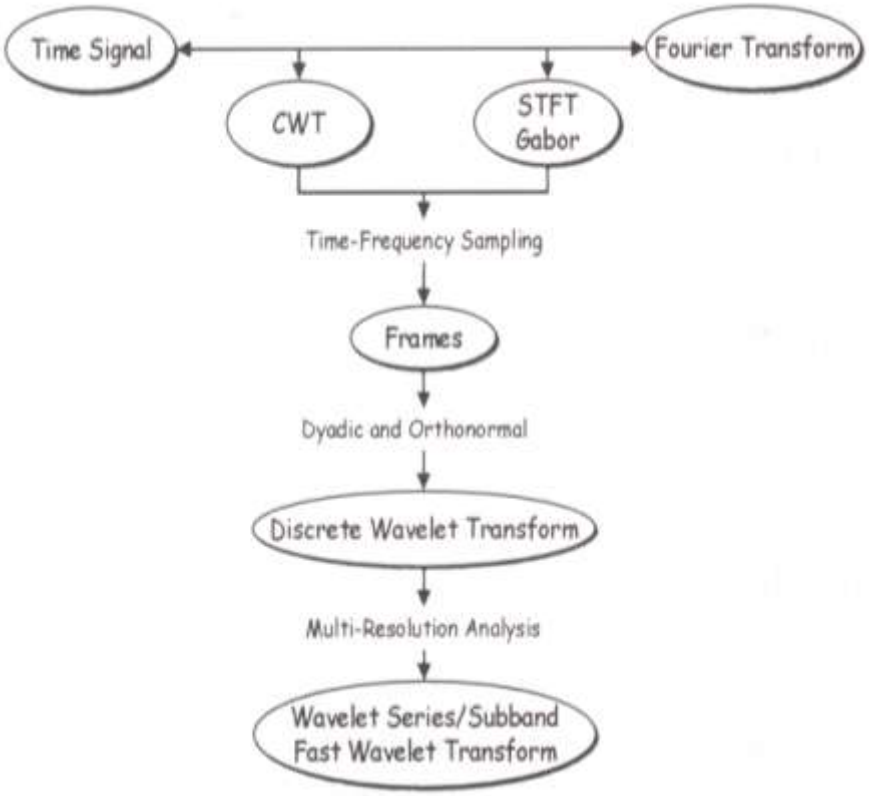

Figure 3.2.1. Signal processing tree representing the different techniques

By introducing the concept of time-frequency sampling, the concept of frames are introduced, whereas using the concept of orthogonal transformation, discrete wavelet transform and ultimately the fast wavelet transform are introduced. This evolution in a concept of wavelet transform from the continuous domain to the Dyadic Multi-resolution and fast transformation can be compared to different layers of onion [81] as shown in figure 3.2.2.

The Continuous Wavelet Transform (CWT) can be considered the most generalized representation of the wavelet transform. The price to pay is the high redundancy of the transform. By using the sampling theorem in time and frequency, one can reduce the redundancy by using frames, which form a subset of the CWT. The inner layers of the onion correspond to more strictly defined, and less general transformations that have

stronger constraints on the basis functions that can be used, but also less redundancy in their output.

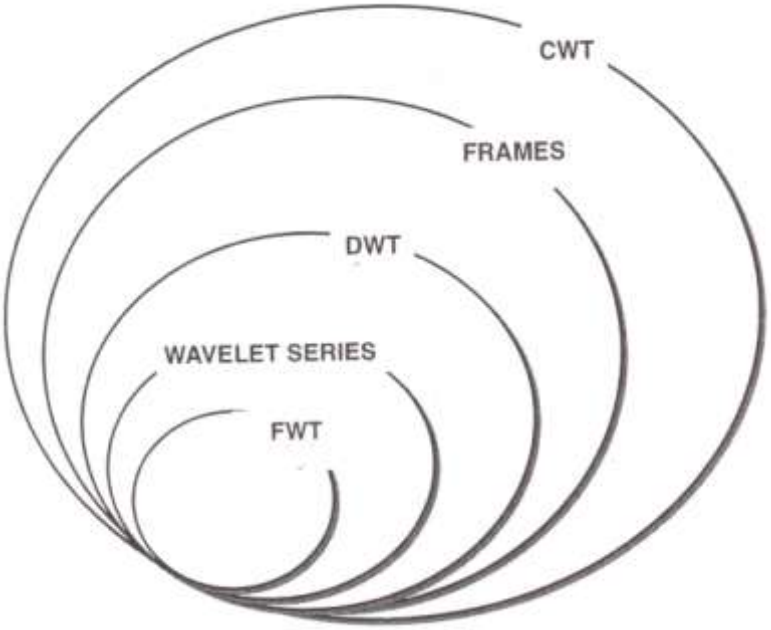

Figure 3.2.2 Wavelet transform signal processing onion

3.3.0 INTRODUCTION OF WAVELET

The concept of wavelets has been discussed in the literature for a very long time. It is based on fundamental ideas, which were first expressed more than a century ago in a variety of forms. However, it is only recently that significant progress has been made in the application of wavelet to practical problem in signal processing. The wavelet transform has been proposed as a flexible tool for the multiresolution decomposition of continuous time signals. Significant practical applications of wavelets have been found in signal and image processing.

In 1909, Haar replaced the sine and cosine functions of the Fourier transforms with another orthonormal basis, now commonly known as the Haar basis.

Daubechies introduced the concept of compactly supported wavelets and theory of frames. She also saw the connection between the wavelet theory, and theory of subband decomposition which was independently being pursued by the digital signal processing community of electrical engineers. Mallat introduced the concept of multiresolution, which is intimately related to multi-rate digital filter used for subband decomposition.

3.3.1 WAVELET

The signal is defined by a function of one variable or many variables. Any function is represented with the help of basis function. An impulse is used as the basis function in the time domain. Any function can be represented in time as a summation of various scaled and shifted impulses. Similarly the sine function is used as the basis in the frequency domain. However these two-basis functions have their individual weaknesses: an impulse is not localized in the frequency domain, and is thus a poor basis function to represent frequency information. Likewise a sine wave is not localized in the time domain [82]. In order to represent complex signals efficiently, a basis function should be localized in both time and frequency domains. The support of such a basis function should be variable, so that a narrow version of the function can be used to represent the high frequency components of a signal while wide version of the function can be used to represent the low frequency components. Wavelets satisfy the conditions to be qualified as the basis functions.

Sinusoidal wave is one of the popular waves, which extend from $-\infty$ to $+\infty$. Sinusoidal signals are smooth and predictable; it is the basis function of Fourier analysis. Fourier analysis consists of breaking up a signal into sine and cosine waves of various frequencies. A wavelet is waveform of limited duration that has an average value of zero [12]. Wavelets are localized waves and they extend not from $-\infty$ to $+\infty$ but only for a finite time duration, as shown in figure 3.3.1.1.

The wavelet as shown in figure 3.3.1.1 is a mother wavelet (*h(t)*).The mother wavelet and its scaled daughter functions are used as a basis for a new transform. Unfortunately, if *h(t)* is centered around t = 0, with extension between – T and + T, no matter how many daughter wavelets we use, it will not be possible to properly represent any point at t >T of a signal *s(t).*

Please note that the wave transform did not have this problem, as the wave function was defined for every value of t. For the case using a localized wave or wavelet, it must be possible to shift the center location of the function [81]. In other words, it must include a shift parameter, b, and the daughter wavelets should be defined as

$$h_{ab}(t) = \frac{1}{\sqrt{a}} h\left(\frac{t-b}{a}\right) \qquad \text{---3.3.1.1}$$

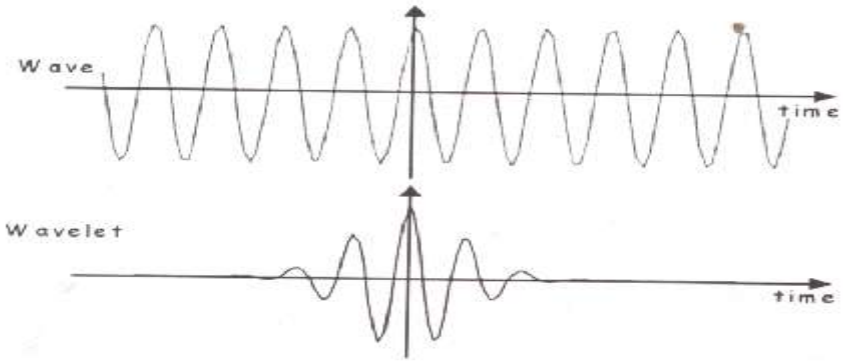

Figure 3.3.1.1 wave and wavelet

The reason for choosing the factor $\frac{1}{\sqrt{a}}$ in the above equation is to keep the energy of the daughter wavelets constant.

Thus, the wavelet transform has to be a two-dimensional transformation with the dimension being *a*, the scale parameter, and *b*, the shift parameter. The wavelet transform maps 1-D time signals to 2–D scale (frequency) and shift parameter signals.

It is observed that for periodic functions, Fourier analysis is ideal. However, wavelet transforms are not restricted to only the periodic function, but for any function, provided it is admissible. In many cases of signal processing, one can choose the signal itself or a theoretical model as the mother wavelet. The advantage of doing this is that only few wavelet transform coefficients are then required to represent the signal. Wavelets tend to be irregular and asymmetric. The original wave is known as Mother wavelet. Wavelet analysis consists of breaking up of signal into shifted and scaled versions of the original (mother) wavelet.

3.4.0 FOURIER ANALYSIS

Fourier analysis consists of breaking up a signal into sine and cosine waves of various frequencies. Another way to think of Fourier analysis is as mathematical technique for transforming our view of the signal from time domain to frequency domain. For signal processing, Fourier analysis is extremely useful because the signal frequency content is of greater importance, so why do we need other techniques like wavelet analysis?

Fourier analysis has a serious drawback that in transforming the signal from time domain to the frequency domain, time information is lost. When looking at a Fourier transform of a signal; it is impossible to tell, when a particular event took place. If the signal property do not change much over the time then signal is said to be stationary signal,

but however, most interesting signals contain the numerous non-stationary or transitory characteristics: drift, trends, abrupt changes, beginnings and ends of the events. These characteristics are often the most important part of the signals and Fourier analysis is not suited to detect them [12].

3.5.0 SHORT TIME FOURIER ANALYSIS

In an effort to correct the deficiency of Fourier analysis, Dennis Gabor (1946), adapted the Fourier transform to analyze only a small section of the signal at a time, this technique is known as windowing the signal. Gabor's adaption, called the Short-Time Fourier Transform (STFT), maps a signal into two-dimensional function of time and frequency as shown in figure 3.5.1

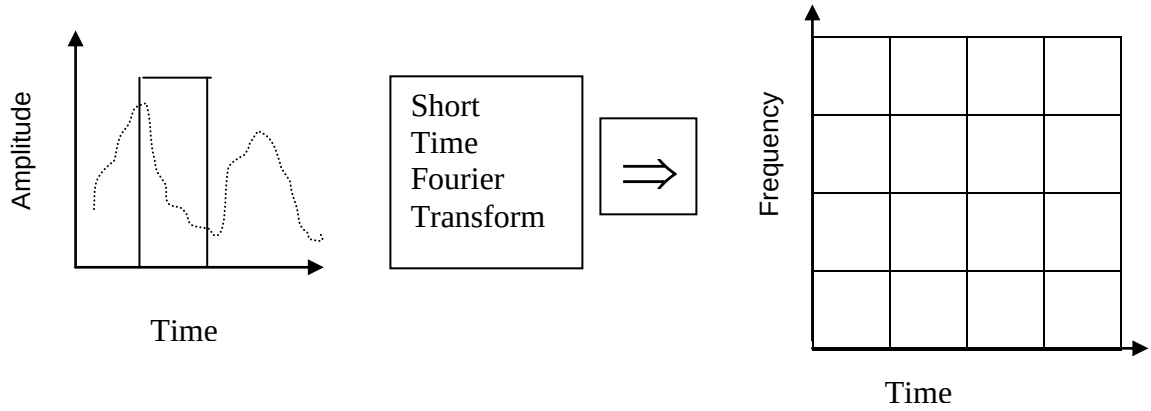

Figure 3.5.1 Short-Time Fourier Transform (STFT), mapping a signal into two-dimensional function of time and frequency

Figure 3.5.1 shows that, the time and frequency spaces are divided into equal segments. Each column represents one application of a Discrete Fourier Transform over specific time interval. The rows in the figure represent the frequency bins into which it divides the signal energy at each time segment. Each row is the result of signal analysis by a basis function of a specific frequency. The Short-Time Fourier Transform represents a sort of compromise between the time and frequency based views of a signal. It provides some information about time and frequency both, when and at what frequencies a signal event occurs. However, one can obtain this information with limited precision, and that precision is determined by the size of the window. While the STFT is the compromise between time and frequency information, a drawback of this technique is that once one chooses a particular size of time window, that window is the same for all frequencies of the

signals. Many signals require more flexible approach – where one can vary the window size to determine more accurately either time or frequency [12].

3.6.0 WAVELET ANALYSIS

Wavelet analysis represents a windowing technique with variable sized regions. Wavelet analysis allows the use of long time intervals, when one wants more precise low frequency information of a signal, and short time intervals, when one wants high frequency information of a signal. Wavelet analysis uses a time scale region as shown in figure 3.6.1

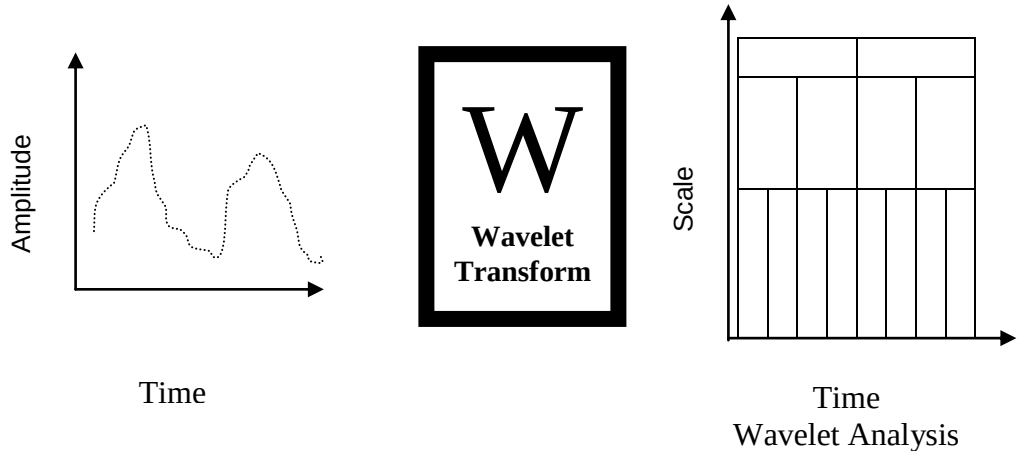

Figure 3.6.1 Wavelet transform, mapping a signal into two-dimensional function of time and scale

Figure 3.6.1 shows, wavelet analysis, which uses time and scale analysis regions, which are not evenly spread. The vertical position of each rectangle shows the frequency of a signal and the vertical size shows the frequency resolution or bandwidth of the signal, as governed by each wavelet or basis function. Wavelet analysis allows the use of long time intervals where one wants to observe low frequency information and short time intervals where one wants to observe high frequency information. If one looks at signal with large window, one sees large features of the signal. If one looks at a signal with small windows, one can fine structure of the signal.

It is noticed that wavelet analysis does not use time-frequency region, but it uses the time scale region. The basis functions used in wavelet are not sine waves, but less regular functions, which are stretched or compressed to get different scales. Small scale or fine scale is analogous to high frequency, and coarse scale is analogous to low frequency. The variable time is often refereed to as shift or position, so rather than referring to the time

frequency region of the DFT, it talks about a shift scale region of the wavelet analysis [12]. The mathematical details of the wavelet transform is discussed as follows:

The word wavelet literally means small wave. The wavelet transform, similar to the short-time Fourier transform, maps a function *s(t)*, into a two-dimensional domain (the time-scale plane) and is denoted by W_S (a, b) given by

$$W_S(a,b) = \frac{1}{\sqrt{a}} \int_{-\infty}^{+\infty} s(t)\, h^*\left(\frac{t-b}{a}\right) dt$$

$$= \int_{-\infty}^{+\infty} s(t)\, h^*_{ab}(t)\, dt \qquad \text{---3.6.1}$$

where *h(t)* is in general called the mother wavelet, and the basis functions h_{ab} of the transform, called daughter wavelet, are given by

$$h_{ab}(t) = \frac{1}{\sqrt{a}} h\left(\frac{t-b}{a}\right) \qquad \text{---3.6.2}$$

Equation 3.6.1 is known as the forward wavelet transform; where $h_{ab}(t)$ is a set of basis functions obtained from the mother wavelet *h(t)* by compression or dilation using scaling parameter *a*, and temporal translation using shift parameter *b*. The scaling parameter *a* is positive and varies form 0 to ∞. For a < 1, the transform performs compression of the signal, and for a > 1, the transform performs dilation of the signal [81]. The signal *s(t)* can be recovered form the wavelet coefficients $W_s(a, b)$ by the inverse wavelet transform, given by:

$$s(t) = \frac{1}{c} \int_{-\infty}^{\infty} \int_{0}^{\infty} W_S(a,b)\, h\left(\frac{t-b}{a}\right) \frac{da}{a^2}\, db \qquad \text{---3.6.3}$$

provided that constant c is

$$c = \int \frac{|H(\omega)|^2}{\omega} d\omega \qquad < \infty \qquad \text{---3.6.4}$$

Equation 3.6.3 is also referred to as reconstruction formula, inverse transform, or synthesis, and equation 3.6.4 is generally known as the admissibility condition.

3.7.0 FOURIER TRANSFORM AS A WAVE TRANSFORM

The Fourier transform $S(\omega)$ is a frequency representation of a time domain signal *s(t)* is given by:

$$S(\omega) = \int_{-\infty}^{+\infty} s(t) e^{-j\omega t}\, dt \qquad \text{---3.7.1}$$

and its inverse transform

$$s(t) = \frac{1}{2\pi} \int_{-\infty}^{+\infty} S(\omega)\, e^{j\omega t}\, d\omega \qquad \text{---3.7.2}$$

where ω is angular frequency, and is equal to 2πf, and f is the frequency of the continuous signal in Hz. Equation 3.7.1 is the traditional definition of a Fourier transform. However, one can choose to utilize different notation using the concept of time scaling, a =1/ω. One can also introduce the concept of a wave function, as the basis function of a transformation

$$h(t) = e^{jt} \qquad \text{---3.7.3}$$

and

$$h\left(\frac{t}{a}\right) = h_a(t) = e^{jt/a} \qquad \text{---3.7.4}$$

Equation 3.7.1 can now be written as the wave transform:

$$W(a) = \int_{-\infty}^{+\infty} s(t) e^{-jt/a}\, dt = \int_{-\infty}^{+\infty} s(t)\, h_a^*(t)\, dt \qquad \text{---3.7.5}$$

As the basis functions are all created by scaling in time of the same mother wave *h(t)*, they are called as daughter waves. A mother wave and two daughter waves are shown in figure 3.7.1.

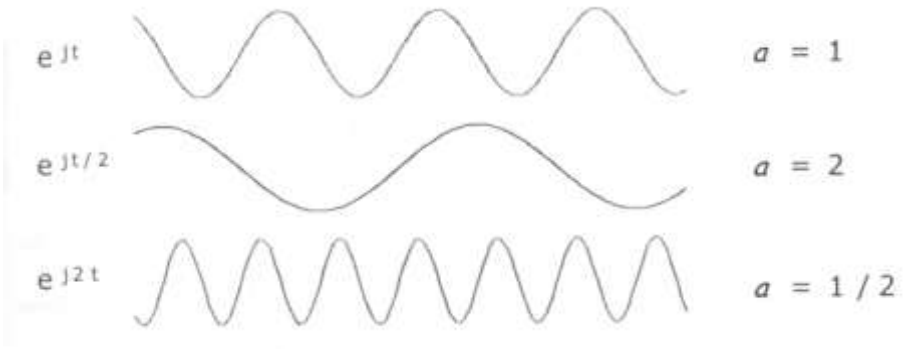

Figure 3.7.1 Mother and Daughter waves (Fourier bases) as a function of time for *a* = 1, 2 and 1 / 2

The functions are periodic waves that extended over the entire time axis form –∞ to +∞. It is important to note that the basis functions are like waves, each having a different frequency obtained by changing the scale of the horizontal axis. The top curve in the figure for *a* = 1 represents the mother wave e^{jt}. For *a* >1, the curve in the middle of the figure, the function is dilated in time, resulting in a lower frequency wave. For *a* <1, the curve at the bottom of figure, the wave is compressed in the time and it has a higher frequency oscillation [81].

As the waves are orthogonal and extend over the entire frequency space, the inverse transformation is obtained as

$$s(t) = \int_{-\infty}^{+\infty} W(a)\, e^{jt/a} \frac{da}{a^2} = \int_{-\infty}^{+\infty} W(a)\, h_a(t) \frac{da}{a^2} \qquad \text{---3.7.6}$$

In order to keep consistency with equation 3.7.2, the limits of integration of equation 3.7.6 are set between $-\infty$ to $+\infty$. In reality most of the applications are limited to real signals, hence it is common practice to consider only positive values of the scaling parameter *a*. Even though only positive values of *a* are considered, there is no loss of information in Fourier transform [81].

The term da/a^2 represents the differential change in frequency and is obtained form differentiating relationship between frequency and scale:

$$d\omega = -\frac{da}{a^2} \qquad \text{---3.7.7}$$

The Fourier transform is the most used signal transformation in the analysis of signals; it is not optimal for many applications, because if it is localized in time domain, then it is not localized in frequency domain and vice versa. As an example, let us look at the Fourier transform S(ω) of the rectangular function s(t) defined as

$$s(t) = \begin{cases} 1 & for \quad |t| < T/2 \\ 0 & otherwise \end{cases} \qquad \text{---3.7.8}$$

given by

$$S(\omega) = T \frac{\sin(\omega T/2)}{(\omega T/2)} = T \sin\left(\frac{\omega T}{2\pi}\right) \qquad \text{---3.7.9}$$

The Fourier transform in equation 3.7.9 is defined (i.e., it has no zero values) over the entire frequency axis. It follows that to define the signal *s(t)* in the frequency domain, the complete set of values of *S*(ω) must be used. The rectangular function, and its Fourier transform are plotted in figure 3.7.2. It is found that the signal *s*(t) is well localized in time, but it is not localized in frequency by its Fourier transform. For time localized signals, like the rectangular function *s*(t) shown in figure 3.7.2, a set of basis functions such as the waves is not convenient, although mathematically correct. A more compact result can be obtained, if the basis functions of the transformation were localized. Thus, there is a need of wavelets, not waves.

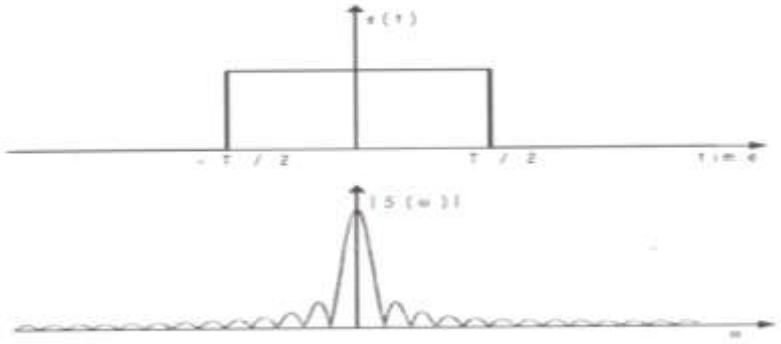

Figure 3.7.2 Rectangular function and its Fourier transform.

3.8.0 CONNECTION BETWEEN WAVELETS AND FILTERS

A wavelet is waveform of limited duration that has an average value of zero [12]. Wavelets are localized waves and they extend not from $-\infty$ to $+\infty$ but only for a finite time duration. The wavelet transform, transforms the signals from one-dimensional to two-dimensional. By definition, equation 3.6.1 describes the wavelet transform according to the following relationship:

$$W_S(a,b) = \frac{1}{\sqrt{a}} \int_{-\infty}^{+\infty} s(t)\, h^*\left(\frac{t-b}{a}\right) dt \qquad \text{---3.8.1}$$

In above equation the variable t is replaced by τ and, b is replaced by t to yeild

$$W_S(a,t) = \frac{1}{\sqrt{a}} \int_{-\infty}^{+\infty} s(\tau)\, h^*\left(\frac{\tau-t}{a}\right) d\tau \qquad \text{---3.8.2}$$

The equation 3.8.2 can be rewritten as

$$W_S(a,t) = s(t) \otimes h_a^*(t) = s(t) * h_a^*(-t) \qquad \text{---3.8.3}$$

where the symbol $\otimes$ represents the correlations operations, and the symbol * the convolution operator, and the function $h_a(t)$ is given as

$$h_a(t) = \frac{1}{\sqrt{a}} h\left(\frac{t}{a}\right) \qquad \text{---3.8.4}$$

The wavelet transform of a signal is nothing but the correlation between the signal and the function $h_a(t)$ [81]. The wavelet transform of a signal $s(t)$ can be obtained by applying the signal as the input to a linear system whose impulse response is given by $h_a(- t)$ as shown in figure 3.8.1 (a) and figure 3.8.1 (b) shown in the Fourier domain

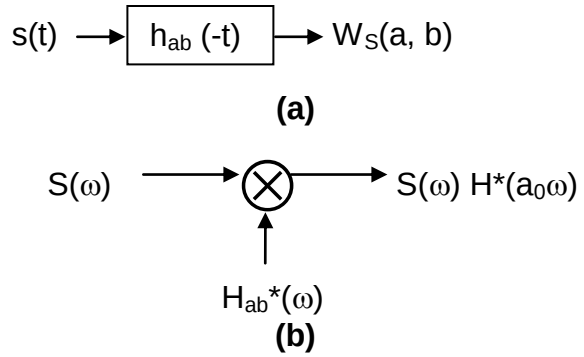

Figure 3.8.1 Filter bank representation of the wavelet transform of a signal *s*(t) in (a) Time domain and (b) Frequency domain

The Fourier transform of equation 3.8.3 is given by

$$\Im\{W_S(a,t)\} = W_S(a,\omega) = S(\omega)\, h_a(\omega) \qquad \text{---3.8.5}$$

where $W_s(a, \omega)$, $S(\omega)$, and $H_a(\omega)$ are the Fourier transform of $W(a, t)$, $s(t)$ and $h_a(t)$ respectively. $S(\omega)$ gives us the frequency components of the signal. $H_a(\omega)$ gives the frequency response of the linear system or filter whose impulse response is given by $h_a(t)$. $H_a(\omega)$ is given by

$$H_a(\omega) = \Im\{h_a(t)\} = \sqrt{a}\, H(a\omega) \qquad \text{---3.8.6}$$

The wavelet transform is thus the response of the filter bank constructed by the filters $H_a(\omega)$to the signal $s(t)$ [81].

The wavelet coefficients are obtained by processing the signal using a filter bank for different values of *a*, whose frequency response are given by $H_a(\omega)$in frequency domain as shown in figure 3.8.2. The time domain implementation using convolvers is shown in figure 3.8.3.

The implementation of a Fourier transform using linear systems involves a time-variant impulse response. In contrast, wavelet transforms as defined can be implemented using time-invariant systems. This is an enormous advantage in connection with implementing wavelet transformers. For example, it is well known that one can perform a correlation of signals in real time or in the spatial domain using optical signals. Because of the time-invariant property, all of these correlators can be used directly for implementing wavelet transformers. A block diagram of a typical wavelet transform signal processor is shown in figure 3.8.4, which is the wavelet transform implementation of the general transform domain processor.

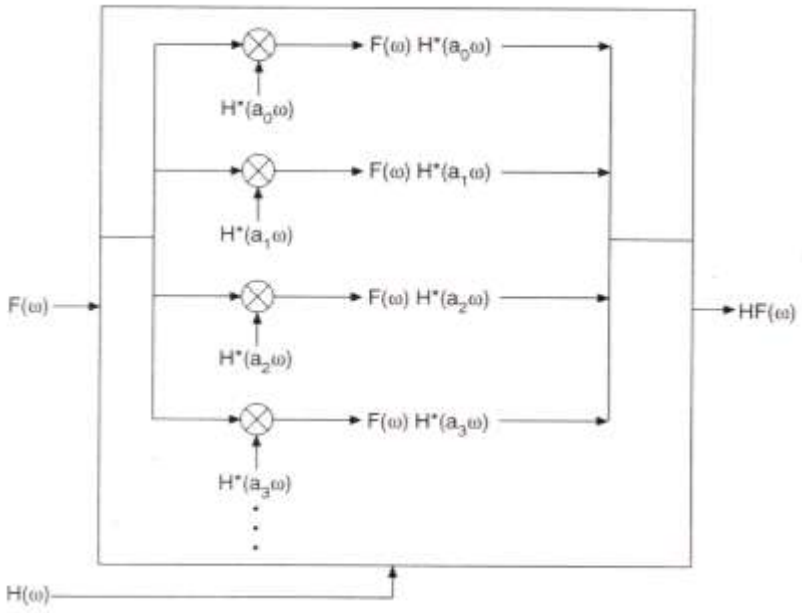

Figure 3.8.2 Filter bank representation of the Continuous Wavelet Transform

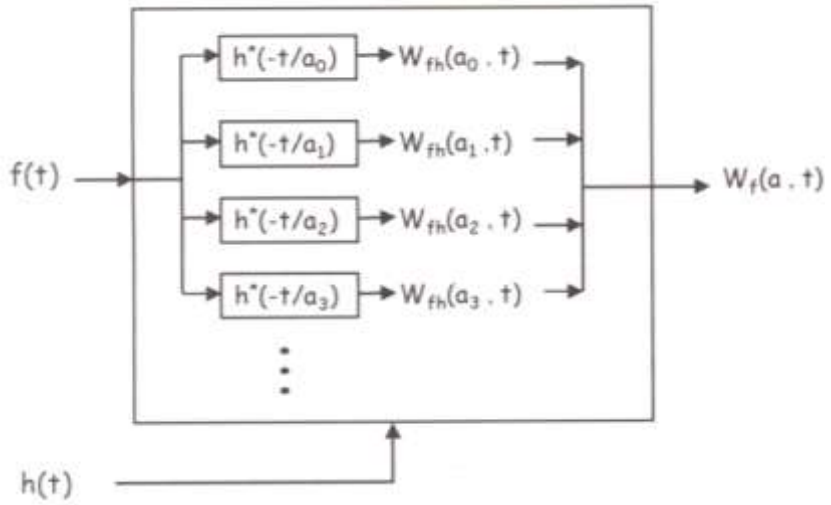

Figure 3.8.3 Time domain filter bank implementation of the continuous wavelet transforms

As discussed earlier, a wavelet transform can be performed either in the time domain or in the frequency domain using filter banks. The frequency domain implementation is shown in figure 3.8.5. In this figure S(ω), H(ω) and W_s(a) represent the Fourier transform of s(t), *h*(t) and w_s(a) respectively. Depending on the application, the block labeled WT filtering multiplies the wavelet transform coefficients with another function.

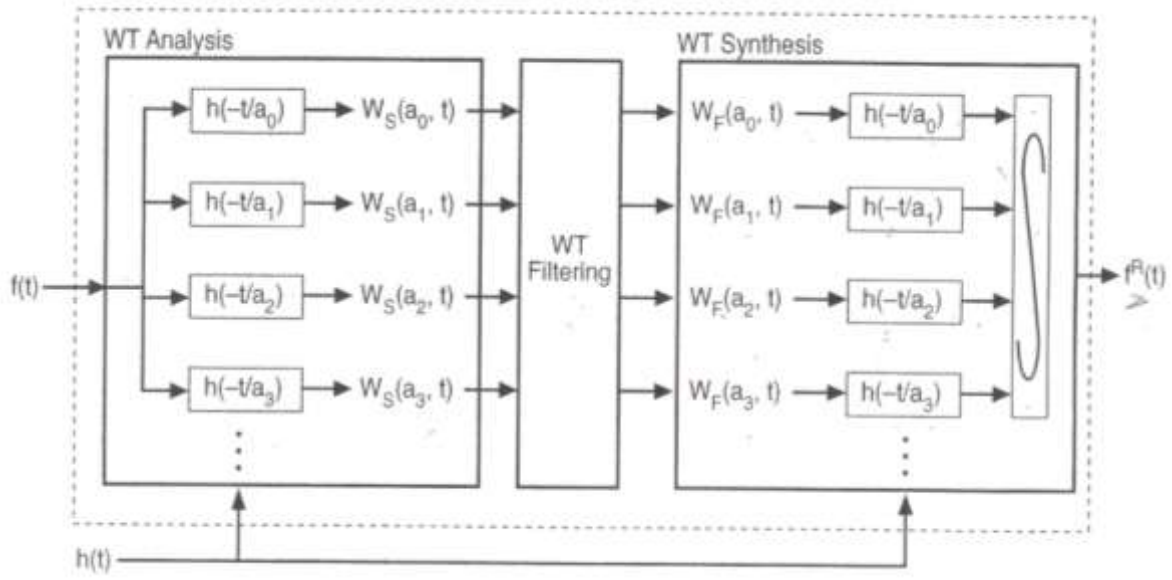

Figure 3.8.4 Block diagram of a wavelet transform signal processor

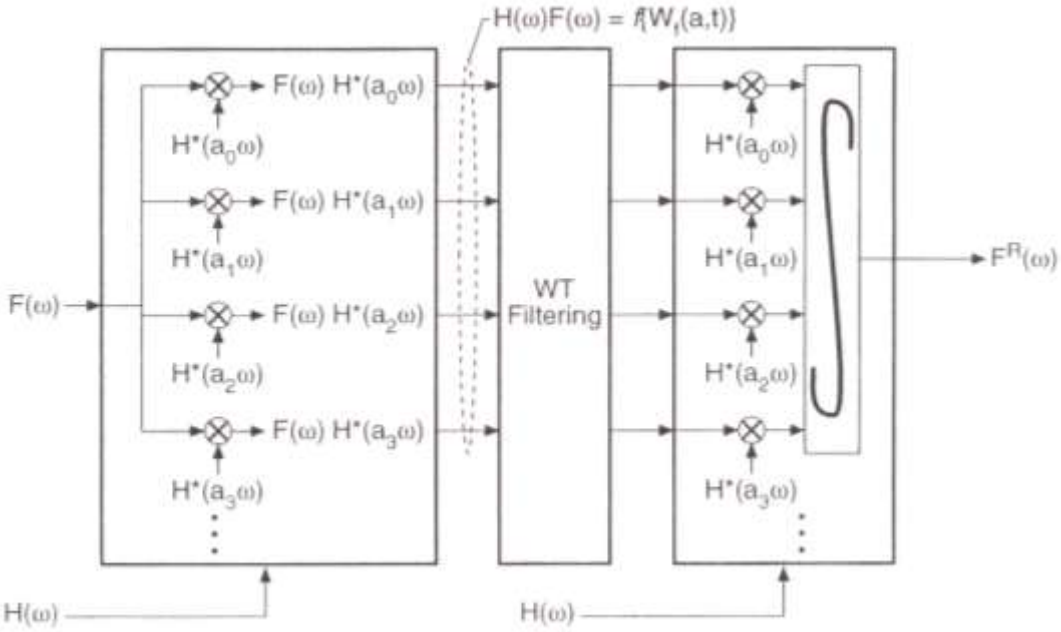

Figure 3.8.5 Frequency domain implementation of the wavelet transforms signal processor

The WT synthesis block diagram is really an inverse wavelet transform, which converts the processed signal back into the time domain.

It is of interest to point out that the block diagrams shown in figure 3.8.4 and 3.8.5 can be modified such that their practical implementation becomes easier. A particular case

is shown in figure 3.8.6 and 3.8.7. In this case, the filtering is performed after the WT synthesis block diagram.

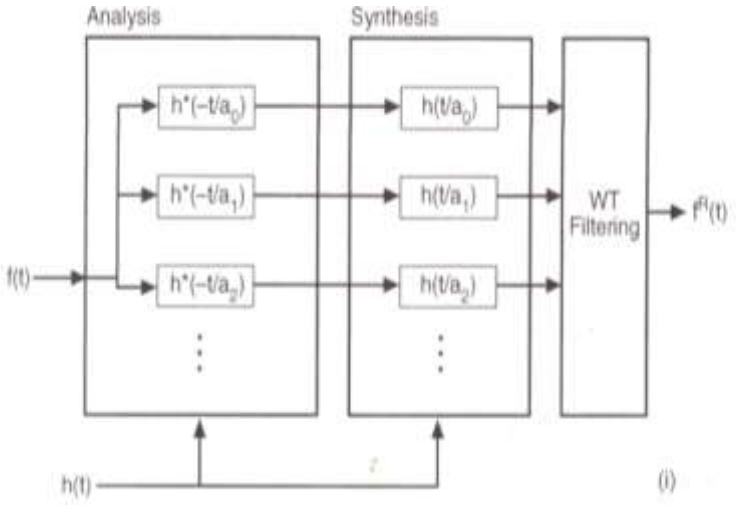

Figure 3.8.6 (i) Time domain representation of the alternative design of the wavelet transform signal processor

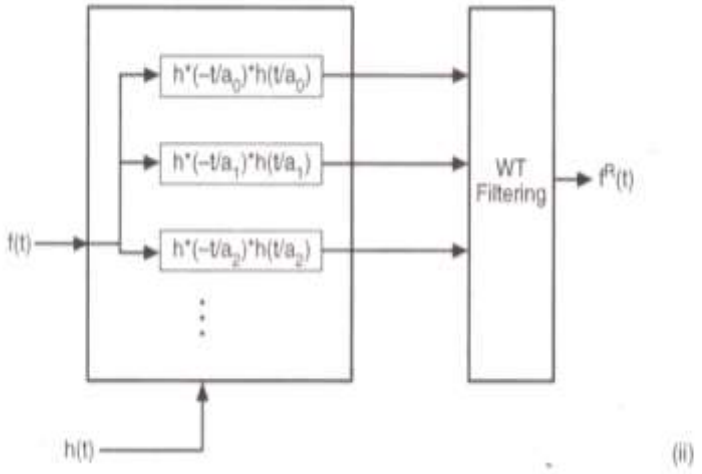

Figure 3.8.6 (ii) Time domain representation of the alternative design of the wavelet transform signal processor

In figure 3.8.6, the synthesis and analysis blocks are combined. For this case, each filter has a combined impulse response given by h*(-t/a) h(t/a). A similar simplification is not possible for the case of Fourier transforms. Figure 3.8.7 shows the frequency domain implementation of the modified structure. Again, the synthesis and analysis blocks can be combined for simplification. For this case the filters have combined frequency response given by $|H(a\ \omega)|^2$.

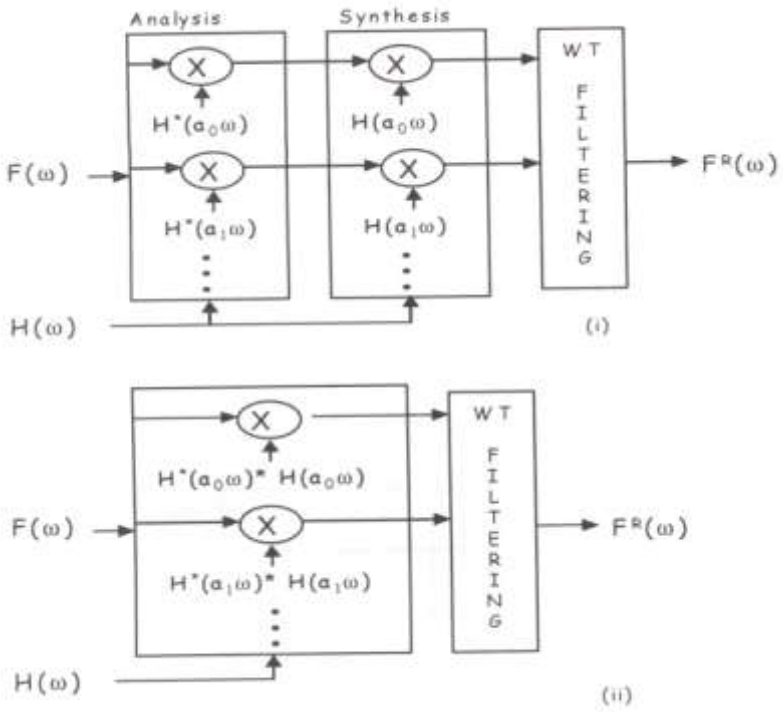

Figure 3.8.7 Frequency domain representation of the alternative design of the wavelet transforms signal processor

It is convenient to discuss the admissibility condition at this point. For the wavelet transform, an inverse wavelet transform should also exist. The inverse wavelet transform is given by:

$$s(t) = \frac{1}{c}\int_{-\infty}^{+\infty}\int_{-\infty}^{+\infty} W_S(a,b)\, h\left(\frac{t-b}{a}\right)\frac{da}{a^2}\,db \qquad \text{---3.8.7}$$

Where C is an unknown constant. If we choose s(t) = δ or S(ω) = 1, then the output of the inverse transform should also be a delta function.

This situation is shown in the frequency domain in figure 3.8.8 with F(ω) = S(ω).

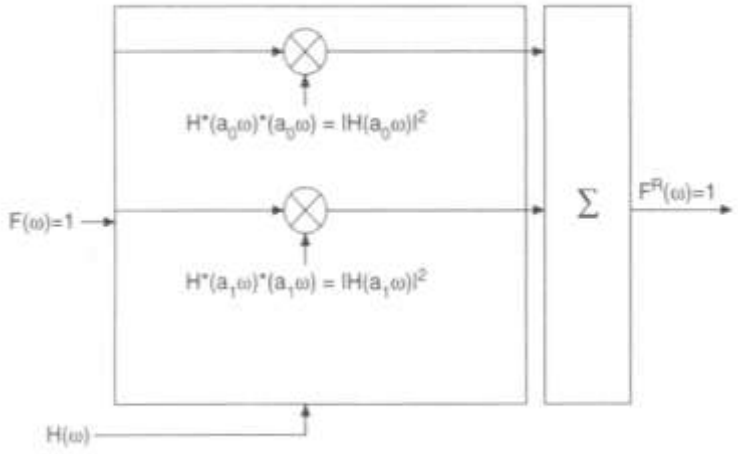

Figure 3.8.8 Filter bank representation of the wavelet transform admissibility condition

It is obvious that the following equation should be satisfied:

$$S(\omega) \equiv 1 = \frac{1}{C} \int_{-\infty}^{+\infty} \left| Ha(\omega) \right|^2 \frac{da}{a^2} \qquad \text{---3.8.8}$$

where $H_a(\omega) = \sqrt{a}\ H(a\omega)$ hence

$$1 = \frac{1}{C} \int_{-\infty}^{+\infty} \frac{\left| H(\omega) \right|^2}{\omega}\, d\omega \qquad \text{---3.8.9}$$

$$C = \int_{-\infty}^{+\infty} \frac{\left| H(\omega) \right|^2}{\grave{}\omega}\, d\omega \ < +\infty$$

The constant C has to be less than infinity for the wavelet transform to be valid. Thus, it is observed that any mother wavelet can be chosen or admissible as long as $C < \infty$. In this way, we obtain the so-called admissibility condition.

Let us point out again the versatility of the wavelet transform. Any function can be chosen as a mother wavelet as long as admissibility condition is satisfied. Thus, one is not confined to a single set of basis function, as is the case in a Fourier transform. This ability to choose the mother wavelet depending on the particular problem is a significant advantage. Actually, one can employ the usual optimization techniques to obtain the minimum mother wavelet for a particular problem by minimizing a proper chosen cost function. This is possible since the wavelet transform is both linear and time invariant; this means that one can choose a linear combination of admissible wavelet functions [81].

3.9.0 THE CONTINUOUS WAVELET TO THE DISCRETE WAVELET

In definition of wavelet transform, the variable considered for the time *t*, scale *a*, shift *b* and angular frequency ω are continuous, and hence the transform is said to be continuous wavelet transform.

In the theory of linear systems, one also deals with continuous and discrete times. In the first case, it is talked about analog signal processing, whereas the latter is called discrete-time signal processing. Analog signal processing involves the Fourier transform, whereas the so-called z-transform plays an important role for the discrete case. Digital signal processing involves not only discrete time but also values, which are quantized.

A Fourier transform maps 1-D signals to 1-D frequency space, whereas a wavelet transform maps 1-D signals to a 2-D space (the dimensions being given by the scale and shift parameters *a* and *b).* Thus, while starting to discretise the variables, the situation becomes quite complex. However, one can have a situation where the signal itself is continuous with continuous *t* and *f* but the basis functions have bounded *t* and discrete *a*. This is the case, which people generally refer to as a Discrete Wavelet Transform (DWT),

One cannot use matrix theory with discrete/values to discuss DWT as the variable *t* is still continuous. Equivalent to the DFT, one has the case where *t* and *a* are both discrete. This is the case generally known as sub-bands and was developed independently starting from the concepts of digital signal processing. In wavelet theory, this is called as wavelet series. Just as we modified the DFT to obtain the FFT, if one restricts sub-bands to the dyadic case; one obtains high computational efficiency like the FFT case, except using polyphase decomposition.

3.10.0 SUBBANDS

The continuous time signal is converted into discrete time signal by taking the samples at fixed intervals of time as per the Nyquist criteria. Let us consider the case of wavelet transform, when the time axis is not continuous but discrete. The sampling rate, f_s, is determined by the Nyquist sampling theorem, which states that for a signal with highest frequency f_{max} the sampling frequency must be $f_s \geq 2f_{max}$ or the sampling interval must be

$$T_S = \frac{1}{f_s} = \frac{1}{2\, f_{max}} \qquad \text{---3.10.1}$$

The continuous signal, *s(t)* becomes $s(nT_s)$. Since in general one normalizes the time

variable T_s as unity and hence $s(nT_s) = s(n)$. A band-limited signal is analyzed with $\omega_{max} = 2\pi f_{max} = \pi f_s = \pi$ as shown in Figure 3.10.1.

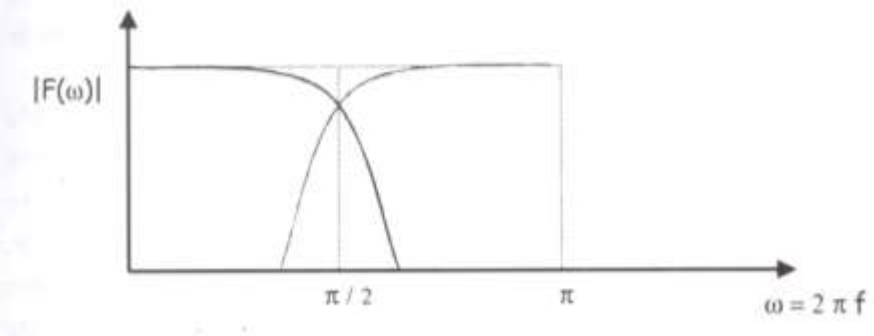

Figure 3.10.1 Frequency space of a discrete-time signal with sampling rate $T_s = 1$ leading to $\omega_{max} = \pi$.

A typical discrete-time linear system is shown in Figure 3.10.2. Similar to the impulse response in the continuous case, impulse response of a linear system is denoted by *h(n).* The convolution integral is replaced by a discrete convolution given by:

$$g(n) = f(n) * h(n) = \sum_m f(m)\, h(n-m) \qquad \text{---3.10.2}$$

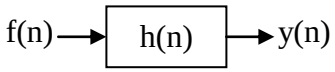

(a)

$$y(n) = f(n)*h(n) = \sum_m f(m)h(n-m) \qquad \text{---3.10.3}$$

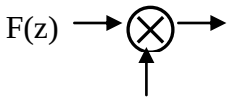

---3.10.4

(b)

Figure 3.10.2 Discrete-time linear system (a) in the time domain and (b) in the *z*-domain

In order to obtain a representation similar to a Fourier transform, for the discrete-time case, substitute $z = e^{j\omega}$ in above equation.

$$G(z) = F(z)\, H(z) \qquad \text{---3.10.5}$$

$$G(z)|_{z = ej\omega} = G(e^{j\omega}) = F(e^{j\omega})\, H(e^{j\omega}) \qquad \text{---3.10.6}$$

$$G(\omega)= F(\omega)\, H(\omega) \qquad \text{---3.10.7}$$

where *G(z), F*(z) and *H*(z) are the z-transforms of *g(n), f{n),* and *h(n),*respectively.

Consider a signal space in the frequency domain, as shown in Figure 3.10.1 going from 0 to π, under the condition sampling frequency normalized to 1. Thus, according to the Nyquist sampling theorem, to avoid aliasing error, the signal's angular or radian frequency cannot exceed π.

The two filters; one low-pass and the other one high-pass are designed, such that it splits the signal space exactly in half a shown in Figure 3.10.3. The low-pass region extends from 0 to π/2 and the high-pass region extends from π/2 to π. Of course, once we design the filters to split a frequency band, we can split it again and again, forming subbands. Thus, in subband theory, we design a set of two prototype filters, such that repeated application of these filters divides the signal frequency band into equal parts. This is also referred to as a filter bank. There are different ways to split up the frequency space; some examples are shown in Figures 3.10.4 and 3.10.5.

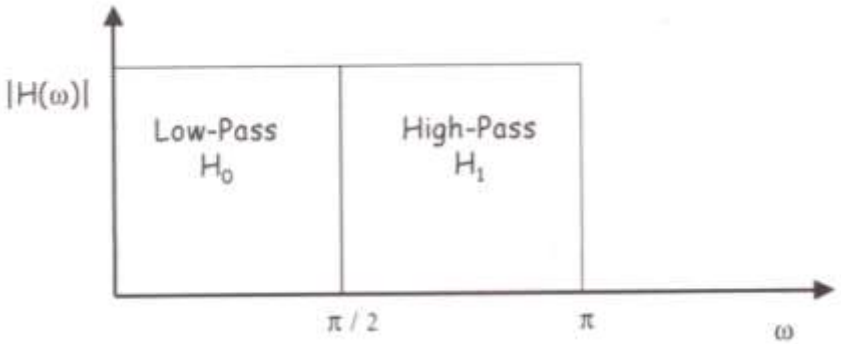

Figure 3.10.3 Splitting of the signal space using and ideal low-pass (H_0) and high-pass (H_1) filters

In a dyadic wavelet transform, one can design a mother wavelet from which set of daughter wavelets is generated, which forms a complete set. In other words, remembering the connection between the wavelet transform, and the filter bank, for this case one filter has been designed, and then using the scaling property, we have constructed a filter bank. All the filters in the filter bank are identical in properties except for their scale. In a subband implementation, initially two filters are designed, which are then scaled to form a filter bank or subband. For most of the applications, it is convenient to construct the wavelet transforms using two filters. Their corresponding impulse responses are then used to obtain a scaling function (low-pass filter) and a wavelet function (high-pass filter). At this point, the difference between subband and wavelet transform becomes very small as, in

general, subbands refer to the discrete-time signal analysis application, whereas wavelet transforms refer to the continuous-time case [81].

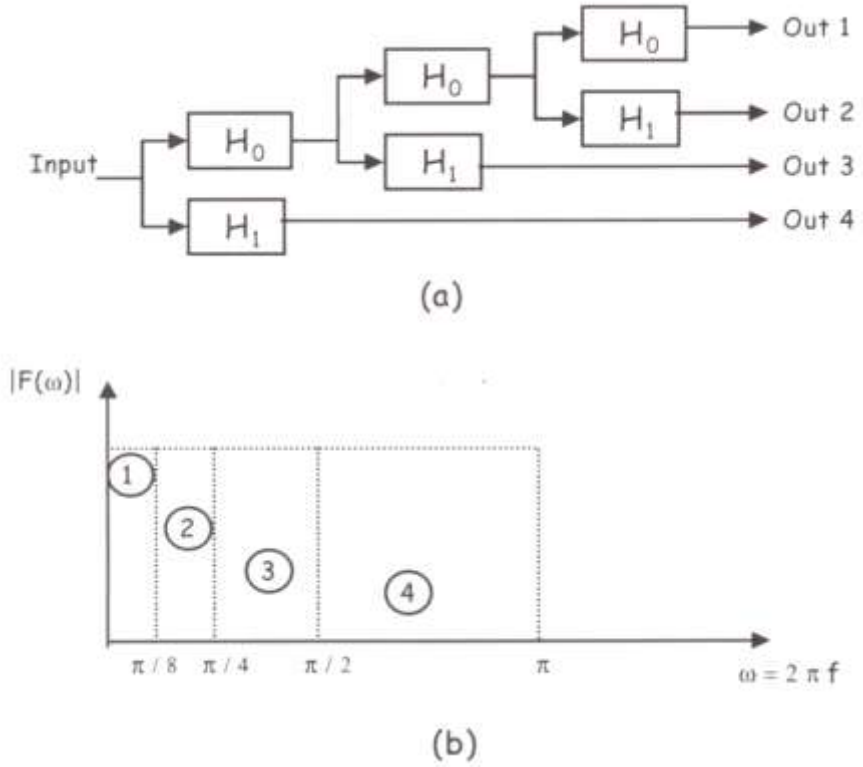

Figure 3.10.4 (a) The filter bank for splitting the signal bandwidth in the low frequency part only. (b) Frequency domain representation of the non-uniform subband.

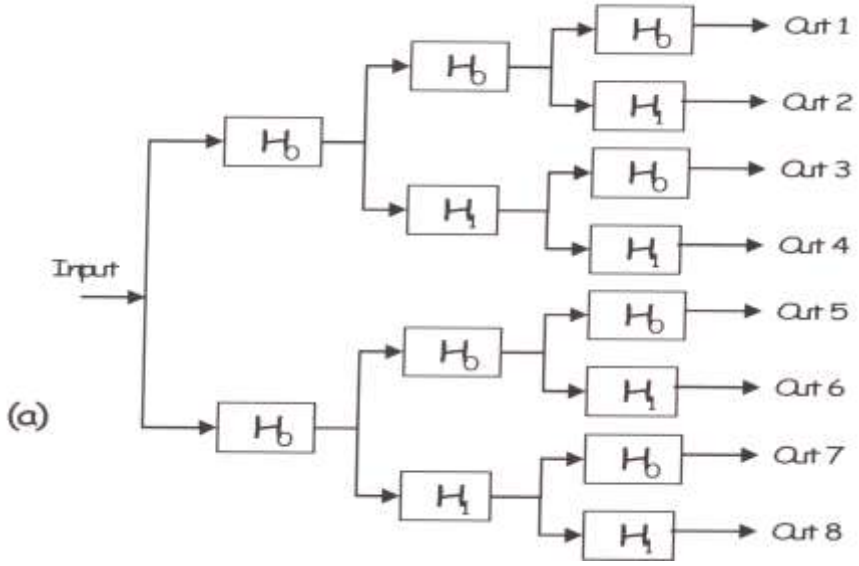

Figure 3.10.5 (a) The filter bank for uniform splitting the signal bandwidth into eight equal parts

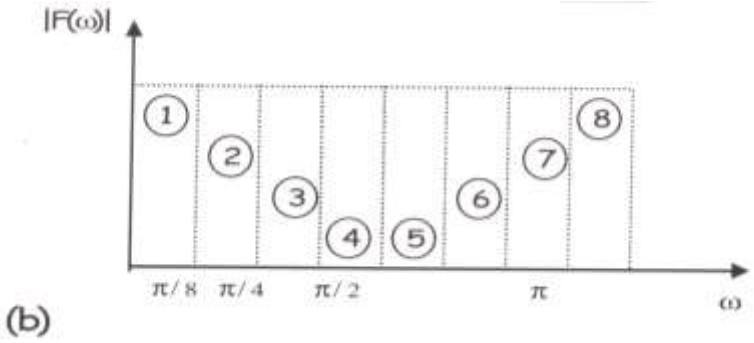

Figure 3.10.5 (b) Frequency domain representation of the subbands.

Consider the design of the subband filters. The obvious choice in the frequency domain is to design two ideal filters, whose frequency responses are rectangular as shown in Figure 3.10.5. The definition of filters is given in the frequency domain; to actually implement them; it is needed to convert it into the time domain. The impulse response of the ideal filter is the well-known sinc function. For the continuous-time case, the response extends to infinity and an exact implementation is therefore impossible. A delay line implementation of an *N-order* filter is shown in Figure 3.10.6. The figure also shows the fundamental elements of digital signal processing. To obtain a perfect response based on the filters in Figure 3.10.3, the number N of coefficients should be infinity. The simplest practical solution to obtain a FIR (finite impulse response) filter is to terminate the delay line coefficients beyond a certain value *N*. This assumes that truncated coefficients are very small in amplitude, with respect to the first *N*. The effect of terminating the coefficients of the impulse response to a finite number *N* results in the modification of the ideal response with the introduction of ripples in the stop-band, as shown in Figure 3.10.7. As it can be seen, some high- frequency information of the signal still leaks in the low- pass filter as can be noticed that the filter response for the low-pass case extends beyond $\pi/2$ and introduces ripples in the pass band. This means that this design will introduce aliasing error and distortion, which one would prefer to avoid.

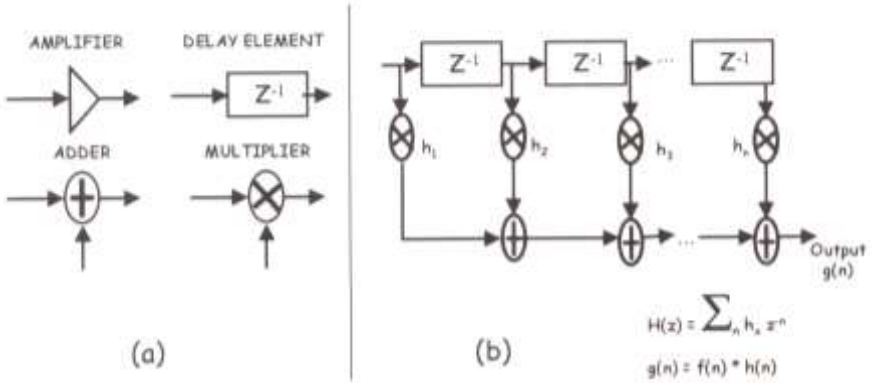

Figure 3.10.6 Finite impulse response (FIR) implementation of (a) elements of single rate digital signal processing and (b) *N*-tap FIR filter

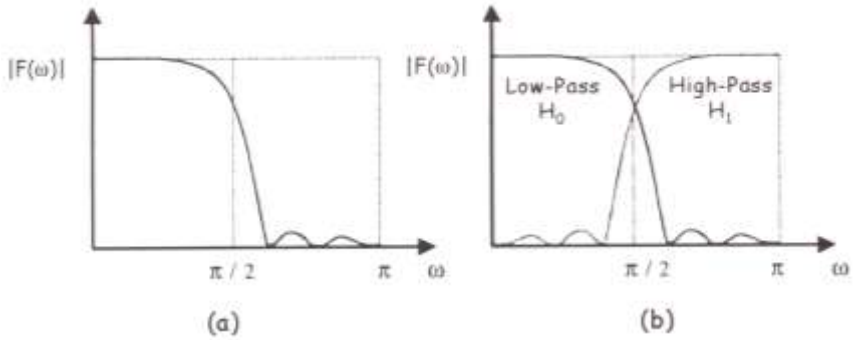

Figure 3.10.7 (a) Typical N-tap FIR low-pass filter response and (b) Typical N-tap FIR high-pass and low-pass filter response showing distortion and aliasing.

To appreciate the problem associated with aliasing and distortion errors, consider Figure 3.10.8, in which the signal is spitted into equal frequency bands. $H_0(z)$ and $H_1(z)$ refer to the z-response of the low-pass and high-pass filters, respectively. Firstly the signal is analyzed by splitting it into low-pass and high-pass frequency bands, this section is known as the analysis filter. The processing is carried out in the frequency domain, and then there is a need to convert it to the time domain. This last part is done through the so-called synthesis filter. Synthesis filters are like the reconstruction formula or the inverse transform. If no alteration of the coefficients in the frequency domain is done, then the input signal *s(n)* must be identical to the output $\hat{s}(n)$.

G_0 and G_1 are the low-pass and high-pass synthesis filters, respectively. However, if H_0 and H_1 are ideal filters, then G_0 and G_1 are also ideal filters. Thus, for this case $G_0 = H_0$ and $G_1 = H_1$. A point of historical interest is the fact that people initially used H_0 and H_1

for both analysis and synthesis filters. The concept of using different filters to cancel out the distortion and aliasing errors was introduced later.

Let us introduce the concept of multirate filters using Figure 3.10.8. We note that the bandwidth at the output of H_0 is only $\pi/2$, although the output has a sampling frequency corresponding to π. So, every other sample in the output is superfluous and carries no information; we might as well discard these samples and hence the output of the filter is down-sampled by two. This is shown by the block diagram with a downward arrow and a 2, indicating that every other sample point is discarded; it is called decimation by 2. Similar operations are performed on the high-pass output. Thus, if the input signal has *N* samples, then the output signal also has *N* samples. However, *N/2* of these correspond to the low-pass version and the other *N/2* correspond to the high-pass version [81]. At the output of the next stage shown in Figure 3.10.8, has *an N* sample because in the processing signal is up sampled by two and then filtered.

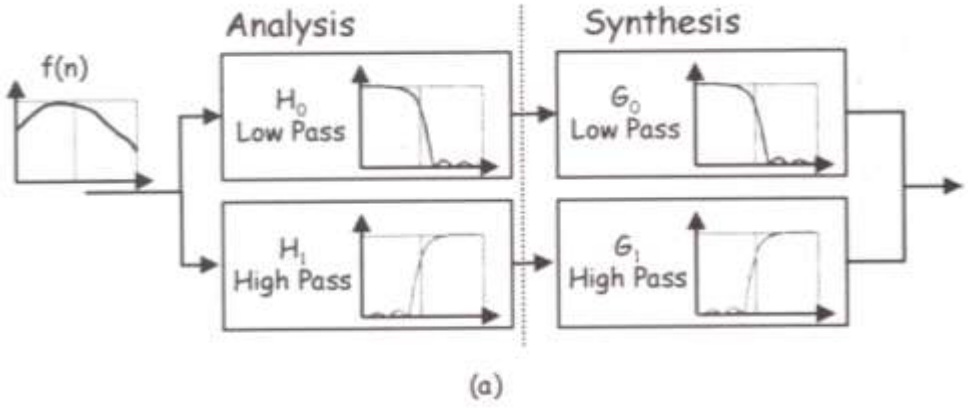

Figure 3.10.8 (a) Analysis and Synthesis filters

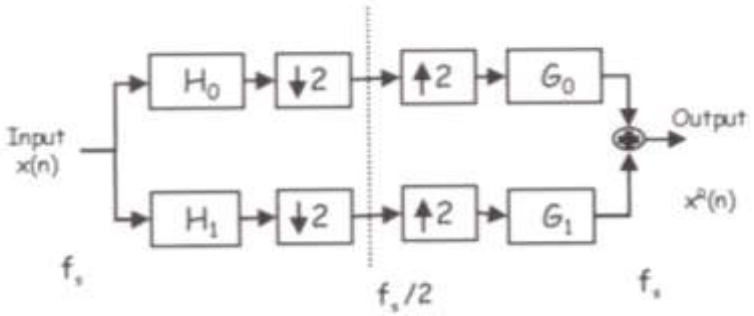

(b)

Figure 3.10.8 (b) with decimation and interpolation

Since the number of samples in the input and output are the same, this process of subband operation is optimum.

When H_0 and H_1 are not ideal; they have ripples and go beyond the $\pi/2$ cutoff frequency as shown in Figure 3.10.7. Distortion error is obvious, as ripples are generated in the pass band. However, aliasing error occurs due to decimation, because the output bandwidths are not limited to $\pi/2$. Initially, the solution for reducing these errors was to use window functions, which reduce ripples in the pass band and extend beyond the cut-off frequency, $\pi/2$. However, one cannot completely eliminate the errors using this technique. The situation is similar to using a Gabor transform, which does not form a complete set of basis functions.

To solve this problem, the so-called quadrature mirror filter (QMF) was introduced, When using a QMF, one does not use the same filters for analysis and synthesis, The basic idea is to use different filters such that the errors in analysis are minimized by the synthesis. The perfect reconstruction filters are also QMF, but they completely cancel both the distortion and aliasing errors. The situation can be understood by considering an analogous situation, (shown in Figure 3.10.9). If one can map linearly between the time and frequency domains, then both the analysis and synthesis filters are identical and linear. However, if the analysis filter is nonlinear due to practical constraints; then one can correct all the nonlinearity for the whole system by imposing the opposite nonlinearity on the synthesis filter [81].

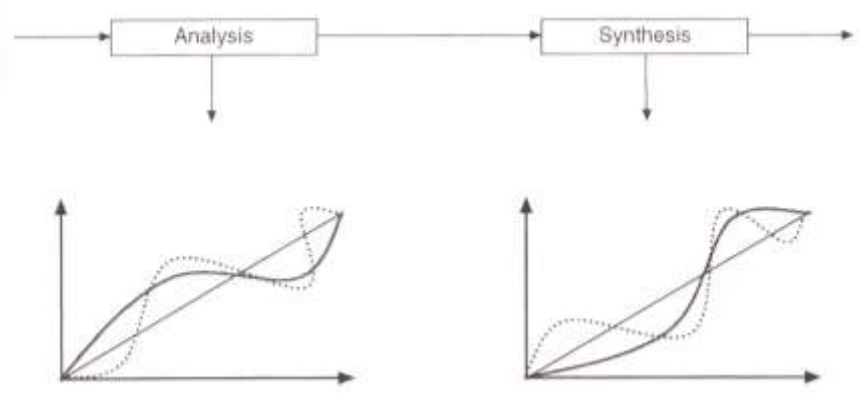

Figure 3.10.9 Linear and nonlinear mapping of the input and the output for the analysis and synthesis filters.

As shown in Figure 3.10.9, one can choose any kind of nonlinearity and correct it. The case of discontinuous signals will be highly susceptible to quantization error and noise,

whereas the continuous, smoother case probably will be more stable. The situation is very similar for the case of perfect reconstruction filter design.

3.11.0 TWO STAGE SUBBAND FILTER

The single-stage decimation-interpolation subband decomposition can be extended easily, as shown in Figure 3.11.1, where the original input sequence *x(n)* of length *N* is mapped into four sequences of *N/4* samples each. This is very important since basically *N* input samples are mapped using a $N \times N$ matrix to next output.

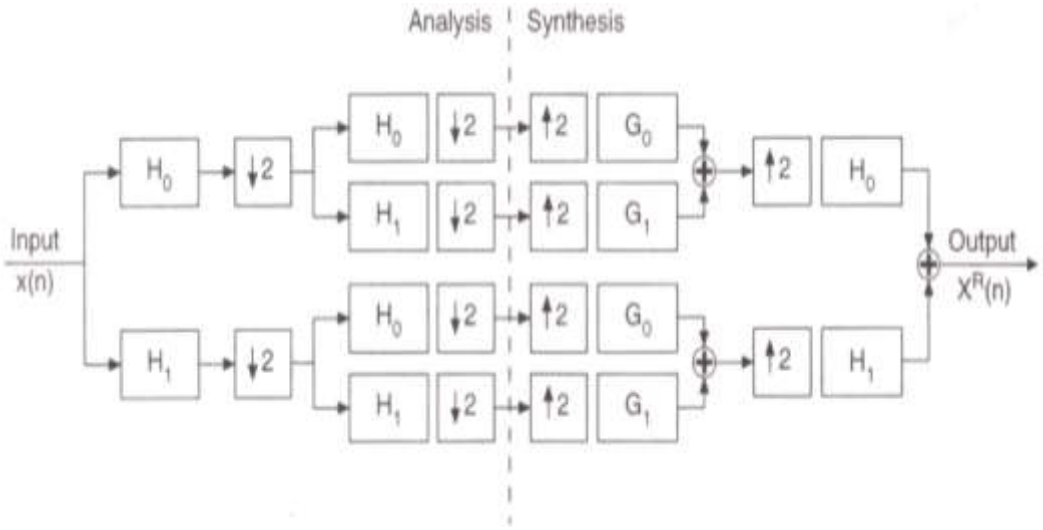

Figure 3.11.1 Two stage subband filter.

Figure 3.11.1, shows a two-stage analysis and synthesis filter. The filter responses are given in Figure 3.10.8a and they are mirror images around π/2; that is the reason for the name Quadrature Mirror Filter. For finite impulse response (FIR) filters which extends to N, the perfect reconstruction condition is satisfied provided that

$$G_0(z) = -H_1(z)$$

$$G_1(z) = -H_0(z) \qquad \text{---3.11.1}$$

$$H_1(z) = z^{-(N-1)} H_0(-z^{-1})$$

and in the discrete-time domain

$$h_1(n) = (-1)^{n+1} h_0(N-1-n)$$

$$g_0(n) = h_0(N-1-n) \qquad \text{---3.11.2}$$

$$g_1(n) = (-1)^n h_0(n)$$

Note that the above equations fully describe all the filters h_1, g_0 and g_1, once the filter *ho* has been defined. The conditions on h_0 are

$$\sum_{k=0}^{N-1} h(k)\ \ h(k+2n) = \delta_n \qquad \text{---3.11.3}$$

$$\left| H_1\left(e^{j\left[\frac{\pi}{2}-\omega\right]} \right) \right| = \left| H_0(e^{j\omega}) \right|$$

The above equation means that H_0 and H_1 are QMF as shown in Figure 3.11.1. As noted previously, they are called quadrature mirror filters because the magnitudes are a mirror image of each other, with the mirror placed at $\omega = \pi/2$. $H_1(z)$ is in quadrature to $G_0(z)$ and $Ho(z)$ is also in quadrature to $G_1(z)$. As H_0 has N taps, it is needed to determine N tap weights; however, only $N/2$ equations are specified. Thus, there is quite a bit of arbitrariness in the design. Theoretically, one can choose any other $N/2$ equations to design the filter, which will be perfect reconstruction.

3.12.0 PROPERTIES OF WAVELET

In this section, the properties of wavelet like Localized in time and frequency, Admissibility, Vanishing Moments, Compact support, Orthogonal, bi-orthogonal and symmetry have been discussed in brief [91].

3.12.1 LOCALIZED IN TIME AND FREQUENCY

Daughter wavelet is given as

$$h_{ab}(t) = \frac{1}{\sqrt{a}} h\frac{(t-b)}{a} \qquad \text{---3.12.1}$$

The Fourier Transform of $h_{ab}(t)$

$$H_{ab}(\omega) = F.T.\left\{ \frac{1}{\sqrt{a}} h\frac{(t-b)}{a} \right\}$$

$$H_{ab}(\omega) = \sqrt{a}\, H(a\omega) e^{-jwb} \qquad \text{---3.12.2}$$

The equation 3.12.1 and 3.12.2 shows that $h_{ab}(t)$ and $H_{ab}(\omega)$ has a finite length. It means that $h_{ab}(t)$ is localized in time and $H_{ab}(\omega)$ is localized in frequency and hence the mother wavelet h(t) is localized in time and frequency.

3.12.2 ADMISSIBILITY

Mother wavelet is said to be admissible if it has finite energy or mother wavelet must be square integrable.

$$\|h\|^2 = \int_{-\infty}^{\infty} |h(t)|^2 \, dt \; < +\infty \qquad \text{---3.12.3}$$

Which satisfies the following admissibility condition

$$C_H = \int_{-\infty}^{\infty} \frac{|H(\omega)|^2}{\omega} \, d\omega \; < \infty \qquad \text{---3.12.4}$$

For a band-limited mother wavelet h (t), the admissibility condition is equivalent to imposing the condition that the function has zero mean.

$$\int_{-\infty}^{\infty} h(t) \, dt \; = 0 \quad or \; H(\omega) \Big/_{\omega = 0} = 0 \qquad \text{---3.12.5}$$

Since mother wavelet is admissible the properties of linearity scaling and time shifting is applicable for CWT.

3.12.3 VANISHING MOMENTS

To measure the local regularity of the signal, it is not important to use wavelet with narrow frequency support, but vanishing moments are crucial. If the wavelet has the n vanishing moment, then we show that the wavelet transform can be interpreted as a multi-scale differential operator of order n. A wavelet has n vanishing moments if and only if its scaling function can generate polynomials of degree smaller than or equal to n. While this property is used to describe the approximating power of scaling functions, in the wavelet case it has a "dual" usage, e.g. the possibility to characterize the order of isolated singularities. The number of vanishing moments is entirely determined by the coefficients h[n] of the filter h which is featured in the scaling equation [83]. The wavelet h(t) has n vanishing moments, if

$$\int_{-\infty}^{+\infty} t^k \, h(t) \, dt = 0, \qquad for \quad 0 \le k \le n \qquad \text{---3.12.3.1}$$

3.12.4 COMPACT SUPPORT

If the impulse response of the filters h_1 and h_2 has a finite support, then the scaling functions have the same support, and the wavelets are compactly supported. If the supports of the scaling functions are respectively [N_1, N_2] and [M_1, M_2], then the

corresponding wavelets have support [(N_1-M_2+1)/2, (N_2-M_1+1)/2] and [(M_1-N_2+1)/2, (M_2-N_1+1)].

3.12.5 ORTHOGONAL

The orthogonal transform is useful tools for signal processing. Many filters have to be design so far to be applied to the transform domain. Suppose there is set of continuous functions {$h_0(t)$, $h_1(t)$, $h_2(t)$, …} of t. These functions, real or complex, are said to be orthogonal functions in the interval [t_0, t_0+T] [83], if

$$\int_{x0}^{x0+X} h_i(t)\,h_j(t)\,dt = \begin{cases} k & \text{if } i = j \\ 0 & \text{otherwise} \end{cases} \qquad \text{---3.12.6.1}$$

When k = 1 the set is called orthonormal.

3.12.6 BI-ORTHOGONAL

In a wavelet transform the separate filter for analysis and synthesis can be used. Let us consider h_1 and g_1 is low pass and high pass filter used for analysis and h_2 and g_2 are low pass and high pas filters used for synthesis [81, 85], then the condition for perfect reconstruction is

$$H_1^*(\omega+\pi)H_2(\omega)+G_1^*(\omega+\pi)G_2(\omega) = 0 \qquad \text{---3.12.7.1}$$

$$H_1^*(\omega)H_2(\omega)+G_1^*(\omega)G_2(\omega) = 2 \qquad \text{---3.12.7.2}$$

As the filter pairs (h_1, g_1) and (h_2, g_2) create basis for the representation of the any signal s[n] ε $L^2(Z)$, then the resulting wavelet and scaling functions represents bi-orthogonal Riesz bases in $L^2(Z)$.

3.12.7 SYMMETRY

Symmetric scaling functions and wavelets are important because they are used to build bases of regular wavelets over an interval, rather than the real axis. If the filters h_1 and h_2 have and odd length and are symmetric with respect to 0, then the scaling functions have an even length and are symmetric, and the wavelets are also symmetric. If the filters have an even length and are symmetric with respect to n=1/2, then the scaling functions are symmetric with respect to n=1/2, while the wavelets are antisymmetric. Daubechies has proved that, for a wavelet to be symmetric or antisymmetric, its filter must have a linear complex phase, and the

only symmetric compactly supported conjugate mirror filter is the Haar filter, which corresponds to a discontinuous wavelet with one vanishing moment. Besides the Haar wavelet, there is no symmetric compactly supported orthogonal wavelet.

3.13.0 WAVELET FAMILIES

In this section, most of the known families of mother wavelets, which have proven to be useful in a variety of signal processing applications, are discussed with their characteristics [12].

3.13.1 HAAR WAVELET

This is the simplest of all wavelets. This wavelet is discontinuous and resembles a step function. It is also referred as 'db_1' and it is defined as

$$h(t) = \begin{cases} 1 & 0 \le t \le 1/2 \\ -1 & 1/2 \le t \le 1 \\ 0 & \text{otherwise} \end{cases}$$

The scaling function and the wavelet function of Haar wavelet is shown in figure 3.13.1.1

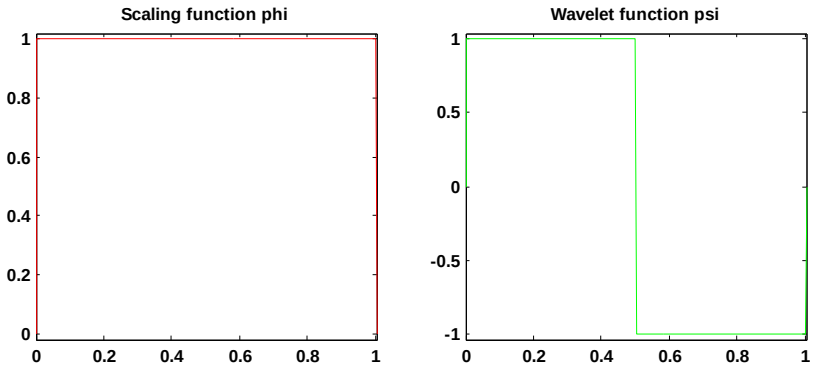

Figure 3.13.1.1 Scale function and wavelet function of Haar wavelet

The Haar wavelet has the shortest support among all orthogonal wavelets; it is not adapted to approximately smooth functions because it has only one vanishing moment.

3.13.2 DAUBECHIE WAVELETS

Ingrid Daubechies invented compactly supported orthogonal wavelets, and makes discrete wavelet analysis practical. The names of the Daubechies family wavelets are written db_N, where N is the order. The db_1 wavelet is same as Haar wavelet. Daubechies wavelets are extremely important, because it can be shown that they have the minimum support size for given number of N. Daubechies constructed her wavelets from the finite response of the conjugate mirror filter. These wavelets have no explicit expression except

for db_1, which is Haar wavelet. However, the square modulus of the transfer function of h is explicit, and fairly simple [12].

$$P(y)=\sum_{k=0}^{N-1} C_k^{N-1+k}\, y^k \qquad \text{---3.13.2.1}$$

where C_k^{N-1+k} *denotes the binomial coefficients.*

Then $$|m_0(\omega)|^2=\left(\cos^2\left(\frac{\omega}{2}\right)\right)^N P\left(\sin^2\left(\frac{\omega}{2}\right)\right) \qquad \text{---3.13.2.2}$$

where $m_0(\omega)=\frac{1}{\sqrt{2}}\sum_{k=0}^{2N-1} h_k e^{-ik\omega}$

The scaling function and the wavelet function of db_N wavelet for N = 1 to 9 is shown in figure 3.13.2.1 to 3.13.2.9

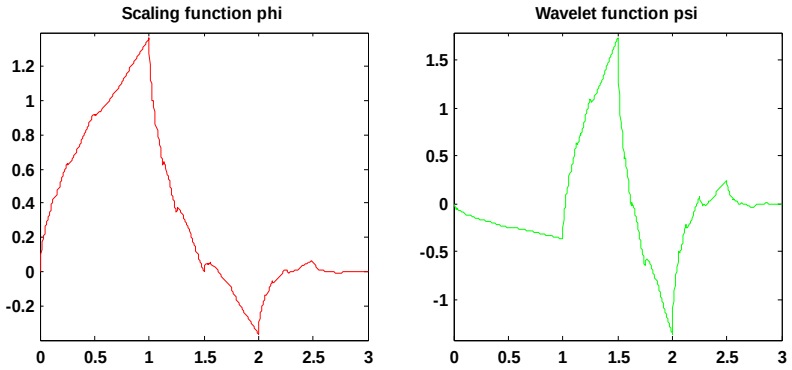

Figure 3.13.2.1 Scale function and wavelet function of db_2 wavelet

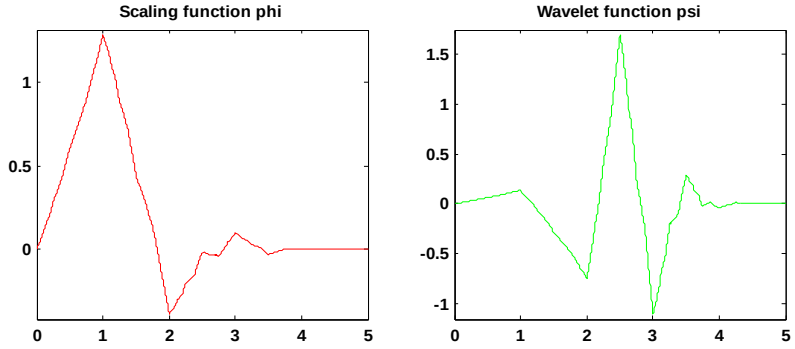

Figure 3.13.2.2 Scale function and wavelet function of db_3 wavelet

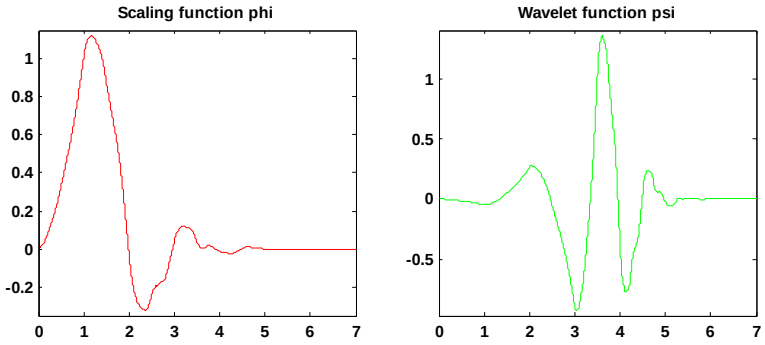

Figure 3.13.2.3 Scale function and wavelet function of db_4 wavelet

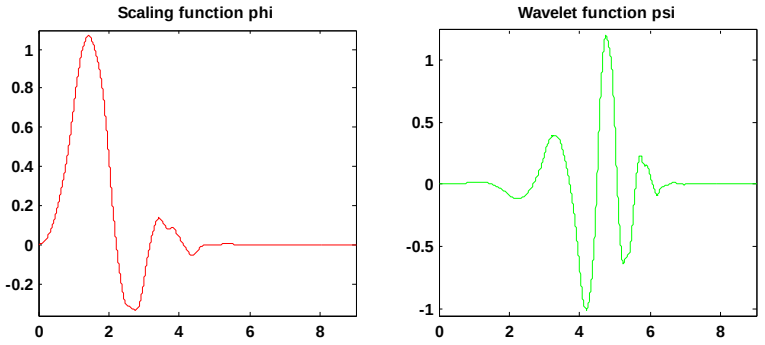

Figure 3.13.2.4 Scale function and wavelet function of db_5 wavelet

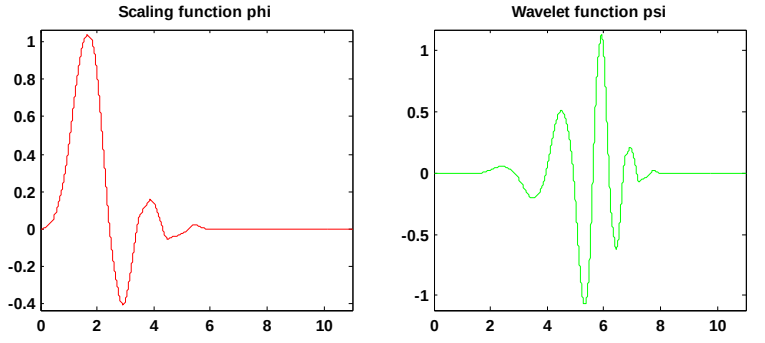

Figure 3.13.2.5 Scale function and wavelet function of db_6 wavelet

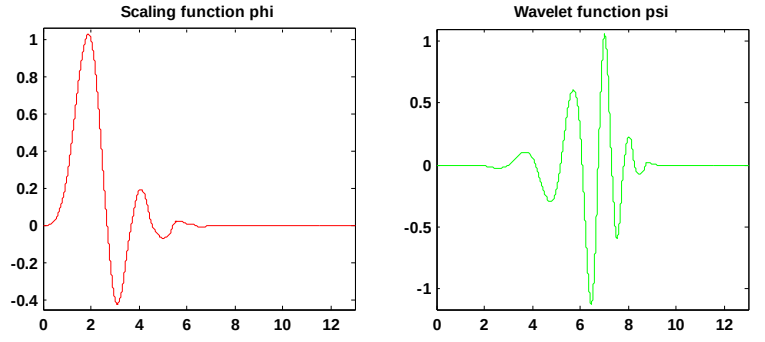

Figure 3.13.2.6 Scale function and wavelet function of db_7 wavelet

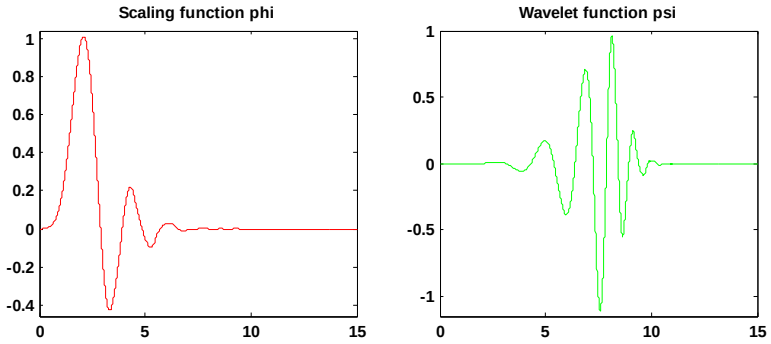

Figure 3.13.2.7 Scale function and wavelet function of db_8 wavelet

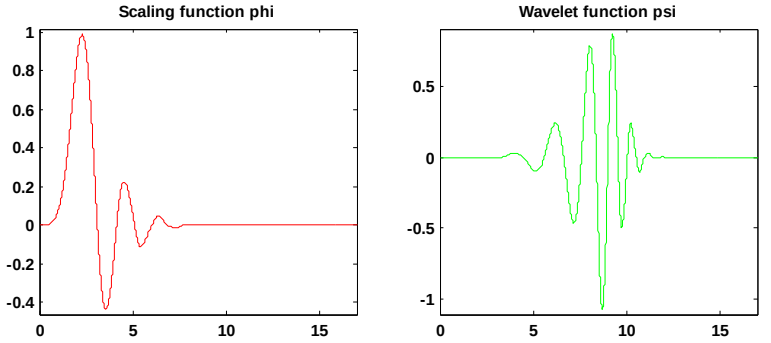

Figure 3.13.2.8 Scale function and wavelet function of db_9 wavelet

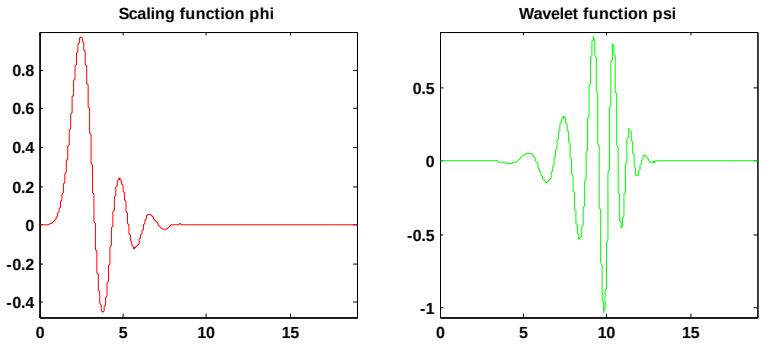

Figure 3.13.2.9 Scale function and wavelet function of db_{10} wavelet

General characteristics of Daubechies wavelet are:

- The supporting length of wavelet function ϕ and scaling function ψ is 2N – 1.
- The number of vanishing moments of ψ is N.
- The analysis is orthogonal.
- Filter length is 2N.

- Discrete wavelet transforms and continuous wavelet transform is possible.
- Order of N is 1, 2 ---- 48.
- It doesn't have explicit expression.
- It is asymmetrical.
- It has arbitrary regularity.
- It is compactly supported orthogonal.
- Exact reconstruction is possible.
- It is implemented using FIR filter.
- Fast algorithm is possible.

3.13.3 COIFLET WAVELETS

These mother wavelets built by Daubechies at the request of Coifman. It is also orthogonal wavelet; it is compactly supported wavelets with highest, number of vanishing moments for both phi and psi for given support width. These wavelets are written as $coif_N$, where N is the order. The function psi has 2N moments equal to zero and, what is more unusal, the function phi has 2N – 1 moments equal to zero. The two functions have a support of length 6N – 1. The $Coif_N$ psi and phi are much more symmetrical than the Db_{NS} with respect to the support length [12]. The scaling function and the wavelet function of $Coif_N$ wavelet for N = 1 to 5 is shown in figure 3.13.3.1 to 3.13.3.5

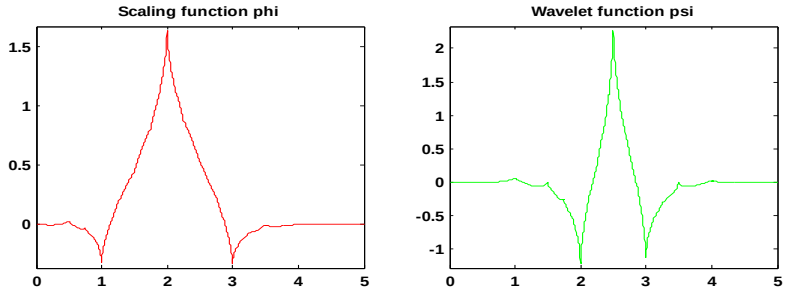

Figure 3.13.3.1 Scale function and wavelet function of $Coif_1$ wavelet

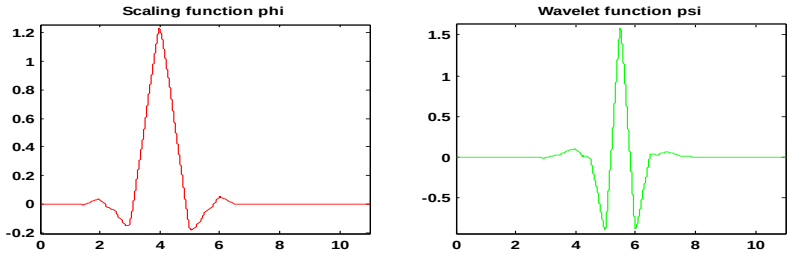

Figure 3.13.3.2 Scale function and wavelet function of $Coif_2$ wavelet

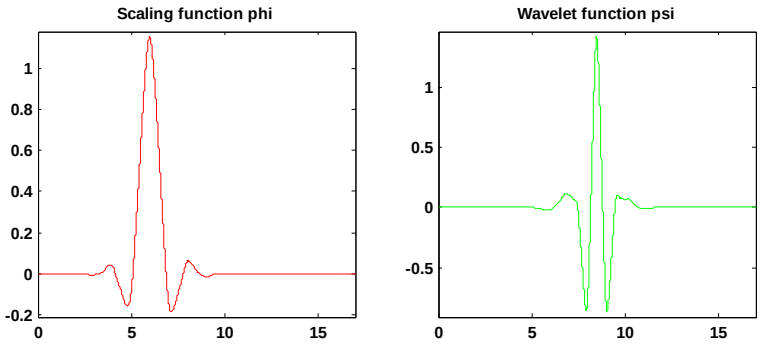

Figure 3.13.3.3 Scale function and wavelet function of Coif$_3$ wavelet

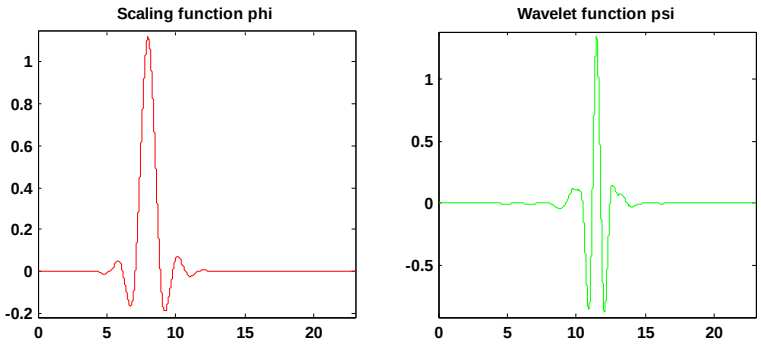

Figure 3.13.3.4 Scale function and wavelet function of Coif$_4$ wavelet

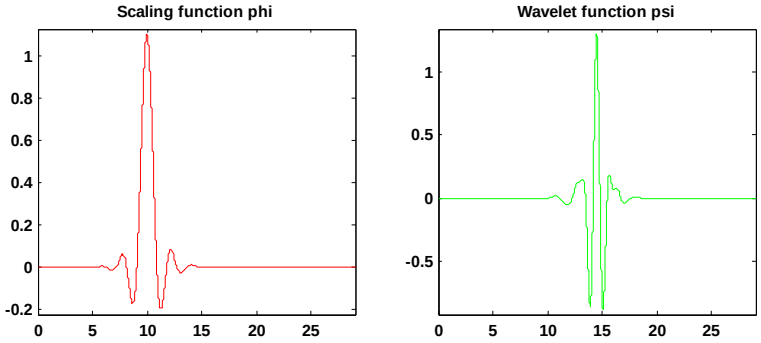

Figure 3.13.3.5 Scale function and wavelet function of Coif$_5$ wavelet

General characteristics of Coiflet wavelets are:

- The supporting length of wavelet function ϕ and scaling function ψ is 6N – 1.
- The number of vanishing moments of ψ is 2N and ϕ is 2N – 1.
- The analysis is orthogonal.
- Filter length is 6N.
- Discrete wavelet transforms and continuous wavelet transform is possible.
- Order of N is 1, 2, ----5.
- It doesn't have explicit expression.

- It is nearly symmetrical.
- It is arbitrary regular.
- It is compactly supported orthogonal.
- Exact reconstruction is possible.
- It is implemented by using FIR filters.
- Fast algorithm is possible.

3.13.4 BIORTHOGONAL WAVELETS

It is compactly supported Biorthogonal wavelets for which symmetry and exact reconstruction are possible with FIR filters. Biorthogonal wavelets written as bior N_r,N_d, where N_r, is order of wavelet, which is used for reconstruction and N_d, is order of wavelet, which is used for decomposition. Two wavelets, instead of just one, are introduced:

- One, $\tilde{\psi}$, is used in the analysis, and the coefficients of a signal s are:

$$\tilde{C}_{j,k} = \int s(x)\tilde{\psi}_{j,k}(x)dx \qquad \text{---3.13.4.1}$$

- The other ψ, is used in the synthesis

$$s = \sum_{j,k} \tilde{C}_{j,k} \psi_{j,k} \qquad \text{---3.13.4.2}$$

The scaling function and the wavelet function of Bior N_r, N_d wavelet for analysis and synthesis are shown in figure 3.13.4.1 to 3.13.4.15.

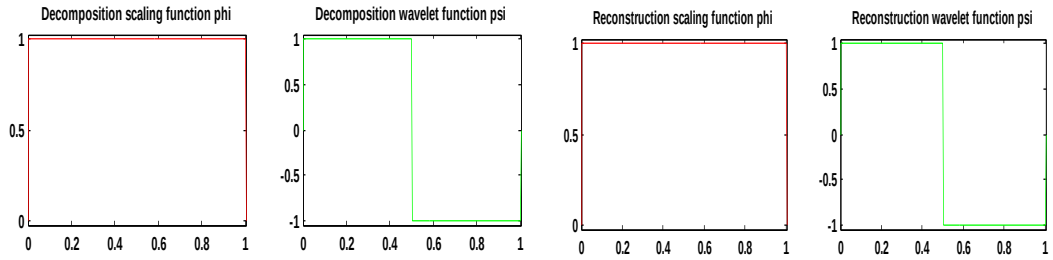

(a) **(b)**

Figure 3.13.4.1 Scale function and wavelet function of Bior1.1 wavelet for (a) analysis and (b) Synthesis

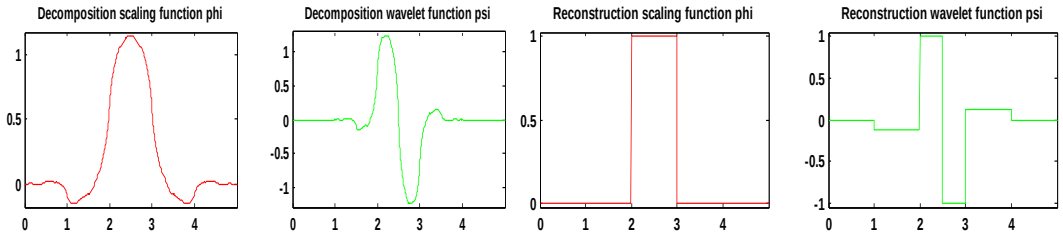

(a) **(b)**

Figure 3.13.4.2 Scale function and wavelet function of Bior1.3 wavelet for (a) analysis and (b) Synthesis

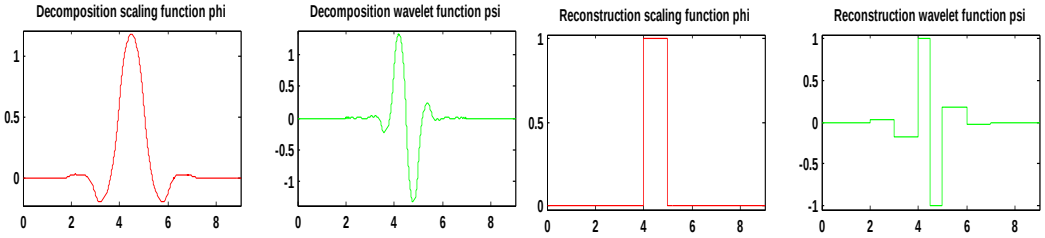

(a) **(b)**

Figure 3.13.4.3 Scale function and wavelet function of Bior1.5 wavelet for (a) analysis and (b) Synthesis

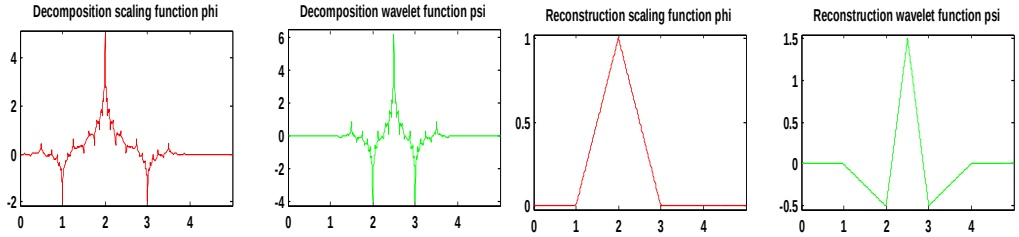

(a) **(b)**

Figure 3.13.4.4 Scale function and wavelet function of Bior2.2 wavelet for (a) analysis and (b) Synthesis

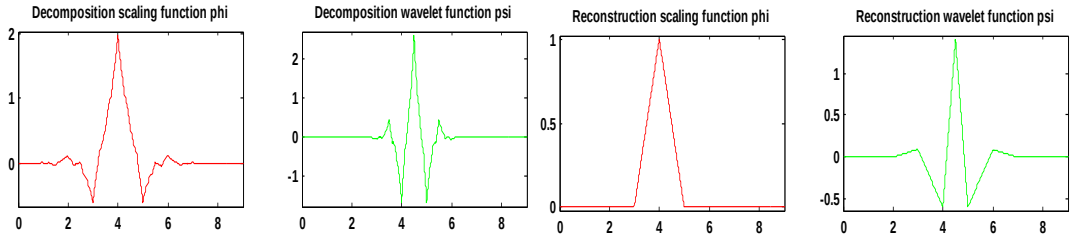

(a) **(b)**

Figure 3.13.4.5 Scale function and wavelet function of Bior2.4 wavelet for (a) analysis and (b) Synthesis

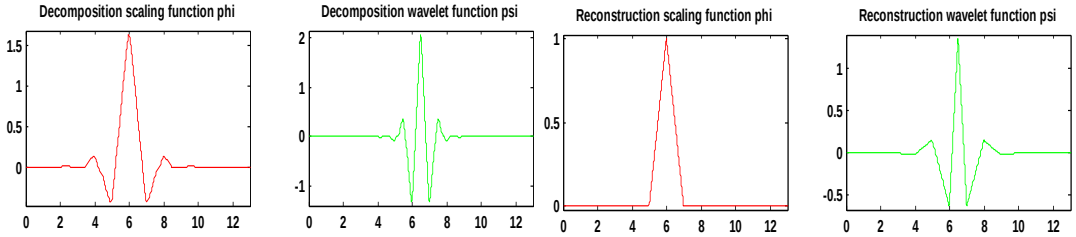

(a) **(b)**

Figure 3.13.4.6 Scale function and wavelet function of Bior2.6 wavelet for (a) analysis and (b) Synthesis

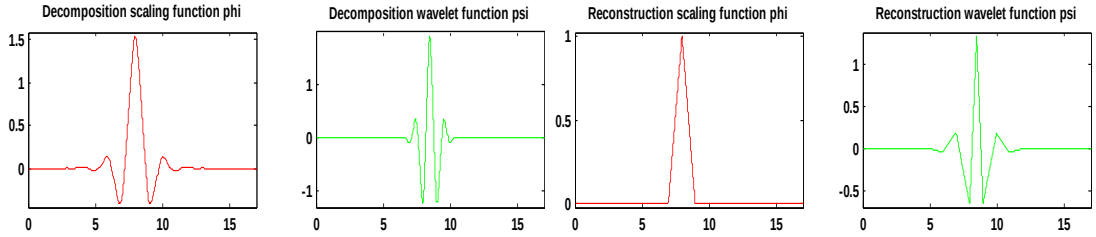

(a) **(b)**

Figure 3.13.4.7 Scale function and wavelet function of Bior2.8 wavelet for (a) analysis and (b) Synthesis

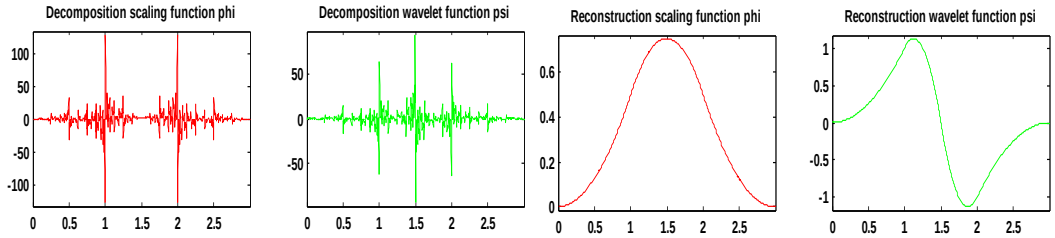

(a) **(b)**

Figure 3.13.4.8 Scale function and wavelet function of Bior3.1 wavelet for (a) analysis and (b) Synthesis

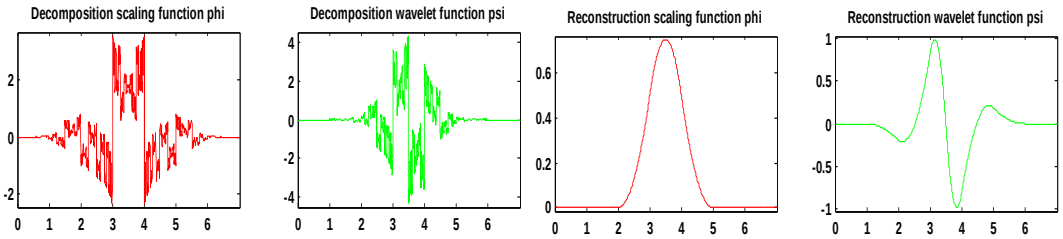

(a) **(b)**

Figure 3.13.4.9 Scale function and wavelet function of Bior3.3 wavelet for (a) analysis and (b) Synthesis

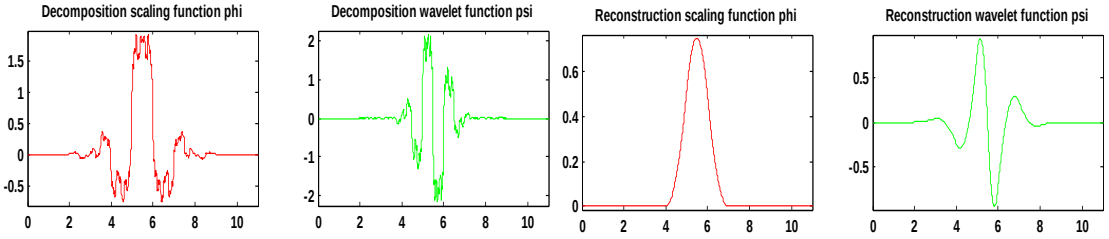

(a) **(b)**

Figure 3.13.4.10 Scale function and wavelet function of Bior3.5 wavelet for (a) analysis and (b) Synthesis

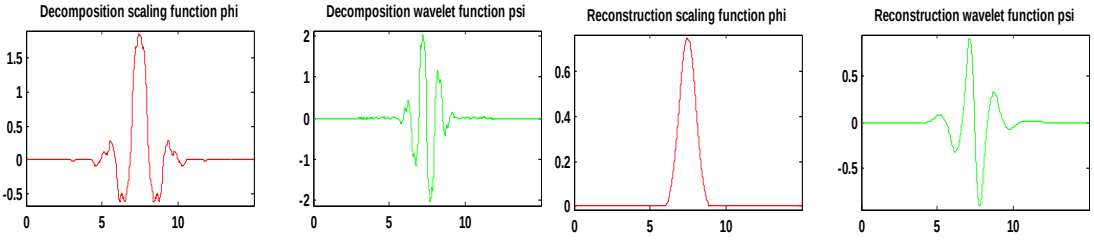

(a) **(b)**

Figure 3.13.4.11 Scale function and wavelet function of Bior3.7 wavelet for (a) analysis and (b) Synthesis

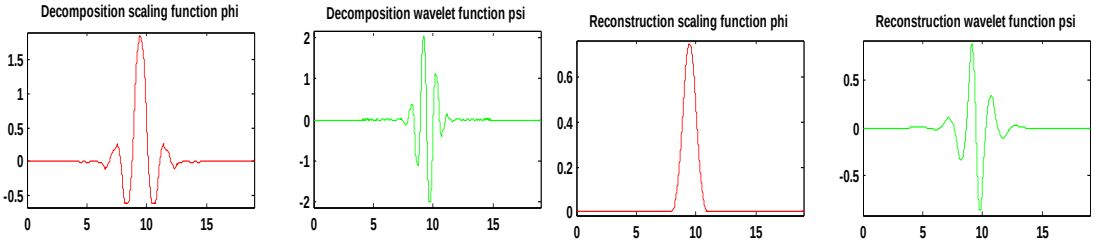

(a) **(b)**

Figure 3.13.4.12 Scale function and wavelet function of Bior3.9 wavelet for (a) analysis and (b) Synthesis

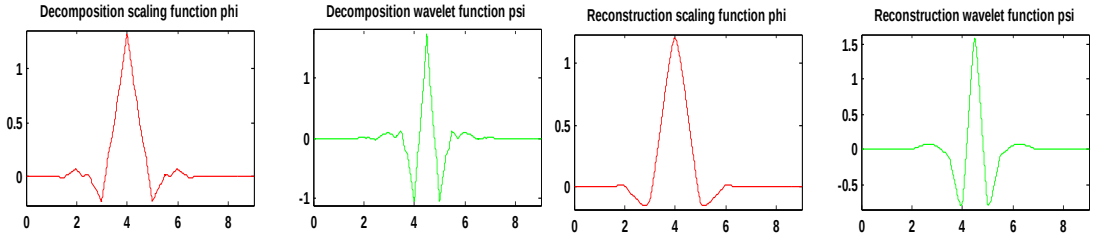

(a) **(b)**

Figure 3.13.4.13 Scale function and wavelet function of Bior4.4 wavelet for (a) analysis and (b) Synthesis

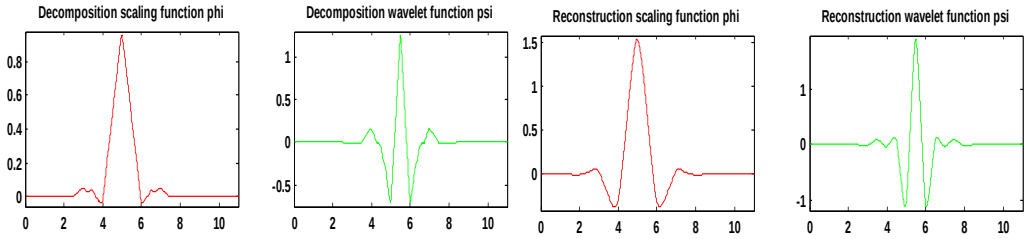

(a) **(b)**

Figure 3.13.4.14 Scale function and wavelet function of Bior5.5 wavelet for (a) analysis and (b) Synthesis

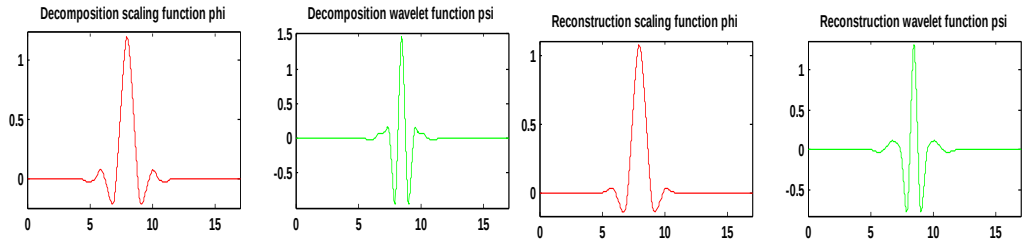

(a) **(b)**

Figure 3.13.4.15 Scale function and wavelet function of Bior6.8 wavelet for (a) analysis and (b) Synthesis

General characteristics of Biorthogonal wavelets are:

- The supporting width of wavelet $2N_r + 1$ for reconstruction and $2N_d + 1$ for decomposition.
- The number of vanishing moments of ψ is N_r.
- The analysis is not orthogonal.
- Filter length is max $(2N_r, 2N_d) + 2$.
- Discrete wavelet transforms and continuous wavelet transform is possible.
- It doesn't have explicit expression except for splines.
- It is symmetrical.
- It is arbitrary regular.
- Exact reconstruction is possible.
- It is implemented by using FIR filters.
- Fast algorithm is possible.

3.14.0 THE DISCRETE WAVELET TRANSFORMS

Calculating wavelet coefficients at every possible scale is a fair amount of work, and it generates huge amount of data. If only a subset of scale, and positions the data are selected then the size of the data may be reduced significantly. It turns out, rather remarkably, that if scales and positions base on the power of two are selected (so called dyadic scales and positions), then the analysis will be much more efficient and accurate. And such analysis is possible from the discrete wavelet transform. In the case of Continuous Wavelet Transform the scaling 'a' and delay 'b' are assumed to be continuous in value and hence in a result of continuous wavelet transform redundancy of signal is present. This redundancy can be reduced by discretizing the transform parameter (a, b).

$$a = a_0^j, \quad a_0 \neq 1, \ j \in z \qquad \text{---3.14.1}$$

Where a_0 is constant but not equal to one, and m is any positive integer. Parameter b is also chosen as power of two.

$$b = k.a_0^j = k.a \qquad \text{where} \qquad k \in z$$

If $a_0 = 2$, $a = 2^j$ and $b = k\ 2^j$

The Discrete Wavelet Transform of continuous time signal is given by the equation.

$$C(a,b) = \int_R s(t)\psi_{ab}(t)dt \qquad \text{---3.14.2}$$

Where $\psi_{ab}(t) = \frac{1}{\sqrt{|a|}} \frac{\psi(t-b)}{a}$ and $a = 2^j$, $b = k\ 2^j$, $(j,k) \in Z^2$

In 1998, Ingrid Daubechies and Mallet [12] discovered that the wavelet transform could be implemented with a specially designed Finite Impulse Response (FIR) filter pair. The filter banks are in effect a fast way of implementing the Discrete Wavelet Transform for orthogonal wavelets the filter banks are a set of Quadrature Mirror Filters [81].

The analysis bank has two filters low pass and high pass. These filter separate the input signal into low and high frequency banks. This process is called as wavelet decomposition. The low frequency components of the signal are known as approximations and high frequency components are known as details. When one performs the filtering operation on real digital signal, then it winds up with twice as much data as one started with

[12]. Using down sampling after the filtering solves this problem. Figure 3.14.1 shows one-stage Discrete Wavelet Transform of signal 'S'.

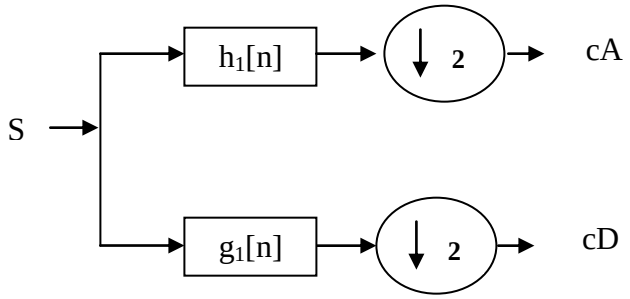

Figure 3.14.1 one-stage Discrete Wavelet Transform of signal S

Where $h_1[n]$ and $g_1[n]$ are the impulse response of low pass and high pass filter, and cD and cA are detail coefficients and approximate coefficients of signal S.

It is observed that the actual length of the detail and approximation coefficients vectors are slightly more than half of the length of the original signal, because filtering process is implemented by convolving the signal with filter.

The decomposition process can be iterated, with successive approximations being decomposed in turn, so that one signal is broken down into many lower resolution components. This is called the wavelet decomposition tree as shown in figure 3.14.2.

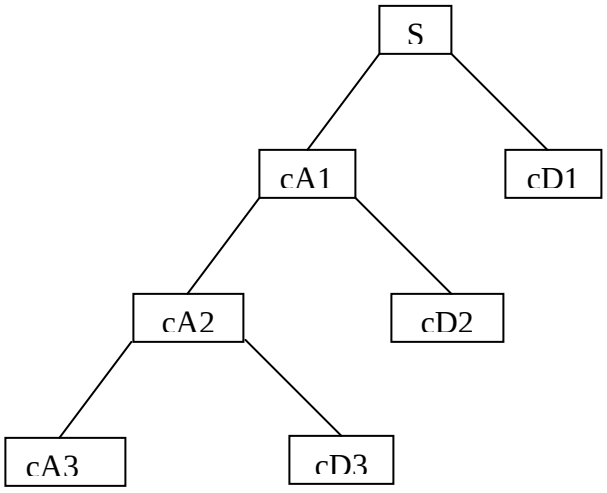

Figure 3.14.2 Three level decomposition tree

The wavelet reconstruction process is just reversed to the decomposition process. It consists of up sampling and filtering as shown in figure 3.14.3.

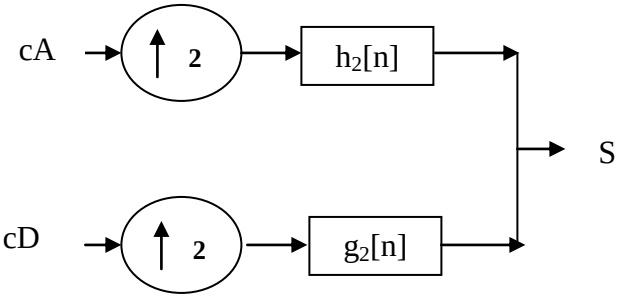

Figure 3.14.3 Signal reconstruction process

Where $h_2[n]$ and $g_2[n]$ are the impulse response of low pass and high pass filter, and cD and cA are detail coefficients and approximate coefficients of signal S.

3.15.0 TWO DIMENSIONAL DWT

Two dimensional wavelet transform is applicable to analyze the two-dimensional signal such as image. A two-dimensional wavelet transform is readily computed by combining the one-dimensional basis transform for both the dimensions (horizontal and vertical). In two dimensional wavelet transform the process breaks the original band into four sub-bands: one tuned for low frequency (approximation), one tuned for vertical high frequency (vertical details), one tuned for horizontal high frequency (horizontal detail), and one tuned for both orientations of diagonal high frequency (diagonal details). This kind of two-dimensional DWT leads to decomposition of approximation coefficients at level j in four components: the approximation at level j+1 and the details in three orientations (horizontal, vertical and diagonal). The figure 3.15.1 shows the basic decomposition steps.

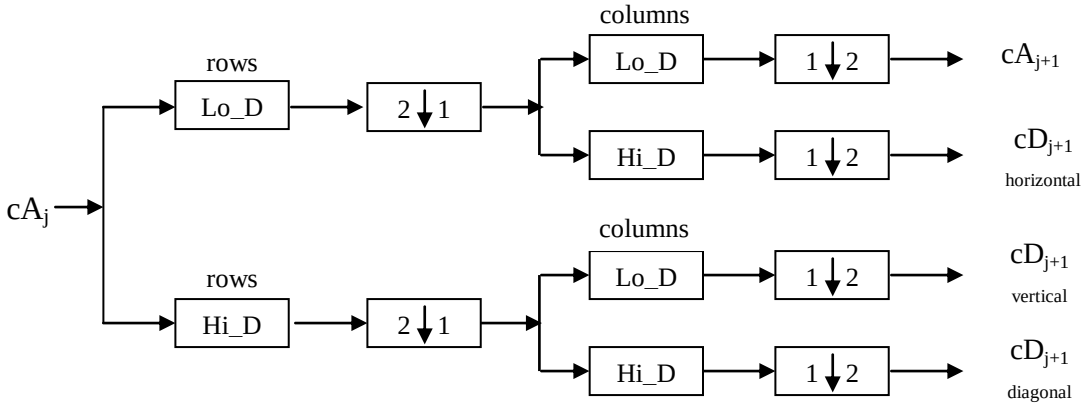

Figure 3.15.1 Two-Dimensional DWT Decomposition

The decomposition phase has two filters: low pass and high pass. These filters separate the input signal into low and high frequency components. The two-dimensional signal first filtered row wise, and down sampled by the amount of two. Then, the procedure is repeated for the column components of two-dimensional signals. This process is called as wavelet decomposition of two-dimensional signal. The low frequency components of row and column of two-dimensional signals are known as approximations, low frequency components of row and high frequency components of column of two-dimensional signal are known as horizontal details, high frequency components of row and low frequency components of column of two-dimensional signal are known as vertical details, and high

frequency components of row and high frequency components of column of two-dimensional signal are known as diagonal.

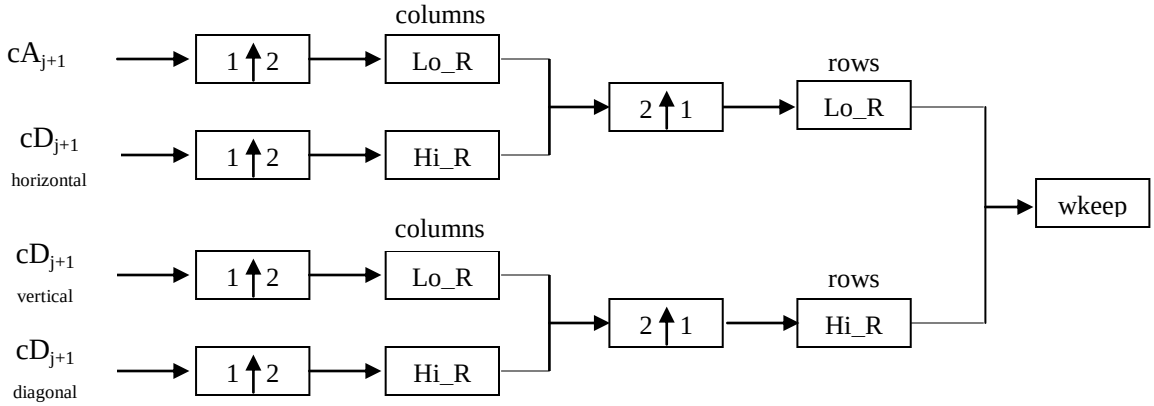

Figure 3.15.2 shows the basic reconstruction steps

In reconstruction stage the approximate and detail components are first up sampled with the factor of two, and the row components, and column components are separately filtered with the reconstruction low pass, and high pass filters. Sum of the filtered components are again up sampled with the factor of two, and again filtered with low pass and high pass filters. The filtered components when added reconstruct the original signal.

3.16.0 WAVELET PACKET

The weakness of wavelet transform is that it fails to capture high frequency components of an image, and hence, another transform method must be employed. Coifman, Meyer and Wickerhauser developed the technique, which was based on the wavelet transform and known as wavelet packets. Wavelet packets are better able to represent the high frequency information [74].

Wavelet packets represent a generalization of multi-resolution decomposition. In wavelet, the decomposition is applied recursively to the coarse scale approximation, whereas in the wavelet packets decomposition, the recursive procedure is applied to the coarse scale approximation along with horizontal detail, vertical detail, and diagonal detail, which leads to a complete binary tree. Wavelet packets is an extension of the octave band wavelet decomposition to a full tree decomposition by allowing the low pass filtering, high pass filtering and down sampling procedure to be iterated on approximate and details. High pass branches in the tree, add more flexibility in frequency resolution. Wavelet packets decomposition leads to the 4^J sub-bands at decomposition level 'J' [79].

Tree structure of wavelet packets decomposition up to third level is shown in figure 3.16.1.

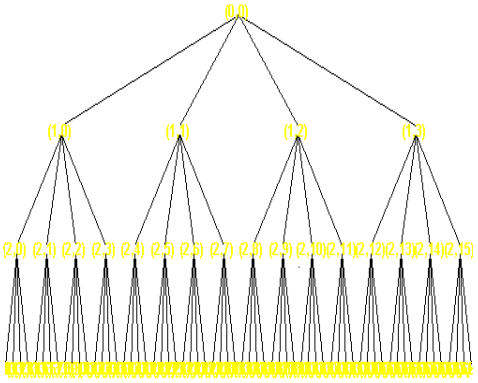

Figure 3.16.1:The tree structure of wavelet packets decomposition up to third level

The original signal S, referred as (0,0) is decomposed at first level to generate four successors as approximation (1,0), horizontal detail (1,1), vertical detail (1,2), and diagonal detail (1,3). Further, these successors are decomposed at second level to generate total sixteen successors namely (2,0), (2,1), (2,2), (2,3), (2,4), (2,5), (2,6), (2,7), (2,8), (2,9), (2,10), (2,11), (2,12), (2,13), (2,14), (2,15). Similar process is carried out at third level also to yield total sixty-four successors as leaves of the tree. Decomposition process includes low pass, high pass filtering for rows of two-dimensional signal followed by down sampling with amount of two. Then, the procedure is repeated for the column components of two-dimensional signals.

CHAPTER 4
IMPLEMENTATION OF ALGORITHMS

4.1.0 INTRODUCTION

Literature survey reveals that the majority of the compression techniques used were focused on Discrete Cosine Transform (DCT) and Discrete Wavelet Transform (DWT). The Discrete Wavelet Transform (DWT) has become the popular transform for image compression. The varieties of Discrete Wavelet Transform (DWT) were invented and used for image compression. The Discrete Wavelet Transforms have many advantages and disadvantages, which are already discussed in chapter two. The fundamentals of wavelet and wavelet packet tree are discussed in chapter three. There is a wide scope to develop the new methods of image compression using wavelet packet tree. Generally the image compression methodology is constituted by three stages mainly: i) Transformation ii) Qunatization / Thresholding, and iii) Encoding. For the optimum image compression, that is, high compression ratio and good visual image quality, there is a need, to select appropriate and efficient transformation technique, to select the proper values of threshold, and efficient encoding technique. This chapter includes: selection of wavelet transform, the comparison of wavelet and wavelet packet tree, selection of best basis based on various entropies, proposed technique of best basis selection, proposed adaptive threshold calculations based on nature of image, modified lossy encoding techniques with quantitative results, and intermediate conclusions.

4.2.0 WAVELET SELECTION FOR IMAGE COMPRESSION

Haar [23] described the first wavelet basis in 1910. In 1986 many researchers performed pioneering work in wavelets, particularly in multi-resolution and fast wavelet transforms. The researchers developed a wide variety of wavelets. The major wavelets are Daubechies Wavelet, Coiflets Wavelet, Biorthogonal Wavelet, Symlets Wavelet, Morlet Wavelet, and Mayer Wavelet. These wavelets are used to transform the signals from one domain to another domain. Wavelet transform is a two-dimensional time-frequency signal analysis method. Wavelet Transform (WT) represents an image as a sum of wavelet functions (wavelets) with different locations and scales [86]. Any decomposition of an image using wavelet involves a pair of waveforms, one to represent the high frequencies corresponding to the detail parts of an image (wavelet function), and another for the low frequencies or smooth parts of an image (scaling function). Integer Wavelet Transform and Discrete Wavelet Transform would be used for lossy

compression. In the paper [41] the researchers claimed that Integer Wavelet Transform could lead to too much larger degradation than the Discrete Wavelet Transform; especially Discrete Wavelet Transform is popular in the field of compression for small quantization rather than Integer Wavelet Transform. All the wavelets are not suitable for the image compression. Among the many suitable wavelets, for image compression choice of wavelet is crucial for coding performance in image compression [5]. The choice of the wavelet function should be adjusted to image content. The compression performance for images with high spectral activity is fairly insensitive to choice of compression method (for example, test image Mandrill), on the other hand coding performance for the images with moderate spectral activity (for example, test image Lena), are more sensitive to choice of compression method. The best way for choosing wavelet function is to select optimal basis for images with moderate spectral activity. This wavelet gives satisfying results for other types of images. It is also noticed that selection of the optimal wavelet for image compression is based on objective picture quality measures, and subjective picture quality measures.

Important properties of wavelet in image compression are: compact support (leads to efficient implementation), symmetry (useful in avoiding dephasing in image processing), orthogonality (allows fast algorithm), regularity and degree of smoothness (related to filter order or filter length) [86]. These properties of most of the well-known wavelets are discussed in detail in chapter three. The wavelets are implemented by using different ordered quadratic filters. The subband coding system is based on the frequency selectivity property of the filter banks. An alias free frequency split and perfect inter-band decorrelation of coefficients can be achieved only with ideal filter bands with infinite duration basis functions. Since time localization of the filters is very important in visual signal processing, one cannot use an arbitrarily long filter. In addition properties such as vanishing moments, phase linearity, time-frequency localization, energy compaction etc., influence the coding performance. Filter length is determined by filter order, the relationship between filter order and filter length is different for different wavelet families. Higher filter order gives wide function in the time domain with higher degree of smoothness its results blurring of an image even if the PSNR is high, and filter has good frequency localization, which in turns increases, the energy compaction. The regularity of wavelets also increases with filter order. In addition more vanishing moments can be obtained with a higher order filter. Filter with lower order has a better time localization and preserves important edge information. The low order filters provides less energy compaction and more blockiness. Wavelet based image

compression prefers smooth functions, but complexity of calculating Discrete Wavelet Transform increases by increasing the filter length. Therefore, in image compression there is a need to find a balance between filter length, degree of smoothness and computational complexity. Inside each wavelet family, one can find wavelet function that represents optimal solution related to filter length and degree of smoothness, but this solution depends on image contents [86]. The length of the filter and computational complexity of the wavelet transform for an image of size M × M, employing dyadic decomposition is approximately.

$$L = 2 \times N \text{ for Daubechies Wavelet family,}$$

$$L = 6 \times N \text{ for Coiflet Wavelet Family and}$$

$$L = \max(2Nd, 2Nr) + 2 \text{ for Biorthogonal Wavelet family}$$

Computational Complexity, $C = 16 \times M^2 \times L\,(1 - 4^{-J}) / 3$

Where N is the order of filter, L is the length of the filter; J is number of level decomposition.

In the analysis process four families of wavelets, mostly used and examined by the researchers named as: Haar wavelet, Daubechies wavelet, Coiflet wavelet, and Biorthogonal wavelet. These wavelets are tested over many test images, which include different natural images of varying frequencies, and synthetic images having characteristics different than natural images. Each wavelet family can be parameterized by integer N, which determines the filter order. Biorthogonal wavelets can use filters with similar or dissimilar order for decomposition and reconstruction of signals. Nd denotes the order of decomposition filter, and Nr denotes the order of reconstruction filter. Each wavelet family is tested with different filter orders. The Daubechies wavelets db_N is tested for the order of filter, N = 1 to 44, the Coiflet wavelet $Coif_N$ is tested for the order of filter, N = 1, 2, 3, 4, 5; and the Biorthogonal wavelet Bior $_{NrNd}$ is tested for the order of reconstruction and decomposition filter (Nr . Nd) = 1.1, 1.3, 1.5, 2.2, 2.4, 2.6, 2.8, 3.1, 3.3, 3.5, 3.7, 3.9, 4.4, 5.5, and 6.8. The experimental results are given in terms of percentage of zeros, energy retained, and peak signal to noise ratio for the fixed value of threshold. The peak signal to noise ratio is one of the important objective measures. Higher the value of PSNR better the quality of an image, more percentage of zeros might be responsible for more compression, and high value of the energy retained shows the less loss of the information.

Table 4.2.1 to 4.2.5 shows the comparative results of wavelet db_1 to db_{45} for different natural and synthetic images. Table 4.2.6 to 4.2.10 shows the comparative results of wavelet Bior1.1 to Bior6.8 for different natural and synthetic images. Table

4.2.11 to 4.2.15 shows the comparative results of wavelet $Coif_1$ to $Coif_5$ for different natural and synthetic images. The results are given in terms of percentage of zeros, energy retained, and peak signal to noise ratio. The natural test images are Aishwarya, Cheetah, Lena, Woman, Barbara, Mandrill, and synthetic test images are butterfly, diagonal line based images, vertical line based images, and horizontal line based images.

Table 4.2.1 Results of Daubechies wavelets db_N (where N = 1 to 44) for Aishwarya and Cheetah images

Wavelet	AISHWARYA			CHEETAH		
	Percentage of Zeros	Percentage of Energy Recover	Peak Signal to Noise Ratio (dB)	Percentage of Zeros	Percentage of Energy Recover	Peak Signal to Noise Ratio (dB)
db1	92.515	99.8901	82.9103	88.5544	99.773	71.361
db2	93.1336	99.9464	89.9897	90.2095	99.8496	75.3626
db3	**93.1808**	**99.9561**	**91.9226**	**90.515**	**99.8677**	**76.6027**
db4	**93.0832**	**99.9591**	**92.476**	**90.4597**	**99.8769**	**77.2279**
db5	**93.1008**	**99.9616**	**92.8383**	**90.5461**	**99.8869**	**78.0073**
db6	**93.0035**	**99.963**	**93.1425**	**90.2583**	**99.8957**	**78.8606**
db7	92.9712	99.9624	92.9496	90.1724	99.9025	79.5673
db8	92.8942	99.9633	93.0017	90.0284	99.9055	79.877
db9	92.8538	99.9642	93.1481	90.0271	99.9042	79.5326
db10	92.7375	99.9645	93.1523	89.9486	99.9071	79.1013
db11	92.693	99.9643	93.09	89.8772	99.8986	79.0239
db12	92.5936	99.9651	93.1111	89.7706	99.901	79.1585
db13	92.5617	99.9642	93.0721	89.6793	99.9042	79.574
db14	92.4536	99.9645	92.824	89.4334	99.9071	80.045
db15	92.4031	99.9643	92.8945	89.3155	99.9093	80.2545
db16	92.3236	99.9635	92.8266	89.2107	99.9081	80.155
db17	92.2705	99.9643	92.6923	89.1185	99.9044	79.747
db18	92.1824	99.9632	92.6993	89.084	99.9016	79.3924
db19	92.1767	99.9642	92.7258	89.1027	99.9014	79.3373
db20	92.0505	99.963	92.4308	88.7479	99.9027	79.6414
db21	92.0348	99.9631	92.514	88.8215	99.9043	79.8837
db22	91.9617	99.9642	92.4659	88.6029	99.9065	80.258
db23	91.9298	99.9614	92.1929	88.4092	99.9051	80.2552
db24	91.8647	99.9631	92.2589	88.4261	99.9042	80.0913
db25	91.822	99.9632	92.2884	88.4178	99.9016	79.6871
db26	91.7446	99.9626	92.1675	88.2374	99.8999	79.5619
db27	91.7181	99.9635	92.152	88.2947	99.9	79.5961
db28	91.6306	99.9624	92.0132	88.1738	99.9008	79.6998
db29	91.607	99.9626	91.9303	87.9984	99.903	80.1496
db30	91.5358	99.9623	91.8635	87.8645	99.9033	80.3484
db31	91.4883	99.9621	91.7832	87.873	99.9021	80.1254
db32	91.4269	99.9613	91.6806	87.6527	99.9005	80.0021
db33	91.392	99.962	91.7793	87.7164	99.8984	79.6744
db34	91.2833	99.9622	91.6369	87.6492	99.8969	79.463
db35	91.2929	99.9608	91.6279	87.5358	99.8981	79.6343
db36	91.1922	99.9617	91.5382	87.3335	99.8996	79.8305
db37	91.1729	99.9599	91.3749	87.3335	99.9001	79.9594
db38	91.0956	99.9612	91.3469	87.0985	99.9016	80.1797
db39	91.0747	99.9598	91.3551	86.9662	99.9004	80.0921
db40	91.0126	99.96	91.2378	87.0167	99.8998	79.8067
db41	90.9727	99.9612	91.2972	86.9191	99.8985	79.5819
db42	91.2929	99.9608	91.6279	87.5358	99.8981	79.6343
db43	91.1729	99.9599	91.3749	87.3335	99.9001	79.9594
db44	91.0747	99.9598	91.3551	86.9662	99.9004	80.0921

Table 4.2.2 Results of Daubechies wavelets db_N (where N = 1 to 44) for Lena and Woman images

Wavelet	LENA			WOMAN		
	Percentage of Zeros	Percentage of Energy Recover	Peak Signal to Noise Ratio (dB)	Percentage of Zeros	Percentage of Energy Recover	Peak Signal to Noise Ratio (dB)
db1	91.1836	99.8702	79.6658	78.3301	99.6721	65.0408
db2	92.4404	99.933	86.1184	80.4057	99.6941	65.5944
db3	**92.7403**	**99.9454**	**88.0905**	**80.9294**	**99.7133**	**65.8308**
db4	**92.7068**	**99.951**	**89.031**	**81.0816**	**99.721**	**65.9379**
db5	**92.7186**	**99.9535**	**89.478**	**80.7867**	**99.735**	**66.0668**
db6	**92.6819**	**99.9552**	**89.7161**	**81.0561**	**99.7366**	**65.9977**
db7	**92.6472**	**99.9563**	**89.8909**	**80.8188**	**99.7465**	**66.0396**
db8	92.5582	99.9566	89.8198	80.7029	99.749	65.9844
db9	92.5291	99.959	89.9924	80.4564	99.7773	66.0426
db10	92.4682	99.9592	90.0067	80.5045	99.7783	66.0189
db11	92.4298	99.958	89.8304	80.14	99.7676	66.0174
db12	92.3296	99.9589	89.8477	80.0252	99.7707	65.9982
db13	92.3487	99.959	89.7844	79.8227	99.7773	66.0597
db14	92.2401	99.9592	89.7291	79.5312	99.7783	66.0011
db15	92.1995	99.9595	89.7272	79.4413	99.7843	65.9779
db16	92.1455	99.9601	89.6914	79.2044	99.7866	65.9706
db17	92.107	99.9599	89.6199	79.0838	99.7923	65.9781
db18	92.0079	99.9601	89.4307	78.9788	99.7945	65.9262
db19	92.0082	99.961	89.5035	78.8199	99.7977	65.8304
db20	91.9199	99.9603	89.4201	78.6394	99.7996	65.8367
db21	91.8787	99.9603	89.2959	78.1963	99.8062	65.8968
db22	91.8103	99.9617	89.3957	78.2304	99.8086	65.9645
db23	91.7799	99.9616	89.3471	77.9205	99.8126	65.9127
db24	91.6912	99.9618	89.1455	78.0109	99.8138	65.8101
db25	91.6771	99.9628	89.2491	77.8227	99.817	65.7777
db26	91.5996	99.963	89.1445	77.6906	99.8207	65.8762
db27	91.5676	99.963	89.0055	77.4395	99.8225	65.8504
db28	91.501	99.9637	88.9942	77.4949	99.8213	65.7463
db29	91.4814	99.9641	89.076	77.2088	99.8251	65.7189
db30	91.382	99.964	88.8462	77.1548	99.8238	65.7188
db31	91.3756	99.965	88.9181	77.1762	99.8287	65.7845
db32	91.2949	99.9654	88.9856	76.9799	99.8292	65.7691
db33	91.2653	99.965	88.7309	76.9165	99.8311	65.6901
db34	91.1967	99.9655	88.724	76.8687	99.8321	65.7176
db35	91.182	99.9659	88.737	76.5212	99.8333	65.6477
db36	91.0873	99.9657	88.5533	76.4937	99.8339	65.7218
db37	91.0683	99.9663	88.6598	76.3784	99.8356	65.7157
db38	91.0055	99.9664	88.602	76.1415	99.8369	65.6556
db39	90.961	99.9661	88.5301	76.1926	99.8385	65.631
db40	90.8878	99.9667	88.5193	76.0546	99.8389	65.6728
db41	90.8854	99.9671	80.5068	74.844	99.7005	51.4404
db42	91.182	99.9659	88.737	74.5983	99.7037	51.4772
db43	91.0683	99.9663	8836598	74.6984	99.7043	51.4725
db44	90.961	99.9661	88.5301	74.4872	99.7056	51.4063

Table 4.2.3 Results of Daubechies wavelets db_N (where N = 1 to 44) for Barbara and Mandrill images

Wavelet	BARBARA			MANDRILL		
	Percentage of Zeros	Percentage of Energy Recover	Peak Signal to Noise Ratio (dB)	Percentage of Zeros	Percentage of Energy Recover	Peak Signal to Noise Ratio (dB)
db1	87.1597	99.7161	73.0629	76.8967	99.6125	67.5123
db2	88.9319	99.7539	74.1302	78.428	99.6596	68.6186
db3	**89.3148**	**99.7714**	**74.7091**	**78.8176**	**99.6804**	**69.1943**
db4	**89.0538**	**99.7847**	**75.0357**	**78.9087**	**99.6887**	**69.3453**
db5	**89.1265**	**99.7909**	**75.243**	**79.0197**	**99.686**	**69.2509**
db6	88808	99.7963	75.2605	78.5821	99.6874	69.2263
db7	88.58	99.7998	75.3643	78.5166	99.6879	69.2499
db8	88.4457	99.8009	75.2876	78.4807	99.6954	69.4104
db9	88.3398	99.8027	74.9577	78.4537	99.6992	69.5291
db10	87.9506	99.804	74.9891	78.1187	99.699	69.6357
db11	87.9154	99.8019	74.995	78.0738	99.7082	69.5994
db12	87.5889	99.8048	74.995	78.0345	99.7043	69.3326
db13	87.43	99.8027	74.8796	77.8264	99.6992	69.1481
db14	87.2296	99.804	74.9475	77.6767	99.699	69.037
db15	87.0011	99.8039	74.9935	77.532	99.699	69.03
db16	86.8363	99.8005	74.7221	77.2553	99.7071	69.229
db17	86.7069	99.8007	74.7524	77.2944	99.7119	69.3503
db18	86.4457	99.8038	74.7725	77.194	99.7182	69.5347
db19	86.406	99.7994	74.5143	76.9279	997188	69.4952
db20	86.1632	99.8003	74.5305	76.711	99.7155	69.2789
db21	85.9969	99.8008	74.6578	76.6237	99.7108	69.0813
db22	85.7993	99.7981	74.5201	76.6172	99.7098	68.9438
db23	85.6947	99.7971	74.43	76.4294	99.707	68.8774
db24	85.3532	99.805	74.6468	76.4681	99.7109	68.9524
db25	85.3904	99.8015	74.4353	76.4327	99.7169	69.0963
db26	85.0818	99.8016	74.3401	76.2151	99.7208	69.2202
db27	85.0481	99.8057	74.4992	75.9922	99.7246	69.2989
db28	84.7256	99.8061	74.3021	75.818	99.7235	69.1524
db29	84.542	99.8063	74.2774	75.7448	99.7196	68.9872
db30	84.3229	99.8079	74.2628	75.6911	99.7193	68.9154
db31	84.1736	99.8086	74.1562	75.639	99.7177	68.8359
db32	83.8732	99.8125	74.2704	75.4285	99.7215	68.9008
db33	83.7694	99.8157	74.1933	75.4448	99.7254	68.9378
db34	83.79	99.8185	74.1339	75.4691	99.7272	69.0129
db35	83.7517	99.8184	73.9985	74.9451	99.7293	69.0045
db36	83.272	99.8244	74.1678	74.6917	99.7312	68.9952
db37	83.3866	99.8252	74.1161	74.6508	99.7284	68.8705
db38	83.0422	99.8284	74.1828	74.5019	99.7303	68.8227
db39	82.904	99.83	74.0552	74.3695	99.7309	68.8456
db40	82.9162	99.8349	74.0831	74.4241	99.7339	68.8631
db41	83.2574	99.8172	74.6266	74.3731	99.737	68.8907
db42	83.6486	99.8179	74.4971	74.9451	99.7293	69.0045
db43	83.524	99.8201	74.6274	74.6508	99.7284	68.8705
db44	83.355	99.8182	74.5536	74.3695	99.7309	68.8456

Table 4.2.4 Results of Daubechies wavelets db_N (where N = 1 to 44) for Butterfly and Diagonal line based images

Wavelet	BUTTERFLY			DIAGONAL		
	Percentage of Zeros	Percentage of Energy Recover	Peak Signal to Noise Ratio (dB)	Percentage of Zeros	Percentage of Energy Recover	Peak Signal to Noise Ratio (dB)
db1	86.4705	99.9265	77.696	87.5977	99.9197	91.9933
db2	87.7887	99.9383	78.9313	86.1275	99.8096	82.3133
db3	**88.247**	**99.9417**	**78.9407**	**85.9898**	**99.7649**	**80.0928**
db4	**88.209**	**99.945**	**79.0793**	**85.8933**	**99.7392**	**78.9862**
db5	**88.1094**	**99.9467**	**78.8936**	**84.995**	**99.7145**	**78.0282**
db6	87.8601	99.9487	78.8845	84.1694	99.7191	78.0653
db7	87.6895	99.9493	78.5626	84.1664	99.6791	76.3245
db8	87.5319	99.9509	78.5108	83.4593	99.6592	75.7316
db9	87.4588	99.9552	78.2602	83.3084	99.5974	75.4996
db10	87.2466	99.956	78.237	83.0524	99.5924	74.9992
db11	87.1586	99.9537	78.1167	82.7066	99.6112	74.1537
db12	86.9933	99.9545	77.9975	82.3688	99.5952	73.4982
db13	86.6499	99.9552	77.8455	82.2467	99.5974	73.6943
db14	86.4797	99.956	77.8209	81.9104	99.5924	73.278
db15	86.316	99.956	77.5317	81.5652	99.5769	72.8681
db16	86.1592	99.9561	77.4309	81.288	99.5709	72.6657
db17	85.9717	99.9661	77.2761	80.9188	99.5689	72.5851
db18	85.9519	99.9563	77.1587	81.1205	99.5581	72.0575
db19	85.7018	99.9561	77.0458	81.2034	99.5442	71.666
db20	85.4464	99.9562	76.9535	80.5039	99.5376	71.3909
db21	85.2473	99.9564	76.8675	80.4507	99.54	71.3749
db22	85.0479	99.9561	76.7013	80.6836	99.5364	71.157
db23	84.785	99.9562	76.683	80.2946	99.5257	70.8587
db24	84.7686	99.9551	76.4101	80.092	99.5184	70.494
db25	84.5249	99.9556	76.4639	80.2632	99.5101	70.2488
db26	84.4186	99.9558	76.454	80.0424	99.5273	70.5568
db27	84.2166	99.9556	76.2444	80.0043	99.5105	70.0436
db28	84.0944	99.9553	76.1594	79.9533	99.5047	69.7915
db29	83.7766	99.9553	76.0854	79.74	99.5079	69.6615
db30	83.5709	99.9546	75.8353	79.4393	99.5106	69.6963
db31	83.4976	99.9545	75.7772	79.7148	99.5008	69.3112
db32	83.2613	99.4547	75.7602	79.3316	99.496	69.1422
db33	83.1851	99.9547	75.7418	79.3499	99.5029	69.1031
db34	83.0677	99.955	75.6355	79.2109	99.4997	69.0201
db35	82.8755	99.9547	75.5948	79.2261	99.4903	68.8425
db36	82.7101	99.9541	75.4735	78.964	99.4828	68.511
db37	82.4999	99.9543	75.3941	78.9254	99.4861	68.483
db38	82.361	99.9538	75.2885	78.8894	99.4982	68.6986
db39	82.0555	99.9534	75.0989	78.4696	99.475	68.2346
db40	82.0395	99.9532	75.0895	78.6555	99.4729	67.9834
db41	81.9044	99.9532	75.0625	78.6705	99.4753	68.0288
db42	82.8755	99.9547	75.5948	79.2261	99.4903	68.8425
db43	82.4999	99.9543	75.3941	78.9254	99.4861	68.483
db44	82.0555	99.9534	75.0989	78.4696	99.475	68.2346

Table 4.2.5 Results of Daubechies wavelets db_N (where N = 1 to 44) for Horizontal and Vertical line based images

Wavelet	HORIZONTAL			VERTICAL		
	Percentage of Zeros	Percentage of Energy Recover	Peak Signal to Noise Ratio (dB)	Percentage of Zeros	Percentage of Energy Recover	Peak Signal to Noise Ratio (dB)
db1	**90.5807**	**99.9998**	**141.8606**	**89.6906**	**99.9994**	**129.0678**
db2	87.9801	99.9764	92.1412	87.6507	99.9737	92.0882
db3	86.0544	99.9813	94.739	85.7543	99.9644	89.0369
db4	86.3986	99.967	89.0313	84.3615	99.9604	88.0752
db5	83.8869	99.9678	88.9092	82.8151	99.9712	91.7549
db6	83.4849	99.9598	86.7037	83.1172	99.9436	84.5041
db7	83.4699	99.9637	87.3624	81.4279	99.9513	86.2282
db8	82.7425	99.9482	83.9312	80.6732	99.9411	83.9541
db9	81.8921	99.9516	83.2115	80.9066	99.9458	84.7572
db10	82.0809	99.9484	85.7097	80.7984	99.9482	82.4657
db11	81.6307	99.9521	84.4208	79.2368	99.9452	83.3758
db12	80.3611	99.9494	83.9313	78.9336	99.9349	81.0413
db13	79.5822	99.9516	84.3359	78.2297	99.9458	83.439
db14	79.1497	99.9484	83.4058	77.3262	99.9482	84.2376
db15	78.1144	99.9599	85.6589	77.412	99.9327	80.5607
db16	78.2833	99.9477	82.552	76.5705	99.9387	81.9401
db17	77.5908	99.9558	84.6852	76.8844	99.9305	80.5995
db18	78.107	99.9496	82.1104	77.2655	99.9365	80.9924
db19	78.1574	99.9514	82.9466	77.2478	99.9174	77.6881
db20	77.1106	99.9364	79.7384	75.5473	99.937	80.9689
db21	77.1937	99.9353	79.4358	75.7022	99.9225	79.0759
db22	76.5257	99.9509	81.5729	74.8951	99.9288	80.0012
db23	76.3786	99.9468	81.0507	74.9125	99.9067	76.6035
db24	76.0181	99.9379	78.6059	74.795	99.9139	77.9108
db25	76.6549	99.9411	79.0551	75.2576	99.9252	78.9502
db26	76.0509	99.945	80.1656	74.8901	99.9187	77.8289
db27	75.006	99.9549	83.1629	75.3564	99.9051	75.6424
db28	74.8177	99.9448	80.0043	73.348	99.9191	77.8926
db29	75.1647	99.9231	76.2631	72.8263	99.9225	78.2648
db30	73.848	99.9467	80.3597	72.6959	99.9127	77.1094
db31	74.0339	99.94	78.5886	72.2712	99.9169	77.6733
db32	72.2468	99.9336	77.34	72.7678	99.9169	77.4971
db33	73.3881	99.9513	81.5444	73.5048	99.9093	76.6569
db34	73.9848	99.9427	79.7249	73.8311	99.9187	77.4633
db35	72.9265	99.9452	80.9512	72.7095	99.9001	75.14
db36	73.2061	99.9267	77.3958	71.4738	99.9207	77.6825
db37	72.7884	99.9326	77.7164	71.2882	99.9228	78.4557
db38	72.967	99.9299	77.6145	71.4682	99.9119	77.2697
db39	71.9951	99.9411	78.9345	71.5374	99.9064	75.9434
db40	72.6989	99.9311	79.5928	71.0152	99.9105	76.2003
db41	73.0846	99.9419	78.7539	71.1963	99.9255	78.1694
db42	72.9265	99.9452	80.9512	72.7095	99.9001	75.14
db43	72.7884	99.9326	77.7164	71.2882	99.9228	78.4557
db44	71.9951	99.5411	78.9345	71.5374	99.9064	75.9434

Table 4.2.6 Results of Biorthogonal wavelets Bior $_{NrNd}$ (where Nr.Nd = 1.1 to 6.8) for Aishwarya and Cheetah images

Wavelet	AISHWARYA			CHEETAH		
	Percentage of Zeros	Percentage of Energy Recover	Peak Signal to Noise Ratio (dB)	Percentage of Zeros	Percentage of Energy Recover	Peak Signal to Noise Ratio (dB)
Bior1.1	92.515	99.8901	82.9103	88.5544	99.773	71.361
Bior1.3	92.3279	99.8925	83.1685	87.4506	990774	71.7984
Bior1.5	92.0145	99.8896	82.7746	86.646	99.7738	71.6622
Bior2.2	**93.1977**	**99.9577**	**92.0476**	**90.2404**	**99.8871**	**77.5968**
Bior2.4	92.9932	99.9568	93.0115	89.607	99.8858	78.6389
Bior2.6	92.8339	99.9568	93.0158	89.1916	99.885	78.9781
Bior2.8	92.6838	99.9577	93.3433	88.7701	99.8849	79.1754
Bior3.1	93.1738	99.9622	91.5198	89.8164	99.9123	76.2828
Bior3.3	92.9691	99.9611	94.0776	89.3159	99.9114	79.0814
Bior3.5	92.8068	99.9611	95.0184	88.9409	99.9098	80.0858
Bior3.7	92.6604	99.9611	95.3497	88.502	99.9105	80.7554
Bior3.9	92.5015	99.9621	95.6907	88.1325	99.909	80.9962
Bior4.4	**93.1709**	**99.9653**	**92.7367**	**90.9208**	**99.9011**	**77.9022**
Bior5.5	93.1399	99.9683	91.3622	91.575	99.9054	75.5642
Bior6.8	92.8618	99.9669	93.6798	90.174	99.9048	79.4862

Table 4.2.7 Results of Biorthogonal wavelets Bior $_{NrNd}$ (where Nr.Nd = 1.1 to 6.8) for Lena and Woman images

Wavelet	LENA			WOMAN		
	Percentage of Zeros	Percentage of Energy Recover	Peak Signal to Noise Ratio (dB)	Percentage of Zeros	Percentage of Energy Recover	Peak Signal to Noise Ratio (dB)
Bior1.1	91.1836	99.8702	79.6658	78.3301	99.6721	65.0408
Bior1.3	90.8806	99.871	79.7226	77.7278	99.6975	65.0371
Bior1.5	90.6552	99.872	79.5049	76.8835	99.714	64.8894
Bior2.2	**92.7155**	**99.9501**	**88.7139**	**80.9913**	**99.72**	**64.9219**
Bior2.4	**92.5391**	**99.9496**	**89.5255**	**80.5637**	**99.7388**	**65.1403**
Bior2.6	92.3476	99.92492	89.7282	79.9979	99.7531	65.1959
Bior2.8	92.2153	99.9498	89.8572	79.5679	99.7639	65.1681
Bior3.1	92.819	99.9576	88.5461	76.159	99.7283	62.2942
Bior3.3	92.6395	99.958	90.9716	78.6955	99.7377	64.4196
Bior3.5	92.4972	99.9576	91.8911	78.6477	99.7527	64.8366
Bior3.7	92.3199	99.958	92.2877	78.4681	99.7657	650012
Bior3.9	92.2042	99.9572	92.5056	78.0588	99.7754	65.0392
Bior4.4	92.9063	99.9597	89.3324	81.0144	99.7298	65.9157
Bior5.5	92.9398	99.9609	87.5979	79.695	99.7228	66.136
Bior6.8	92.5969	99.9612	90.3925	80.5114	99.7626	66.1039

Table 4.2.8 Results of Biorthogonal wavelets Bior $_{NrNd}$ (where Nr.Nd = 1.1 to 6.8) for Barbara and Mandrill images

Wavelet	BARBARA			MANDRILL		
	Percentage of Zeros	Percentage of Energy Recover	Peak Signal to Noise Ratio (dB)	Percentage of Zeros	Percentage of Energy Recover	Peak Signal to Noise Ratio (dB)
Bior1.1	87.1597	99.7161	73.0629	76.8967	99.6125	67.5123
Bior1.3	86.3086	99.7275	73.1251	75.6872	99.6255	67.7541
Bior1.5	85.6884	99.7303	73.0218	74.5255	99.6312	67.6353
Bior2.2	**89.4328**	**99.7958**	**74.9362**	**79.1526**	**99.7157**	**68.1968**
Bior2.4	88.78.56	99.8014	75.4736	78.5208	99.7174	68.6136
Bior2.6	88.306	99.8024	75.4715	77.9448	99.7253	68.7658
Bior2.8	87.8296	99.8059	75.5932	77.4888	99.7296	68.7803
Bior3.1	**89.0403**	**99.8366**	**72.8833**	**77.1783**	**99.7786**	**65.8669**
Bior3.3	88.4952	99.8332	74.8914	77.3859	99.7698	67.8016
Bior3.5	87.9842	99.8361	75.588	77.0747	99.7755	68.3526
Bior3.7	87.4441	99.8327	75.8289	76.7616	99.7772	68.5422
Bior3.9	87.0677	99.8353	75.9746	76.305	99.7823	68.6782
Bior4.4	**89.5578**	**99.8028**	**75.2008**	**79.5193**	**99.702**	**69.0367**
Bior5.5	89.617	99.7902	73.9709	79.0711	99.6887	68.4013
Bior6.8	88.7139	99.8123	75.6583	78.7894	99.7175	69.51

Table 4.2.9 Results of Biorthogonal wavelets Bior $_{NrNd}$ (where Nr.Nd = 1.1 to 6.8) for Butterfly and Diagonal line based images

Wavelet	BUTERFLY			DIAGONAL		
	Percentage of Zeros	Percentage of Energy Recover	Peak Signal to Noise Ratio (dB)	Percentage of Zeros	Percentage of Energy Recover	Peak Signal to Noise Ratio (dB)
Bior1.1	86.4705	99.9265	77.696	87.5977	99.9297	91.9923
Bior1.3	86.1507	99.9316	77.3916	86.9088	99.9024	99.5234
Bior1.5	85.8098	99.9371	77.1579	86.0054	99.8807	86.0722
Bior2.2	**88.6174**	**99.9498**	**78.915**	**86.4097**	**99.78.55**	**78.9708**
Bior2.4	88.3737	99.9541	79.3845	86.0039	99.7822	79.3556
Bior2.6	88.021	99.9572	79.4897	85.3134	99.786	79.81
Bior2.8	87.9198	99.9601	79.5026	84.9226	99.7815	79.3572
Bior3.1	**88.487**	**99.9526**	**75.7841**	**85.2757**	**99.8322**	**72.5067**
Bior3.3	88.4205	99.9569	78.0183	84.4357	99.8065	75.3657
Bior3.5	88.1986	99.9595	78.591	84.478	99.7941	76.9759
Bior3.7	98.0556	99.9625	78.9449	83.8964	99.7905	76.4806
Bior3.9	87.7616	99.4696	79.0681	83.5237	99.7966	76.7913
Bior4.4	88.9876	**99.9509**	**78.891**	**85.8317**	**99.7896**	**81.3103**
Bior5.5	88.8204	99.949	77.9598	85.367	99.7554	79.5208
Bior6.8	88.5575	99.9578	79.0433	85.0252	99.7802	80.294

Table 4.2.10 Results of Biorthogonal wavelets Bior $_{NrNd}$ (where Nr.Nd = 1.1 to 6.8) for Horizontal and Vertical line based images

Wavelet	HORIZONTAL			VERTICAL		
	Percentage of Zeros	Percentage of Energy Recover	Peak Signal to Noise Ratio (dB)	Percentage of Zeros	Percentage of Energy Recover	Peak Signal to Noise Ratio (dB)
Bior1.1	**90.5807**	**99.9998**	**141.8606**	**89.6906**	**99.9994**	**129.0678**
Bior1.3	89.827	99.9954	107.8747	88.8065	99.994	106.8088
Bior1.5	89.2695	99.9983	117.9047	87.4669	99.9949	111.2401
Bior2.2	88.5299	99.9773	89.091	88.21	99.9561	86.4728
Bior2.4	88.1099	99.9802	90.1071	87.0784	99.9633	88.4526
Bior2.6	87.9476	99.9779	89.2849	86.7609	99.9609	87.6797
Bior2.8	87.8456	99.9736	87.8634	86.3064	99.9608	87.1243
Bior3.1	87.2012	99.9934	99.336	86.312	99.9878	92.8083
Bior3.3	86.8935	99.9917	98.7425	85.6395	99.9869	93.8358
Bior3.5	86.5848	99.9898	98.1983	85.0048	99.9805	93.039
Bior3.7	86.2401	99.9884	97.1879	84.5695	99.9793	92.2589
Bior3.9	85.8657	99.9894	96.6793	84.0103	99.9804	92.2369
Bior4.4	86.9539	99.9586	85.8119	85.3907	99.9458	84.9707
Bior5.5	85.1037	99.9663	88.9886	83.1772	99.9532	87.9473
Bior6.8	85.5756	99.9714	88.6548	83.4828	99.9633	88.4515

Table 4.2.11 Results of Coiflet wavelet Coif$_N$ (N = 1 to 5) for Aishwarya and Cheetah images

Wavelet	AISHWARYA			CHEETAH		
	Percentage of Zeros	Percentage of Energy Recover	Peak Signal to Noise Ratio (dB)	Percentage of Zeros	Percentage of Energy Recover	Peak Signal to Noise Ratio (dB)
coif1	93.0993	99.9472	89.9422	90.2315	99.8519	75.4467
coif2	92.9629	99.9606	92.5138	90.2167	99.8875	78.1318
coif3	92.8275	99.9646	93.1689	90.034	99.8983	79.0777
coif4	92.6025	99.9667	93.4433	89.6852	99.9029	79.4945
coif5	92.4552	99.9681	93.5706	89.4566	99.9055	79.7609

Table 4.2.12 Results of Coiflet wavelet Coif$_N$ (N = 1 to 5) for Lena and Woman images

Wavelet	LENA			WOMAN		
	Percentage of Zeros	Percentage of Energy Recover	Peak Signal to Noise Ratio (dB)	Percentage of Zeros	Percentage of Energy Recover	Peak Signal to Noise Ratio (dB)
coif1	92.4594	99.9344	86.2557	80.2502	99.7062	65.629
coif2	92.5852	99.9537	89.4145	80.5051	99.7365	66.0701
coif3	92.5124	99.9576	90.0661	80.261	99.7604	66.2195
coif4	92.331	99.9599	90.32	80.0306	99.7733	66.2625
coif5	92.204	99.9614	90.444	79.6633	99.7882	66.2849

Table 4.2.13 Results of Coiflet wavelet $Coif_N$ (N = 1 to 5) for Barbara and Mandrill images

Wavelet	BARBARA			MANDRILL		
	Percentage of Zero	Percentage of Energy Recover	Peak Signal to Noise Ratio (dB)	Percentage of Zero	Percentage of Energy Recover	Peak Signal to Noise Ratio (dB)
coif1	88.8473	99.7632	74.4199	78.3398	99.6632	68.6755
coif2	88.8311	99.7955	75.3616	78.6141	99.6913	69.3394
coif3	88.4352	99.8072	75.7584	78.4193	99.7032	69.5422
coif4	87.8656	99.8172	75.6235	78.0875	99.7143	69.6527
coif5	87.4195	99.8212	75.6718	77.8292	99.7205	69.708

Table 4.2.14 Results of Coiflet wavelet $Coif_N$ (N = 1 to 5) for Butterfly and Diagonal line based images

Wavelet	BUTTERFLY			DIAGONAL		
	Percentage of Zero	Percentage of Energy Recover	Peak Signal to Noise Ratio (dB)	Percentage of Zero	Percentage of Energy Recover	Peak Signal to Noise Ratio (dB)
coif1	87.7537	99.9421	79.0146	86.1643	99.8113	82.5575
coif2	88.2891	99.9508	79.2511	85.5763	99.7848	80.6617
coif3	88.1259	99.9561	79.1396	85.0207	99.7756	80.1113
coif4	87.92	99.9599	79.0298	84.5075	99.7752	79.7368
coif5	87.6613	99.963	78.9415	84.142	99.7706	79.3684

Table 4.2.15 Results of Coiflet wavelet $Coif_N$ (N = 1 to 5) for Horizontal and Vertical line based images

Wavelet	HORIZONTAL			VERTICAL		
	Percentage of Zero	Percentage of Energy Recover	Peak Signal to Noise Ratio (dB)	Percentage of Zero	Percentage of Energy Recover	Peak Signal to Noise Ratio (dB)
coif1	88.3589	99.9762	92.6496	87.4958	99.9646	90.825
coif2	86.7364	99.9593	85.8262	84.88	99.9488	85.5071
coif3	85.3682	99.9672	87.5704	83.3506	99.9575	86.8353
coif4	84.75	99.9647	86.7689	82.9411	99.9534	85.5086
coif5	84.084	99.9619	85.6793	82.583	99.9493	84.1841

4.2.1 CONCLUSION

From the results, it is observed that the choice of mother wavelet depends on nature of image as described by the researcher [36, 81]. Haar wavelets, which is also known as db_1, give good results for synthetic images, and db_3, db_4, db_5, db_6 give the good results for natural images. Daubechies and Coiflet wavelets are families of orthogonal wavelets that are compactly supported. Compactly supported wavelets correspond to finite impulse response (FIR) filters, and thus lead to efficient implementation [5]. It is also observed, that larger number of taps does not imply better peak signal to noise ratio, and visual quality.

A major disadvantage of Daubechies and Coiflet wavelets is their asymmetry, which can cause artifacts at borders of the wavelet sub-band, as it is observed in the results. Symmetry is one of the important properties of the wavelet transform. It can be obtained in wavelet by losing either compact support or orthogonality. Haar wavelet is the only wavelet, which is orthogonal, compactly supported and symmetric. Mayer wavelet family is non-compactly supported but symmetric, and orthogonal wavelet. For this wavelet Discrete Wavelet Transform is possible without Fast Wavelet Transform (FWT), its support width is infinite. The use of Mayer wavelets adds computational burden, and does not provide efficient implementation. For good visual quality, and more compression ratio, wavelet must support symmetry and compact properties. If both symmetry and compact support is required in wavelets, then one should relax the orthogonality condition and allow non-orthogonal wavelet functions. Bi-orthogonal wavelets are compactly supported and symmetric [36]. Results of wavelets for different spectral density images are discussed here.

Aishwarya and Cheetah are widely used natural images, which do not contain large amounts of high frequency or oscillating patterns. The peak signal to noise ratio and percentage of zeros show that the db_3 to db_6, and Bior2.2, Bior4.4 wavelets give the best performance.

Lena is widely used natural image that does not contain large amount of high frequency or oscillating patterns. The peak signal to noise ratio, and percentage of zeros show that the db_3 to db_7, and Bior2.2, Bior2.4 wavelets give the best performance.

Barbara is popular choice from the class of natural test images that exhibits large amount of high frequency and oscillating patterns. The peak signal to noise ratio and percentage of zeros show that the db_3, db_4, db_5, Bior2.2, Bior3.1 and Bior4.4 wavelets give the best performance.

Mandrill image is another image that is quite difficult to compress significantly. In a texture of the Mandrill image, it has a large amount of high frequency content, and spread over most of the image. The peak signal to noise ratio and percentage of zeros show that the db_3, db_4, db_5, Bior2.2, Bior3.1, and Bior4.4 wavelets give the best performance.

Synthetic test images used for the tests are Butterfly, Diagonal, Horizontal and Vertical images. Diagonal, Vertical, and Horizontal images are constructed by using the strands of lines. It is observed that for the synthetic images db_1 wavelet gives the best performance.

Percentage of zeros in Bi-orthogonal wavelet is decreased by the amount of one to two percent as compared to the Daubechies wavelet. Bi-orthogonal wavelets possess the symmetry property, though the percentage of zeros is slightly less than Daubechies wavelet, the symmetry property present in Bi-orthogonal wavelets is responsible for good visual quality of an image. From comparative study of different wavelets, in still image compression techniques, the final choice of optimal wavelet depends on subjective and objective image quality measures, and computational complexity. It is found that the best of known wavelet is Bior2.2 wavelets. It provides the best visual image quality for different image contents with comparable percentage of zeros. The Bior2.2 has low computational complexity in comparison with Bior3.1, Bior4.4, and Bior6.8.

4.3.0 WAVELET AND WAVELET PACKET

Signals are represented with basis function. For example an impulse is used as the basis function in the time domain representation, any function can be represented in time domain as a summation of various scaled and shifted impulses. Similarly the sine function is used as the basis in the frequency domain representation. However, these two-basis functions have their individual weaknesses: an impulse is not localized in the frequency domain, and hence impulse function is a poor basis function to be used to represent frequency information. Likewise a sine wave is not localized in the time domain, and hence, sine function is a poor basis function to be used to represent time information. In order to represent complex signals efficiently, a basis function should be localized in both time and frequency domains. The support of such a basis function should be variable, so that a narrow version of the function can be used to represent the high frequency components of a signal, while wide version of the function can be used to represent the low frequency components. The function that is localized in time

domain as well as in frequency domain, and it is a function of variable parameters. The wavelet is an example of such a function; it has variable parameters scale and shift.

A wide variety of wavelet based image compression schemes had been represented in literature ranging from simple entropy coding [27] to more complex technique such as vector quantization, adaptive transform, tree encoding, multi-wavelet and multi wavelet packet [16, 74, 78, 79] and edge based coding [31]. In all these techniques wavelet transform is used to de-correlate the image data. A pair of approximately designed Quadrature Mirror Filter (QMF) can efficiently implement the wavelet transform. The low pass and high pass filters are applied to the image in both the horizontal and vertical directions, then the filter outputs are sub-sampled by a factor of two. It generates four different horizontal frequencies and vertical frequencies outputs. These outputs are referred as approximation, horizontal detail, vertical detail, and diagonal detail. The approximation contains low frequency horizontal and vertical components of the image. Most of the natural images have maximum low frequency components, and hence the filtering and sub-sampling process is then repeated on the approximation sub-band to generate the next level of the decomposition, and so on. It is leading to well known pyramidal decomposition tree. Wavelet yields a multi-scale decomposition: low frequency trends occurring at large scale in the image, can be as efficiently coded. Wavelets with many vanishing yield sparse decomposition of piece wise smooth surface; therefore they provide a very appropriate tool to compactly code smooth images. Wavelets however, are ill suited to represent oscillatory patterns [76, 90] or the wavelet transform often fail to accurately capture high frequency information. A special from a texture, oscillating variations, rapid variations in the intensity can only be described by the small-scale wavelet coefficients. Unfortunately, these small-scale coefficients carry very little energy, and are often quantized to zero even at high bit rate. Fingerprint, Barbara, Mandrill, and Seismic signals are few examples of non wavelet-friendly images [75, 76, 78, 80].

The weakness of wavelet transform is that it fails to capture high frequency components of an image, and hence, another transform method must be employed. Coifman, Meyer and Wickerhauser developed the technique, which was based on the wavelet transform and known as wavelet packets. Wavelet packets are better able to represent the high frequency information [74].

Wavelet packets represent a generalization of multi-resolution decomposition. In wavelet, the decomposition is applied recursively to the coarse scale approximation, whereas in the wavelet packets decomposition, the recursive procedure is applied to the

coarse scale approximation along with horizontal detail, vertical detail, and diagonal detail, which leads to a complete binary tree. Wavelet packets is an extension of the octave band wavelet decomposition to a full tree decomposition by allowing the low pass filtering, high pass filtering and down sampling procedure to be iterated on approximate and details. High pass branches in the tree, add more flexibility in frequency resolution. Wavelet packets decomposition leads to the 4^J sub-bands at decomposition level 'J' [79].

The details of wavelet and wavelet packet are explained in chapter 3. The pyramid structure of wavelet decomposition up to third level is shown in figure 4.3.1, tree structure of wavelet decomposition up to third level is shown in figure 4.3.2, structure of three level decomposition of wavelet packet is shown in figure 4.3.3, and tree structure of wavelet packets decomposition up to third level is shown in figure 4.3.4.

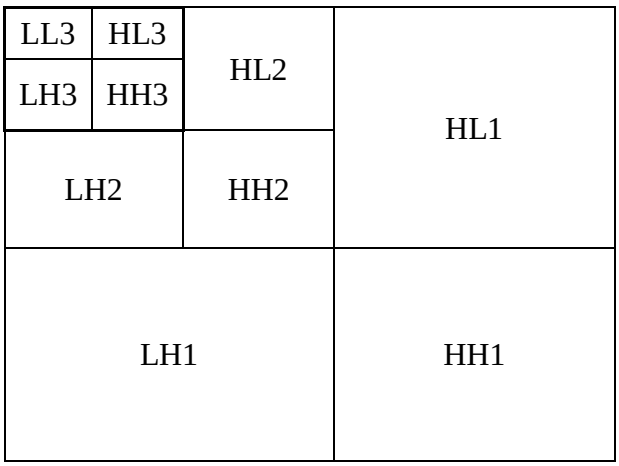

Figure 4.3.1:The pyramid structure of wavelet decomposition up to third level

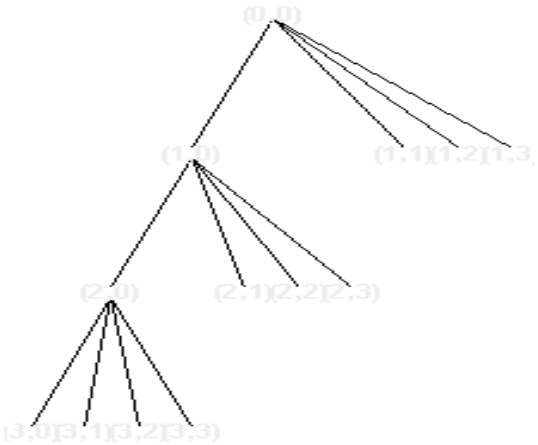

Figure 4.3.2:The tree structure of wavelet decomposition up to third level

LL_1LL_2	LL_1HL_2	HL_1LL_2	HL_1HL_2
LL_1LH_2	LL_1HH_2	HL_1LH_2	HL_1HH_2
LH_1LL_2	LH_1LH_2	HH_1LL_2	HH_1HL_2
LH_1LH_2	LH_1HH_2	HH_1LH_2	HH_1HH_2

Figure 4.3.3:The structure of two level decomposition of wavelet packet

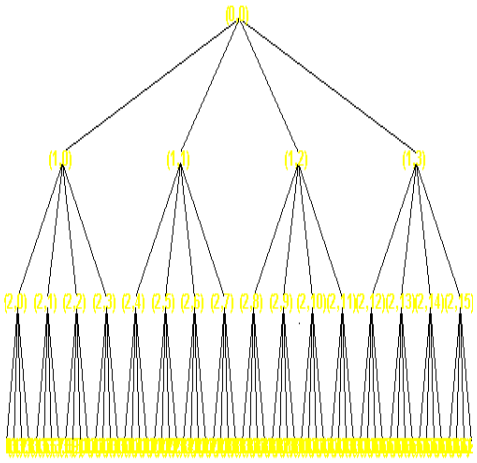

Figure 4.3.4:The tree structure of wavelet packets decomposition up to third level

In wavelet packets number of sub-bands are more, and hence, there is flexibility to the user to select wide range of thresholds, and it results in extracting the important information from the sub-bands. The overall result is better compression ratio by maintaining the image quality. It is one of the main objectives of this research work.

Multiwavelets and multiwavelet packets are new areas of research for image compression. Complexity of multiwavelets is very high. The researchers [72] claimed that the unbalanced multiwavelets usually perform about 0.3 – 1.2 dB worse than the balance multiwavelets. In unbalanced multiwavelet packets several checkerboard artifacts are observed and bi-orthogonal wavelet achieved 0.2 to 0.5 dB have higher peak signal to noise ratio than balanced multiwavelets. The researchers [80] claimed that multiwavelet packets typically gave the best results for the synthetic images, and wavelet packet gives better results for most of the natural images. By considering time

complexity of multiwavelet packets, the wavelet packet is selected as a tool to decompose the image for image compression in the proposed technique.

The experimental results of wavelet and wavelet packets for few test images are examined. The natural test images are Aishwarya, Cheetah, Lena, Woman, Barbara, Mandrill, Fingure-print, Bird, Rose, Donkey and synthetic images are Butterfly, diagonal line based image, horizontal line based image and vertical line based image. The results are given in terms of percentage of zeros, energy reatined and peak signal to noise ratio.

Table 4.3.1 Results of Bi-orthogonal wavelet packets and wavelet for the natural and synthetic images

Name of the image	Wavelet Packets			Wavelet		
	Percentage of Zero	Percentage of Energy Recover	Peak Signal to Noise Ratio (dB)	Percentage of Zero	Percentage of Energy Recover	Peak Signal to Noise Ratio (dB)
AISHWARYA	97.1793	99.9334	89.4282	97.0586	99.9399	89.1467
CHEETAH	92.0904	99.8697	77.0622	91.9023	99.8816	76.8707
LENA	96.2739	99.9276	86.6867	96.1055	99.9362	86.6578
WOMAN	83.3723	99.7185	65.0393	83.3889	99.7404	64.6974
BARBARA	92.2719	99.7805	74.8745	91.7535	99.8011	74.3187
MANDRILL	67.1875	99.282	45.1783	64.5509	99.4625	48.4843
FINGURE	91.0963	98.8756	44.0425	91.0793	99.0296	43.3431
BIRD	96.5036	99.8716	83.2414	96.5066	99.8919	83.8035
ROSE	83.4973	99.4616	67.7474	83.4729	99.5166	68.7544
DONKEY	89.457	99.7415	70.5969	89.5955	99.7632	73.8438
BUTTERFLY	91.11	99.9377	74.9865	91.6432	99.953	78.4872
DIAGONAL	85.9984	99.4666	68.4852	89.0459	99.7715	78.3489
HORIZONTAL	91.422	99.9752	88.7784	92.1195	99.9775	88.7484
VERTICAL	90.3629	99.9534	84.6848	91.6001	99.9552	86.0328

4.3.1 CONCLUSION

It is observed that for most of natural images percentage of zeros of wavelet packets increases than wavelet by the amount of 2.6366 to 0.0437 percent. This change is significant for the high frequency images and insignificant for low frequency images. For the synthetic images, percentage of zeros decreases by the amount of 1.2372 to 0.003. There is a negligible change in peak signal to noise ratio. The wavelet packets tree preserves the high frequency components, those are lost in wavelet decomposition, and therefore it is strongly recommended that the wavelet packets decomposition for image compression even though the changes in percentage of zeros is not significant in few natural and synthetic images.

4.4.0 WAVELET PACKET BEST TREE

Modern image compression techniques use the wavelet transform for image compression. It is observed that wavelet decomposition often fails to accurately capture high frequency information even at high bit rates [75]. This limitation of wavelet transform is overcome in wavelet packets, and hence it is strongly recommended for image compression. Wavelet packets represent a generalization of multi-resolution decomposition. In wavelet packets decomposition, the recursive procedure is applied to the coarse scale approximation along with horizontal detail, vertical detail, and diagonal detail, which leads to a complete binary tree. Wavelet packets decomposition leads to 4^J sub-bands where J is decomposition level'[78]. For three level wavelet packets decomposition, number of sub-bands is $4^3 = 64$ and for high-level decomposition number of sub-bands are very large. The number of computations are more, and hence, it takes more time for decomposition. The wavelet packets has to pay with an increase of complexity from O (N) in the wavelet case to ((N log (N)) in the wavelet packet case [75, 79]. Where N is number of pixels in an image. To reduce the time complexity of wavelet packets decomposition, there is a need to select the sub-bands, which include significant information in compact form. The researchers [79, 75, 77] suggested, the best basis selection techniques. The selection of the best basis is based on given cost function C. The cost function should be separable or additive i.e. $C(X)=\sum_K \mu(X_K)$, where $\{X_K, K= 0, 1, -----, (N - 1)\}$ are the elements of wavelet packet decomposed image and μ is positive function such that $\mu(0) = 0$.

4.4.1. ROLE OF COST FUNCTION

The best basis selection is based on cost function. It is the function of information contain in sub-bands. First seminar paper published in 1948, laid the foundation of wonderful field of information theory, a theory initiated by the American Electrical Engineer, Claude E. Shannon. The notation of the best wavelet packet basis is limited to the cost function based on which the full wavelet packet tree is pruned to obtain an optimal tree. It is therefore crucial that an appropriate cost function is chosen taking into consideration the quantization strategy employed by the coder. When best basis selection should be performed, a cost function on transform coefficients is defined, which measures the information cost, in the sense of concentration of information. The cost function gives the large values, when the coefficients are roughly the same size, and small values when all but a few coefficients are negligible. Initially a cost function used by Coifman and Wickeshauser [75] is given as

$$h(x) = -\sum_{k}\left(\frac{|X_k|^2}{\|X\|^2}\log\frac{|X_k|^2}{\|X\|^2}\right) \qquad \text{--- 4.4.1.1}$$

It is noticed that h(x) hears no connection with the entropy H(x) of the probability distribution of the X_k. If all X_k are equal, then h(x) is maximal, but the entropy of the distribution H(x) is minimal. The researchers [77] claimed that, in practice h(x) is usually not capable of discovering any meaningful basis. The researchers [76, 78 79] have used the Threshold entropy, Log entropy, and Shannon entropy criteria as a cost function to select the best basis for the wavelet packets best tree. Their algorithm suffers from more time complexity. In proposed research work, the suggested algorithms are implemented and tested with low time complexity, and the results are compared with new proposed energy based technique and conclusions are given.

4.4.2 ENTROPY

The average self-information of a random variable X is known as entropy.
The self information of the event X= Xi is given by:

$$I(Xi) = \log\left(1/P(Xi)\right) = -\log P(Xi) \qquad \text{---4.4.2.1}$$

where P(Xi) is probability of the coefficient Xi, the amount of information I(Xi) is function of coefficient Xi. It gives the information in single outcome, in data compression, it is much more interesting to know the average information content of a source. This average is given by the expected value of the self-information with respect to the source's probability distribution. This average of self-information is called the source entropy [87]. The entropy of a discrete random variable X is a function of its probability mass function and is defined as:

$$H(X) = -\sum_{i=1}^{N} P(Xi)\,.\log P(Xi) \qquad \text{---4.4.2.2}$$

Wavelet packets decomposition gives a lot of bases from which we can look for the best representation with respective design objectives: time complexity, compression ratio, and peak signal to noise ratio. The well-known log entropy would be used as cost functions to select the best basis for wavelet packets best tree. Log entropy criteria, finds the information content of the signal X, and its log entropy is obtained by the equation

$$Entropy = \sum_{l=1}^{N}\log\,(Xi)^2 \qquad \text{---4.4.2.3}$$

The properties of entropy are,

a) The entropy is always greater than or equal to zero and less than or equal to N.
b) H(x) = 0, if and only if the probability P(Xi) = 1 for some 'i' and the remaining probabilities in the set are all zeros. This lower bound on entropy corresponds to no uncertainty.
c) H(x) = $\log_2$N, if and only if P(Xi) = 1/N for all 'i'. This upper bound on entropy corresponds to maximum uncertainty [88].

It is noted that the high probability event conveys less information than low probability event. Shannon entropy, log entropy and threshold entropy are popular to use as cost function to select the best basis in wavelet packets compression.

4.4.3 ALGORITHM FOR BEST BASIS SELECTION

The researchers [76, 78, 79] suggested the algorithm for best basis selection: Firstly wavelet packets decomposition of image at level 'J' takes place, and cost functions of all nodes in the decomposition tree are evaluated. Beginning at the bottom (leaf nodes) of the tree, the cost function of each parent node is compared to the sum of the cost function of his child nodes. If the parent's cost is higher than sum of the cost function of his child nodes, then child nodes are considered as leaf nodes of the tree. If the parent's cost is lower than sum of the cost function of child nodes then child nodes are neglected and parent node would be considered as leaf node of tree. This procedure is applied recursively at each level of the tree until the top most node (root node) of the tree is reached. Obiviously this method is complex and time consuming. In the proposed work this method is implemented, tested and published [110, 112, 113]. The algorithms are named as ***Wavelet packets best tree with threshold entropy, wavelet packets best tree with log entropy, wavelet packets best tree with Shannon entropy***. The time complexity of implemented algorithm is low.

4.4.3.1 SELECTION OF BEST BASIS BASED ON THRESHOLD ENTROPY

The wavelet packets are offering a more complex and flexible analysis. In wavelet packets analysis the details as well as the approximation are splitted**.** As there is large number of sub-bands obtained after the wavelet packets decomposition, the time complexity of the algorithm is high. To reduce the time complexity, in this algorithm threshold entropy criterion is used to construct the best tree (to select the best basis for wavelet packet image compression). Threshold entropy criteria find the information contain in signal X.

$$Entropy = \sum_{i=0}^{N-1} abs(Xi) > Threshold \qquad \text{---4.4.3.1}$$

Where Xi is the i^{th} coefficient of sub-band and N is the length of sub-band.

The information contains of decomposed components of wavelet packets may be greater than or less than the information contain of component, which has been decomposed. The sum of cost (entropy) of decomposed components (child nodes) is checked with cost of component, which has been decomposed (parent node). If sum of the cost of child nodes is less than the cost of parent node, then the child nodes are considered as leaf nodes of the tree, otherwise child nodes are neglected from the tree, and parent node becomes leaf node of the tree. This process is iterated up to the last level of decomposition. The generated result is function of threshold, which is used to find the cost function. Selection of threshold value is crucial for best basis selection. For the experimental results the value of threshold is treated as a constant.

The time complexity of proposed algorithm is less as compared to algorithm in paper [76] is discussed. In the given algorithm, the first wavelet packets decomposition of level 'J' takes place, and cost functions of all nodes in the decomposition tree are evaluated. Beginning at bottom of the tree, the cost function of the parent node is compared with union of cost functions of child nodes. According to the comparison of results the best basis node is selected. This procedure is applied recursively at each level of the tree until the top most node of the tree is reached. In proposed algorithm there is no need of full wavelet packets decomposition of level 'J' and no need to evaluate cost function of all nodes initially. Algorithm of best basis selection based on Threshold entropy is:

1. Load the image
2. Set current node equal to input image
3. Decompose the current node using wavelet packet tree
4. Evaluate the cost of current node, and decomposed components
5. Compare the cost of parent node (current node) with the sum of cost of child nodes (decomposed components). If the sum of cost of child nodes is greater than the parent node, consider the parent node as leaf node of the tree, and child nodes are pruned, else repeat the steps 3, 4, and 5 for each child node by considering a child node as a current node, until last level of the tree reached.

This algorithm reduces the time complexity, because there is no need to decompose the full wavelet packets tree and no need to evaluate the costs initially. The decision of further decomposition, and cost calculation is based on the run time strategy of the

algorithm, and it decides at run time whether to retain or prune the decomposed components [113]. The flow chart of the above algorithm is given in figure 4.4.3.1.

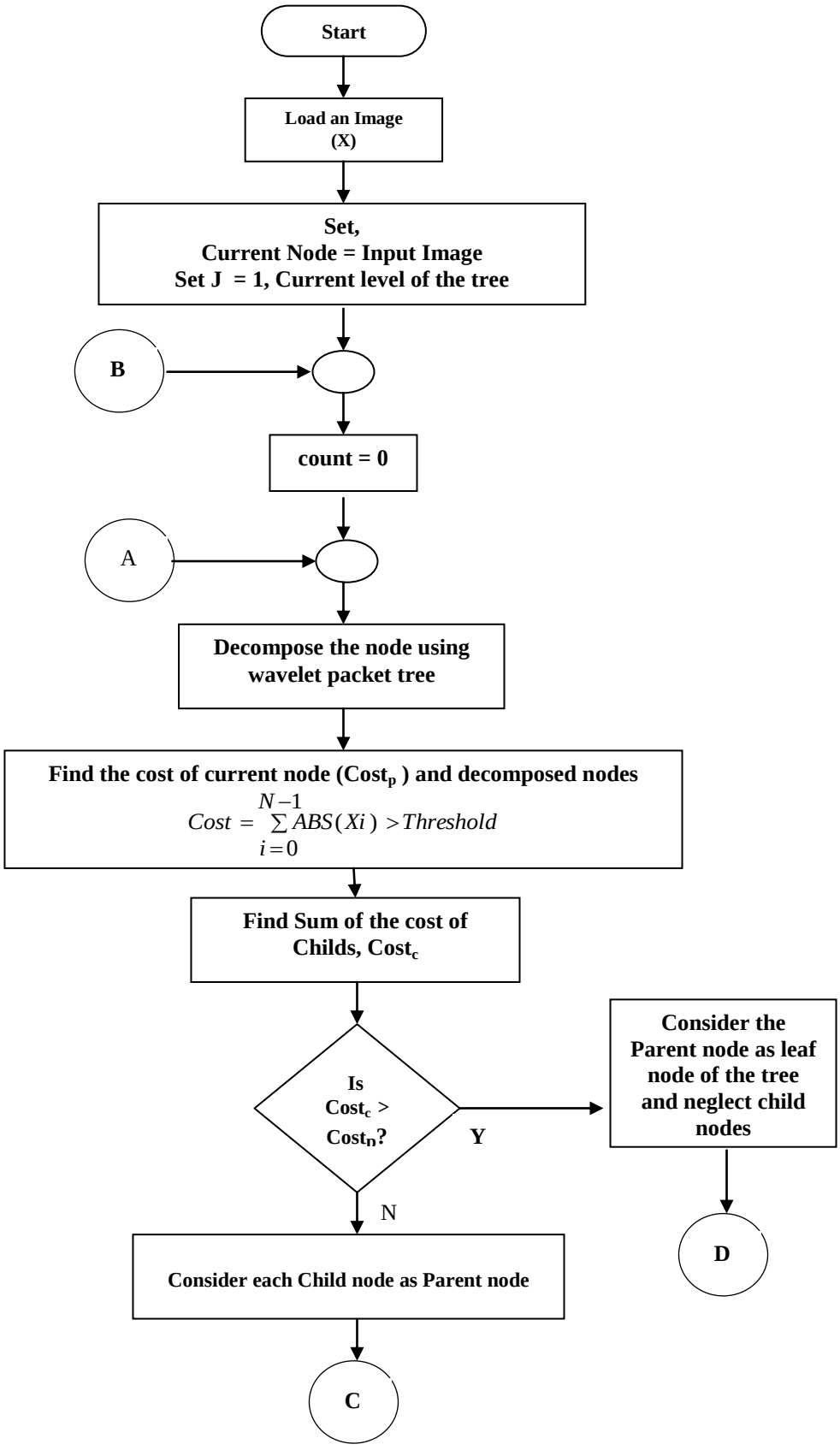

Figure 4.4.3.1: The flow chart of selection of best basis based on threshold entropy (Continued)

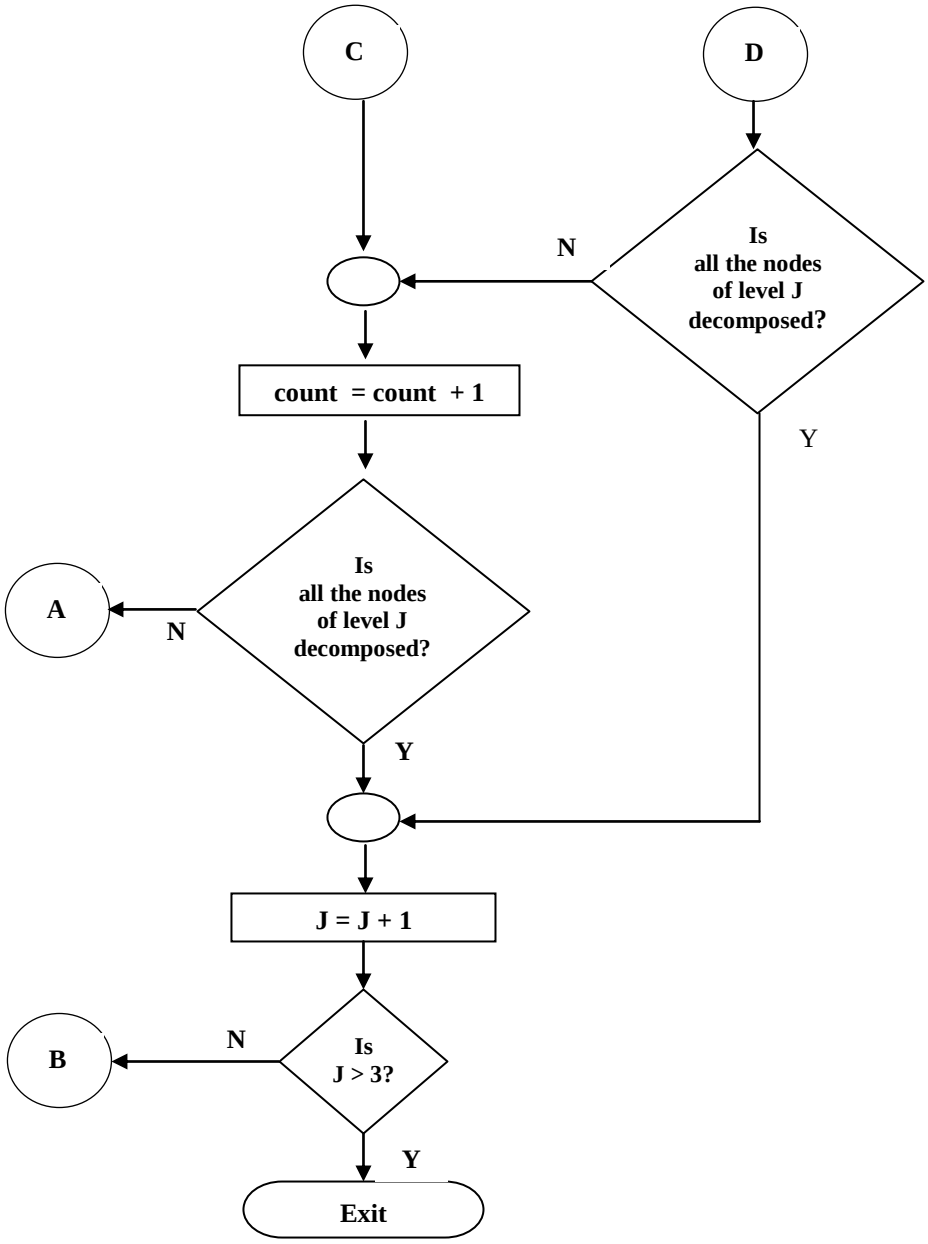

Figure 4.4.3.1: The flow chart of selection of best basis based on threshold entropy

The experimental results of the selection of best basis based on threshold entropy in terms of percentage of zeros, energy retained and peak signal to noise ratio for the natural and synthetic images are given in table 4.4.3.1

Table 4.4.3.1 Results of selection of best basis based on threshold entropy for the natural and synthetic images

Name of The images	Proposed Wavelet Packet Tree		
	Percentage of zeros	Percentage of Energy in retained	PSNR in dB
AISHWARYA	97.1604	99.9456	88.82
CHEETAH	92.8554	99.8748	76.5433
LENA	96.3538	99.9387	86.4307
WOMAN	84.6043	99.5216	64.9548
BARBARA	91.0828	99.7633	73.7503
MANDRILL	81.9664	99.7082	69.5213
FINGURE	91.2581	98.9244	72.6834
BIRD	96.7604	99.8894	83.3235
ROSE	84.9632	99.4486	69.6195
DONKEY	89.5941	99.7462	73.9705
BUTTERFLY	92.0675	99.9438	77.0963
DIAGONAL	88.8387	99.5876	74.422
HORIZONTAL	90.0897	99.9692	89.3711
VERTICAL	87.6484	99.9624	89.7418

4.4.3.2 SELECTION OF BEST BASIS BASED ON LOG ENTROPY

The wavelet packets are offering a more complex and flexible analysis. In wavelet packets analysis the details as well as the approximation are splitted**.** As there is large number of sub-bands obtained after the wavelet packets decomposition, the time complexity of the algorithm is high. To reduce the time complexity, in this algorithm well known log entropy criterion is used to construct the best tree (to select the best basis for wavelet packet image compression). The cost function is used to select the best basis in paper [78]. The fast algorithm to select the best basis for wavelet packet best tree based on log entropy is implemented and tested. The log entropy criterion finds the information contains of transform coefficients of sub-bands. Log entropy is obtained by the equation

$$Entropy = \sum_{l=1}^{N} \log Xi^2 \qquad \text{---4.4.3.2}$$

Where Xi is the i^{th} coefficient of sub-band and N is the length of sub-band.

The information contain of decomposed components of wavelet packets may be greater than or less than the information contain of component, which has been decomposed. The sum of cost (log entropy) of decomposed components (child nodes) is checked with cost of component, which has been decomposed (parent node). If sum of the cost of child nodes is less than the cost of parent node, then the child nodes are considered as leaf nodes of the tree, otherwise child nodes are neglected from the tree,

and parent node becomes leaf node of the tree. This process is iterated up to the last level of decomposition.

The time complexity of proposed algorithm is less as compared to the algorithm in paper [78] is discussed. In the given algorithm, the first wavelet packets decomposition of level 'J' takes place, and cost functions of all nodes in the decomposition tree are evaluated. Beginning at bottom of the tree, the cost function of the parent node is compared with union of cost functions of child nodes. According to the comparison of results the best basis node(s) is selected. This procedure is applied recursively at each level of the tree until the top most node of the tree is reached. In proposed algorithm there is no need of full wavelet packets decomposition of level 'J' and no need to evaluate cost function of all nodes initially. Algorithm of best basis selection based on Log entropy is:

1. Load the image
2. Set current node equal to input image
3. Decompose the current node using wavelet packet tree
4. Evaluate the cost of current node, and decomposed components
5. Compare the cost of parent node (current node) with the sum of cost of child nodes (decomposed components). If the sum of cost of child nodes is greater than the parent node, consider the parent node as leaf node of the tree, and child nodes are pruned, else repeat the steps 3, 4, and 5 for each child node by considering a child node as a current node, until last level of the tree reached.

This algorithm reduces the time complexity, because there is no need to decompose the full wavelet packets tree and no need to evaluate the costs initially. The decision of further decomposition, and cost calculation is based on the run time strategy of the algorithm, and it decides at run time whether to retain or prune the decomposed components [112]. The flow chart of the above algorithm is given in figure 4.4.3.2.

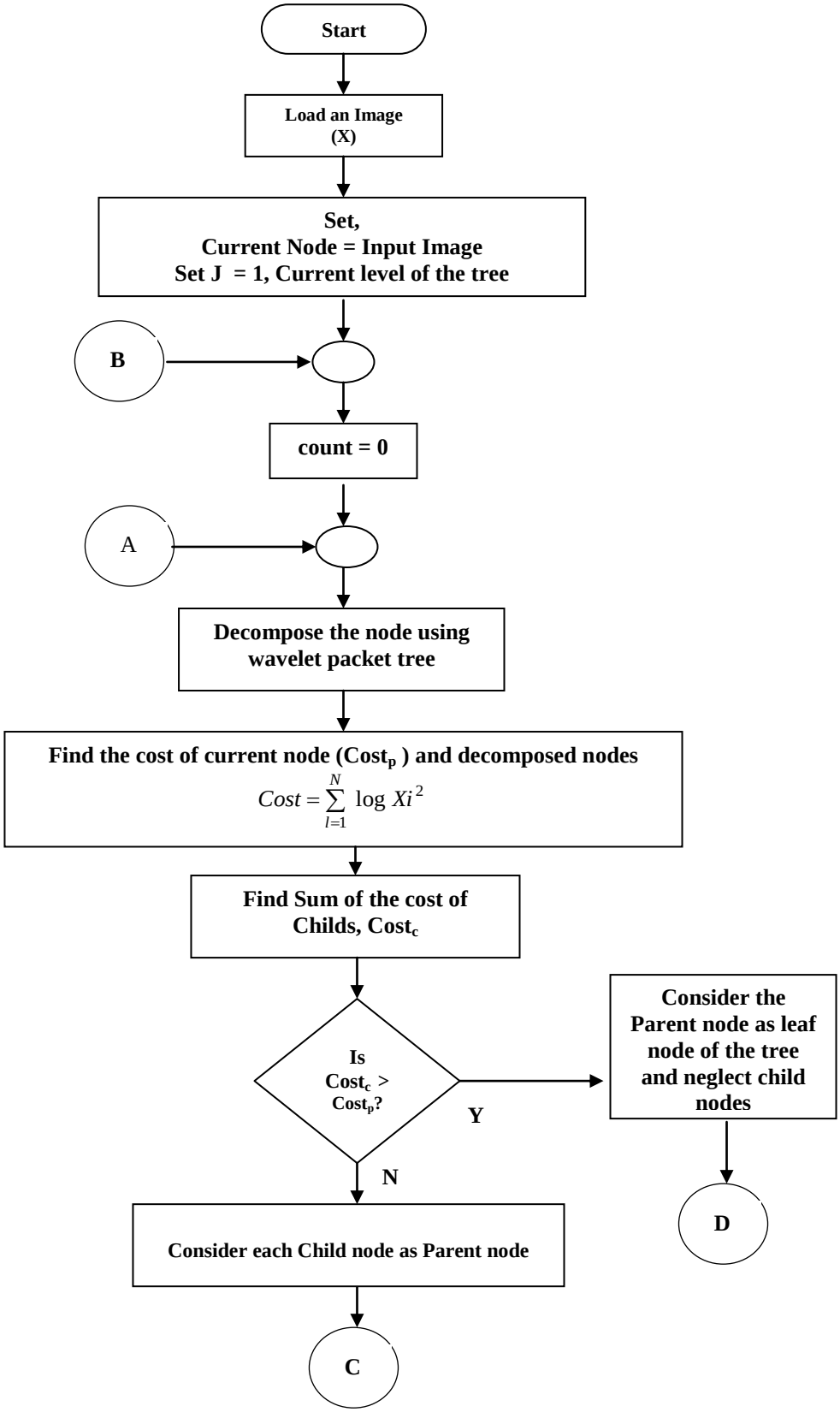

Figure 4.4.3.2: The flow chart of selection of best basis based on Log entropy

(Continued)

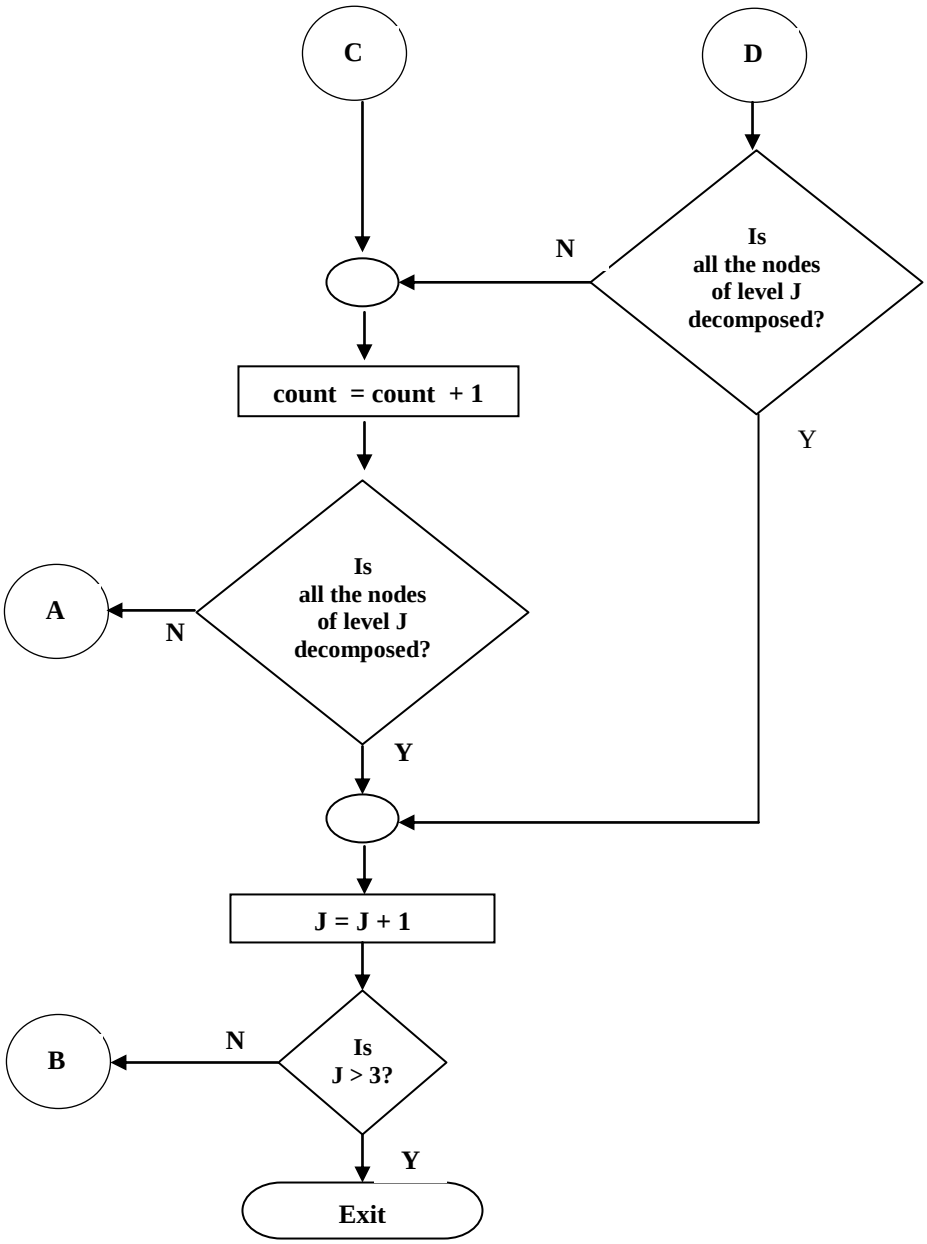

Figure 4.4.3.2: The flow chart of selection of best basis based on Log entropy

The experimental results of the selection of best basis based on log entropy in terms of percentage of zeros, energy retained and peak signal to noise ratio for the natural and synthetic images are given in table 4.4.3.2

Table 4.4.3.2 Results of selection of best basis based on Log entropy for the natural and synthetic images

Name of The images	Proposed Wavelet Packet Tree		
	Percentage of zeros	Percentage of Energy in retained	PSNR in dB
AISHWARYA	97.3539	99.9453	89.0559
CHEETAH	93.4543	99.8795	77.5847
LENA	96.7052	99.9403	86.9598
WOMAN	82.3964	99.5533	64.9028
BARBARA	91.6104	99.7769	74.6009
MANDRILL	81.6895	99.7051	69.3463
FINGURE	92.1989	98.8912	73.7326
BIRD	96.8896	99.8824	83.0857
ROSE	85.1602	99.393	69.3545
DONKEY	90.0651	99.7285	73.5779
BUTTERFLY	92.2415	99.9407	76.6458
DIAGONAL	88.6991	99.7156	77.592
HORIZONTAL	90.1315	99.9689	91.2219
VERTICAL	88.3207	99.9468	87.6995

4.4.4.3 SELECTION OF BEST BASIS BASED ON SHANNON ENTROPY

The wavelet packets are offering a more complex and flexible analysis. In wavelet packets analysis the details as well as the approximation are splitted**.** As there is large number of sub-bands obtained after the wavelet packets decomposition, the time complexity of the algorithm is high. To reduce the time complexity, in this algorithm well known Shannon entropy criterion is used to construct the best tree (to select the best basis for wavelet packet image compression). The cost function is used to select the best basis in paper [79]. The fast algorithm to select the best basis for wavelet packet best tree based on Shannon entropy is implemented and tested. The Shannon entropy criterion finds the information contains of transform coefficients of sub-bands. Shannon entropy is obtained by the equation

$$Entropy = -\sum_{i=1}^{N} Xi^2 \log Xi^2 \qquad \text{---4.4.3.3}$$

Where Xi is the i^{th} coefficient of sub-band and N is the length of sub-band.

The information contain of decomposed components of wavelet packets may be greater than or less than the information contain of component, which has been decomposed. The sum of cost (Shannon entropy) of decomposed components (child nodes) is checked with cost of component, which has been decomposed (parent node). If sum of the cost of child nodes is less than the cost of parent node, then the child nodes are considered as leaf nodes of the tree, otherwise child nodes are neglected from the

tree, and parent node becomes leaf node of the tree. This process is iterated up to the last level of decomposition.

The time complexity of proposed algorithm is less as compared to algorithm in paper [79] is discussed. In the given algorithm, the first wavelet packets decomposition of level 'J' takes place, and cost functions of all nodes in the decomposition tree are evaluated. Beginning at bottom of the tree, the cost function of the parent node is compared with union of cost functions of child nodes. According to the comparison of results the best basis node(s) is selected. This procedure is applied recursively at each level of the tree until the top most node of the tree is reached. In proposed algorithm there is no need of full wavelet packets decomposition of level 'J' and no need to evaluate cost function of all nodes initially. Algorithm of best basis selection based on Shannon entropy is:

1. Load the image
2. Set current node equal to input image
3. Decompose the current node using wavelet packet tree
4. Evaluate the cost of current node, and decomposed components
5. Compare the cost of parent node (current node) with the sum of cost of child nodes (decomposed components). If the sum of cost of child nodes is greater than the parent node, consider the parent node as leaf node of the tree, and child nodes are pruned, else repeat the steps 3, 4, and 5 for each child node by considering a child node as a current node, until last level of the tree reached.

This algorithm reduces the time complexity, because there is no need to decompose the full wavelet packets tree and no need to evaluate the costs initially. The decision of further decomposition, and cost calculation is based on the run time strategy of the algorithm, and it decides at run time whether to retain or prune the decomposed components [110]. The flow chart of the above algorithm is given in figure 4.4.3.3.

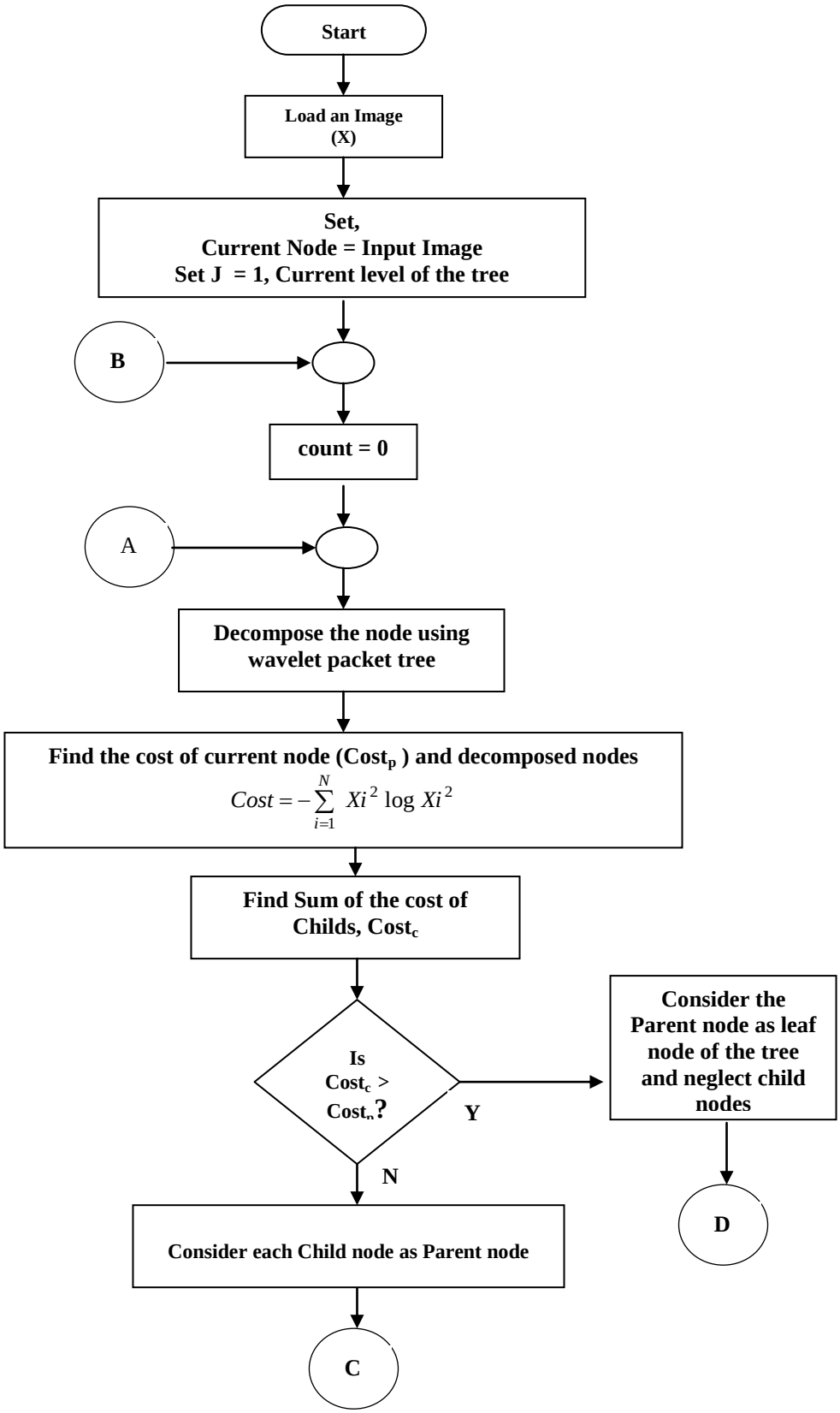

Figure 4.4.3.3: The flow chart of selection of best basis based on Shannon entropy (Continued)

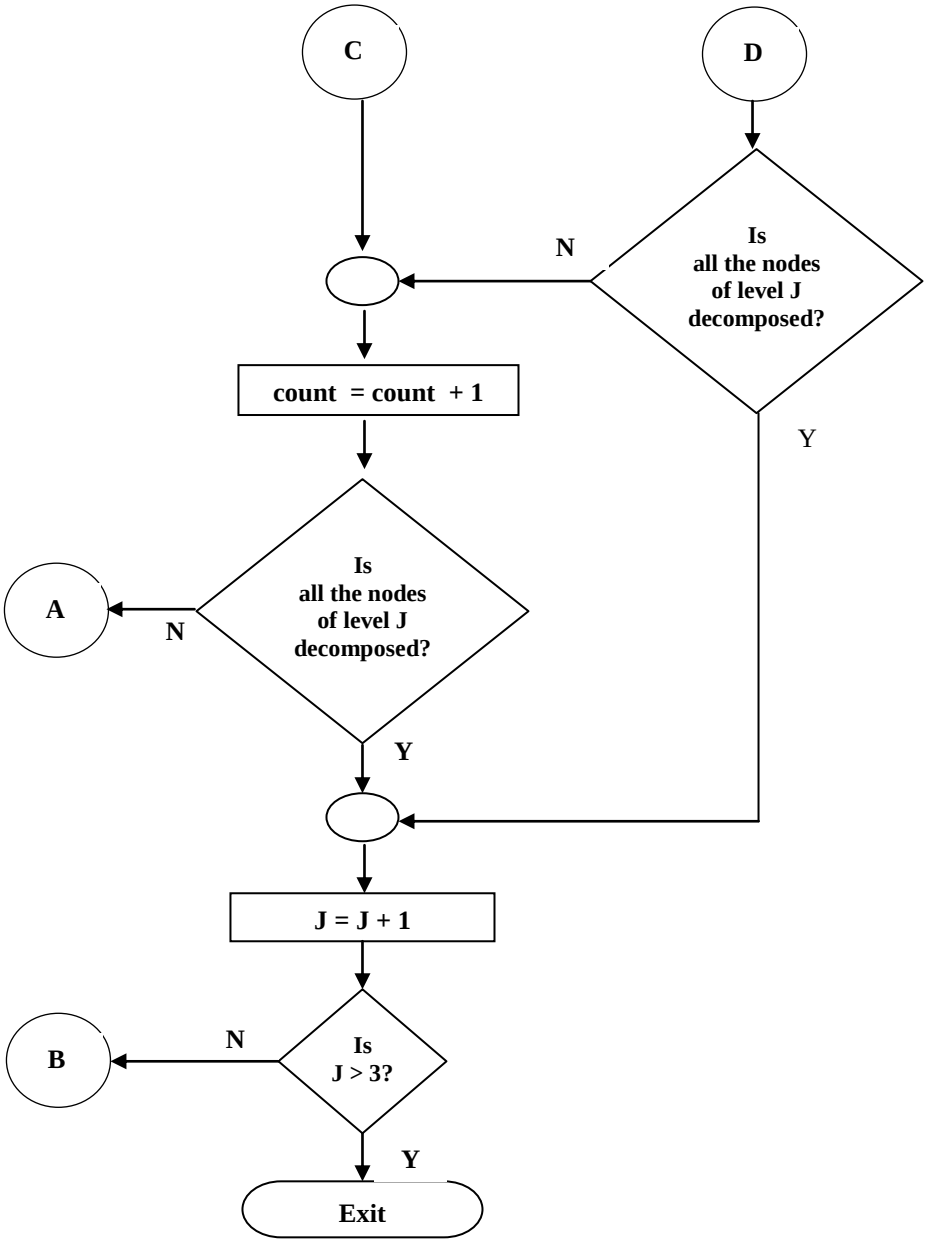

Figure 4.4.3.3: The flow chart of selection of best basis based on Shannon entropy

The experimental results of the selection of best basis based on Shannon entropy in terms of percentage of zeros, energy retained and peak signal to noise ratio for the natural and synthetic images are given in table 4.4.3.3

Table 4.4.3.3 Results of selection of best basis based on Shannon entropy for the natural and synthetic images

Name of The images	Proposed Wavelet Packet Tree		
	Percentage of zeros	Percentage of Energy in retained	PSNR in dB
AISHWARYA	97.3539	99.9453	89.0559
CHEETAH	93.4543	99.8795	77.5847
LENA	96.7052	99.9403	86.9598
WOMAN	86.0381	99.4586	65.1179
BARBARA	91.6104	99.7769	74.6009
MANDRILL	82.5804	99.6784	69.2524
FINGURE	92.5357	98.8553	73.7627
BIRD	96.8896	99.8824	83.0857
ROSE	85.3911	99.3894	69.3632
DONKEY	90.3995	99.7197	73.397
BUTTERFLY	92.1114	99.9412	76.7155
DIAGONAL	88.4518	99.5197	72.9791
HORIZONTAL	90.1315	99.9689	91.2219
VERTICAL	88.3709	99.9473	89.6969

4.4.4.4 SELECTION OF BEST BASIS BASED ON ENERGY

The wavelet packets are offering a more complex and flexible analysis. In wavelet packets analysis the details as well as the approximation are splitted**.** As there is large number of sub-bands obtained after the wavelet packets decomposition, the time complexity of the algorithm is high. To reduce the time complexity, the researcher suggests energy of a component, used as cost function to select the best basis for wavelet packet best tree [111]. The energy of the components is obtained by the equation

$$Entropy = \sum_{i=1}^{N} Xi^{2} \qquad \text{---4.4.3.4}$$

Where Xi is the i^{th} coefficient of sub-band and N is the length of sub-band.

Wavelet and wavelet packets has a compact support. The energy is concentrated in a few coefficients and most of the coefficients are zero. The less entropy means more information, and more energy means the more information concentration, resulting more compactness.

The energy contain of decomposed components of wavelet packets may be greater than or less than the energy contain of component, which has been decomposed. The sum of cost (Energy) of decomposed components (child nodes) is checked with cost of component, which has been decomposed (parent node). If sum of the cost of child nodes is greater than the cost of parent node, then the child nodes are considered

as leaf nodes of the tree, otherwise child nodes are neglected from the tree, and parent node becomes leaf node of the tree. This process is iterated up to the last level of decomposition. Algorithm of best basis selection based on Energy contain is:

1. Load the image
2. Set current node equal to input image
3. Decompose the current node using wavelet packet tree
4. Evaluate the cost of current node, and decomposed components
5. Compare the cost of parent node (current node) with the sum of cost of child nodes (decomposed components). If the sum of cost of child nodes is less than the parent node, consider the parent node as leaf node of the tree, and child nodes are pruned, else repeat the steps 3, 4, and 5 for each child node by considering a child node as a current node, until last level of the tree reached.

This algorithm is efficient in terms of time complexity, because there is no need to decompose the full wavelet packets tree and no need to evaluate the costs initially. The decision of further decomposition, and cost calculation is based on the run time strategy of the algorithm, and it decides at run time whether to retain or prune the decomposed components. The flow chart of the above algorithm is given in figure 4.4.3.4.

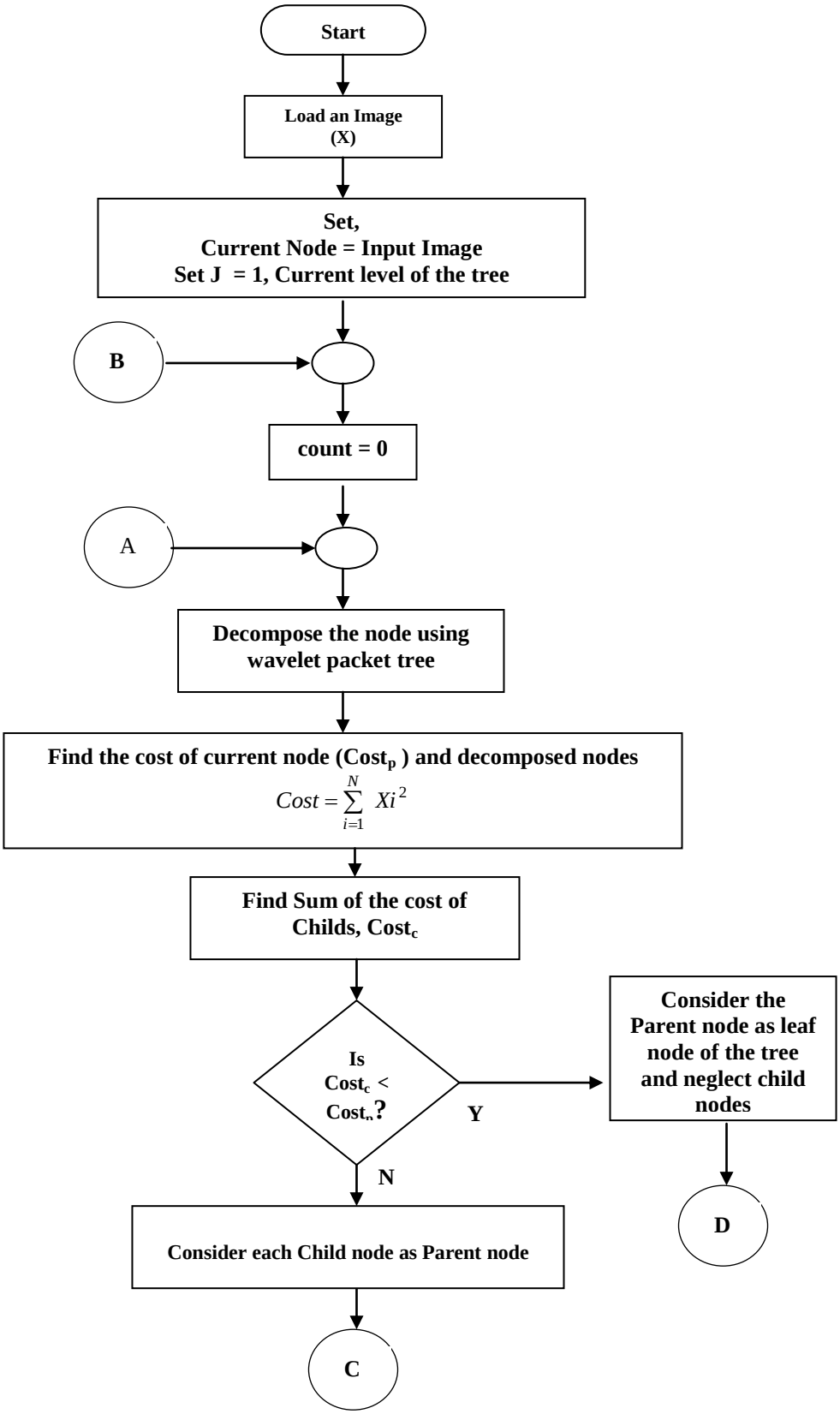

Figure 4.4.3.4: The flow chart of selection of best basis based on Energy contain
(Continued)

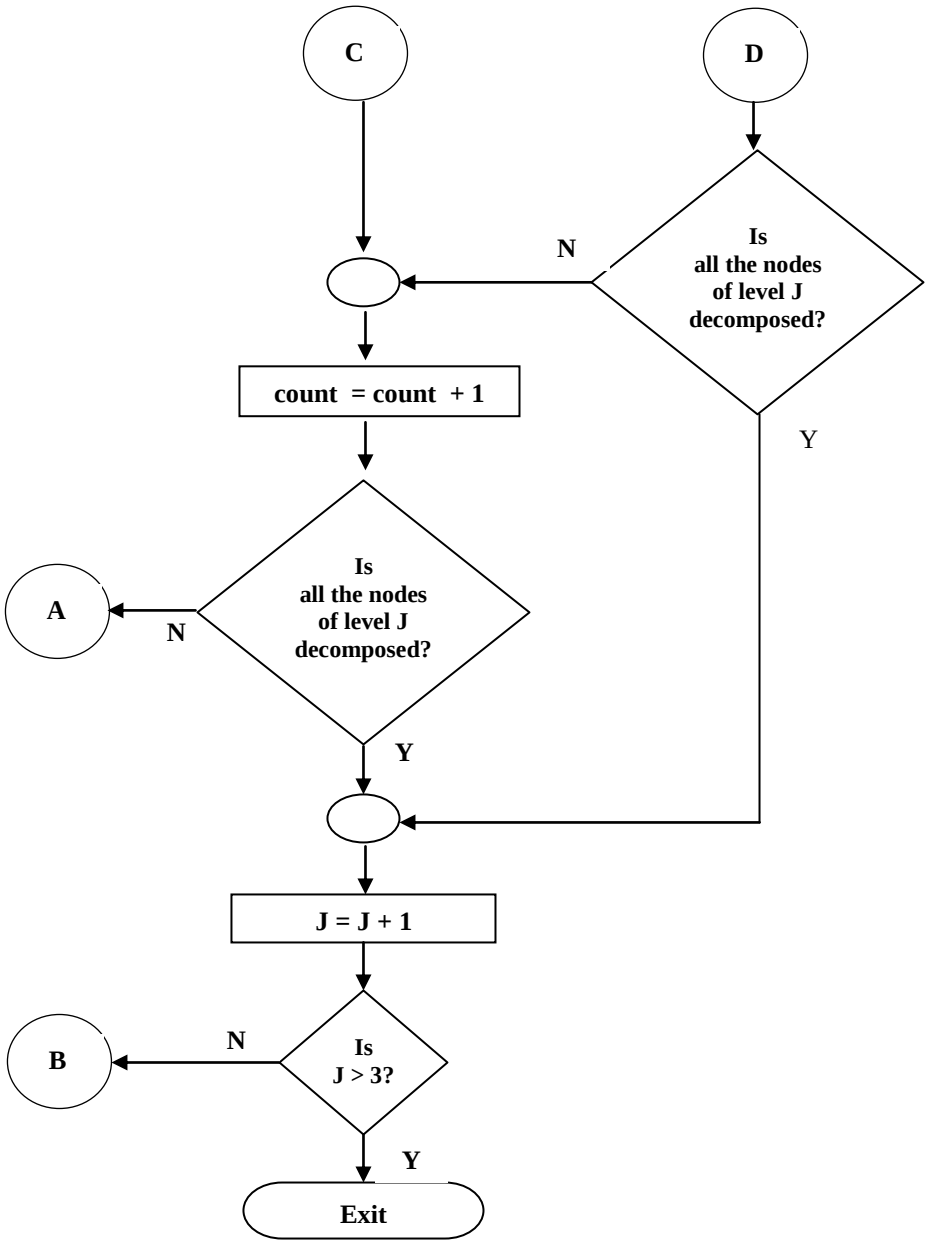

Figure 4.4.3.4: The flow chart of selection of best basis based on Energy contain

The experimental results of selection of best basis based on Energy contain in terms of percentage of zeros, energy retained and peak signal to noise ratio for the natural and synthetic images are given in table 4.4.3.4.

Table 4.4.3.4 Results of selection of best basis based on Energy contain for the natural and synthetic images

Name of The images	Proposed Wavelet Packet Tree		
	Percentage of zeros	Percentage of Energy in retained	PSNR in dB
AISHWARYA	97.4437	99.9453	89.0559
CHEETAH	93.4543	99.8795	77.5847
LENA	96.7052	99.9403	86.9598
WOMAN	86.0381	99.4586	65.1179
BARBARA	91.6104	99.7769	74.6009
MANDRILL	82.5804	99.6784	69.2524
FINGURE	92.5357	98.8553	73.7627
BIRD	96.8896	99.8824	83.0857
ROSE	85.3911	99.3894	69.3632
DONKEY	90.3995	99.7197	73.3974
BUTTERFLY	92.2415	99.9407	76.6458
DIAGONAL	87.906	99.4128	70.9919
HORIZONTAL	90.1315	99.9689	91.2219
VERTICAL	88.3709	99.9473	89.6969

4.5.0 COMPARISON OF BEST BASIS SELECTION METHODS

Few researchers discussed the selection of best basis based on Threshold entropy, Log entropy and Shannon entropy [76, 78, 79]. In an efficient image compression process, time complexity should be minimum, and the developed algorithm should not be human dependant such as, in an algorithm of selection of best basis based on Threshold entropy, the human interaction is required for selection of threshold value. As a threshold value changes the structure of a tree also changes, and there is no assurance of visual quality of an image, the important information may be lost in the process. Hence even though the selection of best basis based on Threshold entropy method is simple with less time complexity, it cannot be preferred because of its human dependency.

In case of wavelet packets best tree based on Log entropy and wavelet packets best tree based on Shannon entropy, do not have human dependency, but their time complexity is more. Researcher suggests, the wavelet packets best tree based on energy contain. In proposed method there is no human dependency, and its time complexity is also less. The results of wavelet packet best tree based on threshold entropy for fixed value of threshold and thresholding using fixed value of threshold are given in table 4.4.3.1. The results of wavelet packets best tree based on log entropy and thresholding using fixed value of threshold are given in table 4.4.3.2. The results of wavelet packets best tree based on Shannon entropy and thresholding using fixed value of threshold are

given in table 4.4.3.3. The results of wavelet packets best tree based on energy and thresholding using fixed value of threshold are given in table 4.4.3.4.

It is observed that for most of natural images, percentage of zeros of proposed method is more than percentage of zeros of wavelet packets best tree based on threshold entropy and wavelet packets best tree based on log entropy by the amount of 0.0418 to 1.4332 percent and the amount of 0.0898 to 3.6417 with the good visual quality. The percentage of zeros of proposed method is same as percentage of zeros of wavelet packets best tree based on Shannon entropy. By considering time complexity, human dependency, peak signal to noise ratio and percentage of zeros, researcher strongly recommends the wavelet packets best tree based on energy contain.

4.6.0 ADAPTIVE THRESHOLD

Once the best basis has been selected based on cost function, the image is represented by a set of wavelet packets coefficients. The high compression ratio is achieved by using the thresholding to the wavelet packets coefficients. Embedded zero tree wavelet is one of the techniques proposed by the researchers [65, 66, 67, 68, 69]. This technique begins with coefficients in the coarsest scale, and then the tree is built by noting that a coefficient will have descendants at finer scales with the same spatial location. The coefficient value is compared with defined threshold, if the value of the coefficient is less than the threshold, then that coefficients are said to be insignificant. If any one coefficient is insignificant then their descendants will also be insignificant for natural image. This technique is not suitable for proposed algorithm because threshold is not constant and tree is also not regular.

Since wavelets are ill suited to represent oscillatory patterns: rapid variations of intensity can only be described by small scale wavelet coefficients, which are often quantized to zero, even at high bit rate. Hence the proposed algorithm uses wavelet packets decomposition for image compression. The advantages of wavelet packets can be gained by proper selection of thresholds. In image compression the selection of threshold plays the crucial role. In the proposed algorithm threshold is adaptive, and the adaptive threshold is calculated on the basis of nature of image.

The statistical properties of the sub-images of different orientations are usually different, and thus different thresholds should be adaptive to each sub-image. In compression algorithm, the threshold is key factor affecting the overall performance. The threshold is calculated for each resolution and orientation, taking into account the different statistical properties of each sub-image. In order to prevent the major

structures from being smoothened, in thresholding, the coefficient value less than threshold is converted to zero, and others are kept unchanged. For high value of threshold, most of the coefficients are zero, and it results in high compression, but visual quality of image is poor, and the peak signal to noise ratio is very low. For low value of threshold the visual quality of signal is good, peak signal to noise ratio is high, but compression ratio is low. The basic aim of the research is to improve the compression ratio with maintaining the quality of image, by exploiting the advantages of wavelet packets tree. For fixed global threshold the result is good for one image but for same value of threshold the result for other images may be poor. Therefore selection of threshold is one of main areas of researcher in image compression.

To obtain good visual quality results, human perception is main factor to select the threshold. Human eye is less sensitive to high frequency signal and more sensitive to low frequency signal. Hence most of the researchers suggest the low value of threshold for high frequency spectrum and high value of threshold for low frequency spectrum. But these thresholds can work well, if image has maximum low frequency components, and less value of high frequency components. The result for the image, which includes more high frequency spectrum distributed all over the image, is poor. The goal to select, variable threshold is to achieve the good visual picture quality at low bit rate. In order to benefit from variable threshold, proper model for determining the threshold, based on perceptual value of the human eye must be employed.

Thus the technique of evaluating adaptive threshold is suggested, which is based on:

- What type of mother wavelet is used to decompose the image?
- How much energy is concentrated in sub-bands?
- What is relative visibility after discarding various coefficients of equal energy at different levels of tree?

Algorithm to find the adaptive threshold is given below:

1. The RGB color components of the color image are converted in to YCrCb color components,
2. Decompose color components Y, Cr, and Cb of the image using wavelet packets tree,
3. Find the percentage of energy of each child node for each color component

$$Percentage\ Energy = \frac{Energy\ of\ child\ node}{Energy\ of\ parent\ node} \times 100 \qquad \text{---4.6.1}$$

4. Find the median of each child node for each color component

5. Calculate the threshold of each node for each color component

$$Threshold = (K - \sqrt{Percentage\ of\ energy}) \times (P - median) \quad \text{---4.6.2}$$

where the K and P are constants. To reduce the dependency of algorithm, the researcher has tested this algorithm over many natural and synthetic images. By considering the compression ratio and visual quality researcher fixes the value of K as 3. The value of P is not fixed, that provides the flexibility to the user in terms of visual quality, and compression ratio. As human eye is more sensitive to lower frequency components and less sensitive to high frequency components, the value of P for higher-level decomposition is more and lower for low-level decomposition. The researcher uses the three level wavelet packets decomposition. The value of P for first level is variable, which is provided by the user according to applications demand. The value of P for second level is P1, which is P + h_{11}. The value of P for third level is P2, which is equal to P+h_{22}, where h_{11} is a square root of median of horizontal, vertical, and diagonal components at level one of decomposition, and where h_{22} is a square root of median of horizontal, vertical, and diagonal components at level two of decomposition.

The human visual system is more sensitive to low frequency components, and less sensitive to high frequency components. Therefore, for high frequency sub-bands the threshold value should be more to neglect the high frequency components. But researcher observes that if the energy contain of high frequency component is low in a sub-bands, then the above observation holds true. But if the energy of high frequency component in a sub-band is more, then we cannot neglect the high frequency components. And hence in threshold calculation researcher has considered the energy contain of a sub-band and the median of the sub-band.

The value of the threshold suggested and implemented in Matlab 6.5 in the function “ddencmp” is constant. It is calculated by using Daubechies mother wavelet db1. In proposed algorithm the value of the threshold evaluated is also the function of the type of mother wavelet used to decompose the image. In short the recommended threshold is adaptive, which is based on nature of the image, and type of wavelet used [109]. In addition to this the researcher has provided the flexibility to select the value of P. For the low value of the P, the compression ratio is low, and visual quality of the image is good. For high value of P, the compression ratio is high, and quality of the image is degraded. This flexibility can be used according to the application demand. If the application demands the high compression ratio, and ready to accept the compromised quality of the image, then user can specify high value of P. But if application demands good quality of the image with less compression ratio, then user

can specify the low value of P. It is important to note that the minimum value of P should always be greater than the median of a sub-band. The values of the thresholds for the different values of P, for the natural and synthetic images for the color components Y, Cr, and Cb are given in a table 4.6.1 to 4.6.12.

Table 4.6.1 Thresholds for Y color component of the natural and synthetic images for P = 10 for the sub-bands 1 to 47

Images → / Threshold↓	Aishwarya	Lena	Donkey	Barbara	Mandrill	Rose	Horizontal	Vertical
TH1	1.0000	1.0000	1.0000	1.0000	1.0000	1.0000	1.0000	1.0000
TH2	27.9003	27.8009	18.3429	21.9720	6.5471	14.2113	17.4258	26.2610
TH3	27.5322	27.9667	19.5571	8.8517	13.6433	10.5887	27.9123	17.2727
TH4	29.3379	29.5174	26.9560	25.0954	24.4254	24.4721	29.7362	29.5964
TH5	1.0000	1.0000	1.0000	1.0000	1.0000	1.0000	1.0000	1.0000
TH6	30.9454	29.3670	22.6024	39.0089	20.6965	29.6282	17.4258	26.2610
TH7	29.1732	29.2462	24.7538	20.5257	35.9747	23.4393	27.9123	17.2727
TH8	35.4858	34.3688	39.2468	46.2310	58.2815	49.1330	29.7362	29.5964
TH9	55.4805	54.1816	20.2530	14.6152	85.2171	45.1983	70.0000	70.0000
TH10	30.9454	29.3670	22.6024	39.0089	20.6965	29.6282	17.4258	26.2610
TH11	29.1732	29.2462	24.7538	20.5257	35.9747	23.4393	27.9123	17.2727
TH12	35.4858	34.3688	39.2468	46.2310	58.2815	49.1330	29.7362	29.5964
TH13	55.4805	54.1816	20.2530	14.6152	85.2171	45.1983	70.0000	70.0000
TH14	30.9454	29.3670	22.6024	39.0089	20.6965	29.6282	17.4258	26.2610
TH15	29.1732	29.2462	24.7538	20.5257	35.9747	23.4393	27.9123	17.2727
TH16	35.4858	34.3688	39.2468	46.2310	58.2815	49.1330	29.7362	29.5964
TH17	55.4805	54.1816	20.2530	14.6152	85.2171	45.1983	70.0000	70.0000
TH18	30.9454	29.3670	22.6024	39.0089	20.6965	29.6282	17.4258	26.2610
TH19	29.1732	29.2462	24.7538	20.5257	35.9747	23.4393	27.9123	17.2727
TH20	30.9454	29.3670	22.6024	39.0089	20.6965	29.6282	17.4258	26.2610
TH21	0.0001	0.0001	0.0001	0.0001	0.0001	0.0001	0.0001	0.0001
TH22	37.3120	34.9349	22.6024	40.0337	20.6965	33.3816	17.4258	90.4644
TH23	29.1732	29.2462	32.6495	20.5257	31.9108	23.4393	99.6670	17.2727
TH24	49.0264	46.6241	60.7051	56.9601	73.1176	66.1946	106.1795	101.9539
TH25	39.9764	31.5686	23.5457	29.0450	81.1779	70.6663	109.9503	70.0000
TH26	37.3120	34.9349	22.6024	40.0337	20.6965	33.3816	17.4258	90.4644
TH27	29.1732	29.2462	32.6495	20.5257	31.9108	23.4393	99.6670	17.2727
TH28	49.0264	46.6241	60.7051	56.9601	73.1176	66.1946	106.1795	101.9539
TH29	39.9764	31.5686	23.5457	29.0450	81.1779	70.6663	109.9503	70.0000
TH30	37.3120	34.9349	22.6024	40.0337	20.6965	33.3816	17.4258	90.4644
TH31	29.1732	29.2462	32.6495	20.5257	31.9108	23.4393	99.6670	17.2727
TH32	49.0264	46.6241	60.7051	56.9601	73.1176	66.1946	106.1795	101.9539
TH33	39.9764	31.5686	23.5457	29.0450	81.1779	70.6663	109.9503	70.0000
TH34	37.3120	34.9349	22.6024	40.0337	20.6965	33.3816	17.4258	90.4644
TH35	29.1732	29.2462	32.6495	20.5257	31.9108	23.4393	99.6670	17.2727
TH36	49.0264	46.6241	60.7051	56.9601	73.1176	66.1946	106.1795	101.9539
TH37	39.9764	31.5686	23.5457	29.0450	81.1779	70.6663	109.9503	70.0000
TH38	37.3120	34.9349	22.6024	40.0337	20.6965	33.3816	17.4258	90.4644
TH39	29.1732	29.2462	32.6495	20.5257	31.9108	23.4393	99.6670	17.2727
TH40	49.0264	46.6241	60.7051	56.9601	73.1176	66.1946	106.1795	101.9539
TH41	39.9764	31.5686	23.5457	29.0450	81.1779	70.6663	109.9503	70.0000
TH42	37.3120	34.9349	22.6024	40.0337	20.6965	33.3816	17.4258	90.4644
TH43	29.1732	29.2462	32.6495	20.5257	31.9108	23.4393	99.6670	17.2727
TH44	49.0264	46.6241	60.7051	56.9601	73.1176	66.1946	106.1795	101.9539
TH45	0	31.5686	23.5457	29.0450	81.1779	70.6663	109.9503	70.0000
TH46	0	34.9349	22.6024	40.0337	20.6965	33.3816	17.4258	90.4644
TH47	0	29.2462	32.6495	20.5257	31.9108	23.4393	99.6670	17.2727

(Continued)

Table 4.6.1 Thresholds for Y color component of the natural and synthetic images for P = 10 for the sub-bands 48 to 84

Images → / Threshold↓	Aishwarya	Lena	Donkey	Barbara	Mandrill	Rose	Horizontal	Vertical
TH48	0	46.6241	60.7051	56.9601	73.1176	66.1946	106.1795	101.9539
TH49	39.9764	31.5686	23.5457	29.0450	81.1779	70.6663	109.9503	70.0000
TH50	37.3120	34.9349	22.6024	40.0337	20.6965	33.3816	17.4258	90.4644
TH51	29.1732	29.2462	32.6495	20.5257	31.9108	23.4393	99.6670	17.2727
TH52	49.0264	46.6241	60.7051	56.9601	73.1176	66.1946	106.1795	101.9539
TH53	84.3401	83.0020	108.1537	114.9941	193.4811	161.7985	70.0000	70.0000
TH54	37.3120	34.9349	22.6024	40.0337	20.6965	33.3816	17.4258	90.4644
TH55	29.1732	29.2462	32.6495	20.5257	31.9108	23.4393	99.6670	17.2727
TH56	49.0264	46.6241	60.7051	56.9601	73.1176	66.1946	106.1795	101.9539
TH57	0	0.7318	0.5458	0.6733	1.8819	1.6382	2.5489	1.6228
TH58	0	34.9349	22.6024	40.0337	20.6965	33.3816	17.4258	90.4644
TH59	0	29.2462	32.6495	20.5257	31.9108	23.4393	99.6670	17.2727
TH60	0	46.6241	60.7051	56.9601	73.1176	66.1946	106.1795	101.9539
TH61	39.9764	31.5686	23.5457	29.0450	81.1779	70.6663	109.9503	70.0000
TH62	37.3120	34.9349	22.6024	40.0337	20.6965	33.3816	17.4258	90.4644
TH63	29.1732	29.2462	32.6495	20.5257	31.9108	23.4393	99.6670	17.2727
TH64	49.0264	46.6241	60.7051	56.9601	73.1176	66.1946	106.1795	101.9539
TH65	39.9764	31.5686	23.5457	29.0450	81.1779	70.6663	109.9503	70.0000
TH66	37.3120	34.9349	22.6024	40.0337	20.6965	33.3816	17.4258	90.4644
TH67	29.1732	29.2462	32.6495	20.5257	31.9108	23.4393	99.6670	17.2727
TH68	49.0264	46.6241	60.7051	56.9601	73.1176	66.1946	106.1795	101.9539
TH69	0	31.5686	23.5457	29.0450	81.1779	70.6663	109.9503	70.0000
TH70	0	34.9349	22.6024	40.0337	20.6965	33.3816	17.4258	90.4644
TH71	0	29.2462	32.6495	20.5257	31.9108	23.4393	99.6670	17.2727
TH72	0	46.6241	60.7051	56.9601	73.1176	66.1946	106.1795	101.9539
TH73	39.9764	31.5686	23.5457	29.0450	81.1779	70.6663	109.9503	70.0000
TH74	37.3120	34.9349	22.6024	40.0337	20.6965	33.3816	17.4258	90.4644
TH75	29.1732	29.2462	32.6495	20.5257	31.9108	23.4393	99.6670	17.2727
TH76	49.0264	46.6241	60.7051	56.9601	73.1176	66.1946	106.1795	101.9539
TH77	39.9764	31.5686	23.5457	29.0450	81.1779	70.6663	109.9503	70.0000
TH78	37.3120	34.9349	22.6024	40.0337	20.6965	33.3816	17.4258	90.4644
TH79	29.1732	29.2462	32.6495	20.5257	31.9108	23.4393	99.6670	17.2727
TH80	49.0264	46.6241	60.7051	56.9601	73.1176	66.1946	106.1795	101.9539
TH81	39.9764	31.5686	23.5457	29.0450	81.1779	70.6663	109.9503	70.0000
TH82	37.3120	34.9349	22.6024	40.0337	20.6965	33.3816	17.4258	90.4644
TH83	29.1732	29.2462	32.6495	20.5257	31.9108	23.4393	99.6670	17.2727
TH84	49.0264	46.6241	60.7051	56.9601	73.1176	66.1946	106.1795	101.9539

Table 4.6.2 Thresholds for Y color component of the natural and synthetic images for P = 20 for the sub-bands 1 to 10

Images → / Threshold↓	Aishwarya	Lena	Donkey	Barbara	Mandrill	Rose	Horizontal	Vertical
TH1	1.0000	1.0000	1.0000	1.0000	1.0000	1.0000	1.0000	1.0000
TH2	57.2690	57.0650	40.9453	49.4371	27.2436	38.6175	34.8515	52.5221
TH3	56.7054	57.2129	42.9961	29.3773	38.6023	34.0280	55.8246	34.5455
TH4	59.1870	59.4084	54.9623	53.3719	52.0950	52.7551	59.4723	59.1927
TH5	1.0000	1.0000	1.0000	1.0000	1.0000	1.0000	1.0000	1.0000
TH6	60.3142	58.6311	45.2047	66.4740	41.3929	54.0344	34.8515	52.5221
TH7	58.3464	58.4924	48.1929	41.0513	60.9338	46.8786	55.8246	34.5455
TH8	65.3349	64.2598	67.2531	74.5075	85.9512	77.4160	59.4723	59.1927
TH9	125.4805	124.1816	90.2530	84.6152	15.2171	24.8017	140.0000	140.0000
TH10	60.3142	58.6311	45.2047	66.4740	41.3929	54.0344	34.8515	52.5221

(Continued)

Table 4.6.2 Thresholds for Y color component of the natural and synthetic images for P = 20 for the sub-bands 11 to 64

Images → / Threshold↓	Aishwarya	Lena	Donkey	Barbara	Mandrill	Rose	Horizontal	Vertical
TH11	58.3464	58.4924	48.1929	41.0513	60.9338	46.8786	55.8246	34.5455
TH12	65.3349	64.2598	67.2531	74.5075	85.9512	77.4160	59.4723	59.1927
TH13	125.4805	124.1816	90.2530	84.6152	15.2171	24.8017	140.0000	140.0000
TH14	60.3142	58.6311	45.2047	66.4740	41.3929	54.0344	34.8515	52.5221
TH15	58.3464	58.4924	48.1929	41.0513	60.9338	46.8786	55.8246	34.5455
TH16	65.3349	64.2598	67.2531	74.5075	85.9512	77.4160	59.4723	59.1927
TH17	125.4805	124.1816	90.2530	84.6152	15.2171	24.8017	140.0000	140.0000
TH18	60.3142	58.6311	45.2047	66.4740	41.3929	54.0344	34.8515	52.5221
TH19	58.3464	58.4924	48.1929	41.0513	60.9338	46.8786	55.8246	34.5455
TH20	60.3142	58.6311	45.2047	66.4740	41.3929	54.0344	34.8515	52.5221
TH21	0.0001	0.0001	0.0001	0.0001	0.0001	0.0001	0.0001	0.0001
TH22	66.6808	64.1990	45.2047	67.4987	41.3929	57.7878	34.8515	116.7254
TH23	58.3464	58.4924	56.0885	41.0513	56.8698	46.8786	127.5792	34.5455
TH24	78.8754	76.5151	88.7114	85.2367	100.7873	94.4776	135.9156	131.5503
TH25	109.9764	101.5686	46.4543	99.0450	11.1779	0.6663	39.9503	140.0000
TH26	66.6808	64.1990	45.2047	67.4987	41.3929	57.7878	34.8515	116.7254
TH27	58.3464	58.4924	56.0885	41.0513	56.8698	46.8786	127.5792	34.5455
TH28	78.8754	76.5151	88.7114	85.2367	100.7873	94.4776	135.9156	131.5503
TH29	109.9764	101.5686	46.4543	99.0450	11.1779	0.6663	39.9503	140.0000
TH30	66.6808	64.1990	45.2047	67.4987	41.3929	57.7878	34.8515	116.7254
TH31	58.3464	58.4924	56.0885	41.0513	56.8698	46.8786	127.5792	34.5455
TH32	78.8754	76.5151	88.7114	85.2367	100.7873	94.4776	135.9156	131.5503
TH33	109.9764	101.5686	46.4543	99.0450	11.1779	0.6663	39.9503	140.0000
TH34	66.6808	64.1990	45.2047	67.4987	41.3929	57.7878	34.8515	116.7254
TH35	58.3464	58.4924	56.0885	41.0513	56.8698	46.8786	127.5792	34.5455
TH36	78.8754	76.5151	88.7114	85.2367	100.7873	94.4776	135.9156	131.5503
TH37	109.9764	101.5686	46.4543	99.0450	11.1779	0.6663	39.9503	140.0000
TH38	66.6808	64.1990	45.2047	67.4987	41.3929	57.7878	34.8515	116.7254
TH39	58.3464	58.4924	56.0885	41.0513	56.8698	46.8786	127.5792	34.5455
TH40	78.8754	76.5151	88.7114	85.2367	100.7873	94.4776	135.9156	131.5503
TH41	109.9764	101.5686	46.4543	99.0450	11.1779	0.6663	39.9503	140.0000
TH42	66.6808	64.1990	45.2047	67.4987	41.3929	57.7878	34.8515	116.7254
TH43	58.3464	58.4924	56.0885	41.0513	56.8698	46.8786	127.5792	34.5455
TH44	78.8754	76.5151	88.7114	85.2367	100.7873	94.4776	135.9156	131.5503
TH45	0	101.5686	46.4543	99.0450	11.1779	0.6663	39.9503	140.0000
TH46	0	64.1990	45.2047	67.4987	41.3929	57.7878	34.8515	116.7254
TH47	0	58.4924	56.0885	41.0513	56.8698	46.8786	127.5792	34.5455
TH48	0	76.5151	88.7114	85.2367	100.7873	94.4776	135.9156	131.5503
TH49	109.9764	101.5686	46.4543	99.0450	11.1779	0.6663	39.9503	140.0000
TH50	66.6808	64.1990	45.2047	67.4987	41.3929	57.7878	34.8515	116.7254
TH51	58.3464	58.4924	56.0885	41.0513	56.8698	46.8786	127.5792	34.5455
TH52	78.8754	76.5151	88.7114	85.2367	100.7873	94.4776	135.9156	131.5503
TH53	154.3401	153.0020	178.1537	184.9941	263.4811	231.7985	140.0000	140.0000
TH54	66.6808	64.1990	45.2047	67.4987	41.3929	57.7878	34.8515	116.7254
TH55	58.3464	58.4924	56.0885	41.0513	56.8698	46.8786	127.5792	34.5455
TH56	78.8754	76.5151	88.7114	85.2367	100.7873	94.4776	135.9156	131.5503
TH57	0	2.3546	1.0769	2.2961	0.2591	0.0154	0.9261	3.2456
TH58	0	64.1990	45.2047	67.4987	41.3929	57.7878	34.8515	116.7254
TH59	0	58.4924	56.0885	41.0513	56.8698	46.8786	127.5792	34.5455
TH60	0	76.5151	88.7114	85.2367	100.7873	94.4776	135.9156	131.5503
TH61	109.9764	101.5686	46.4543	99.0450	11.1779	0.6663	39.9503	140.0000
TH62	66.6808	64.1990	45.2047	67.4987	41.3929	57.7878	34.8515	116.7254
TH63	58.3464	58.4924	56.0885	41.0513	56.8698	46.8786	127.5792	34.5455
TH64	78.8754	76.5151	88.7114	85.2367	100.7873	94.4776	135.9156	131.5503

(Continued)

Table 4.6.2 Thresholds for Y color component of the natural and synthetic images for P = 20 for the sub-bands 65 to 84

Images → / Threshold↓	Aishwarya	Lena	Donkey	Barbara	Mandrill	Rose	Horizontal	Vertical
TH65	109.9764	101.5686	46.4543	99.0450	11.1779	0.6663	39.9503	140.0000
TH66	66.6808	64.1990	45.2047	67.4987	41.3929	57.7878	34.8515	116.7254
TH67	58.3464	58.4924	56.0885	41.0513	56.8698	46.8786	127.5792	34.5455
TH68	78.8754	76.5151	88.7114	85.2367	100.7873	94.4776	135.9156	131.5503
TH69	0	101.5686	46.4543	99.0450	11.1779	0.6663	39.9503	140.0000
TH70	0	64.1990	45.2047	67.4987	41.3929	57.7878	34.8515	116.7254
TH71	0	58.4924	56.0885	41.0513	56.8698	46.8786	127.5792	34.5455
TH72	0	76.5151	88.7114	85.2367	100.7873	94.4776	135.9156	131.5503
TH73	109.9764	101.5686	46.4543	99.0450	11.1779	0.6663	39.9503	140.0000
TH74	66.6808	64.1990	45.2047	67.4987	41.3929	57.7878	34.8515	116.7254
TH75	58.3464	58.4924	56.0885	41.0513	56.8698	46.8786	127.5792	34.5455
TH76	78.8754	76.5151	88.7114	85.2367	100.7873	94.4776	135.9156	131.5503
TH77	109.9764	101.5686	46.4543	99.0450	11.1779	0.6663	39.9503	140.0000
TH78	66.6808	64.1990	45.2047	67.4987	41.3929	57.7878	34.8515	116.7254
TH79	58.3464	58.4924	56.0885	41.0513	56.8698	46.8786	127.5792	34.5455
TH80	78.8754	76.5151	88.7114	85.2367	100.7873	94.4776	135.9156	131.5503
TH81	109.9764	101.5686	46.4543	99.0450	11.1779	0.6663	39.9503	140.0000
TH82	66.6808	64.1990	45.2047	67.4987	41.3929	57.7878	34.8515	116.7254
TH83	58.3464	58.4924	56.0885	41.0513	56.8698	46.8786	127.5792	34.5455
TH84	78.8754	76.5151	88.711	85.2367	100.7873	94.4776	135.9156	131.5503

Table 4.6.3 Thresholds for Y color component of the natural and synthetic images for P = 30 for the sub-bands 1 to 28

Images → / Threshold↓	Aishwarya	Lena	Donkey	Barbara	Mandrill	Rose	Horizontal	Vertical
TH1	1.0000	1.0000	1.0000	1.0000	1.0000	1.0000	1.0000	1.0000
TH2	86.6378	86.3291	63.5476	76.9021	47.9400	63.0236	52.2773	78.7831
TH3	85.8786	86.4591	66.4352	49.9030	63.5614	57.4674	83.7369	51.8182
TH4	89.0360	89.2994	82.9685	81.6484	79.7647	81.0381	89.2085	88.7891
TH5	1.0000	1.0000	1.0000	1.0000	1.0000	1.0000	1.0000	1.0000
TH6	89.6829	87.8952	67.8071	93.9390	62.0894	78.4405	52.2773	78.7831
TH7	87.5196	87.7387	71.6319	61.5770	85.8928	70.3180	83.7369	51.8182
TH8	95.1840	94.1508	95.2593	102.7840	113.6208	105.6991	89.2085	88.7891
TH9	195.4805	194.1816	160.2530	154.6152	54.7829	94.8017	210.0000	210.0000
TH10	89.6829	87.8952	67.8071	93.9390	62.0894	78.4405	52.2773	78.7831
TH11	87.5196	87.7387	71.6319	61.5770	85.8928	70.3180	83.7369	51.8182
TH12	95.1840	94.1508	95.2593	102.7840	113.6208	105.6991	89.2085	88.7891
TH13	195.4805	194.1816	160.2530	154.6152	54.7829	94.8017	210.0000	210.0000
TH14	89.6829	87.8952	67.8071	93.9390	62.0894	78.4405	52.2773	78.7831
TH15	87.5196	87.7387	71.6319	61.5770	85.8928	70.3180	83.7369	51.8182
TH16	95.1840	94.1508	95.2593	102.7840	113.6208	105.6991	89.2085	88.7891
TH17	195.4805	194.1816	160.2530	154.6152	54.7829	94.8017	210.0000	210.0000
TH18	89.6829	87.8952	67.8071	93.9390	62.0894	78.4405	52.2773	78.7831
TH19	87.5196	87.7387	71.6319	61.5770	85.8928	70.3180	83.7369	51.8182
TH20	89.6829	87.8952	67.8071	93.9390	62.0894	78.4405	52.2773	78.7831
TH21	0.0001	0.0001	0.0001	0.0001	0.0001	0.0001	0.0001	0.0001
TH22	96.0495	93.4631	67.8071	94.9637	62.0894	82.1939	52.2773	142.9865
TH23	87.5196	87.7387	79.5276	61.5770	81.8288	70.3180	155.4915	51.8182
TH24	108.7245	106.4062	116.7176	113.5132	128.4569	122.7606	165.6518	161.1466
TH25	179.9764	171.5686	116.4543	169.0450	58.8221	69.3337	30.0497	210.0000
TH26	96.0495	93.4631	67.8071	94.9637	62.0894	82.1939	52.2773	142.9865
TH27	87.5196	87.7387	79.5276	61.5770	81.8288	70.3180	155.4915	51.8182
TH28	108.7245	106.4062	116.7176	113.5132	128.4569	122.7606	165.6518	161.1466

(Continued)

Table 4.6.3 Thresholds for Y color component of the natural and synthetic images for P = 30 for the sub-bands 29 to 84

TH29	179.9764	171.5686	116.4543	169.0450	58.8221	69.3337	30.0497	210.0000
TH30	96.0495	93.4631	67.8071	94.9637	62.0894	82.1939	52.2773	142.9865
TH31	87.5196	87.7387	79.5276	61.5770	81.8288	70.3180	155.4915	51.8182
TH32	108.7245	106.4062	116.7176	113.5132	128.4569	122.7606	165.6518	161.1466
TH33	179.9764	171.5686	116.4543	169.0450	58.8221	69.3337	30.0497	210.0000
TH34	96.0495	93.4631	67.8071	94.9637	62.0894	82.1939	52.2773	142.9865
TH35	87.5196	87.7387	79.5276	61.5770	81.8288	70.3180	155.4915	51.8182
TH36	108.7245	106.4062	116.7176	113.5132	128.4569	122.7606	165.6518	161.1466
TH37	179.9764	171.5686	116.4543	169.0450	58.8221	69.3337	30.0497	210.0000
TH38	96.0495	93.4631	67.8071	94.9637	62.0894	82.1939	52.2773	142.9865
TH39	87.5196	87.7387	79.5276	61.5770	81.8288	70.3180	155.4915	51.8182
TH40	108.7245	106.4062	116.7176	113.5132	128.4569	122.7606	165.6518	161.1466
TH41	179.9764	171.5686	116.4543	169.0450	58.8221	69.3337	30.0497	210.0000
TH42	96.0495	93.4631	67.8071	94.9637	62.0894	82.1939	52.2773	142.9865
TH43	87.5196	87.7387	79.5276	61.5770	81.8288	70.3180	155.4915	51.8182
TH44	108.7245	106.4062	116.7176	113.5132	128.4569	122.7606	165.6518	161.1466
TH45	0	171.5686	116.4543	169.0450	58.8221	69.3337	30.0497	210.0000
TH46	0	93.4631	67.8071	94.9637	62.0894	82.1939	52.2773	142.9865
TH47	0	87.7387	79.5276	61.5770	81.8288	70.3180	155.4915	51.8182
TH48	0	106.4062	116.7176	113.5132	128.4569	122.7606	165.6518	161.1466
TH49	179.9764	171.5686	116.4543	169.0450	58.8221	69.3337	30.0497	210.0000
TH50	96.0495	93.4631	67.8071	94.9637	62.0894	82.1939	52.2773	142.9865
TH51	87.5196	87.7387	79.5276	61.5770	81.8288	70.3180	155.4915	51.8182
TH52	108.7245	106.4062	116.7176	113.5132	128.4569	122.7606	165.6518	161.1466
TH53	224.3401	223.0020	248.1537	254.9941	333.4811	301.7985	210.0000	210.0000
TH54	96.0495	93.4631	67.8071	94.9637	62.0894	82.1939	52.2773	142.9865
TH55	87.5196	87.7387	79.5276	61.5770	81.8288	70.3180	155.4915	51.8182
TH56	108.7245	106.4062	116.7176	113.5132	128.4569	122.7606	165.6518	161.1466
TH57	0	3.9774	2.6997	3.9189	1.3636	1.6073	0.6966	4.8683
TH58	0	93.4631	67.8071	94.9637	62.0894	82.1939	52.2773	142.9865
TH59	0	87.7387	79.5276	61.5770	81.8288	70.3180	155.4915	51.8182
TH60	0	106.4062	116.7176	113.5132	128.4569	122.7606	165.6518	161.1466
TH61	179.9764	171.5686	116.4543	169.0450	58.8221	69.3337	30.0497	210.0000
TH62	96.0495	93.4631	67.8071	94.9637	62.0894	82.1939	52.2773	142.9865
TH63	87.5196	87.7387	79.5276	61.5770	81.8288	70.3180	155.4915	51.8182
TH64	108.7245	106.4062	116.7176	113.5132	128.4569	122.7606	165.6518	161.1466
TH65	179.9764	171.5686	116.4543	169.0450	58.8221	69.3337	30.0497	210.0000
TH66	96.0495	93.4631	67.8071	94.9637	62.0894	82.1939	52.2773	142.9865
TH67	87.5196	87.7387	79.5276	61.5770	81.8288	70.3180	155.4915	51.8182
TH68	108.7245	106.4062	116.7176	113.5132	128.4569	122.7606	165.6518	161.1466
TH69	0	171.5686	116.4543	169.0450	58.8221	69.3337	30.0497	210.0000
TH70	0	93.4631	67.8071	94.9637	62.0894	82.1939	52.2773	142.9865
TH71	0	87.7387	79.5276	61.5770	81.8288	70.3180	155.4915	51.8182
TH72	0	106.4062	116.7176	113.5132	128.4569	122.7606	165.6518	161.1466
TH73	179.9764	171.5686	116.4543	169.0450	58.8221	69.3337	30.0497	210.0000
TH74	96.0495	93.4631	67.8071	94.9637	62.0894	82.1939	52.2773	142.9865
TH75	87.5196	87.7387	79.5276	61.5770	81.8288	70.3180	155.4915	51.8182
TH76	108.7245	106.4062	116.7176	113.5132	128.4569	122.7606	165.6518	161.1466
TH77	179.9764	171.5686	116.4543	169.0450	58.8221	69.3337	30.0497	210.0000
TH78	96.0495	93.4631	67.8071	94.9637	62.0894	82.1939	52.2773	142.9865
TH79	87.5196	87.7387	79.5276	61.5770	81.8288	70.3180	155.4915	51.8182
TH80	108.7245	106.4062	116.7176	113.5132	128.4569	122.7606	165.6518	161.1466
TH81	179.9764	171.5686	116.4543	169.0450	58.8221	69.3337	30.0497	210.0000
TH82	96.0495	93.4631	67.8071	94.9637	62.0894	82.1939	52.2773	142.9865
TH83	87.5196	87.7387	79.5276	61.5770	81.8288	70.3180	155.4915	51.8182
TH84	108.7245	106.4062	116.7176	113.5132	128.4569	122.7606	165.6518	161.1466

Table 4.6.4 Thresholds for Y color component of the natural and synthetic images for P = 40 for the sub-bands 1 to 54

Images → / Threshold↓	Aishwarya	Lena	Donkey	Barbara	Mandrill	Rose	Horizontal	Vertical
TH1	1.0000	1.0000	1.0000	1.0000	1.0000	1.0000	1.0000	1.0000
TH2	116.0065	115.5932	86.1500	104.3671	68.6365	87.4297	69.7031	105.0442
TH3	115.0518	115.7054	89.8742	70.4286	88.5204	80.9067	111.6492	69.0910
TH4	118.8851	119.1904	110.9747	109.9249	107.4343	109.3212	118.9446	118.3854
TH5	1.0000	1.0000	1.0000	1.0000	1.0000	1.0000	1.0000	1.0000
TH6	119.0516	117.1593	90.4094	121.4040	82.7858	102.8467	69.7031	105.0442
TH7	116.6928	116.9849	95.0710	82.1026	110.8518	93.7573	111.6492	69.0910
TH8	125.0330	124.0418	123.2656	131.0605	141.2905	133.9821	118.9446	118.3854
TH9	265.4805	264.1816	230.2530	224.6152	124.7829	164.8017	280.0000	280.0000
TH10	119.0516	117.1593	90.4094	121.4040	82.7858	102.8467	69.7031	105.0442
TH11	116.6928	116.9849	95.0710	82.1026	110.8518	93.7573	111.6492	69.0910
TH12	125.0330	124.0418	123.2656	131.0605	141.2905	133.9821	118.9446	118.3854
TH13	265.4805	264.1816	230.2530	224.6152	124.7829	164.8017	280.0000	280.0000
TH14	119.0516	117.1593	90.4094	121.4040	82.7858	102.8467	69.7031	105.0442
TH15	116.6928	116.9849	95.0710	82.1026	110.8518	93.7573	111.6492	69.0910
TH16	125.0330	124.0418	123.2656	131.0605	141.2905	133.9821	118.9446	118.3854
TH17	265.4805	264.1816	230.2530	224.6152	124.7829	164.8017	280.0000	280.0000
TH18	119.0516	117.1593	90.4094	121.4040	82.7858	102.8467	69.7031	105.0442
TH19	116.6928	116.9849	95.0710	82.1026	110.8518	93.7573	111.6492	69.0910
TH20	119.0516	117.1593	90.4094	121.4040	82.7858	102.8467	69.7031	105.0442
TH21	0.0001	0.0001	0.0001	0.0001	0.0001	0.0001	0.0001	0.0001
TH22	125.4182	122.7272	90.4094	122.4288	82.7858	106.6001	69.7031	169.2475
TH23	116.6928	116.9849	102.9666	82.1026	106.7879	93.7573	183.4038	69.0910
TH24	138.5736	136.2972	144.7239	141.7897	156.1266	151.0437	195.3880	190.7430
TH25	249.9764	241.5686	186.4543	239.0450	128.8221	139.3337	100.0497	280.0000
TH26	125.4182	122.7272	90.4094	122.4288	82.7858	106.6001	69.7031	169.2475
TH27	116.6928	116.9849	102.9666	82.1026	106.7879	93.7573	183.4038	69.0910
TH28	138.5736	136.2972	144.7239	141.7897	156.1266	151.0437	195.3880	190.7430
TH29	249.9764	241.5686	186.4543	239.0450	128.8221	139.3337	100.0497	280.0000
TH30	125.4182	122.7272	90.4094	122.4288	82.7858	106.6001	69.7031	169.2475
TH31	116.6928	116.9849	102.9666	82.1026	106.7879	93.7573	183.4038	69.0910
TH32	138.5736	136.2972	144.7239	141.7897	156.1266	151.0437	195.3880	190.7430
TH33	249.9764	241.5686	186.4543	239.0450	128.8221	139.3337	100.0497	280.0000
TH34	125.4182	122.7272	90.4094	122.4288	82.7858	106.6001	69.7031	169.2475
TH35	116.6928	116.9849	102.9666	82.1026	106.7879	93.7573	183.4038	69.0910
TH36	138.5736	136.2972	144.7239	141.7897	156.1266	151.0437	195.3880	190.7430
TH37	249.9764	241.5686	186.4543	239.0450	128.8221	139.3337	100.0497	280.0000
TH38	125.4182	122.7272	90.4094	122.4288	82.7858	106.6001	69.7031	169.2475
TH39	116.6928	116.9849	102.9666	82.1026	106.7879	93.7573	183.4038	69.0910
TH40	138.5736	136.2972	144.7239	141.7897	156.1266	151.0437	195.3880	190.7430
TH41	249.9764	241.5686	186.4543	239.0450	128.8221	139.3337	100.0497	280.0000
TH42	125.4182	122.7272	90.4094	122.4288	82.7858	106.6001	69.7031	169.2475
TH43	116.6928	116.9849	102.9666	82.1026	106.7879	93.7573	183.4038	69.0910
TH44	138.5736	136.2972	144.7239	141.7897	156.1266	151.0437	195.3880	190.7430
TH45	0	241.5686	186.4543	239.0450	128.8221	139.3337	100.0497	280.0000
TH46	0	122.7272	90.4094	122.4288	82.7858	106.6001	69.7031	169.2475
TH47	0	116.9849	102.9666	82.1026	106.7879	93.7573	183.4038	69.0910
TH48	0	136.2972	144.7239	141.7897	156.1266	151.0437	195.3880	190.7430
TH49	249.9764	241.5686	186.4543	239.0450	128.8221	139.3337	100.0497	280.0000
TH50	125.4182	122.7272	90.4094	122.4288	82.7858	106.6001	69.7031	169.2475
TH51	116.6928	116.9849	102.9666	82.1026	106.7879	93.7573	183.4038	69.0910
TH52	138.5736	136.2972	144.7239	141.7897	156.1266	151.0437	195.3880	190.7430
TH53	294.3401	293.0020	318.1537	324.9941	403.4811	371.7985	280.0000	280.0000
TH54	125.4182	122.7272	90.4094	122.4288	82.7858	106.6001	69.7031	169.2475

(Continued)

Table 4.6.4 Thresholds for Y color component of the natural and synthetic images for P = 40 for the sub-bands 55 to 84

Images → / Threshold↓	Aishwarya	Lena	Donkey	Barbara	Mandrill	Rose	Horizontal	Vertical
TH55	116.6928	116.9849	102.9666	82.1026	106.7879	93.7573	183.4038	69.0910
TH56	138.5736	136.2972	144.7239	141.7897	156.1266	151.0437	195.3880	190.7430
TH57	0	5.6002	4.3225	5.5417	2.9864	3.2301	2.3194	6.4911
TH58	0	122.7272	90.4094	122.4288	82.7858	106.6001	69.7031	169.2475
TH59	0	116.9849	102.9666	82.1026	106.7879	93.7573	183.4038	69.0910
TH60	0	136.2972	144.7239	141.7897	156.1266	151.0437	195.3880	190.7430
TH61	249.9764	241.5686	186.4543	239.0450	128.8221	139.3337	100.0497	280.0000
TH62	125.4182	122.7272	90.4094	122.4288	82.7858	106.6001	69.7031	169.2475
TH63	116.6928	116.9849	102.9666	82.1026	106.7879	93.7573	183.4038	69.0910
TH64	138.5736	136.2972	144.7239	141.7897	156.1266	151.0437	195.3880	190.7430
TH65	249.9764	241.5686	186.4543	239.0450	128.8221	139.3337	100.0497	280.0000
TH66	125.4182	122.7272	90.4094	122.4288	82.7858	106.6001	69.7031	169.2475
TH67	116.6928	116.9849	102.9666	82.1026	106.7879	93.7573	183.4038	69.0910
TH68	138.5736	136.2972	144.7239	141.7897	156.1266	151.0437	195.3880	190.7430
TH69	0	241.5686	186.4543	239.0450	128.8221	139.3337	100.0497	280.0000
TH70	0	122.7272	90.4094	122.4288	82.7858	106.6001	69.7031	169.2475
TH71	0	116.9849	102.9666	82.1026	106.7879	93.7573	183.4038	69.0910
TH72	0	136.2972	144.7239	141.7897	156.1266	151.0437	195.3880	190.7430
TH73	249.9764	241.5686	186.4543	239.0450	128.8221	139.3337	100.0497	280.0000
TH74	125.4182	122.7272	90.4094	122.4288	82.7858	106.6001	69.7031	169.2475
TH75	116.6928	116.9849	102.9666	82.1026	106.7879	93.7573	183.4038	69.0910
TH76	138.5736	136.2972	144.7239	141.7897	156.1266	151.0437	195.3880	190.7430
TH77	249.9764	241.5686	186.4543	239.0450	128.8221	139.3337	100.0497	280.0000
TH78	125.4182	122.7272	90.4094	122.4288	82.7858	106.6001	69.7031	169.2475
TH79	116.6928	116.9849	102.9666	82.1026	106.7879	93.7573	183.4038	69.0910
TH80	138.5736	136.2972	144.7239	141.7897	156.1266	151.0437	195.3880	190.7430
TH81	249.9764	241.5686	186.4543	239.0450	128.8221	139.3337	100.0497	280.0000
TH82	125.4182	122.7272	90.4094	122.4288	82.7858	106.6001	69.7031	169.2475
TH83	116.6928	116.9849	102.9666	82.1026	106.7879	93.7573	183.4038	69.0910
TH84	138.5736	136.2972	144.7239	141.7897	156.1266	151.0437	195.3880	190.7430

Table 4.6.5 Thresholds for Cr color component of the natural and synthetic images for P = 10 for the sub-bands 1 to 18

Images → / Threshold↓	Aishwarya	Lena	Donkey	Barbara	Mandrill	Rose	Horizontal	Vertical
TH1	1.0000	1.0000	1.0000	1.0000	.0000	1.0000	1.0000	1.0000
TH2	28.7728	17.9941	27.3857	35.3166	27.7784	27.0572	20.6647	26.6379
TH3	28.2570	20.9119	27.1055	36.2807	27.1202	26.7730	27.9127	20.2253
TH4	29.4556	0.8195	28.7830	17.1020	29.1844	28.9150	29.8042	29.6900
TH5	1.0000	1.0000	1.0000	1.0000	1.0000	1.0000	1.0000	1.0000
TH6	29.6852	17.9941	27.9065	35.3166	28.8513	29.0985	20.6647	26.6379
TH7	28.9163	20.9119	27.8885	36.2807	29.6296	28.1802	27.9127	20.2253
TH8	30.8428	0.8195	30.1697	17.1020	32.8296	33.6947	29.8042	29.6900
TH9	66.8853	70.0000	65.8044	70.0000	59.9302	57.1131	70.0000	70.0000
TH10	29.6852	17.9941	27.9065	35.3166	28.8513	29.0985	20.6647	26.6379
TH11	28.9163	20.9119	27.8885	36.2807	29.6296	28.1802	27.9127	20.2253
TH12	30.8428	0.8195	30.1697	17.1020	32.8296	33.6947	29.8042	29.6900
TH13	66.8853	70.0000	65.8044	70.0000	59.9302	57.1131	70.0000	70.0000
TH14	29.6852	17.9941	27.9065	35.3166	28.8513	29.0985	20.6647	26.6379
TH15	28.9163	20.9119	27.8885	36.2807	29.6296	28.1802	27.9127	20.2253
TH16	30.8428	0.8195	30.1697	17.1020	32.8296	33.6947	29.8042	29.6900
TH17	66.8853	70.0000	65.8044	70.0000	59.9302	57.1131	70.0000	70.0000
TH18	29.6852	17.9941	27.9065	35.3166	28.8513	29.0985	20.6647	26.6379

(Continued)

Table 4.6.5 Thresholds for Cr color component of the natural and synthetic images for P = 10 for the sub-bands 18 to 71

Images → / Threshold↓	Aishwarya	Lena	Donkey	Barbara	Mandrill	Rose	Horizontal	Vertical
TH19	28.9163	20.9119	27.8885	36.2807	29.6296	28.1802	27.9127	20.2253
TH20	29.6852	17.9941	27.9065	35.3166	28.8513	29.0985	20.6647	26.6379
TH21	0.0001	0.0001	0.0001	0.0001	0.0001	0.0001	0.0001	0.0001
TH22	31.4897	17.9941	20.5031	28.1772	23.7518	22.9917	5.6817	141.7985
TH23	28.9163	20.9119	21.8345	28.6772	19.3185	19.3683	133.8540	4.0801
TH24	35.2033	0.8195	32.0360	21.7286	41.5132	40.9457	154.9642	164.1832
TH25	61.8169	70.0000	0	18.3692	1.7650	1.9926	19.3735	4.6652
TH26	31.4897	17.9941	0	1.5931	30.3029	33.8188	27.7327	166.9569
TH27	28.9163	20.9119	0	2.0594	29.5955	29.5360	159.0141	27.5236
TH28	35.2033	0.8195	0	7.2172	45.6174	48.4220	161.4910	171.3859
TH29	61.8169	70.0000	3.1837	18.3692	1.7650	1.9926	19.3735	4.6652
TH30	31.4897	17.9941	29.4569	1.5931	30.3029	33.8188	27.7327	166.9569
TH31	28.9163	20.9119	31.0808	2.0594	29.5955	29.5360	159.0141	27.5236
TH32	35.2033	0.8195	35.6794	7.2172	45.6174	48.4220	161.4910	171.3859
TH33	61.8169	70.0000	3.1837	18.3692	1.7650	1.9926	19.3735	4.6652
TH34	31.4897	17.9941	29.4569	1.5931	30.3029	33.8188	27.7327	166.9569
TH35	28.9163	20.9119	31.0808	2.0594	29.5955	29.5360	159.0141	27.5236
TH36	35.2033	0.8195	35.6794	7.2172	45.6174	48.4220	161.4910	171.3859
TH37	61.8169	70.0000	3.1837	18.3692	1.7650	1.9926	0	4.6652
TH38	31.4897	17.9941	29.4569	1.5931	30.3029	33.8188	0	166.9569
TH39	28.9163	20.9119	31.0808	2.0594	29.5955	29.5360	0	27.5236
TH40	35.2033	0.8195	35.6794	7.2172	45.6174	48.4220	0	171.3859
TH41	1.8169	70.0000	3.1837	18.3692	1.7650	1.9926	19.3735	4.6652
TH42	31.4897	17.9941	29.4569	1.5931	30.3029	33.8188	27.7327	166.9569
TH43	28.9163	20.9119	31.0808	2.0594	29.5955	29.5360	159.0141	27.5236
TH44	35.2033	0.8195	35.6794	7.2172	45.6174	48.4220	161.4910	171.3859
TH45	61.8169	70.0000	3.1837	18.3692	1.7650	1.9926	19.3735	4.6652
TH46	31.4897	17.9941	29.4569	1.5931	30.3029	33.8188	27.7327	166.9569
TH47	28.9163	20.9119	31.0808	2.0594	29.5955	29.5360	159.0141	27.5236
TH48	35.2033	0.8195	35.6794	7.2172	45.6174	48.4220	161.4910	171.3859
TH49	61.8169	70.0000	3.1837	18.3692	1.7650	1.9926	19.3735	4.6652
TH50	31.4897	17.9941	29.4569	1.5931	30.3029	33.8188	27.7327	166.9569
TH51	28.9163	20.9119	31.0808	2.0594	29.5955	29.5360	159.0141	27.5236
TH52	35.2033	0.8195	35.6794	7.2172	45.6174	48.4220	161.4910	171.3859
TH53	72.8405	70.0000	4.2250	18.3692	4.6031	5.2367	5.7122	4.6652
TH54	31.4897	17.9941	29.4569	1.5931	30.3029	33.8188	27.7327	166.9569
TH55	28.9163	20.9119	31.0808	2.0594	29.5955	29.5360	159.0141	27.5236
TH56	35.2033	0.8195	35.6794	7.2172	45.6174	48.4220	161.4910	171.3859
TH57	1.4331	1.6228	17.1058	14.7043	9.1920	9.7080	75.6984	21.9884
TH58	31.4897	17.9941	29.4569	1.5931	30.3029	33.8188	27.7327	166.9569
TH59	28.9163	20.9119	31.0808	2.0594	29.5955	29.5360	159.0141	27.5236
TH60	35.2033	0.8195	35.6794	7.2172	45.6174	48.4220	161.4910	171.3859
TH61	61.8169	70.0000	3.1837	18.3692	1.7650	1.9926	19.3735	4.6652
TH62	31.4897	17.9941	29.4569	1.5931	30.3029	33.8188	27.7327	166.9569
TH63	28.9163	20.9119	31.0808	2.0594	29.5955	29.5360	159.0141	27.5236
TH64	35.2033	0.8195	35.6794	7.2172	45.6174	48.4220	161.4910	171.3859
TH65	61.8169	70.0000	3.1837	18.3692	1.7650	1.9926	19.3735	4.6652
TH66	31.4897	17.9941	29.4569	1.5931	30.3029	33.8188	27.7327	166.9569
TH67	28.9163	20.9119	31.0808	2.0594	29.5955	29.5360	159.0141	27.5236
TH68	35.2033	0.8195	35.6794	7.2172	45.6174	48.4220	161.4910	171.3859
TH69	61.8169	70.0000	3.1837	18.3692	1.7650	1.9926	19.3735	4.6652
TH70	31.4897	17.9941	29.4569	1.5931	30.3029	33.8188	27.7327	166.9569
TH71	28.9163	20.9119	31.0808	2.0594	29.5955	29.5360	159.0141	27.5236

(Continued)

Table 4.6.5 Thresholds for Cr color component of the natural and synthetic images for P = 10 for the sub-bands 72 to 84

Images → / Threshold↓	Aishwarya	Lena	Donkey	Barbara	Mandrill	Rose	Horizontal	Vertical
TH72	35.2033	0.8195	35.6794	7.2172	45.6174	48.4220	161.4910	171.3859
TH73	61.8169	70.0000	3.1837	18.3692	1.7650	1.9926	19.3735	4.6652
TH74	31.4897	17.9941	29.4569	1.5931	30.3029	33.8188	27.7327	166.9569
TH75	28.9163	20.9119	31.0808	2.0594	29.5955	29.5360	159.0141	27.5236
TH76	35.2033	0.8195	35.6794	7.2172	45.6174	48.4220	161.4910	171.3859
TH77	61.8169	70.0000	3.1837	18.3692	1.7650	1.9926	19.3735	4.6652
TH78	31.4897	17.9941	29.4569	1.5931	30.3029	33.8188	27.7327	166.9569
TH79	28.9163	20.9119	31.0808	2.0594	29.5955	29.5360	159.0141	27.5236
TH80	35.2033	0.8195	35.6794	7.2172	45.6174	48.4220	161.4910	171.3859
TH81	61.8169	70.0000	3.1837	18.3692	1.7650	1.9926	19.3735	4.6652
TH82	31.4897	17.9941	29.4569	1.5931	30.3029	33.8188	27.7327	166.9569
TH83	28.9163	20.9119	31.0808	2.0594	29.5955	29.5360	159.0141	27.5236
TH84	35.2033	0.8195	35.6794	7.2172	45.6174	48.4220	161.4910	171.3859

Table 4.6.6 Thresholds for Cr color component of the natural and synthetic images for P = 20 for the sub-bands 1 to 35

Images → / Threshold↓	Aishwarya	Lena	Donkey	Barbara	Mandrill	Rose	Horizontal	Vertical
TH1	1.0000	1.0000	1.0000	1.0000	1.0000	1.0000	1.0000	1.0000
TH2	57.9079	35.9881	55.2921	70.6333	56.6297	55.3394	41.3293	53.2758
TH3	57.1733	41.8238	54.7200	72.5614	55.5528	54.9532	55.8254	40.4506
TH4	59.0439	1.6390	57.7311	34.2039	58.8035	58.3459	59.6084	59.3799
TH5	1.0000	1.0000	1.0000	1.0000	1.0000	1.0000	1.0000	1.0000
TH6	58.8202	35.9881	55.8129	70.6333	57.7026	57.3807	41.3293	53.2758
TH7	57.8326	41.8238	55.5030	72.5614	58.0623	56.3604	55.8254	40.4506
TH8	60.4312	1.6390	59.1178	34.2039	62.4487	63.1255	59.6084	59.3799
TH9	136.8853	140.0000	135.8044	140.0000	129.9302	127.1131	140.0000	140.0000
TH10	58.8202	35.9881	55.8129	70.6333	57.7026	57.3807	41.3293	53.2758
TH11	57.8326	41.8238	55.5030	72.5614	58.0623	56.3604	55.8254	40.4506
TH12	60.4312	1.6390	59.1178	34.2039	62.4487	63.1255	59.6084	59.3799
TH13	136.8853	140.0000	135.8044	140.0000	129.9302	127.1131	140.0000	140.0000
TH14	58.8202	35.9881	55.8129	70.6333	57.7026	57.3807	41.3293	53.2758
TH15	57.8326	41.8238	55.5030	72.5614	58.0623	56.3604	55.8254	40.4506
TH16	60.4312	1.6390	59.1178	34.2039	62.4487	63.1255	59.6084	59.3799
TH17	136.8853	140.0000	135.8044	140.0000	129.9302	127.1131	140.0000	140.0000
TH18	58.8202	35.9881	55.8129	70.6333	57.7026	57.3807	41.3293	53.2758
TH19	57.8326	41.8238	55.5030	72.5614	58.0623	56.3604	55.8254	40.4506
TH20	58.8202	35.9881	55.8129	70.6333	57.7026	57.3807	41.3293	53.2758
TH21	0.0001	0.0001	0.0001	0.0001	0.0001	0.0001	0.0001	0.0001
TH22	56.7127	55.7188	55.8129	70.6333	58.2848	60.6369	41.3293	179.2160
TH23	52.1075	60.7881	56.8265	72.5614	56.8654	56.3604	178.4063	40.4506
TH24	63.4857	32.9180	63.6924	34.2039	74.8054	77.1651	190.4960	199.7500
TH25	8.6147	19.5622	0	140.0000	99.4625	100.9778	167.4105	140.0000
TH26	61.9669	21.8149	0	70.6333	58.2848	60.6369	41.3293	179.2160
TH27	59.4489	19.4934	0	72.5614	56.8654	56.3604	178.4063	40.4506
TH28	65.4639	35.4793	0	34.2039	74.8054	77.1651	190.4960	199.7500
TH29	8.6147	19.5622	124.9370	140.0000	99.4625	100.9778	167.4105	140.0000
TH30	61.9669	21.8149	55.8129	70.6333	58.2848	60.6369	41.3293	179.2160
TH31	59.4489	19.4934	56.8265	72.5614	56.8654	56.3604	178.4063	40.4506
TH32	65.4639	35.4793	63.6924	34.2039	74.8054	77.1651	190.4960	199.7500
TH33	8.6147	19.5622	124.9370	140.0000	99.4625	100.9778	167.4105	140.0000
TH34	61.9669	21.8149	55.8129	70.6333	58.2848	60.6369	41.3293	179.2160
TH35	59.4489	19.4934	56.8265	72.5614	56.8654	56.3604	178.4063	40.4506

(Continued)

Table 4.6.6 Thresholds for Cr color component of the natural and synthetic images for P = 20 for the sub-bands 36 to 84

Images → / Threshold↓	Aishwarya	Lena	Donkey	Barbara	Mandrill	Rose	Horizontal	Vertical
TH36	65.4639	35.4793	63.6924	34.2039	74.8054	77.1651	190.4960	199.7500
TH37	8.6147	19.5622	124.9370	140.0000	99.4625	100.9778	0	140.0000
TH38	61.9669	21.8149	55.8129	70.6333	58.2848	60.6369	0	179.2160
TH39	59.4489	19.4934	56.8265	72.5614	56.8654	56.3604	0	40.4506
TH40	65.4639	35.4793	63.6924	34.2039	74.8054	77.1651	0	199.7500
TH41	8.6147	19.5622	124.9370	140.0000	99.4625	100.9778	167.4105	140.0000
TH42	61.9669	21.8149	55.8129	70.6333	58.2848	60.6369	41.3293	179.2160
TH43	59.4489	19.4934	56.8265	72.5614	56.8654	56.3604	178.4063	40.4506
TH44	65.4639	35.4793	63.6924	34.2039	74.8054	77.1651	190.4960	199.7500
TH45	8.6147	19.5622	124.9370	140.0000	99.4625	100.9778	167.4105	140.0000
TH46	61.9669	21.8149	55.8129	70.6333	58.2848	60.6369	41.3293	179.2160
TH47	59.4489	19.4934	56.8265	72.5614	56.8654	56.3604	178.4063	40.4506
TH48	65.4639	35.4793	63.6924	34.2039	74.8054	77.1651	190.4960	199.7500
TH49	8.6147	19.5622	124.9370	140.0000	99.4625	100.9778	167.4105	140.0000
TH50	61.9669	21.8149	55.8129	70.6333	58.2848	60.6369	41.3293	179.2160
TH51	59.4489	19.4934	56.8265	72.5614	56.8654	56.3604	178.4063	40.4506
TH52	65.4639	35.4793	63.6924	34.2039	74.8054	77.1651	190.4960	199.7500
TH53	9.3351	19.5622	142.9052	140.0000	146.8384	151.4116	140.0000	140.0000
TH54	61.9669	21.8149	55.8129	70.6333	58.2848	60.6369	41.3293	179.2160
TH55	59.4489	19.4934	56.8265	72.5614	56.8654	56.3604	178.4063	40.4506
TH56	65.4639	35.4793	63.6924	34.2039	74.8054	77.1651	190.4960	199.7500
TH57	41.3525	34.8402	2.8964	3.2456	2.3058	2.3409	3.8810	3.2456
TH58	61.9669	21.8149	55.8129	70.6333	58.2848	60.6369	41.3293	179.2160
TH59	59.4489	19.4934	56.8265	72.5614	56.8654	56.3604	178.4063	40.4506
TH60	65.4639	35.4793	63.6924	34.2039	74.8054	77.1651	190.4960	199.7500
TH61	8.6147	19.5622	124.9370	140.0000	99.4625	100.9778	167.4105	140.0000
TH62	61.9669	21.8149	55.8129	70.6333	58.2848	60.6369	41.3293	179.2160
TH63	59.4489	19.4934	56.8265	72.5614	56.8654	56.3604	178.4063	40.4506
TH64	65.4639	35.4793	63.6924	34.2039	74.8054	77.1651	190.4960	199.7500
TH65	8.6147	19.5622	124.9370	140.0000	99.4625	100.9778	167.4105	140.0000
TH66	61.9669	21.8149	55.8129	70.6333	58.2848	60.6369	41.3293	179.2160
TH67	59.4489	19.4934	56.8265	72.5614	56.8654	56.3604	178.4063	40.4506
TH68	65.4639	35.4793	63.6924	34.2039	74.8054	77.1651	190.4960	199.7500
TH69	8.6147	19.5622	124.9370	140.0000	99.4625	100.9778	167.4105	140.0000
TH70	61.9669	21.8149	55.8129	70.6333	58.2848	60.6369	41.3293	179.2160
TH71	59.4489	19.4934	56.8265	72.5614	56.8654	56.3604	178.4063	40.4506
TH72	65.4639	35.4793	63.6924	34.2039	74.8054	77.1651	190.4960	199.7500
TH73	8.6147	19.5622	124.9370	140.0000	99.4625	100.9778	167.4105	140.0000
TH74	61.9669	21.8149	55.8129	70.6333	58.2848	60.6369	41.3293	179.2160
TH75	59.4489	19.4934	56.8265	72.5614	56.8654	56.3604	178.4063	40.4506
TH76	65.4639	35.4793	63.6924	34.2039	74.8054	77.1651	190.4960	199.7500
TH77	8.6147	19.5622	124.9370	140.0000	99.4625	100.9778	167.4105	140.0000
TH78	61.9669	21.8149	55.8129	70.6333	58.2848	60.6369	41.3293	179.2160
TH79	59.4489	19.4934	56.8265	72.5614	56.8654	56.3604	178.4063	40.4506
TH80	65.4639	35.4793	63.6924	34.2039	74.8054	77.1651	190.4960	199.7500
TH81	8.6147	19.5622	124.9370	140.0000	99.4625	100.9778	167.4105	140.0000
TH82	61.9669	21.8149	55.8129	70.6333	58.2848	60.6369	41.3293	179.2160
TH83	59.4489	19.4934	56.8265	72.5614	56.8654	56.3604	178.4063	40.4506
TH84	65.4639	35.4793	63.6924	34.2039	74.805	77.1651	190.4960	199.7500

Table 4.6.7 Thresholds for Cr color component of the natural and synthetic images for P = 30 for the sub-bands 1 to 54

Images → / Threshold↓	Aishwarya	Lena	Donkey	Barbara	Mandrill	Rose	Horizontal	Vertical
TH1	1.0000	1.0000	1.0000	1.0000	1.0000	1.0000	1.0000	1.0000
TH2	87.0429	53.9822	83.1986	105.9499	85.4810	83.6216	61.9940	79.9137
TH3	86.0897	62.7357	82.3345	108.8421	83.9855	83.1334	83.7382	60.6759
TH4	88.6323	2.4585	86.6791	51.3059	88.4226	87.7767	89.4126	89.0699
TH5	1.0000	1.0000	1.0000	1.0000	1.0000	1.0000	1.0000	1.0000
TH6	87.9553	53.9822	83.7194	105.9499	86.5539	85.6629	61.9940	79.9137
TH7	86.7490	62.7357	83.1176	108.8421	86.4949	84.5406	83.7382	60.6759
TH8	90.0195	2.4585	88.0658	51.3059	92.0678	92.5563	89.4126	89.0699
TH9	206.8853	210.0000	205.8044	210.0000	199.9302	197.1131	210.0000	210.0000
TH10	87.9553	53.9822	83.7194	105.9499	86.5539	85.6629	61.9940	79.9137
TH11	86.7490	62.7357	83.1176	108.8421	86.4949	84.5406	83.7382	60.6759
TH12	90.0195	2.4585	88.0658	51.3059	92.0678	92.5563	89.4126	89.0699
TH13	206.8853	210.0000	205.8044	210.0000	199.9302	197.1131	210.0000	210.0000
TH14	87.9553	53.9822	83.7194	105.9499	86.5539	85.6629	61.9940	79.9137
TH15	86.7490	62.7357	83.1176	108.8421	86.4949	84.5406	83.7382	60.6759
TH16	90.0195	2.4585	88.0658	51.3059	92.0678	92.5563	89.4126	89.0699
TH17	206.8853	210.0000	205.8044	210.0000	199.9302	197.1131	210.0000	210.0000
TH18	87.9553	53.9822	83.7194	105.9499	86.5539	85.6629	61.9940	79.9137
TH19	86.7490	62.7357	83.1176	108.8421	86.4949	84.5406	83.7382	60.6759
TH20	87.9553	53.9822	83.7194	105.9499	86.5539	85.6629	61.9940	79.9137
TH21	0.0001	0.0001	0.0001	0.0001	0.0001	0.0001	0.0001	0.0001
TH22	89.7597	53.9822	83.7194	105.9499	87.1361	88.9191	61.9940	205.8538
TH23	86.7490	62.7357	84.4411	108.8421	85.2980	84.5406	206.3191	60.6759
TH24	94.3800	2.4585	92.6404	51.3059	104.4245	106.5959	220.3002	229.4399
TH25	201.8169	210.0000	0	210.0000	169.4625	170.9778	97.4105	210.0000
TH26	89.7597	53.9822	0	105.9499	87.1361	88.9191	61.9940	205.8538
TH27	86.7490	62.7357	0	108.8421	85.2980	84.5406	206.3191	60.6759
TH28	94.3800	2.4585	0	51.3059	104.4245	106.5959	220.3002	229.4399
TH29	201.8169	210.0000	194.9370	210.0000	169.4625	170.9778	97.4105	210.0000
TH30	89.7597	53.9822	83.7194	105.9499	87.1361	88.9191	61.9940	205.8538
TH31	86.7490	62.7357	84.4411	108.8421	85.2980	84.5406	206.3191	60.6759
TH32	94.3800	2.4585	92.6404	51.3059	104.4245	106.5959	220.3002	229.4399
TH33	201.8169	210.0000	194.9370	210.0000	169.4625	170.9778	97.4105	210.0000
TH34	89.7597	53.9822	83.7194	105.9499	87.1361	88.9191	61.9940	205.8538
TH35	86.7490	62.7357	84.4411	108.8421	85.2980	84.5406	206.3191	60.6759
TH36	94.3800	2.4585	92.6404	51.3059	104.4245	106.5959	220.3002	229.4399
TH37	201.8169	210.0000	194.9370	210.0000	169.4625	170.9778	0	210.0000
TH38	89.7597	53.9822	83.7194	105.9499	87.1361	88.9191	0	205.8538
TH39	86.7490	62.7357	84.4411	108.8421	85.2980	84.5406	0	60.6759
TH40	94.3800	2.4585	92.6404	51.3059	104.4245	106.5959	0	229.4399
TH41	201.8169	210.0000	194.9370	210.0000	169.4625	170.9778	97.4105	210.0000
TH42	89.7597	53.9822	83.7194	105.9499	87.1361	88.9191	61.9940	205.8538
TH43	86.7490	62.7357	84.4411	108.8421	85.2980	84.5406	206.3191	60.6759
TH44	94.3800	2.4585	92.6404	51.3059	104.4245	106.5959	220.3002	229.4399
TH45	201.8169	210.0000	194.9370	210.0000	169.4625	170.9778	97.4105	210.0000
TH46	89.7597	53.9822	83.7194	105.9499	87.1361	88.9191	61.9940	205.8538
TH47	86.7490	62.7357	84.4411	108.8421	85.2980	84.5406	206.3191	60.6759
TH48	94.3800	2.4585	92.6404	51.3059	104.4245	106.5959	220.3002	229.4399
TH49	201.8169	210.0000	194.9370	210.0000	169.4625	170.9778	97.4105	210.0000
TH50	89.7597	53.9822	83.7194	105.9499	87.1361	88.9191	61.9940	205.8538
TH51	86.7490	62.7357	84.4411	108.8421	85.2980	84.5406	206.3191	60.6759
TH52	94.3800	2.4585	92.6404	51.3059	104.4245	106.5959	220.3002	229.4399
TH53	212.8405	210.0000	212.9052	210.0000	216.8384	221.4116	210.0000	210.0000
TH54	89.7597	53.9822	83.7194	105.9499	87.1361	88.9191	61.9940	205.8538

(Continued)

Table 4.6.7 Thresholds for Cr color component of the natural and synthetic images for P = 30 for the sub-bands 55 to 84

TH55	86.7490	62.7357	84.4411	108.8421	85.2980	84.5406	206.3191	60.6759
TH56	94.3800	2.4585	92.6404	51.3059	104.4245	106.5959	220.3002	229.4399
TH57	4.6786	4.8683	4.5191	4.8683	3.9286	3.9637	2.2582	4.8683
TH58	89.7597	53.9822	83.7194	105.9499	87.1361	88.9191	61.9940	205.8538
TH59	86.7490	62.7357	84.4411	108.8421	85.2980	84.5406	206.3191	60.6759
TH60	94.3800	2.4585	92.6404	51.3059	104.4245	106.5959	220.3002	229.4399
TH61	201.8169	210.0000	194.9370	210.0000	169.4625	170.9778	97.4105	210.0000
TH62	89.7597	53.9822	83.7194	105.9499	87.1361	88.9191	61.9940	205.8538
TH63	86.7490	62.7357	84.4411	108.8421	85.2980	84.5406	206.3191	60.6759
TH64	94.3800	2.4585	92.6404	51.3059	104.4245	106.5959	220.3002	229.4399
TH65	201.8169	210.0000	194.9370	210.0000	169.4625	170.9778	97.4105	210.0000
TH66	89.7597	53.9822	83.7194	105.9499	87.1361	88.9191	61.9940	205.8538
TH67	86.7490	62.7357	84.4411	108.8421	85.2980	84.5406	206.3191	60.6759
TH68	94.3800	2.4585	92.6404	51.3059	104.4245	106.5959	220.3002	229.4399
TH69	201.8169	210.0000	194.9370	210.0000	169.4625	170.9778	97.4105	210.0000
TH70	89.7597	53.9822	83.7194	105.9499	87.1361	88.9191	61.9940	205.8538
TH71	86.7490	62.7357	84.4411	108.8421	85.2980	84.5406	206.3191	60.6759
TH72	94.3800	2.4585	92.6404	51.3059	104.4245	106.5959	220.3002	229.4399
TH73	201.8169	210.0000	194.9370	210.0000	169.4625	170.9778	97.4105	210.0000
TH74	89.7597	53.9822	83.7194	105.9499	87.1361	88.9191	61.9940	205.8538
TH75	86.7490	62.7357	84.4411	108.8421	85.2980	84.5406	206.3191	60.6759
TH76	94.3800	2.4585	92.6404	51.3059	104.4245	106.5959	220.3002	229.4399
TH77	201.8169	210.0000	194.9370	210.0000	169.4625	170.9778	97.4105	210.0000
TH78	89.7597	53.9822	83.7194	105.9499	87.1361	88.9191	61.9940	205.8538
TH79	86.7490	62.7357	84.4411	108.8421	85.2980	84.5406	206.3191	60.6759
TH80	94.3800	2.4585	92.6404	51.3059	104.4245	106.5959	220.3002	229.4399
TH81	201.8169	210.0000	194.9370	210.0000	169.4625	170.9778	97.4105	210.0000
TH82	89.7597	53.9822	83.7194	105.9499	87.1361	88.9191	61.9940	205.8538
TH83	86.7490	62.7357	84.4411	108.8421	85.2980	84.5406	206.3191	60.6759
TH84	94.3800	2.4585	92.6404	51.3059	104.4245	106.5959	220.3002	229.4399

Table 4.6.8 Thresholds for Cr color component of the natural and synthetic images for P = 40 for the sub-bands 1 to 65

Images → / **Threshold↓**	**Aishwarya**	**Lena**	**Donkey**	**Barbara**	**Mandrill**	**Rose**	**Horizontal**	**Vertical**
TH1	1.0000	1.0000	1.0000	1.0000	1.0000	1.0000	1.0000	1.0000
TH2	116.1779	71.9762	111.1050	141.2666	114.3323	111.9038	82.6587	106.5515
TH3	115.0060	83.6476	109.9490	145.1227	112.4182	111.3136	111.6509	80.9012
TH4	118.2207	3.2781	115.6272	68.4078	118.0417	117.2075	119.2169	118.7599
TH5	1.0000	1.0000	1.0000	1.0000	1.0000	1.0000	1.0000	1.0000
TH6	117.0903	71.9762	111.6259	141.2666	115.4052	113.9450	82.6587	106.5515
TH7	115.6653	83.6476	110.7321	145.1227	114.9276	112.7208	111.6509	80.9012
TH8	119.6079	3.2781	117.0138	68.4078	121.6869	121.9871	119.2169	118.7599
TH9	276.8853	280.0000	275.8044	280.0000	269.9302	267.1131	280.0000	280.0000
TH10	117.0903	71.9762	111.6259	141.2666	115.4052	113.9450	82.6587	106.5515
TH11	115.6653	83.6476	110.7321	145.1227	114.9276	112.7208	111.6509	80.9012
TH12	119.6079	3.2781	117.0138	68.4078	121.6869	121.9871	119.2169	118.7599
TH13	276.8853	280.0000	275.8044	280.0000	269.9302	267.1131	280.0000	280.0000
TH14	117.0903	71.9762	111.6259	141.2666	115.4052	113.9450	82.6587	106.5515
TH15	115.6653	83.6476	110.7321	145.1227	114.9276	112.7208	111.6509	80.9012
TH16	119.6079	3.2781	117.0138	68.4078	121.6869	121.9871	119.2169	118.7599
TH17	276.8853	280.0000	275.8044	280.0000	269.9302	267.1131	280.0000	280.0000
TH18	117.0903	71.9762	111.6259	141.2666	115.4052	113.9450	82.6587	106.5515
TH19	115.6653	83.6476	110.7321	145.1227	114.9276	112.7208	111.6509	80.9012
TH20	117.0903	71.9762	111.6259	141.2666	115.4052	113.9450	82.6587	106.5515

(Continued)

Table 4.6.8 Thresholds for Cr color component of the natural and synthetic images for P = 40 for the sub-bands 21 to 74

Images → / Threshold↓	Aishwarya	Lena	Donkey	Barbara	Mandrill	Rose	Horizontal	Vertical
TH21	0.0001	0.0001	0.0001	0.0001	0.0001	0.0001	0.0001	0.0001
TH22	118.8948	71.9762	111.6259	141.2666	115.9874	117.2013	82.6587	232.4917
TH23	115.6653	83.6476	112.0556	145.1227	113.7307	112.7208	234.2318	80.9012
TH24	123.9684	3.2781	121.5885	68.4078	134.0436	136.0267	250.1044	259.1299
TH25	271.8169	280.0000	0	280.0000	239.4625	240.9778	27.4105	280.0000
TH26	118.8948	71.9762	0	141.2666	115.9874	117.2013	82.6587	232.4917
TH27	115.6653	83.6476	0	145.1227	113.7307	112.7208	234.2318	80.9012
TH28	123.9684	3.2781	0	68.4078	134.0436	136.0267	250.1044	259.1299
TH29	271.8169	280.0000	264.9370	280.0000	239.4625	240.9778	27.4105	280.0000
TH30	118.8948	71.9762	111.6259	141.2666	115.9874	117.2013	82.6587	232.4917
TH31	115.6653	83.6476	112.0556	145.1227	113.7307	112.7208	234.2318	80.9012
TH32	123.9684	3.2781	121.5885	68.4078	134.0436	136.0267	250.1044	259.1299
TH33	271.8169	280.0000	264.9370	280.0000	239.4625	240.9778	27.4105	280.0000
TH34	118.8948	71.9762	111.6259	141.2666	115.9874	117.2013	82.6587	232.4917
TH35	115.6653	83.6476	112.0556	145.1227	113.7307	112.7208	234.2318	80.9012
TH36	123.9684	3.2781	121.5885	68.4078	134.0436	136.0267	250.1044	259.1299
TH37	271.8169	280.0000	264.9370	280.0000	239.4625	240.9778	0	280.0000
TH38	118.8948	71.9762	111.6259	141.2666	115.9874	117.2013	0	232.4917
TH39	115.6653	83.6476	112.0556	145.1227	113.7307	112.7208	0	80.9012
TH40	123.9684	3.2781	121.5885	68.4078	134.0436	136.0267	0	259.1299
TH41	271.8169	280.0000	264.9370	280.0000	239.4625	240.9778	27.4105	280.0000
TH42	118.8948	71.9762	111.6259	141.2666	115.9874	117.2013	82.6587	232.4917
TH43	115.6653	83.6476	112.0556	145.1227	113.7307	112.7208	234.2318	80.9012
TH44	123.9684	3.2781	121.5885	68.4078	134.0436	136.0267	250.1044	259.1299
TH45	271.8169	280.0000	264.9370	280.0000	239.4625	240.9778	27.4105	280.0000
TH46	118.8948	71.9762	111.6259	141.2666	115.9874	117.2013	82.6587	232.4917
TH47	115.6653	83.6476	112.0556	145.1227	113.7307	112.7208	234.2318	80.9012
TH48	123.9684	3.2781	121.5885	68.4078	134.0436	136.0267	250.1044	259.1299
TH49	271.8169	280.0000	264.9370	280.0000	239.4625	240.9778	27.4105	280.0000
TH50	118.8948	71.9762	111.6259	141.2666	115.9874	117.2013	82.6587	232.4917
TH51	115.6653	83.6476	112.0556	145.1227	113.7307	112.7208	234.2318	80.9012
TH52	123.9684	3.2781	121.5885	68.4078	134.0436	136.0267	250.1044	259.1299
TH53	282.8405	280.0000	282.9052	280.0000	286.8384	291.4116	280.0000	280.0000
TH54	118.8948	71.9762	111.6259	141.2666	115.9874	117.2013	82.6587	232.4917
TH55	115.6653	83.6476	112.0556	145.1227	113.7307	112.7208	234.2318	80.9012
TH56	123.9684	3.2781	121.5885	68.4078	134.0436	136.0267	250.1044	259.1299
TH57	6.3014	6.4911	6.1419	6.4911	5.5513	5.5865	0.6354	6.4911
TH58	118.8948	71.9762	111.6259	141.2666	115.9874	117.2013	82.6587	232.4917
TH59	115.6653	83.6476	112.0556	145.1227	113.7307	112.7208	234.2318	80.9012
TH60	123.9684	3.2781	121.5885	68.4078	134.0436	136.0267	250.1044	259.1299
TH61	271.8169	280.0000	264.9370	280.0000	239.4625	240.9778	27.4105	280.0000
TH62	118.8948	71.9762	111.6259	141.2666	115.9874	117.2013	82.6587	232.4917
TH63	115.6653	83.6476	112.0556	145.1227	113.7307	112.7208	234.2318	80.9012
TH64	123.9684	3.2781	121.5885	68.4078	134.0436	136.0267	250.1044	259.1299
TH65	271.8169	280.0000	264.9370	280.0000	239.4625	240.9778	27.4105	280.0000
TH66	118.8948	71.9762	111.6259	141.2666	115.9874	117.2013	82.6587	232.4917
TH67	115.6653	83.6476	112.0556	145.1227	113.7307	112.7208	234.2318	80.9012
TH68	123.9684	3.2781	121.5885	68.4078	134.0436	136.0267	250.1044	259.1299
TH69	271.8169	280.0000	264.9370	280.0000	239.4625	240.9778	27.4105	280.0000
TH70	118.8948	71.9762	111.6259	141.2666	115.9874	117.2013	82.6587	232.4917
TH71	115.6653	83.6476	112.0556	145.1227	113.7307	112.7208	234.2318	80.9012
TH72	123.9684	3.2781	121.5885	68.4078	134.0436	136.0267	250.1044	259.1299
TH73	271.8169	280.0000	264.9370	280.0000	239.4625	240.9778	27.4105	280.0000
TH74	118.8948	71.9762	111.6259	141.2666	115.9874	117.2013	82.6587	232.4917

(Continued)

Table 4.6.8 Thresholds for Cr color component of the natural and synthetic images for P = 40 for the sub-bands 75 to 84

Images → / Threshold↓	Aishwarya	Lena	Donkey	Barbara	Mandrill	Rose	Horizontal	Vertical
TH75	115.6653	83.6476	112.0556	145.1227	113.7307	112.7208	234.2318	80.9012
TH76	123.9684	3.2781	121.5885	68.4078	134.0436	136.0267	250.1044	259.1299
TH77	271.8169	280.0000	264.9370	280.0000	239.4625	240.9778	27.4105	280.0000
TH78	118.8948	71.9762	111.6259	141.2666	115.9874	117.2013	82.6587	232.4917
TH79	115.6653	83.6476	112.0556	145.1227	113.7307	112.7208	234.2318	80.9012
TH80	123.9684	3.2781	121.5885	68.4078	134.0436	136.0267	250.1044	259.1299
TH81	271.8169	280.0000	264.9370	280.0000	239.4625	240.9778	27.4105	280.0000
TH82	118.8948	71.9762	111.6259	141.2666	115.9874	117.2013	82.6587	232.4917
TH83	115.6653	83.6476	112.0556	145.1227	113.7307	112.7208	234.2318	80.9012
TH84	123.9684	3.2781	121.5885	68.4078	134.0436	136.0267	250.1044	259.1299

Table 4.6.9 Thresholds for Cb color component of the natural and synthetic images for P = 10 for the sub-bands 1 to 38

Images → / Threshold↓	Aishwarya	Lena	Donkey	Barbara	Mandrill	Rose	Horizontal	Vertical
TH1	1.0000	1.0000	1.0000	1.0000	1.0000	1.0000	1.0000	1.0000
TH2	28.5220	4.2083	26.9627	17.8535	26.7954	26.1802	20.1975	22.6220
TH3	28.0283	7.3249	26.4082	19.7826	26.4729	25.7583	27.8923	19.4462
TH4	29.4023	7.9431	28.7292	4.5592	28.7381	28.4637	29.7546	29.6515
TH5	1.0000	1.0000	1.0000	1.0000	1.0000	1.0000	1.0000	1.0000
TH6	29.4549	4.2083	27.3567	17.8535	28.3081	28.2981	20.1975	22.6220
TH7	28.6106	7.3249	26.9728	19.7826	30.5617	27.0738	27.8923	19.4462
TH8	30.8743	7.9431	29.7914	4.5592	34.9041	33.1093	29.7546	29.6515
TH9	66.5597	70.0000	66.6288	70.0000	53.2270	58.0819	70.0000	70.0000
TH10	29.4549	4.2083	27.3567	17.8535	28.3081	28.2981	20.1975	22.6220
TH11	28.6106	7.3249	26.9728	19.7826	30.5617	27.0738	27.8923	19.4462
TH12	30.8743	7.9431	29.7914	4.5592	34.9041	33.1093	29.7546	29.6515
TH13	66.5597	70.0000	66.6288	70.0000	53.2270	58.0819	70.0000	70.0000
TH14	29.4549	4.2083	27.3567	17.8535	28.3081	28.2981	20.1975	22.6220
TH15	28.6106	7.3249	26.9728	19.7826	30.5617	27.0738	27.8923	19.4462
TH16	30.8743	7.9431	29.7914	4.5592	34.9041	33.1093	29.7546	29.6515
TH17	66.5597	70.0000	66.6288	70.0000	53.2270	58.0819	70.0000	70.0000
TH18	29.4549	4.2083	27.3567	17.8535	28.3081	28.2981	20.1975	22.6220
TH19	28.6106	7.3249	26.9728	19.7826	30.5617	27.0738	27.8923	19.4462
TH20	29.4549	4.2083	27.3567	17.8535	28.3081	28.2981	20.1975	22.6220
TH21	0.0001	0.0001	0.0001	0.0001	0.0001	0.0001	0.0001	0.0001
TH22	32.2947	4.2083	27.3567	17.8535	29.6438	34.3199	20.1975	204.0991
TH23	28.6106	7.3249	27.0281	19.7826	28.3027	27.0738	173.6104	19.4462
TH24	36.1844	7.9431	33.0939	4.5592	53.9887	52.7574	185.2020	267.5203
TH25	61.7475	70.0000	59.1137	70.0000	7.1876	23.8641	295.7019	70.0000
TH26	32.2947	4.2083	27.3567	17.8535	29.6438	34.3199	20.1975	204.0991
TH27	28.6106	7.3249	27.0281	19.7826	28.3027	27.0738	173.6104	19.4462
TH28	36.1844	7.9431	33.0939	4.5592	53.9887	52.7574	185.2020	267.5203
TH29	61.7475	70.0000	59.1137	70.0000	7.1876	23.8641	295.7019	70.0000
TH30	32.2947	4.2083	27.3567	17.8535	29.6438	34.3199	20.1975	204.0991
TH31	28.6106	7.3249	27.0281	19.7826	28.3027	27.0738	173.6104	19.4462
TH32	36.1844	7.9431	33.0939	4.5592	53.9887	52.7574	185.2020	267.5203
TH33	61.7475	70.0000	59.1137	70.0000	7.1876	23.8641	295.7019	70.0000
TH34	32.2947	4.2083	27.3567	17.8535	29.6438	34.3199	20.1975	204.0991
TH35	28.6106	7.3249	27.0281	19.7826	28.3027	27.0738	173.6104	19.4462
TH36	36.1844	7.9431	33.0939	4.5592	53.9887	52.7574	185.2020	267.5203
TH37	61.7475	70.0000	59.1137	70.0000	7.1876	23.8641	295.7019	70.0000
TH38	32.2947	4.2083	27.3567	17.8535	29.6438	34.3199	20.1975	204.0991

(Continued)

Table 4.6.9 Thresholds for Cb color component of the natural and synthetic images for P = 10 for the sub-bands 39 to 84

Images → / Threshold↓	Aishwarya	Lena	Donkey	Barbara	Mandrill	Rose	Horizontal	Vertical
TH39	28.6106	7.3249	27.0281	19.7826	28.3027	27.0738	173.6104	19.4462
TH40	36.1844	7.9431	33.0939	4.5592	53.9887	52.7574	185.2020	267.5203
TH41	61.7475	70.0000	09.1137	70.0000	7.1876	23.8641	295.7019	70.0000
TH42	32.2947	4.2083	27.3567	17.8535	29.6438	34.3199	20.1975	204.0991
TH43	28.6106	7.3249	27.0281	19.7826	28.3027	27.0738	173.6104	19.4462
TH44	36.1844	7.9431	33.0939	4.5592	53.9887	52.7574	185.2020	267.5203
TH45	61.7475	70.0000	59.1137	70.0000	7.1876	23.8641	295.7019	70.0000
TH46	32.2947	4.2083	27.3567	17.8535	29.6438	34.3199	20.1975	204.0991
TH47	28.6106	7.3249	27.0281	19.7826	28.3027	27.0738	173.6104	19.4462
TH48	36.1844	7.9431	33.0939	4.5592	53.9887	52.7574	185.2020	267.5203
TH49	61.7475	70.0000	59.1137	70.0000	7.1876	23.8641	295.7019	70.0000
TH50	32.2947	4.2083	27.3567	17.8535	29.6438	34.3199	20.1975	204.0991
TH51	28.6106	7.3249	27.0281	19.7826	28.3027	27.0738	173.6104	19.4462
TH52	36.1844	7.9431	33.0939	4.5592	53.9887	52.7574	185.2020	267.5203
TH53	73.3448	70.0000	72.3247	70.0000	82.2475	80.8487	70.0000	70.0000
TH54	32.2947	4.2083	27.3567	17.8535	29.6438	34.3199	20.1975	204.0991
TH55	28.6106	7.3249	27.0281	19.7826	28.3027	27.0738	173.6104	19.4462
TH56	36.1844	7.9431	33.0939	4.5592	53.9887	52.7574	185.2020	267.5203
TH57	1.4315	1.6228	1.3704	1.6228	0.1666	0.5532	6.8551	1.6228
TH58	32.2947	4.2083	27.3567	17.8535	29.6438	34.3199	20.1975	204.0991
TH59	28.6106	7.3249	27.0281	19.7826	28.3027	27.0738	173.6104	19.4462
TH60	36.1844	7.9431	33.0939	4.5592	53.9887	52.7574	185.2020	267.5203
TH61	61.7475	70.0000	59.1137	70.0000	7.1876	23.8641	295.7019	70.0000
TH62	32.2947	4.2083	27.3567	17.8535	29.6438	34.3199	20.1975	204.0991
TH63	28.6106	7.3249	27.0281	19.7826	28.3027	27.0738	173.6104	19.4462
TH64	36.1844	7.9431	33.0939	4.5592	53.9887	52.7574	185.2020	267.5203
TH65	61.7475	70.0000	59.1137	70.0000	7.1876	23.8641	295.7019	70.0000
TH66	32.2947	4.2083	27.3567	17.8535	29.6438	34.3199	20.1975	204.0991
TH67	28.6106	7.3249	27.0281	19.7826	28.3027	27.0738	173.6104	19.4462
TH68	36.1844	7.9431	33.0939	4.5592	53.9887	52.7574	185.2020	267.5203
TH69	61.7475	70.0000	59.1137	70.0000	7.1876	23.8641	295.7019	70.0000
TH70	32.2947	4.2083	27.3567	17.8535	29.6438	34.3199	20.1975	204.0991
TH71	28.6106	7.3249	27.0281	19.7826	28.3027	27.0738	173.6104	19.4462
TH72	36.1844	7.9431	33.0939	4.5592	53.9887	52.7574	185.2020	267.5203
TH73	61.7475	70.0000	59.1137	70.0000	7.1876	23.8641	295.7019	70.0000
TH74	32.2947	4.2083	27.3567	17.8535	29.6438	34.3199	20.1975	204.0991
TH75	28.6106	7.3249	27.0281	19.7826	28.3027	27.0738	173.6104	19.4462
TH76	36.1844	7.9431	33.0939	4.5592	53.9887	52.7574	185.2020	267.5203
TH77	61.7475	70.0000	59.1137	70.0000	7.1876	23.8641	295.7019	70.0000
TH78	32.2947	4.2083	27.3567	17.8535	29.6438	34.3199	20.1975	204.0991
TH79	28.6106	7.3249	27.0281	19.7826	28.3027	27.0738	173.6104	19.4462
TH80	36.1844	7.9431	33.0939	4.5592	53.9887	52.7574	185.2020	267.5203
TH81	61.7475	70.0000	59.1137	70.0000	7.1876	23.8641	295.7019	70.0000
TH82	32.2947	4.2083	27.3567	17.8535	29.6438	34.3199	20.1975	204.0991
TH83	28.6106	7.3249	27.0281	19.7826	28.3027	27.0738	173.6104	19.4462
TH84	36.1844	7.9431	33.0939	4.5592	53.9887	52.7574	185.2020	267.5203

Table 4.6.10 Thresholds for Cb color component of the natural and synthetic images for P = 20 for the sub-bands 1 to 54

Images → / Threshold↓	Aishwarya	Lena	Donkey	Barbara	Mandrill	Rose	Horizontal	Vertical
TH1	1.0000	1.0000	1.0000	1.0000	1.0000	1.0000	1.0000	1.0000
TH2	57.4281	8.4165	54.3194	35.7069	55.1036	53.5661	40.3951	45.2441
TH3	56.6389	14.6499	53.2172	39.5652	54.7755	52.8321	55.7846	38.8925
TH4	58.9109	15.8862	57.5661	9.1185	58.1273	57.4654	59.5092	59.3031
TH5	1.0000	1.0000	1.0000	1.0000	1.0000	1.0000	1.0000	1.0000
TH6	58.3610	8.4165	54.7134	35.7069	56.6163	55.6840	40.3951	45.2441
TH7	57.2211	14.6499	53.7819	39.5652	58.8643	54.1475	55.7846	38.8925
TH8	60.3829	15.8862	58.6283	9.1185	64.2932	62.1110	59.5092	59.3031
TH9	136.5597	140.0000	136.6288	140.0000	123.2270	128.0819	140.0000	140.0000
TH10	58.3610	8.4165	54.7134	35.7069	56.6163	55.6840	40.3951	45.2441
TH11	57.2211	14.6499	53.7819	39.5652	58.8643	54.1475	55.7846	38.8925
TH12	60.3829	15.8862	58.6283	9.1185	64.2932	62.1110	59.5092	59.3031
TH13	136.5597	140.0000	136.6288	140.0000	123.2270	128.0819	140.0000	140.0000
TH14	58.3610	8.4165	54.7134	35.7069	56.6163	55.6840	40.3951	45.2441
TH15	57.2211	14.6499	53.7819	39.5652	58.8643	54.1475	55.7846	38.8925
TH16	60.3829	15.8862	58.6283	9.1185	64.2932	62.1110	59.5092	59.3031
TH17	136.5597	140.0000	136.6288	140.0000	123.2270	128.0819	140.0000	140.0000
TH18	58.3610	8.4165	54.7134	35.7069	56.6163	55.6840	40.3951	45.2441
TH19	57.2211	14.6499	53.7819	39.5652	58.8643	54.1475	55.7846	38.8925
TH20	58.3610	8.4165	54.7134	35.7069	56.6163	55.6840	40.3951	45.2441
TH21	0.0001	0.0001	0.0001	0.0001	0.0001	0.0001	0.0001	0.0001
TH22	61.2008	8.4165	54.7134	35.7069	57.9519	61.7058	40.3951	226.7211
TH23	57.2211	14.6499	53.8371	39.5652	56.6053	54.1475	201.5028	38.8925
TH24	65.6930	15.8862	61.9308	9.1185	83.3778	81.7591	214.9566	297.1718
TH25	131.7475	140.0000	129.1137	140.0000	77.1876	93.8641	225.7019	140.0000
TH26	61.2008	8.4165	54.7134	35.7069	57.9519	61.7058	40.3951	226.7211
TH27	57.2211	14.6499	53.8371	39.5652	56.6053	54.1475	201.5028	38.8925
TH28	65.6930	15.8862	61.9308	9.1185	83.3778	81.7591	214.9566	297.1718
TH29	131.7475	140.0000	129.1137	140.0000	77.1876	93.8641	225.7019	140.0000
TH30	61.2008	8.4165	54.7134	35.7069	57.9519	61.7058	40.3951	226.7211
TH31	57.2211	14.6499	53.8371	39.5652	56.6053	54.1475	201.5028	38.8925
TH32	65.6930	15.8862	61.9308	9.1185	83.3778	81.7591	214.9566	297.1718
TH33	131.7475	140.0000	129.1137	140.0000	77.1876	93.8641	225.7019	140.0000
TH34	61.2008	8.4165	54.7134	35.7069	57.9519	61.7058	40.3951	226.7211
TH35	57.2211	14.6499	53.8371	39.5652	56.6053	54.1475	201.5028	38.8925
TH36	65.6930	15.8862	61.9308	9.1185	83.3778	81.7591	214.9566	297.1718
TH37	131.7475	140.0000	129.1137	140.0000	77.1876	93.8641	225.7019	140.0000
TH38	61.2008	8.4165	54.7134	35.7069	57.9519	61.7058	40.3951	226.7211
TH39	57.2211	14.6499	53.8371	39.5652	56.6053	54.1475	201.5028	38.8925
TH40	65.6930	15.8862	61.9308	9.1185	83.3778	81.7591	214.9566	297.1718
TH41	131.7475	140.0000	129.1137	140.0000	77.1876	93.8641	225.7019	140.0000
TH42	61.2008	8.4165	54.7134	35.7069	57.9519	61.7058	40.3951	226.7211
TH43	57.2211	14.6499	53.8371	39.5652	56.6053	54.1475	201.5028	38.8925
TH44	65.6930	15.8862	61.9308	9.1185	83.3778	81.7591	214.9566	297.1718
TH45	131.7475	140.0000	129.1137	140.0000	77.1876	93.8641	225.7019	140.0000
TH46	61.2008	8.4165	54.7134	35.7069	57.9519	61.7058	40.3951	226.7211
TH47	57.2211	14.6499	53.8371	39.5652	56.6053	54.1475	201.5028	38.8925
TH48	65.6930	15.8862	61.9308	9.1185	83.3778	81.7591	214.9566	297.1718
TH49	131.7475	140.0000	129.1137	140.0000	77.1876	93.8641	225.7019	140.0000
TH50	61.2008	8.4165	54.7134	35.7069	57.9519	61.7058	40.3951	226.7211
TH51	57.2211	14.6499	53.8371	39.5652	56.6053	54.1475	201.5028	38.8925
TH52	65.6930	15.8862	61.9308	9.1185	83.3778	81.7591	214.9566	297.1718
TH53	143.3448	140.0000	142.3247	140.0000	152.2475	150.8487	140.0000	140.0000
TH54	61.2008	8.4165	54.7134	35.7069	57.9519	61.7058	40.3951	226.7211

(Continued)

Table 4.6.10 Thresholds for Cb color component of the natural and synthetic images for P = 20 for the sub-bands 55 to 84

Images → / Threshold↓	Aishwarya	Lena	Donkey	Barbara	Mandrill	Rose	Horizontal	Vertical
TH55	57.2211	14.6499	53.8371	39.5652	56.6053	54.1475	201.5028	38.8925
TH56	65.6930	15.8862	61.9308	9.1185	83.3778	81.7591	214.9566	297.1718
TH57	3.0542	3.2456	2.9932	3.2456	1.7894	2.1760	5.2323	3.2456
TH58	61.2008	8.4165	54.7134	35.7069	57.9519	61.7058	40.3951	226.7211
TH59	57.2211	14.6499	53.8371	39.5652	56.6053	54.1475	201.5028	38.8925
TH60	65.6930	15.8862	61.9308	9.1185	83.3778	81.7591	214.9566	297.1718
TH61	131.7475	140.0000	129.1137	140.0000	77.1876	93.8641	225.7019	140.0000
TH62	61.2008	8.4165	54.7134	35.7069	57.9519	61.7058	40.3951	226.7211
TH63	57.2211	14.6499	53.8371	39.5652	56.6053	54.1475	201.5028	38.8925
TH64	65.6930	15.8862	61.9308	9.1185	83.3778	81.7591	214.9566	297.1718
TH65	131.7475	140.0000	129.1137	140.0000	77.1876	93.8641	225.7019	140.0000
TH66	61.2008	8.4165	54.7134	35.7069	57.9519	61.7058	40.3951	226.7211
TH67	57.2211	14.6499	53.8371	39.5652	56.6053	54.1475	201.5028	38.8925
TH68	65.6930	15.8862	61.9308	9.1185	83.3778	81.7591	214.9566	297.1718
TH69	131.7475	140.0000	129.1137	140.0000	77.1876	93.8641	225.7019	140.0000
TH70	61.2008	8.4165	54.7134	35.7069	57.9519	61.7058	40.3951	226.7211
TH71	57.2211	14.6499	53.8371	39.5652	56.6053	54.1475	201.5028	38.8925
TH72	65.6930	15.8862	61.9308	9.1185	83.3778	81.7591	214.9566	297.1718
TH73	131.7475	140.0000	129.1137	140.0000	77.1876	93.8641	225.7019	140.0000
TH74	61.2008	8.4165	54.7134	35.7069	57.9519	61.7058	40.3951	226.7211
TH75	57.2211	14.6499	53.8371	39.5652	56.6053	54.1475	201.5028	38.8925
TH76	65.6930	15.8862	61.9308	9.1185	83.3778	81.7591	214.9566	297.1718
TH77	131.7475	140.0000	129.1137	140.0000	77.1876	93.8641	225.7019	140.0000
TH78	61.2008	8.4165	54.7134	35.7069	57.9519	61.7058	40.3951	226.7211
TH79	57.2211	14.6499	53.8371	39.5652	56.6053	54.1475	201.5028	38.8925
TH80	65.6930	15.8862	61.9308	9.1185	83.3778	81.7591	214.9566	297.1718
TH81	131.7475	140.0000	129.1137	140.0000	77.1876	93.8641	225.7019	140.0000
TH82	61.2008	8.4165	54.7134	35.7069	57.9519	61.7058	40.3951	226.7211
TH83	57.2211	14.6499	53.8371	39.5652	56.6053	54.1475	201.5028	38.8925
TH84	65.6930	15.8862	61.9308	9.1185	83.3778	81.7591	214.9566	297.1718

Table 4.6.11 Thresholds for Cb color component of the natural and synthetic images for P = 30 for the sub-bands 1 to 18

Images → / Threshold↓	Aishwarya	Lena	Donkey	Barbara	Mandrill	Rose	Horizontal	Vertical
TH1	1.0000	1.0000	1.0000	1.0000	1.0000	1.0000	1.0000	1.0000
TH2	86.3342	12.6248	81.6761	53.5604	83.4117	80.9520	60.5926	67.8661
TH3	85.2495	21.9748	80.0262	59.3478	83.0782	79.9058	83.6769	58.3387
TH4	88.4195	23.8293	86.4031	13.6777	87.5164	86.4671	89.2638	88.9546
TH5	1.0000	1.0000	1.0000	1.0000	1.0000	1.0000	1.0000	1.0000
TH6	87.2671	12.6248	82.0700	53.5604	84.9244	83.0699	60.5926	67.8661
TH7	85.8317	21.9748	80.5909	59.3478	87.1670	81.2213	83.6769	58.3387
TH8	89.8914	23.8293	87.4653	13.6777	93.6823	91.1127	89.2638	88.9546
TH9	206.5597	210.0000	206.6288	210.0000	193.2270	198.0819	210.0000	210.0000
TH10	87.2671	12.6248	82.0700	53.5604	84.9244	83.0699	60.5926	67.8661
TH11	85.8317	21.9748	80.5909	59.3478	87.1670	81.2213	83.6769	58.3387
TH12	89.8914	23.8293	87.4653	13.6777	93.6823	91.1127	89.2638	88.9546
TH13	206.5597	210.0000	206.6288	210.0000	193.2270	198.0819	210.0000	210.0000
TH14	87.2671	12.6248	82.0700	53.5604	84.9244	83.0699	60.5926	67.8661
TH15	85.8317	21.9748	80.5909	59.3478	87.1670	81.2213	83.6769	58.3387
TH16	89.8914	23.8293	87.4653	13.6777	93.6823	91.1127	89.2638	88.9546
TH17	206.5597	210.0000	206.6288	210.0000	193.2270	198.0819	210.0000	210.0000
TH18	87.2671	12.6248	82.0700	53.5604	84.9244	83.0699	60.5926	67.8661

(Continued)

Table 4.6.11 Thresholds for Cb color component of the natural and synthetic images for P = 30 for the sub-bands 19 to 72

Images → / Threshold↓	Aishwarya	Lena	Donkey	Barbara	Mandrill	Rose	Horizontal	Vertical
TH19	85.8317	21.9748	80.5909	59.3478	87.1670	81.2213	83.6769	58.3387
TH20	87.2671	12.6248	82.0700	53.5604	84.9244	83.0699	60.5926	67.8661
TH21	0.0001	0.0001	0.0001	0.0001	0.0001	0.0001	0.0001	0.0001
TH22	90.1068	12.6248	82.0700	53.5604	86.2601	89.0917	60.5926	249.3432
TH23	85.8317	21.9748	80.6461	59.3478	84.9080	81.2213	229.3951	58.3387
TH24	95.2016	23.8293	90.7678	13.6777	112.7669	110.7608	244.7112	326.8233
TH25	201.7475	210.0000	199.1137	210.0000	147.1876	163.8641	155.7019	210.0000
TH26	90.1068	12.6248	82.0700	53.5604	86.2601	89.0917	60.5926	249.3432
TH27	85.8317	21.9748	80.6461	59.3478	84.9080	81.2213	229.3951	58.3387
TH28	95.2016	23.8293	90.7678	13.6777	112.7669	110.7608	244.7112	326.8233
TH29	201.7475	210.0000	199.1137	210.0000	147.1876	163.8641	155.7019	210.0000
TH30	90.1068	12.6248	82.0700	53.5604	86.2601	89.0917	60.5926	249.3432
TH31	85.8317	21.9748	80.6461	59.3478	84.9080	81.2213	229.3951	58.3387
TH32	95.2016	23.8293	90.7678	13.6777	112.7669	110.7608	244.7112	326.8233
TH33	201.7475	210.0000	199.1137	210.0000	147.1876	163.8641	155.7019	210.0000
TH34	90.1068	12.6248	82.0700	53.5604	86.2601	89.0917	60.5926	249.3432
TH35	85.8317	21.9748	80.6461	59.3478	84.9080	81.2213	229.3951	58.3387
TH36	95.2016	23.8293	90.7678	13.6777	112.7669	110.7608	244.7112	326.8233
TH37	201.7475	210.0000	199.1137	210.0000	147.1876	163.8641	155.7019	210.0000
TH38	90.1068	12.6248	82.0700	53.5604	86.2601	89.0917	60.5926	249.3432
TH39	85.8317	21.9748	80.6461	59.3478	84.9080	81.2213	229.3951	58.3387
TH40	95.2016	23.8293	90.7678	13.6777	112.7669	110.7608	244.7112	326.8233
TH41	201.7475	210.0000	199.1137	210.0000	147.1876	163.8641	155.7019	210.0000
TH42	90.1068	12.6248	82.0700	53.5604	86.2601	89.0917	60.5926	249.3432
TH43	85.8317	21.9748	80.6461	59.3478	84.9080	81.2213	229.3951	58.3387
TH44	95.2016	23.8293	90.7678	13.6777	112.7669	110.7608	244.7112	326.8233
TH45	201.7475	210.0000	199.1137	210.0000	147.1876	163.8641	155.7019	210.0000
TH46	90.1068	12.6248	82.0700	53.5604	86.2601	89.0917	60.5926	249.3432
TH47	85.8317	21.9748	80.6461	59.3478	84.9080	81.2213	229.3951	58.3387
TH48	95.2016	23.8293	90.7678	13.6777	112.7669	110.7608	244.7112	326.8233
TH49	201.7475	210.0000	199.1137	210.0000	147.1876	163.8641	155.7019	210.0000
TH50	90.1068	12.6248	82.0700	53.5604	86.2601	89.0917	60.5926	249.3432
TH51	85.8317	21.9748	80.6461	59.3478	84.9080	81.2213	229.3951	58.3387
TH52	95.2016	23.8293	90.7678	13.6777	112.7669	110.7608	244.7112	326.8233
TH53	213.3448	210.0000	212.3247	210.0000	222.2475	220.8487	210.0000	210.0000
TH54	90.1068	12.6248	82.0700	53.5604	86.2601	89.0917	60.5926	249.3432
TH55	85.8317	21.9748	80.6461	59.3478	84.9080	81.2213	229.3951	58.3387
TH56	95.2016	23.8293	90.7678	13.6777	112.7669	110.7608	244.7112	326.8233
TH57	4.6770	4.8683	4.6160	4.8683	3.4122	3.7988	3.6096	4.8683
TH58	90.1068	12.6248	82.0700	53.5604	86.2601	89.0917	60.5926	249.3432
TH59	85.8317	21.9748	80.6461	59.3478	84.9080	81.2213	229.3951	58.3387
TH60	95.2016	23.8293	90.7678	13.6777	112.7669	110.7608	244.7112	326.8233
TH61	201.7475	210.0000	199.1137	210.0000	147.1876	163.8641	155.7019	210.0000
TH62	90.1068	12.6248	82.0700	53.5604	86.2601	89.0917	60.5926	249.3432
TH63	85.8317	21.9748	80.6461	59.3478	84.9080	81.2213	229.3951	58.3387
TH64	95.2016	23.8293	90.7678	13.6777	112.7669	110.7608	244.7112	326.8233
TH65	201.7475	210.0000	199.1137	210.0000	147.1876	163.8641	155.7019	210.0000
TH66	90.1068	12.6248	82.0700	53.5604	86.2601	89.0917	60.5926	249.3432
TH67	85.8317	21.9748	80.6461	59.3478	84.9080	81.2213	229.3951	58.3387
TH68	95.2016	23.8293	90.7678	13.6777	112.7669	110.7608	244.7112	326.8233
TH69	201.7475	210.0000	199.1137	210.0000	147.1876	163.8641	155.7019	210.0000
TH70	90.1068	12.6248	82.0700	53.5604	86.2601	89.0917	60.5926	249.3432
TH71	85.8317	21.9748	80.6461	59.3478	84.9080	81.2213	229.3951	58.3387
TH72	95.2016	23.8293	90.7678	13.6777	112.7669	110.7608	244.7112	326.8233

(Continued)

Table 4.6.11 Thresholds for Cb color component of the natural and synthetic images for P = 30 for the sub-bands 73 to 84

TH73	201.7475	210.0000	199.1137	210.0000	147.1876	163.8641	155.7019	210.0000
TH74	90.1068	12.6248	82.0700	53.5604	86.2601	89.0917	60.5926	249.3432
TH75	85.8317	21.9748	80.6461	59.3478	84.9080	81.2213	229.3951	58.3387
TH76	95.2016	23.8293	90.7678	13.6777	112.7669	110.7608	244.7112	326.8233
TH77	201.7475	210.0000	199.1137	210.0000	147.1876	163.8641	155.7019	210.0000
TH78	90.1068	12.6248	82.0700	53.5604	86.2601	89.0917	60.5926	249.3432
TH79	85.8317	21.9748	80.6461	59.3478	84.9080	81.2213	229.3951	58.3387
TH80	95.2016	23.8293	90.7678	13.6777	112.7669	110.7608	244.7112	326.8233
TH81	201.7475	210.0000	199.1137	210.0000	147.1876	163.8641	155.7019	210.0000
TH82	90.1068	12.6248	82.0700	53.5604	86.2601	89.0917	60.5926	249.3432
TH83	85.8317	21.9748	80.6461	59.3478	84.9080	81.2213	229.3951	58.3387
TH84	95.2016	23.8293	90.7678	13.6777	112.7669	110.7608	244.7112	326.8233

Table 4.6.12 Thresholds for Cb color component of the natural and synthetic images for P = 40 for the sub-bands 1 to 38

Images → / **Threshold↓**	**Aishwarya**	**Lena**	**Donkey**	**Barbara**	**Mandrill**	**Rose**	**Horizontal**	**Vertical**
TH1	1.0000	1.0000	1.0000	1.0000	1.0000	1.0000	1.0000	1.0000
TH2	115.2403	16.8331	109.0328	71.4139	111.7198	108.3379	80.7902	90.4881
TH3	113.8600	29.2997	106.8352	79.1305	111.3808	106.9796	111.5692	77.7849
TH4	117.9280	31.7724	115.2400	18.2369	116.9055	115.4688	119.0184	118.6061
TH5	1.0000	1.0000	1.0000	1.0000	1.0000	1.0000	1.0000	1.0000
TH6	116.1732	16.8331	109.4267	71.4139	113.2325	110.4558	80.7902	90.4881
TH7	114.4422	29.2997	107.3999	79.1305	115.4696	108.2950	111.5692	77.7849
TH8	119.4000	31.7724	116.3022	18.2369	123.0714	120.1144	119.0184	118.6061
TH9	276.5597	280.0000	276.6288	280.0000	263.2270	268.0819	280.0000	280.0000
TH10	116.1732	16.8331	109.4267	71.4139	113.2325	110.4558	80.7902	90.4881
TH11	114.4422	29.2997	107.3999	79.1305	115.4696	108.2950	111.5692	77.7849
TH12	119.4000	31.7724	116.3022	18.2369	123.0714	120.1144	119.0184	118.6061
TH13	276.5597	280.0000	276.6288	280.0000	263.2270	268.0819	280.0000	280.0000
TH14	116.1732	16.8331	109.4267	71.4139	113.2325	110.4558	80.7902	90.4881
TH15	114.4422	29.2997	107.3999	79.1305	115.4696	108.2950	111.5692	77.7849
TH16	119.4000	31.7724	116.3022	18.2369	123.0714	120.1144	119.0184	118.6061
TH17	276.5597	280.0000	276.6288	280.0000	263.2270	268.0819	280.0000	280.0000
TH18	116.1732	16.8331	109.4267	71.4139	113.2325	110.4558	80.7902	90.4881
TH19	114.4422	29.2997	107.3999	79.1305	115.4696	108.2950	111.5692	77.7849
TH20	116.1732	16.8331	109.4267	71.4139	113.2325	110.4558	80.7902	90.4881
TH21	0.0001	0.0001	0.0001	0.0001	0.0001	0.0001	0.0001	0.0001
TH22	119.0129	16.8331	109.4267	71.4139	114.5682	116.4775	80.7902	271.9652
TH23	114.4422	29.2997	107.4551	79.1305	113.2106	108.2950	257.2874	77.7849
TH24	124.7101	31.7724	119.6047	18.2369	142.1561	139.7625	274.4658	356.4748
TH25	271.7475	280.0000	269.1137	280.0000	217.1876	233.8641	85.7019	280.0000
TH26	119.0129	16.8331	109.4267	71.4139	114.5682	116.4775	80.7902	271.9652
TH27	114.4422	29.2997	107.4551	79.1305	113.2106	108.2950	257.2874	77.7849
TH28	124.7101	31.7724	119.6047	18.2369	142.1561	139.7625	274.4658	356.4748
TH29	271.7475	280.0000	269.1137	280.0000	217.1876	233.8641	85.7019	280.0000
TH30	119.0129	16.8331	109.4267	71.4139	114.5682	116.4775	80.7902	271.9652
TH31	114.4422	29.2997	107.4551	79.1305	113.2106	108.2950	257.2874	77.7849
TH32	124.7101	31.7724	119.6047	18.2369	142.1561	139.7625	274.4658	356.4748
TH33	271.7475	280.0000	269.1137	280.0000	217.1876	233.8641	85.7019	280.0000
TH34	119.0129	16.8331	109.4267	71.4139	114.5682	116.4775	80.7902	271.9652
TH35	114.4422	29.2997	107.4551	79.1305	113.2106	108.2950	257.2874	77.7849
TH36	124.7101	31.7724	119.6047	18.2369	142.1561	139.7625	274.4658	356.4748
TH37	271.7475	280.0000	269.1137	280.0000	217.1876	233.8641	85.7019	280.0000
TH38	119.0129	16.8331	109.4267	71.4139	114.5682	116.4775	80.7902	271.9652

(Continued)

Table 4.6.12 Thresholds for Cb color component of the natural and synthetic images for P = 40 for the sub-bands 39 to 84

Images → / Threshold↓	Aishwarya	Lena	Donkey	Barbara	Mandrill	Rose	Horizontal	Vertical
TH39	114.4422	29.2997	107.4551	79.1305	113.2106	108.2950	257.2874	77.7849
TH40	124.7101	31.7724	119.6047	18.2369	142.1561	139.7625	274.4658	356.4748
TH41	271.7475	280.0000	269.1137	280.0000	217.1876	233.8641	85.7019	280.0000
TH42	119.0129	16.8331	109.4267	71.4139	114.5682	116.4775	80.7902	271.9652
TH43	114.4422	29.2997	107.4551	79.1305	113.2106	108.2950	257.2874	77.7849
TH44	124.7101	31.7724	119.6047	18.2369	142.1561	139.7625	274.4658	356.4748
TH45	271.7475	280.0000	269.1137	280.0000	217.1876	233.8641	85.7019	280.0000
TH46	119.0129	16.8331	109.4267	71.4139	114.5682	116.4775	80.7902	271.9652
TH47	114.4422	29.2997	107.4551	79.1305	113.2106	108.2950	257.2874	77.7849
TH48	124.7101	31.7724	119.6047	18.2369	142.1561	139.7625	274.4658	356.4748
TH49	271.7475	280.0000	269.1137	280.0000	217.1876	233.8641	85.7019	280.0000
TH50	119.0129	16.8331	109.4267	71.4139	114.5682	116.4775	80.7902	271.9652
TH51	114.4422	29.2997	107.4551	79.1305	113.2106	108.2950	257.2874	77.7849
TH52	124.7101	31.7724	119.6047	18.2369	142.1561	139.7625	274.4658	356.4748
TH53	283.3448	280.0000	282.3247	280.0000	292.2475	290.8487	280.0000	280.0000
TH54	119.0129	16.8331	109.4267	71.4139	114.5682	116.4775	80.7902	271.9652
TH55	114.4422	29.2997	107.4551	79.1305	113.2106	108.2950	257.2874	77.7849
TH56	124.7101	31.7724	119.6047	18.2369	142.1561	139.7625	274.4658	356.4748
TH57	6.2998	6.4911	6.2387	6.4911	5.0350	5.4216	1.9868	6.4911
TH58	119.0129	16.8331	109.4267	71.4139	114.5682	116.4775	80.7902	271.9652
TH59	114.4422	29.2997	107.4551	79.1305	113.2106	108.2950	257.2874	77.7849
TH60	124.7101	31.7724	119.6047	18.2369	142.1561	139.7625	274.4658	356.4748
TH61	271.7475	280.0000	269.1137	280.0000	217.1876	233.8641	85.7019	280.0000
TH62	119.0129	16.8331	109.4267	71.4139	114.5682	116.4775	80.7902	271.9652
TH63	114.4422	29.2997	107.4551	79.1305	113.2106	108.2950	257.2874	77.7849
TH64	124.7101	31.7724	119.6047	18.2369	142.1561	139.7625	274.4658	356.4748
TH65	271.7475	280.0000	269.1137	280.0000	217.1876	233.8641	85.7019	280.0000
TH66	119.0129	16.8331	109.4267	71.4139	114.5682	116.4775	80.7902	271.9652
TH67	114.4422	29.2997	107.4551	79.1305	113.2106	108.2950	257.2874	77.7849
TH68	124.7101	31.7724	119.6047	18.2369	142.1561	139.7625	274.4658	356.4748
TH69	271.7475	280.0000	269.1137	280.0000	217.1876	233.8641	85.7019	280.0000
TH70	119.0129	16.8331	109.4267	71.4139	114.5682	116.4775	80.7902	271.9652
TH71	114.4422	29.2997	107.4551	79.1305	113.2106	108.2950	257.2874	77.7849
TH72	124.7101	31.7724	119.6047	18.2369	142.1561	139.7625	274.4658	356.4748
TH73	271.7475	280.0000	269.1137	280.0000	217.1876	233.8641	85.7019	280.0000
TH74	119.0129	16.8331	109.4267	71.4139	114.5682	116.4775	80.7902	271.9652
TH75	114.4422	29.2997	107.4551	79.1305	113.2106	108.2950	257.2874	77.7849
TH76	124.7101	31.7724	119.6047	18.2369	142.1561	139.7625	274.4658	356.4748
TH77	271.7475	280.0000	269.1137	280.0000	217.1876	233.8641	85.7019	280.0000
TH78	119.0129	16.8331	109.4267	71.4139	114.5682	116.4775	80.7902	271.9652
TH79	114.4422	29.2997	107.4551	79.1305	113.2106	108.2950	257.2874	77.7849
TH80	124.7101	31.7724	119.6047	18.2369	142.1561	139.7625	274.4658	356.4748
TH81	271.7475	280.0000	269.1137	280.0000	217.1876	233.8641	85.7019	280.0000
TH82	119.0129	16.8331	109.4267	71.4139	114.5682	116.4775	80.7902	271.9652
TH83	114.4422	29.2997	107.4551	79.1305	113.2106	108.2950	257.2874	77.7849
TH84	124.7101	31.7724	119.6047	18.2369	142.1561	139.7625	274.4658	356.4748

4.7.0 ENCODING

After the process of thresholding, most of the components are adjusted to zero values, and encoder further compresses the coefficients of wavelet packets tree to give better overall compression. An encoding process removes the redundancy in the form of repetitive bit patterns in the output of thresholding. It uses a model to determine accurately the probabilities for each coefficient value and produces an appropriate code based on these probabilities, so that the resultant output code-stream will be smaller than the input stream. The most commonly used entropy encoders are Huffman encoder, and Arithmetic encoder. Simple Run-Length Encoding (RLE) has proven very effective encoding in many applications. Run-Length Encoding is a pattern recognition scheme that searches for the repetition (redundancy) of identical data values in the code-stream. The data set can be compressed by replacing the repetitive sequence with a single data value and length of that data. Huffman and Arithmetic codes substitute bit patterns for symbols based on the frequencies of the symbols [93]. The Huffman algorithm requires each code to have an integral number of bits. And arithmetic coding method allows for fractional number of bits per code by grouping two or more such codes together into a block composed of an integral number of bits [23]. This allows arithmetic code to outperform Huffman code, and consequently arithmetic code is more commonly used encoding in wavelet-based algorithms. The researcher has provided the results using Huffman encoding as well as Arithmetic encoding with conclusion.

The researcher suggests the modified technique for the encoding. After the thresholding, repetitions of the coefficients of a wavelet packets tree can be a eliminated by using suggested ***Enhanced Run-Length Encoding,*** and then for the bit coding well known Huffman coding or Arithmetic coding methods are used.

The problems with existing Run Length Encoding, is that the compression ratio obtained from run-length encoding schemes vary depending on the type of data to be encoded, and the repetitions present within the data set. Some data sets can be highly compressed by run-length encoding whereas other data sets can actually grow larger due to the encoding [23]. This problem of an existing run-length encoding techniques are eliminated up to the certain extent by using ***Enhanced Run-Length Encoding*** technique. In the proposed ***Enhanced RLE,*** the coefficients X_i and X_{i+1} are compared, and if $|X_i - X_{i+1}|$ is less than acceptable value then X_i and X_{i+1} are treated as X_i only. This ***Enhanced RLE*** introduces an error. The error introduced is a function of acceptable value. This acceptable value, suggested by the researcher is the function of

the energy contain of an image. The acceptable value is calculated as, ($E - \sqrt{mean\,of\ (energy\,of\ image \times 100)}$).

Although this method overcomes the problem of RLE, it introduces little error, which is not much noticeable. As the flexibility is already extended to the user about required quality of resultant image verses compression ratio by selecting the value of P, the effect of error introduced by ***Enhanced RLE*** technique is compensated. The proposed algorithm is tested over the natural and synthetic images, for the different values of P, which is given in the results and the conclusions, are drawn based on it.

CHAPTER 5

RESULTS

There are various methods available for still image compression. JPEG and JPEG-2000 are the popular standards available for still image compression. JPEG uses the Discrete Cosine Transform for the transformation while JPEG-2000 uses Discrete Wavelet Transform. The disadvantages of the existing compression methods are discussed in chapter-2. In the proposed image compression technique, wavelet packets best tree based on energy contents with adaptive thresholds are used. The parameter P provides the flexibility to the user to select desired image quality and compression ratio. The results for the different values of P for different natural and synthetic images are given in this chapter.

5.1.0 PERCENTAGE OF ZEROS vs THRESHOLD

Wavelet transform transforms, the image from spatial domain to frequency domain. Wavelet transform and wavelet packets are nearly similar, the only difference is that in wavelet transform the approximate component is further decomposed but in wavelet packets the decomposition is carried out with approximate as well as detail components. After the transformation the image is represented by a set of wavelet packets coefficients. The high compression ratio is achieved by using the thresholding to the wavelet packets coefficients. The relation between the percentage of zeros vs threshold for Bior2.2 wavelet for natural and synthetic images is given in the figure 5.1.1 to 5.1.12. More percentage of zeros yields more compression. The natural test images are AISHWARYA, CHEETAH, LENA, BARBARA, MANDRILL, FINGURE, BIRD, ROSE, DONKEY and synthetic images are BUTTERFLY, DIAGONAL, HORIZONTAL, and VERTICAL.

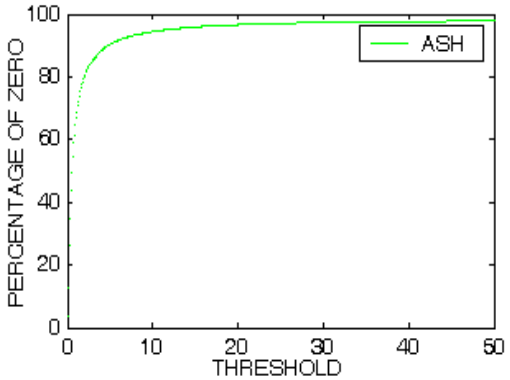

Figure 5.1.1 Percentage of Zeros vs Threshold for the image AISHWARYA

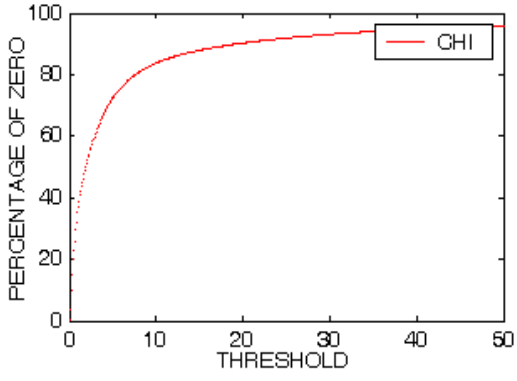

Figure 5.1.2 Percentage of Zeros vs Threshold for the image CHEETAH

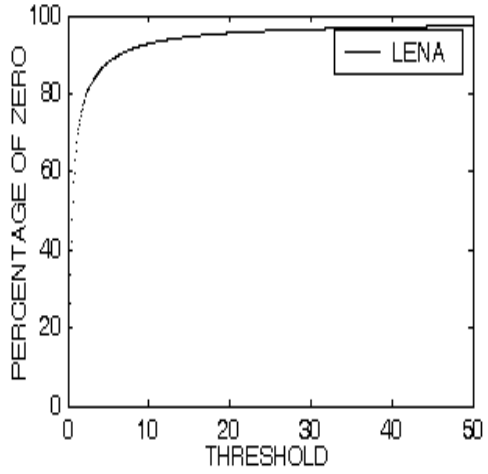

Figure 5.1.3 Percentage of Zeros vs Threshold for the image LENA

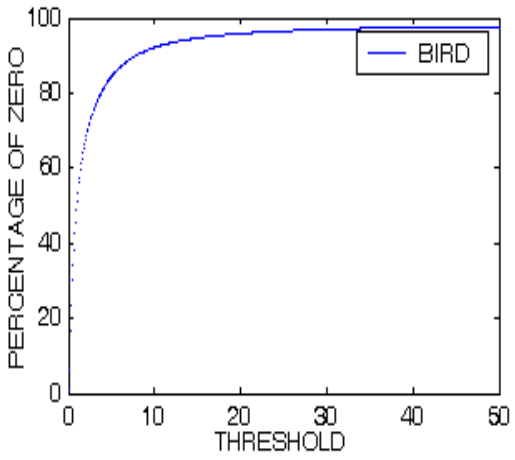

Figure 5.1.4 Percentage of Zeros vs Threshold for the image BIRD

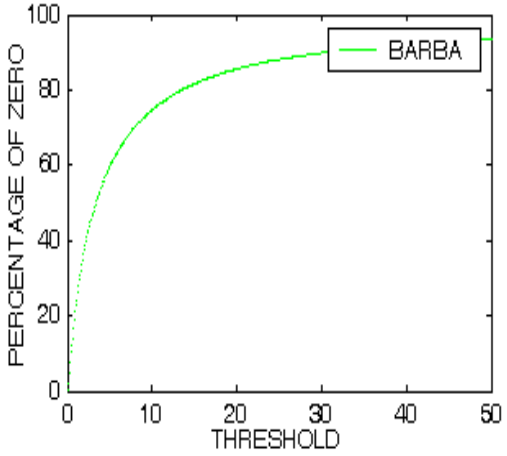

Figure 5.1.5 Percentage of Zeros vs Threshold for the image BARBARA

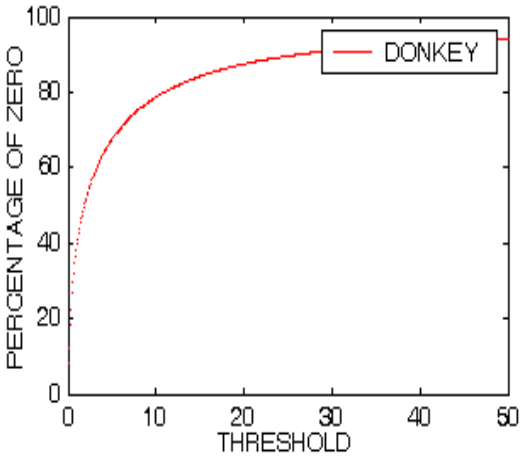

Figure 5.1.6 Percentage of Zeros vs Threshold for the image DONKEY

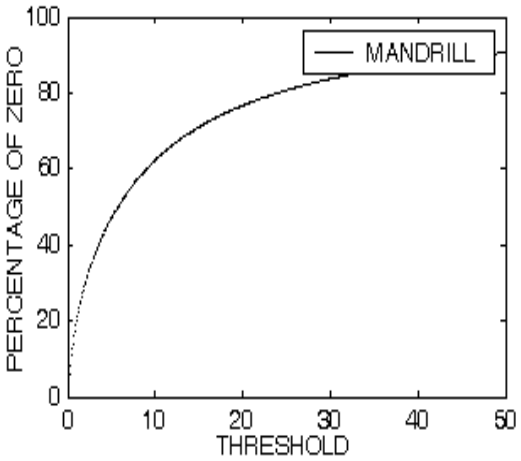

Figure 5.1.7 Percentage of Zeros vs Threshold for the image MANDRILL

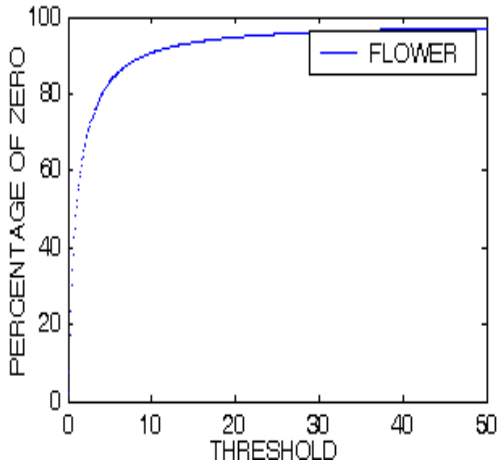

Figure 5.1.8 Percentage of Zeros vs Threshold for the image FLOWER

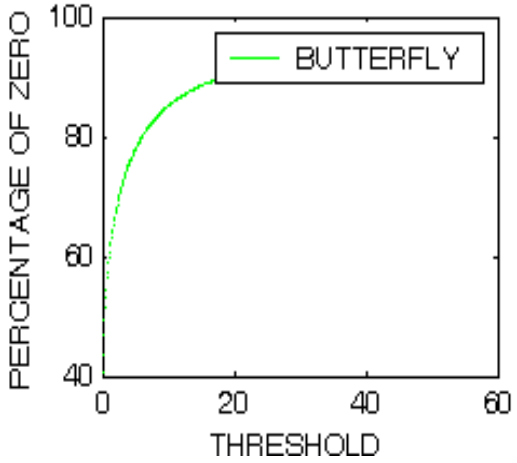

Figure 5.1.9 Percentage of Zeros vs Threshold for the image BUTTERFLY

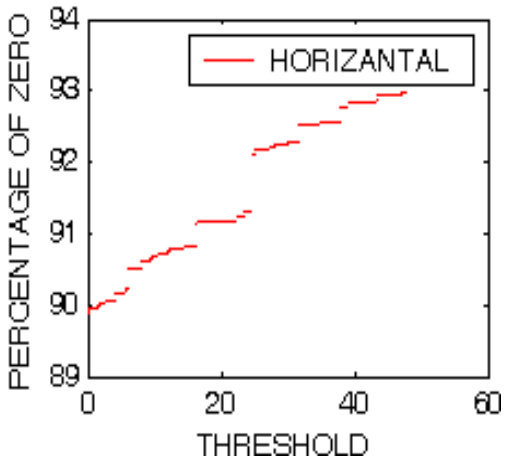

Figure 5.1.10 Percentage of Zeros vs Threshold for the image HORIZONTAL

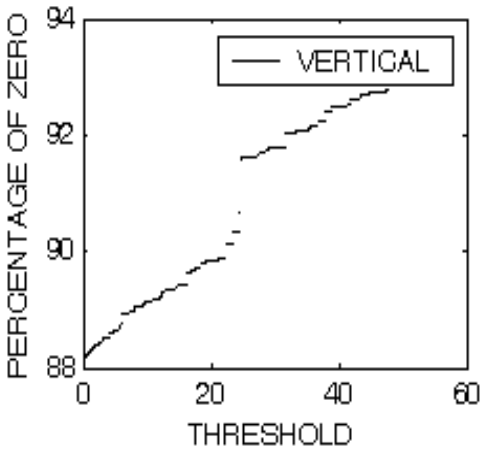

Figure 5.1.11 Percentage of Zeros vs Threshold for the image VERTICAL

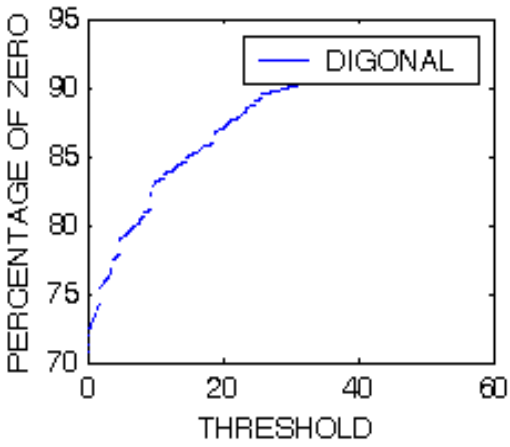

Figure 5.1.12 Percentage of Zeros vs Threshold for the image DIAGONAL

5.2.0 RESULTS FOR THE PROPOSED METHODS

The proposed algorithm is implemented and tested over the range of natural and synthetic images. The results are given in terms of percentage of compression, compression ratio, and peak signal to noise ratio. Every set of result corresponds to a value of P, the flexibility parameter. The natural test images used are AISHWARYA, CHEETAH, LENA, BARBARA, MANDRILL, BIRD, ROSE, DONKEY, and synthetic images used are BUTTERFLY, HORIZONTAL, and VERTICAL. The tables 5.2.1 to 5.2.4 show the results for the proposed methods with a value of P as 5, 10, 20, 30, 40, 50 and 60 using Arithmetic Coding. The tables 5.2.5 to 5.2.8 show the results for the proposed methods with a value of P as 5, 10, 20, 30, 40, 50 and 60 using Huffman Coding. The results for existing standards JPEG-2000 are also given in the table 5.2.9.

Table 5.2.1 Results of selected Images using Arithmetic Coding

	Constant P = 5			Constant P = 10		
Image	**Percentage of compression**	**Compression ratio**	**Peak signal to noise ratio (dB)**	**Percentage of compression**	**Compression ratio**	**Peak signal to noise ratio (dB)**
AISHWARYA	94.6834	19	80.0646	96.1687	27	84.2313
CHEETAH	90.1475	11	79.1685	92.6	14	73.6295
LENA	95.7446	24	85.6561	97.1908	36	85.9624
BARBARA	84.634	7	71.921	90.231	11	67.8158
MANDRILL	72.5561	4	62.1245	80.702	6	60.0194
BIRD	90.1223	11	75.417	94.0162	17	73.7004
ROSE	74.2142	4	65.134	82.2271	6	62.7118
DONKEY	83.9696	7	72.2084	88.0107	9	69.2338
BUTTERFLY	81.8855	6	77.4233	88.3102	9	68.8355
HORIZONTAL	80.0731	6	60.1863	82.6058	6	59.5537
VERTICAL	92.8208	14	77.3835	95.8693	25	12.6192

Table 5.2.2 Results of selected Images using Arithmetic Coding

	Constant P = 20			Constant P = 30		
Image	**Percentage of compression**	**Compression ratio**	**Peak signal to noise ratio (dB)**	**Percentage of compression**	**Compression ratio**	**Peak signal to noise ratio (dB)**
AISHWARYA	96.9113	33	78.9871	97.6032	42	75.9537
CHEETAH	95.415	22	67.0735	96.5636	30	63.6988
LENA	97.894	48	79.6256	98.4183	64	74.8504
BARBARA	94.3057	18	61.49	96.3771	28	56.3253
MANDRILL	83.7612	7	56.812	90.9178	12	18.163
BIRD	95.6095	23	67.4469	96.7617	31	65.7065
ROSE	84.1035	7	58.5079	91.8946	13	51.9217
DONKEY	92.7269	14	30.7286	95.0737	21	30.7342
BUTTERFLY	92.5796	14	61.1711	94.5351	19	50.7274
HORIZONTAL	86.2933	8	54.9828	88.0867	9	54.4989
VERTICAL	95.8693	25	19.88	96.6574	30	57.2394

Table 5.2.3 Results of selected Images using Arithmetic Coding

	Constant P = 40			Constant P = 50		
Image	**Percentage of compression**	**Compression ratio**	**Peak signal to noise ratio (dB)**	**Percentage of compression**	**Compression ratio**	**Peak signal to noise ratio (dB)**
AISHWARYA	97.8096	46	71.231	97.958	49	67.891
CHEETAH	97.1794	36	61.5553	97.4353	39	60.1865
LENA	98.542	69	70.1371	98.6133	73	67.7423
BARBARA	96.953	33	54.0879	97.0091	34	52.8408
MANDRILL	93.3606	16	48.5085	94.4997	19	47.074
BIRD	97.1253	35	62.339	97.2886	37	59.9416
ROSE	93.4251	16	49.7758	94.2324	18	48.3914
DONKEY	96.1503	26	54.4774	96.709	31	52.5357
BUTTERFLY	95.5221	23	48.5618	96.1497	26	47.5036
HORIZONTAL	89.1933	10	52.1679	90.2355	11	49.1411
VERTICAL	97.1568	36	53.849	97.518	41	51.2781

Table 5.2.4 Results of selected Images using Arithmetic Coding

Constant P = 60			
Image	**Percentage of compression**	**Compression ratio**	**Peak signal to noise ratio (dB)**
AISHWARYA	98.0875	53	64.8412
CHEETAH	97.574	42	59.1732
LENA	98.6628	75	66.7228
BARBARA	97.2696	37	51.9716
MANDRILL	95.2328	21	46.1098
BIRD	97.4229	39	57.2633
ROSE	94.8824	20	46.7576
DONKEY	97.0665	35	50.6168
BUTTERFLY	96.5764	30	46.5698
HORIZONTAL	91.5253	12	47.7637
VERTICAL	97.7864	46	49.5102

Table 5.2.5 Results of selected Images using Huffman Coding

	Constant P = 5			Constant P = 10		
Image	**Percentage of compression**	**Compression ratio**	**Peak signal to noise ratio (dB)**	**Percentage of compression**	**Compression ratio**	**Peak signal to noise ratio (dB)**
AISHWARYA	94.0499	17	80.0646	95.8209	24	84.2313
CHEETAH	87.8819	9	79.1685	91.0508	12	73.6295
LENA	94.7726	20	85.6561	96.6427	30	85.9624
BARBARA	81.7345	6	71.921	88.5815	9	67.8158
MANDRILL	72.5561	4	62.1295	76.5062	5	60.0194
BIRD	87.6788	9	75.417	93.0627	15	73.7004
ROSE	69.1386	4	65.134	79.1288	5	62.7118
DONKEY	81.2424	6	72.2084	86.1908	8	69.2338
BUTTERFLY	75.7517	5	77.4233	85.149	7	68.8355
HORIZONTAL	73.1801	4	60.1883	76.2735	5	59.5537
VERTICAL	91.5972	12	77.3835	93.6096	16	67.2358

Table 5.2.6 Results of selected Images using Huffman Coding

	Constant P = 20			Constant P = 30		
Image	**Percentage of compression**	**Compression ratio**	**Peak signal to noise ratio (dB)**	**Percentage of compression**	**Compression ratio**	**Peak signal to noise ratio (dB)**
AISHWARYA	96.7088	31	78.9871	97.4684	40	75.9537
CHEETAH	94.7329	19	67.0735	96.3183	28	63.6988
LENA	97.532	41	79.6256	98.1875	56	74.8504
BARBARA	93.4905	16	61.49	95.5038	23	56.3253
MANDRILL	80.372	6	56.812	89.3435	10	51.9118
BIRD	95.0405	21	67.4469	96.4562	29	65.7065
ROSE	81.6376	6	58.5079	90.8829	11	51.9217
DONKEY	91.8327	13	63.4845	94.5427	19	58.5874
BUTTERFLY	90.7799	11	61.1711	93.5625	16	50.7274
HORIZONTAL	81.0719	6	54.9828	83.2592	6	54.4989
VERTICAL	95.2496	22	62.2183	96.2783	27	57.2394

Table 5.2.7 Results of selected Images using Huffman Coding

Constant P = 40				Constant P = 50		
Image	**Percentage of compression**	**Compression ratio**	**Peak signal to noise ratio (dB)**	**Percentage of compression**	**Compression ratio**	**Peak signal to noise ratio (dB)**
AISHWARYA	97.6873	44	71.231	97.8453	47	67.9816
CHEETAH	96.9972	34	61.5553	97.2941	37	60.1865
18LENA	98.3408	61	70.1371	98.4298	64	67.7423
BARBARA	96.2805	27	54.0879	96.7158	31	52.8408
MANDRILL	92.3307	14	48.5085	93.6994	16	47.074
BIRD	96.8005	32	62.339	96.9788	34	59.9416
ROSE	92.7555	14	49.7758	93.6941	16	48.3914
DONKEY	95.7835	24	54.4774	96.3996	28	52.5357
BUTTERFLY	94.7574	20	48.5618	95.5122	23	47.5036
HORIZONTAL	85.5953	7	52.1679	87.2958	8	49.1411
VERTICAL	96.8418	32	53.849	97.2495	37	51.2781

Table 5.2.8 Results of selected Images using Huffman Coding

Constant P = 60			
Image	**Percentage of compression**	**Compression ratio**	**Peak signal to noise ratio (dB)**
AISHWARYA	97.6873	50	64.8412
CHEETAH	97.3983	39	59.1732
LENA	98.4885	67	66.7228
BARBARA	97.0166	34	51.9716
MANDRILL	94.5585	19	46.1098
BIRD	97.1217	35	57.2633
ROSE	94.4339	18	46.7576
DONKEY	97.0665	35	50.6168
BUTTERFLY	96.0195	26	46.5698
HORIZONTAL	89.2611	10	47.7637
VERTICAL	97.5687	42	49.5102

Table 5.2.9 Results of selected Images using JEPG-2000

Image	**Original size (KB)**	**Compressed size (KB)**	**Compression ratio**	**Percentage of compression**	**Peak signal to noise ratio (dB)**
AISHWARYA	901	216	4.1712	24	191.6040
CHEETAH	901	147	6.1292	16	241.2325
LENA	901	87	10.6	10	170.5337
BARBARA	765	154	4.9675	20	153.3857
MANDRILL	769	341	2.2551	44	185.8936
BIRD	901	339	2.6578	38	200.7146
ROSE	901	402	2.2412	45	186.2608
DONKEY	774	246	3.1463	32	191.3145
BUTTERFLY	385	108	3.5648	28	197.1621
HORIZONTAL	632	18	35.1111	3	192.9029
VERTICAL	685	38	18.0263	5	238.4996

The original image and resultant compressed images of presented algorithm using Arithmetic encoding for different values of P are shown in figure 5.2.1 to 5.2.88.

Figure 5.2.1 Original image AISHWARYA

Compression Ratio = 19
PSNR = 80.0646 dB

Figure 5.2.2 Compressed image with P = 5 using Arithmetic Encoding

Compression Ratio = 27
PSNR = 84.2313 dB

Figure 5.2.3 Compressed image with P = 10 using Arithmetic Encoding

Compression Ratio = 33
PSNR = 78.9871 dB

Figure 5.2.4 Compressed image with P = 20 using Arithmetic Encoding

Compression Ratio = 42
PSNR = 75.9537 dB

Figure 5.2.5 Compressed image with P = 30 using Arithmetic Encoding

Compression Ratio = 46
PSNR = 71.231 dB

Figure 5.2.6 Compressed image with P = 40 using Arithmetic Encoding

Compression Ratio = 49
PSNR = 67.891 dB

Figure 5.2.7 Compressed image with P = 50 using Arithmetic Encoding

Compression Ratio = 53
PSNR = 64.8412 dB

Figure 5.2.8 Compressed image with P = 60 using Arithmetic Encoding

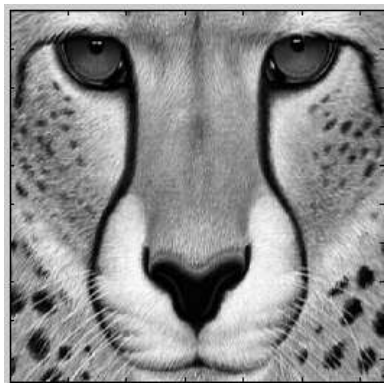

Figure 5.2.9 Original CHEETAH Image

Compression Ratio = 11
PSNR = 79.1685 dB

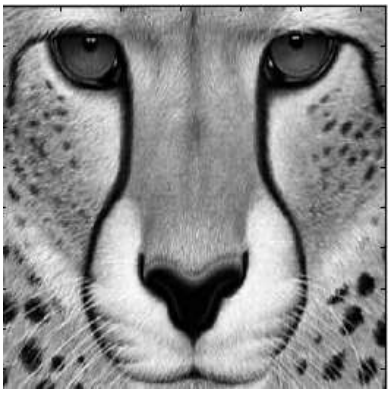

Figure 5.2.10 Compressed image with P = 5 using Arithmetic Encoding

Compression Ratio = 14
PSNR = 73.6295 dB

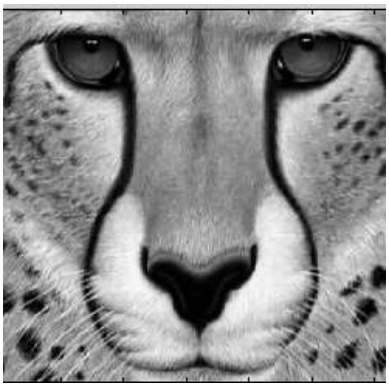

Figure 5.2.11 Compressed image with P = 10 using Arithmetic Encoding

Compression Ratio = 22
PSNR = 67.0735 dB

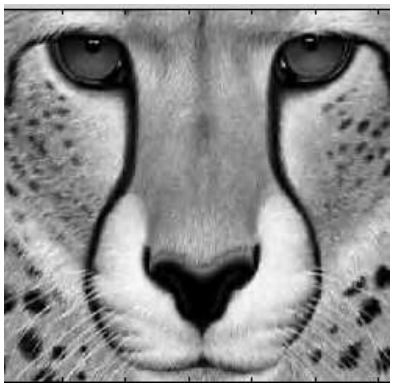

Figure 5.2.12 Compressed image with P = 20 using Arithmetic Encoding

Compression Ratio = 30
PSNR = 63.6988 dB

Figure 5.2.13 Compressed image with P = 30 using Arithmetic Encoding

Compression Ratio = 36
PSNR = 61.5553 dB

Figure 5.2.14 Compressed image with P = 40 using Arithmetic Encoding

Compression Ratio = 39
PSNR = 60.1865 dB

Figure 5.2.15 Compressed image with P = 50 using Arithmetic Encoding

Compression Ratio = 42
PSNR = 59.1732 dB

Figure 5.2.16 Compressed image with P = 60 using Arithmetic Encoding

Figure 5.2.17 Original LENA Image

Compression Ratio = 24
PSNR = 85.6561 dB

Figure 5.2.18 Compressed image with P = 5 using Arithmetic Encoding

Compression Ratio = 36
PSNR = 85.9624 dB

Figure 5.2.19 Compressed image with P =10 using Arithmetic Encoding

Compression Ratio = 48
PSNR = 79.6256 dB

Figure 5.2.20 Compressed image with P = 20 using Arithmetic Encoding

Compression Ratio = 64
PSNR = 74..8504 dB

Figure 5.2.21 Compressed image with P =30 using Arithmetic Encoding

Compression Ratio = 69
PSNR = 70.1371 dB

Figure 5.2.22 Compressed image with P = 40 using Arithmetic Encoding

Compression Ratio = 73
PSNR = 67.7423 dB

Figure 5.2.23 Compressed image with P =50 using Arithmetic Encoding

Compression Ratio = 75
PSNR = 66.7228 dB

Figure 5.2.24 Compressed image with P = 60 using Arithmetic Encoding

Figure 5.2.25 Original BARBARA Image

Compression Ratio = 7
PSNR = 71.921 dB

Figure 5.2.26 Compressed image with P = 5 using Arithmetic Encoding

Compression Ratio = 11
PSNR = 67.8158 dB

Figure 5.2.27 Compressed image with P =10 using Arithmetic Encoding

Compression Ratio = 18
PSNR = 61.49 dB

Figure 5.2.128 Compressed image with P = 20 using Arithmetic Encoding

Compression Ratio = 28
PSNR = 56.3253 dB

Figure 5.2.29 Compressed image with P =30 using Arithmetic Encoding

Compression Ratio =33
PSNR = 54.0879 dB

Figure 5.2.30 Compressed image with P = 40 using Arithmetic Encoding

Compression Ratio = 34
PSNR = 52.8408 dB

Figure 5.2.31 Compressed image with P = 50 using Arithmetic Encoding

Compression Ratio =37
PSNR = 51.9716 dB

Figure 5.2.32 Compressed image with P = 60 using Arithmetic Encoding

Figure 5.2.33 Original MANDRILL Image

Compression Ratio = 4
PSNR = 62.1245 dB

Figure 5.2.34 Compressed image with P = 5 using Arithmetic Encoding

Compression Ratio = 6
PSNR = 60.0194 dB

Figure 5.2.35 Compressed image with P =10 using Arithmetic Encoding

Compression Ratio = 7
PSNR = 56.812 dB

Figure 5.2.36 Compressed image with P = 20 using Arithmetic Encoding

Compression Ratio = 12
PSNR = 18.163 dB

Figure 5.2.37 Compressed image with P =30 using Arithmetic Encoding

Compression Ratio = 16
PSNR = 48.5085 dB

Figure 5.2.38 Compressed image with P = 40 using Arithmetic Encoding

Compression Ratio = 19
PSNR = 47.074 dB

Figure 5.2.39 Compressed image with P = 50 using Arithmetic Encoding

Compression Ratio = 21
PSNR = 46.1098 dB

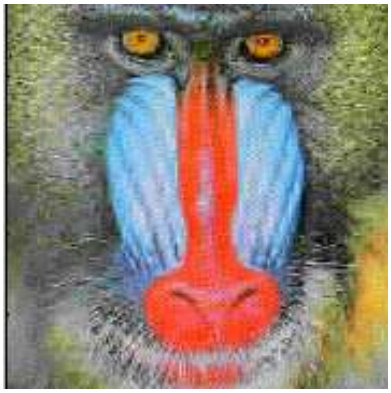

Figure 5.2.40 Compressed image with P = 60 using Arithmetic Encoding

Figure 5.2.41 Original BIRD Image

Compression Ratio = 11
PSNR = 75.417dB

Figure 5.2.42 Compressed image with P = 5 using Arithmetic Encoding

Compression Ratio = 17
PSNR = 73.004 dB

Figure 5.2.43 Compressed image with P =10 using Arithmetic Encoding

Compression Ratio = 23
PSNR = 67.4469 dB

Figure 5.2.44 Compressed image with P = 20 using Arithmetic Encoding

Compression Ratio = 31
PSNR = 65.7065 dB

Figure 5.2.45 Compressed image with P =30 using Arithmetic Encoding

Compression Ratio = 35
PSNR = 62.339 dB

Figure 5.2.46 Compressed image with P = 40 using Arithmetic Encoding

Compression Ratio = 37
PSNR = 59.9416 dB

Figure 5.2.47 Compressed image with P = 50 using Arithmetic Encoding

Compression Ratio = 39
PSNR = 57.2633 dB

Figure 5.2.48 Compressed image with P = 60 using Arithmetic Encoding

Figure 5.2.49 Original ROSE Image

Compression Ratio = 4
PSNR = 65.134 dB

Figure 5.2.50 Compressed image with P = 5 using Arithmetic Encoding

Compression Ratio = 6
PSNR = 62.7118 dB

Figure 5.2.51 Compressed image with P =10 using Arithmetic Encoding

Compression Ratio = 7
PSNR = 58.5079 dB

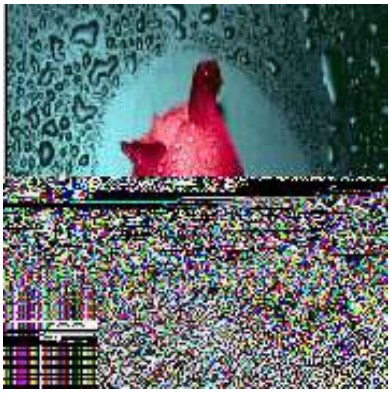

Figure 5.2.52 Compressed image with P = 20 using Arithmetic Encoding

Compression Ratio = 13
PSNR = 51.9217 dB

Figure 5.2.53 Compressed image with P =30 using Arithmetic Encoding

Compression Ratio = 16
PSNR = 49.7758 dB

Figure 5.2.54 Compressed image with P = 40 using Arithmetic Encoding

Compression Ratio = 18
PSNR = 48.3914 dB

Figure 5.2.55 Compressed image with P = 50 using Arithmetic Encoding

Compression Ratio = 20
PSNR = 46.7576 dB

Figure 5.2.56 Compressed image with P = 60 using Arithmetic Encoding

Figure 5.2.57 Original DONKEY Image

Compression Ratio = 7
PSNR = 72.2084 dB

Figure 5.2.58 Compressed image with P = 5 using Arithmetic Encoding

Compression Ratio = 9
PSNR = 69.2338 dB

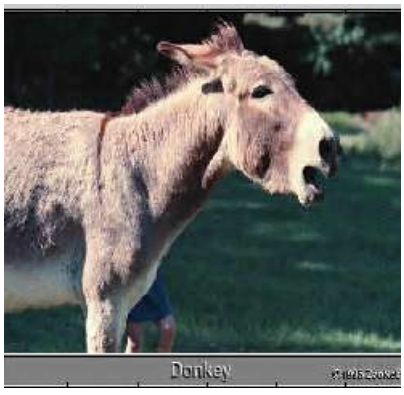

Figure 5.2.59 Compressed image with P =10 using Arithmetic Encoding

Compression Ratio =14
PSNR = 30.7286 dB

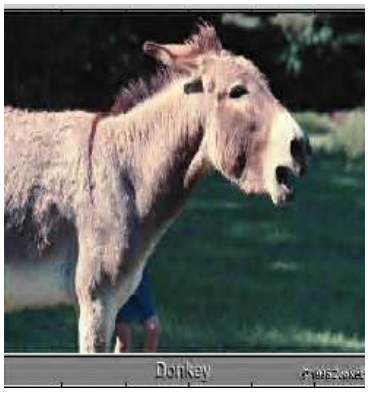

Figure 5.2.60 Compressed image with P = 20 using Arithmetic Encoding

Compression Ratio = 21
PSNR = 30.7342 dB

Figure 5.2.61 Compressed image with P =30 using Arithmetic Encoding

Compression Ratio = 26
PSNR = 54.4774 dB

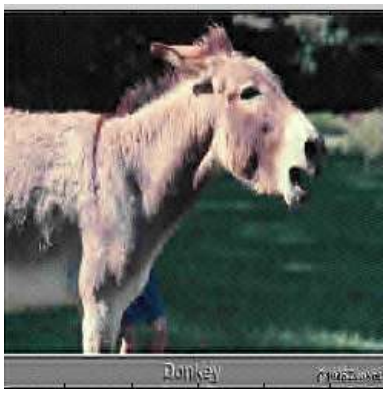

Figure 5.2.62 Compressed image with P = 40 using Arithmetic Encoding

Compression Ratio = 31
PSNR = 52.5357 dB

Figure 5.2.63 Compressed image with P = 50 using Arithmetic Encoding

Compression Ratio = 35
PSNR = 50.6168 dB

Figure 5.2.64 Compressed image with P = 60 using Arithmetic Encoding

Figure 5.2.65 Original BUTTERFLY Image

Compression Ratio = 6
PSNR = 77.4233 dB

Figure 5.2.66 Compressed image with P = 5 using Arithmetic Encoding

Compression Ratio = 9
PSNR = 68.8355 dB

Figure 5.2.67 Compressed image with P =10 using Arithmetic Encoding

Compression Ratio = 14
PSNR = 61.1711 dB

Figure 5.2.68 Compressed image with P = 20 using Arithmetic Encoding

Compression Ratio = 19
PSNR = 50.7274 dB

Figure 5.2.69 Compressed image with P =30 using Arithmetic Encoding

Compression Ratio = 23
PSNR = 48.5618 dB

Figure 5.2.70 Compressed image with P = 40 using Arithmetic Encoding

Compression Ratio = 26
PSNR = 47.5036 dB

Figure 5.2.71 Compressed image with P = 50 using Arithmetic Encoding

Compression Ratio = 30
PSNR = 46.5698 dB

Figure 5.2.72 Compressed image with P = 60 using Arithmetic Encoding

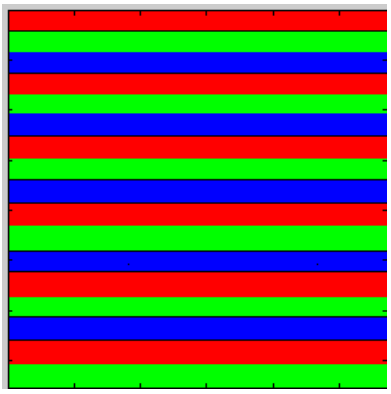

Figure 5.2.73 Original HORIZONTAL LINE Image

Compression Ratio = 6
PSNR = 60.1863dB

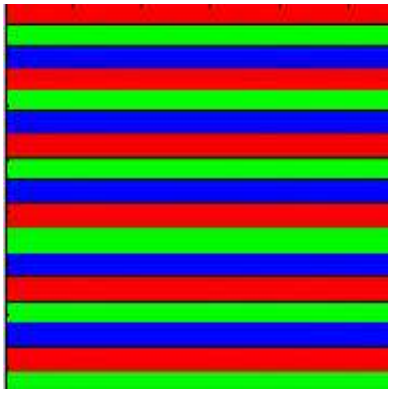

Figure 5.2.74 Compressed image with P = 5 using Arithmetic Encoding

Compression Ratio = 6
PSNR = 59.5537 dB

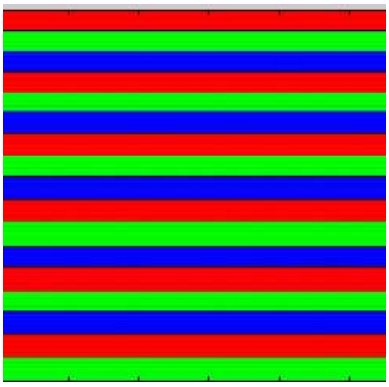

Figure 5.2.75 Compressed image with P =10 using Arithmetic Encoding

Compression Ratio = 8
PSNR = 54.9828 dB

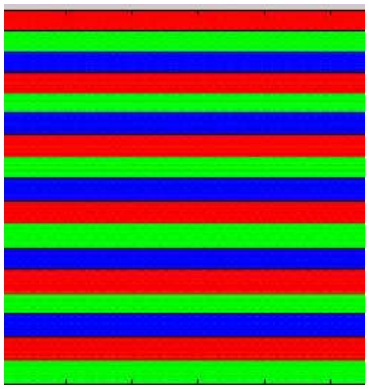

Figure 5.2.76 Compressed image with P = 20 using Arithmetic Encoding

Compression Ratio = 9
PSNR = 54.4989 dB

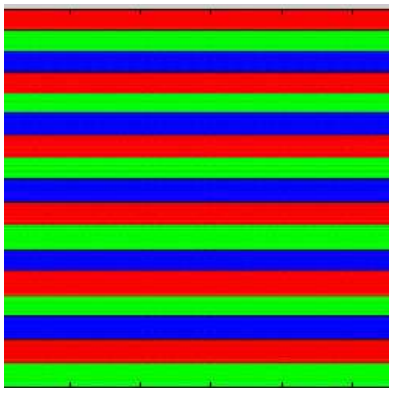

Figure 5.2.77 Compressed image with P =30 using Arithmetic Encoding

Compression Ratio = 10
PSNR = 52.1679 dB

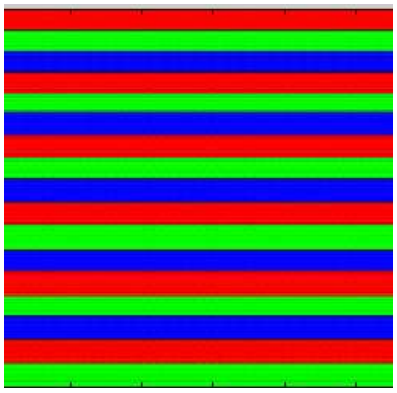

Figure 5.2.78 Compressed image with P = 40 using Arithmetic Encoding

Compression Ratio = 11
PSNR = 49.1411 dB

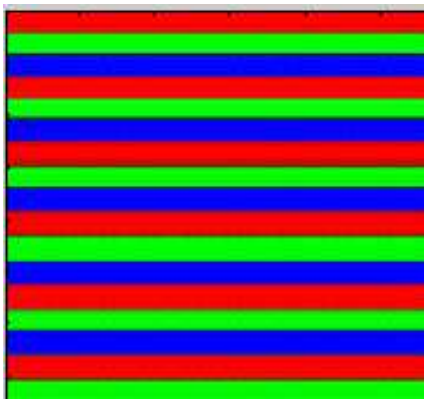

Figure 5.2. 79 Compressed image with P = 50 using Arithmetic Encoding

Compression Ratio = 12
PSNR = 47.7637 dB

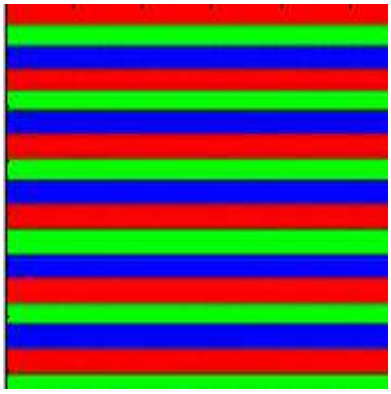

Figure 5.2.80 Compressed image with P = 60 using Arithmetic Encoding

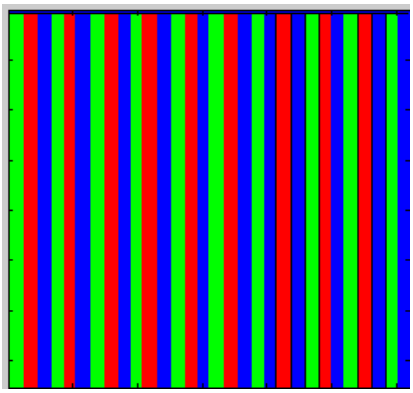

Figure 5.2.81 Original VERTICAL LINE Image

Compression Ratio = 14
PSNR = 77.3835 dB

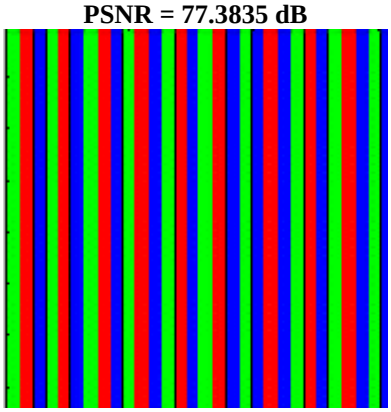

Figure 5.2.82 Compressed image with P = 5 using Arithmetic Encoding

Compression Ratio = 25
PSNR = 12.6192 dB

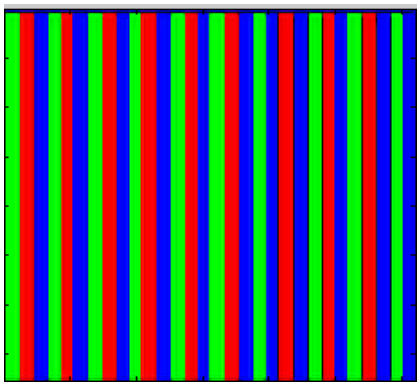

Figure 5.2.83 Compressed image with P =10 using Arithmetic Encoding

Compression Ratio = 25
PSNR = 19.88 dB

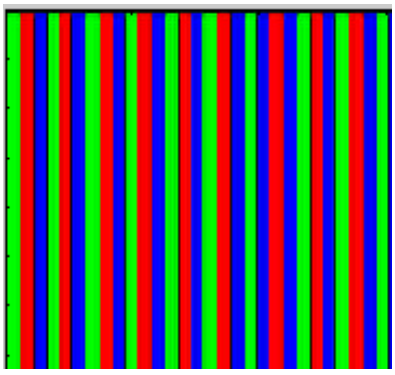

Figure 5.2.84 Compressed image with P = 20 using Arithmetic Encoding

Compression Ratio = 30
PSNR = 57.2394 dB

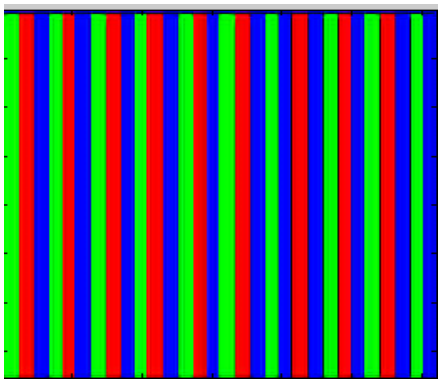

Figure 5.2.85 Compressed image with P =30 using Arithmetic Encoding

Compression Ratio =36
PSNR = 53.849 dB

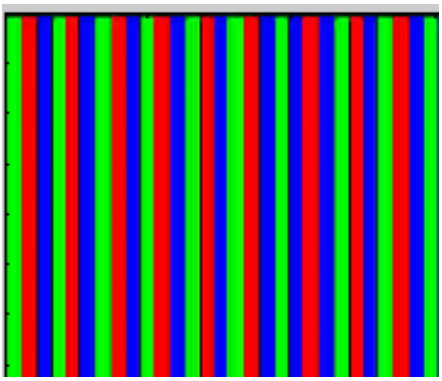

Figure 5.2.86 Compressed image with P = 40 using Arithmetic Encoding

Compression Ratio = 41
PSNR = 51.2781 dB

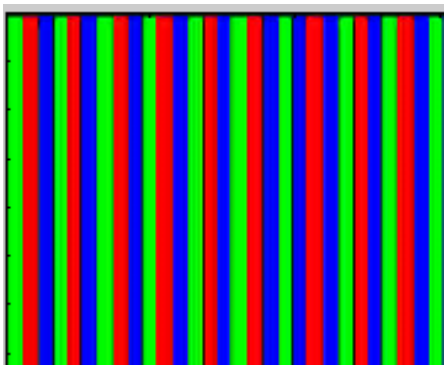

Figure 5.2.87 Compressed image with P = 50 using Arithmetic Encoding

Compression Ratio = 46
PSNR = 49.5102 dB

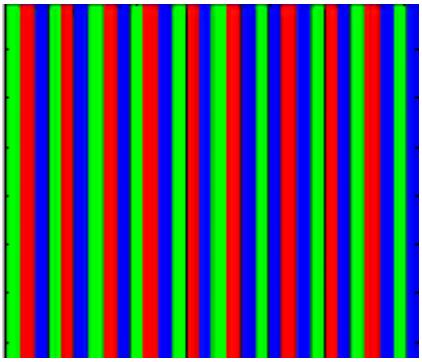

Figure 5.2.88 Compressed image with P = 60 using Arithmetic Encoding

The original image and resultant compressed images of presented algorithm using Huffman encoding for different values of P are shown in figure 5.2.89 to 5.2.176.

Figure 5.2.89 Original image AISHWARYA

Compression Ratio =17
PSNR = 80.0646 dB

Figure 5.2.90 Compressed image with P = 5 using Huffman Encoding

Compression Ratio = 24
PSNR = 84.2313 dB

Figure 5.2.91 Compressed image with P = 10 using Huffman Encoding

Compression Ratio = 31
PSNR = 78.9871 dB

Figure 5.2.92 Compressed image with P = 20 using Huffman Encoding

Compression Ratio = 40
PSNR = 75.9537 dB

Figure 5.2.93 Compressed image with P = 30 using Huffman Encoding

Compression Ratio = 46
PSNR = 71.231 dB

Figure 5.2.94 Compressed image with P = 40 using Huffman Encoding

Compression Ratio = 47
PSNR = 67.9816 dB

Figure 5.2.95 Compressed image with P = 50 using Huffman Encoding

Compression Ratio = 50
PSNR = 64.8412 dB

Figure 5.2.96 Compressed image with P = 60 using Huffman Encoding

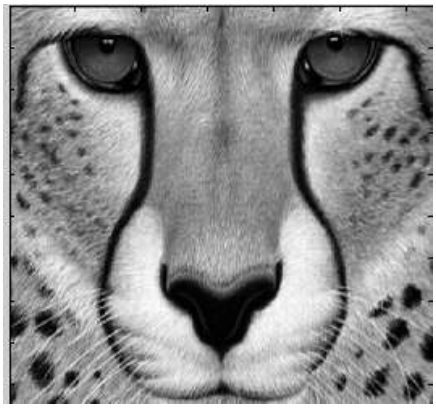

Figure 5.2.97 Original CHEETAH Image

Compression Ratio = 9
PSNR = 79.1685 dB

Figure 5.2.98 Compressed image with P = 5 using Huffman Encoding

Compression Ratio = 12
PSNR = 73.6295 dB

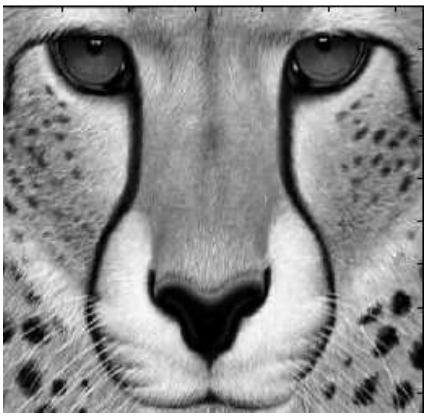

Figure 5.2.99 Compressed image with P = 10 using Huffman Encoding

Compression Ratio = 19
PSNR = 67.0735 dB

Figure 5.2.100 Compressed image with P = 20 using Huffman Encoding

Compression Ratio = 28
PSNR = 63.6988 dB

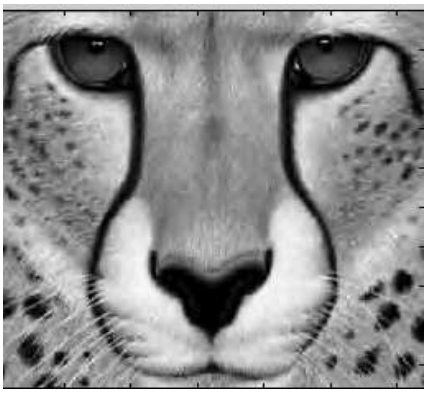

Figure 5.2.101 Compressed image with P = 30 using Huffman Encoding

Compression Ratio = 34
PSNR = 61.5553 dB

Figure 5.2.102 Compressed image with P = 40 using Huffman Encoding

Compression Ratio = 37
PSNR = 60.1865 dB

Figure 5.2.103 Compressed image with P = 50 using Huffman Encoding

Compression Ratio =39
PSNR = 59.1732 dB

Figure 5.2.104 Compressed image with P = 60 using Huffman Encoding

Figure 5.2.105 Original LENA Image

Compression Ratio =20
PSNR = 85.6561 dB

Figure 5.2.106 Compressed image with P = 5 using Huffman Encoding

Compression Ratio = 30
PSNR = 85.9624 dB

Figure 5.2.107 Compressed image with P =10 using Huffman Encoding

Compression Ratio = 41
PSNR = 79.6256 dB

Figure 5.2.108 Compressed image with P = 20 using Huffman Encoding

Compression Ratio = 56
PSNR = 74.8504 dB

Figure 5.2.109 Compressed image with P =30 using Huffman Encoding

Compression Ratio = 61
PSNR = 70.1371 dB

Figure 5.2.110 Compressed image with P = 40 using Huffman Encoding

Compression Ratio = 64
PSNR = 67.7423 dB

Figure 5.2.111 Compressed image with P =50 using Huffman Encoding

Compression Ratio = 67
PSNR = 66.7228 dB

Figure 5.2.112 Compressed image with P = 60 using Huffman Encoding

Figure 5.2.113 Original BARBARA Image

Compression Ratio = 6
PSNR = 71.921 dB

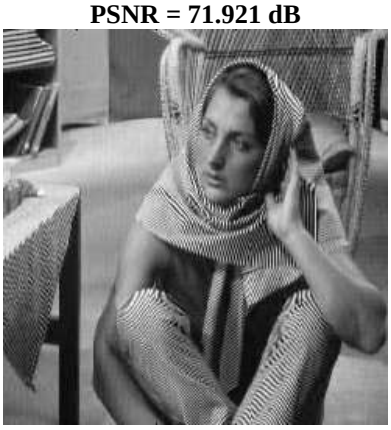

Figure 5.2.114 Compressed image with P = 5 using Huffman Encoding

Compression Ratio = 9
PSNR = 67.8158 dB

Figure 5.2.115 Compressed image with P =10 using Huffman Encoding

Compression Ratio = 16
PSNR = 61.49 dB

Figure 5.2.116 Compressed image with P = 20 using Huffman Encoding

Compression Ratio = 23
PSNR = 56.3253 dB

Figure 5.2.117 Compressed image with P =30 using Huffman Encoding

Compression Ratio = 27
PSNR = 54.0879 dB

Figure 5.2.118 Compressed image with P = 40 using Huffman Encoding

Compression Ratio = 31
PSNR = 52.8408 dB

Figure 5.2.119 Compressed image with P = 50 using Huffman Encoding

Compression Ratio = 34
PSNR = 51.9716 dB

Figure 5.2.120 Compressed image with P = 60 using Huffman Encoding

Figure 5.2.121 Original MANDRILL Image

Compression Ratio = 4
PSNR = 62.1295 dB

Figure 5.2.122 Compressed image with P = 5 using Huffman Encoding

Compression Ratio = 5
PSNR = 60.0194 dB

Figure 5.2.123 Compressed image with P =10 using Huffman Encoding

Compression Ratio = 6
PSNR = 56.812 dB

Figure 5.2.124 Compressed image with P = 20 using Huffman Encoding

Compression Ratio = 10
PSNR = 51.9118 dB

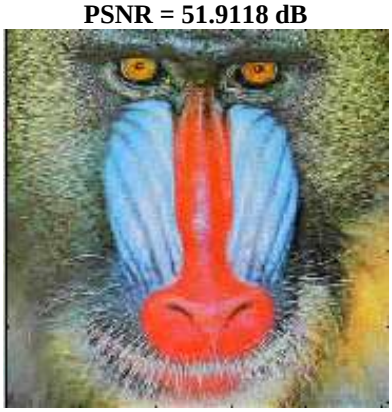

Figure 5.2.125 Compressed image with P =30 using Huffman Encoding

Compression Ratio = 14
PSNR = 48.5085 dB

Figure 5.2.126 Compressed image with P = 40 using Huffman Encoding

Compression Ratio = 16
PSNR = 47.074 dB

Figure 5.2.127 Compressed image with P = 50 using Huffman Encoding

Compression Ratio =19
PSNR = 46.1098 dB

Figure 5.2.128 Compressed image with P = 60 using Huffman Encoding

Figure 5.2.129 Original BIRD Image

Compression Ratio = 9
PSNR = 75.417 dB

Figure 5.2.130 Compressed image with P = 5 using Huffman Encoding

Compression Ratio = 15
PSNR = 73.7004 dB

Figure 5.2.131 Compressed image with P =10 using Huffman Encoding

Compression Ratio = 21
PSNR = 67.4469 dB

Figure 5.2.132 Compressed image with P = 20 using Huffman Encoding

Compression Ratio = 29
PSNR = 65.7065 dB

Figure 5.2.133 Compressed image with P =30 using Huffman Encoding

Compression Ratio = 32
PSNR = 62.339 dB

Figure 5.2.134 Compressed image with P = 40 using Huffman Encoding

Compression Ratio = 34
PSNR = 59.9416 dB

Figure 5.2.135 Compressed image with P = 50 using Huffman Encoding

Compression Ratio =35
PSNR = 57.2633 dB

Figure 5.2.136 Compressed image with P = 60 using Huffman Encoding

Figure 5.2.137 Original ROSE Image

Compression Ratio = 4
PSNR = 65.134 dB

Figure 5.2.138 Compressed image with P = 5 using Huffman Encoding

Compression Ratio = 5
PSNR = 62.7118 dB

Figure 5.2.139 Compressed image with P =10 using Huffman Encoding

Compression Ratio = 6
PSNR = 58.5079 dB

Figure 5.2.140 Compressed image with P = 20 using Huffman Encoding

Compression Ratio = 11
PSNR = 51.9217 dB

Figure 5.2.141 Compressed image with P =30 using Huffman Encoding

Compression Ratio = 14
PSNR = 49.7758 dB

Figure 5.2.142 Compressed image with P = 40 using Huffman Encoding

Compression Ratio = 16
PSNR = 48.3914 dB

Figure 5.2.143 Compressed image with P = 50 using Huffman Encoding

Compression Ratio = 18
PSNR = 46.7576 dB

Figure 5.2.144 Compressed image with P = 60 using Huffman Encoding

Figure 5.2.145 Original DONKEY Image

Compression Ratio = 6
PSNR = 72.2084 dB

Figure 5.2.146 Compressed image with P = 5 using Huffman Encoding

Compression Ratio = 8
PSNR = 69.2338 dB

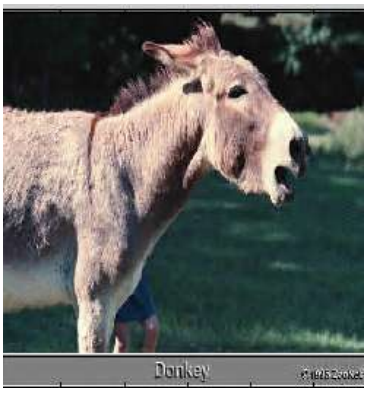

Figure 5.2.147 Compressed image with P =10 using Huffman Encoding

Compression Ratio = 13
PSNR = 63.4845 dB

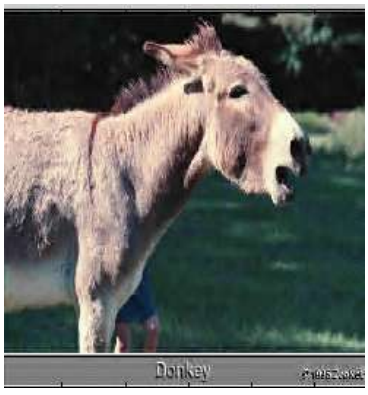

Figure 5.2.148 Compressed image with P = 20 using Huffman Encoding

Compression Ratio = 19
PSNR = 58.5874 dB

Figure 5.2.149 Compressed image with P =30 using Huffman Encoding

Compression Ratio = 24
PSNR = 54.4774 dB

Figure 5.2.150 Compressed image with P = 40 using Huffman Encoding

Compression Ratio = 28
PSNR = 52.5357 dB

Figure 5.2.151 Compressed image with P = 50 using Huffman Encoding

Compression Ratio =35
PSNR = 50.6168 dB

Figure 5.2.152 Compressed image with P = 60 using Huffman Encoding

Figure 5.2.153 Original BUTTERFLY Image

Compression Ratio = 5
PSNR = 77.4233 dB

Figure 5.2.154 Compressed image with P = 5 using Huffman Encoding

Compression Ratio = 7
PSNR = 68.8355 dB

Figure 5.2.155 Compressed image with P =10 using Huffman Encoding

Compression Ratio =11
PSNR = 61.1711 dB

Figure 5.2.156 Compressed image with P = 20 using Huffman Encoding

Compression Ratio = 32
PSNR = 62.339 dB

Figure 5.2.157 Compressed image with P =30 using Huffman Encoding

Compression Ratio = 20
PSNR = 48.5618 dB

Figure 5.2.158 Compressed image with P = 40 using Huffman Encoding

Compression Ratio = 23
PSNR = 47.5036 dB

Figure 5.2.159 Compressed image with P = 50 using Huffman Encoding

Compression Ratio = 26
PSNR = 46.5698 dB

Figure 5.2.160 Compressed image with P = 60 using Huffman Encoding

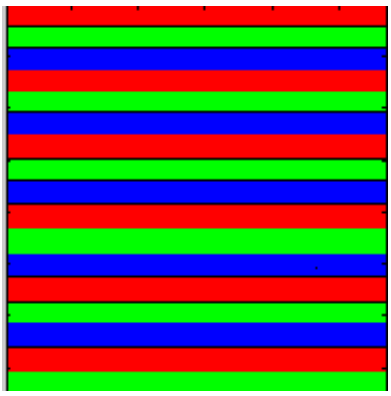

Figure 5.2.161 Original HORIZONTAL LINE Image

Compression Ratio = 4
PSNR = 60.1883 dB

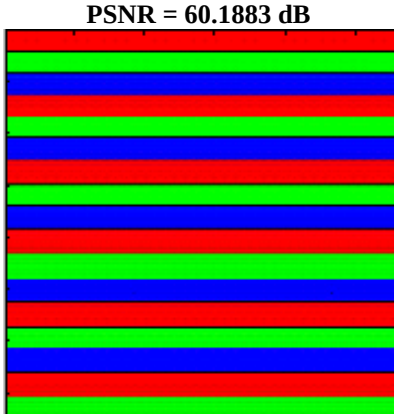

Figure 5.2.162 Compressed image with P = 5 using Huffman Encoding

Compression Ratio = 5
PSNR = 59.5537 dB

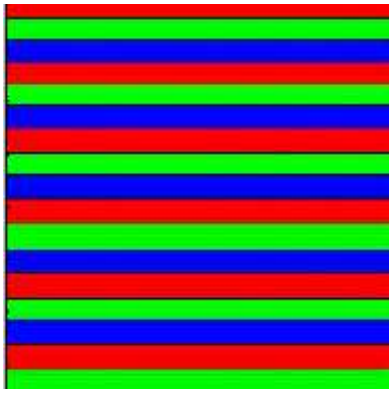

Figure 5.2.163 Compressed image with P =10 using Huffman Encoding

Compression Ratio = 6
PSNR = 54.9828 dB

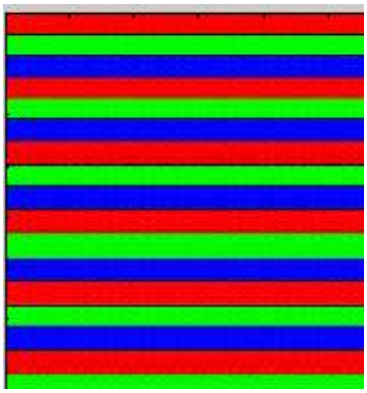

Figure 5.2.164 Compressed image with P = 20 using Huffman Encoding

Compression Ratio = 6
PSNR = 54.4989 dB

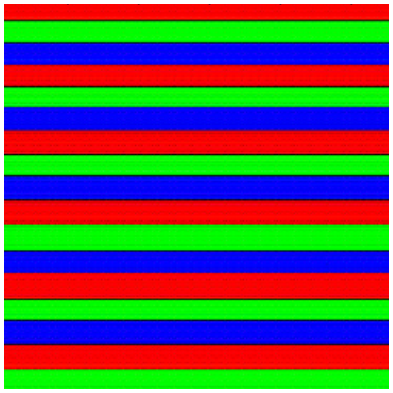

Figure 5.2.165 Compressed image with P =30 using Huffman Encoding

Compression Ratio = 7
PSNR = 52.1679 dB

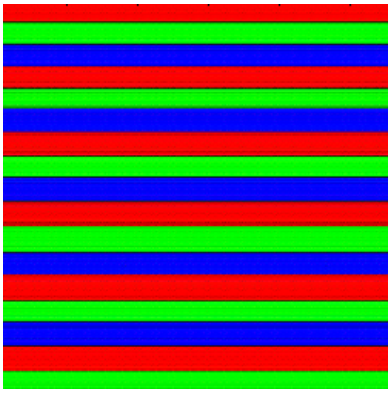

Figure 5.2.166 Compressed image with P = 40 using Huffman Encoding

Compression Ratio = 8
PSNR = 49.1411 dB

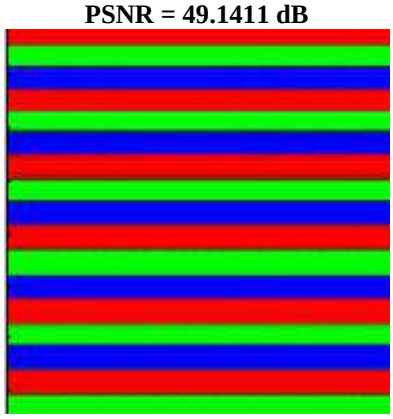

Figure 5.2.167 Compressed image with P = 50 using Huffman Encoding

Compression Ratio = 10
PSNR = 47.7637 dB

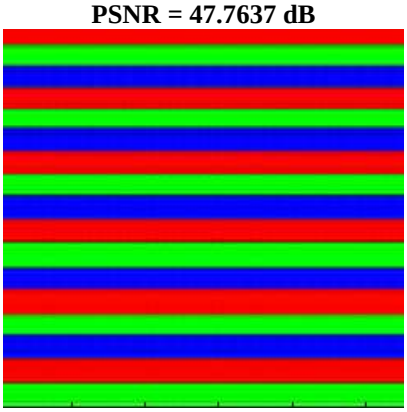

Figure 5.2.168 Compressed image with P = 60 using Huffman Encoding

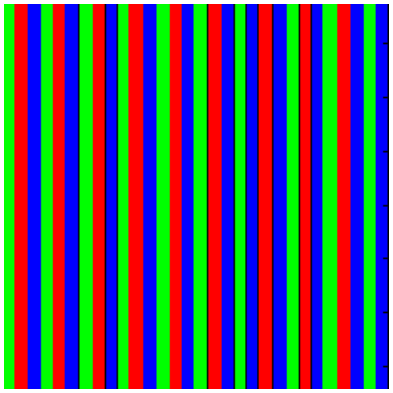

Figure 5.2.169 Original VERTICAL LINE Image

Compression Ratio = 12
PSNR = 77.3835 dB

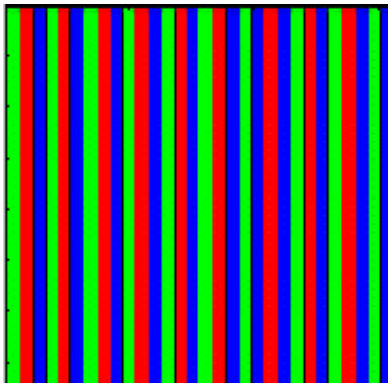

Figure 5.2.170 Compressed image with P = 5 using Huffman Encoding

Compression Ratio = 16
PSNR = 67.2358 dB

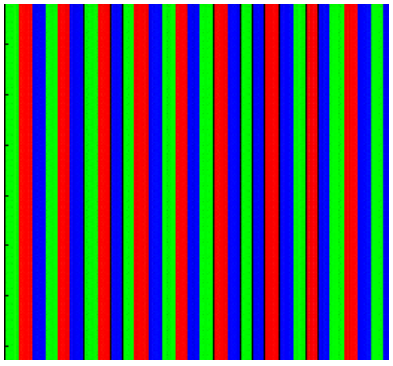

Figure 5.2.171 Compressed image with P =10 using Huffman Encoding

Compression Ratio = 22
PSNR = 62.2183 dB

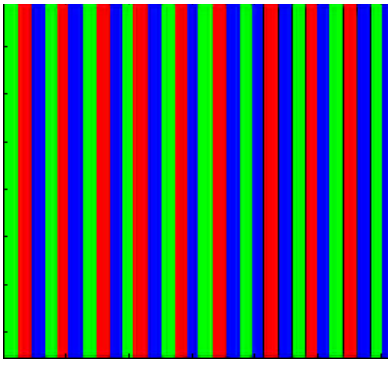

Figure 5.2.172 Compressed image with P = 20 using Huffman Encoding

Compression Ratio = 27
PSNR = 57.2394 dB

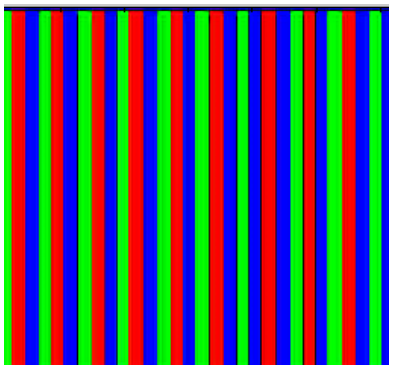

Figure 5.2.173 Compressed image with P =30 using Huffman Encoding

Compression Ratio = 32
PSNR = 53.849 dB

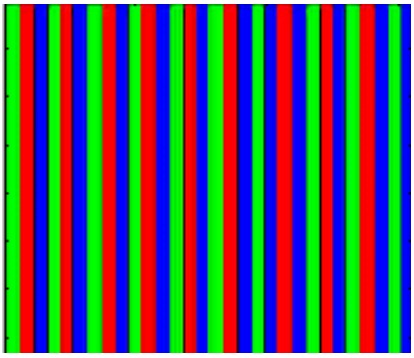

Figure 5.2.174 Compressed image with P = 40 using Huffman Encoding

Compression Ratio = 37
PSNR = 51.2781 dB

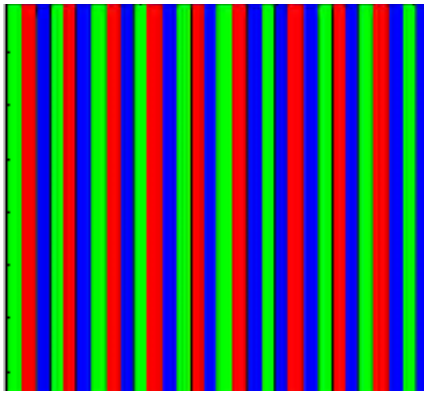

Figure 5.2.175 Compressed image with P = 50 using Huffman Encoding

Compression Ratio =42
PSNR = 49.5102 dB

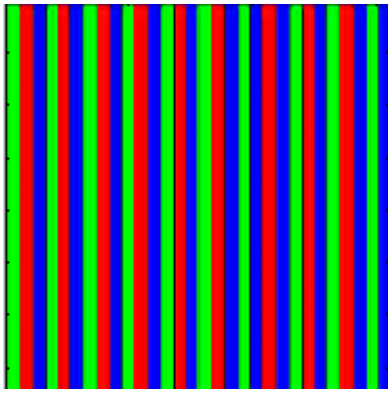

Figure 5.2.176 Compressed image with P = 60 using Huffman Encoding

The resultant compressed images of standard JPEG-2000 application are figure 5.2.177 to 5.2.187.

Compression Ratio = 4.1712
PSNR = 191.6040 dB

Figure 5.2.177 Compressed image of Aishwarya using JPEG-2000

Compression Ratio = 6.1292
PSNR = 241.2325 dB

Figure 5.2.178 Compressed image of Cheetah using JPEG-2000

Compression Ratio = 10.6
PSNR = 170.5337 dB

Figure 5.2.179 Compressed image of Lena using JPEG-2000

Compression Ratio = 4.9675
PSNR = 153.3857 dB

Figure 5.2.180 Compressed image of Barbara using JPEG-2000

Compression Ratio = 2.2551
PSNR = 185.8936 dB

Figure 5.2.181 Compressed image of Mandrill using JPEG-2000

Compression Ratio = 2.6578
PSNR = 200.7146 dB

Figure 5.2.182 Compressed image of Bird using JPEG-2000

Compression Ratio = 2.2412
PSNR = 186.2608 dB

Figure 5.2.183 Compressed image of Rose using JPEG-2000

Compression Ratio = 3.1463
PSNR = 191.3145 dB

Figure 5.2.184 Compressed image of Donkey using JPEG-2000

Compression Ratio = 3.5648
PSNR = 197.1621 dB

Figure 5.2.185 Compressed image of Butterfly using JPEG-2000

Compression Ratio = 35.1111
PSNR =192.9029 dB

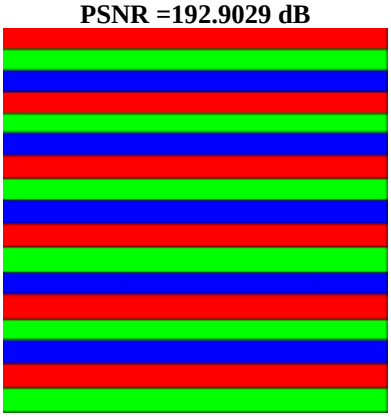

Figure 5.2.186 Compressed image of Horizontal using JPEG-2000

Compression Ratio = 180.263
PSNR = 238.4996 dB

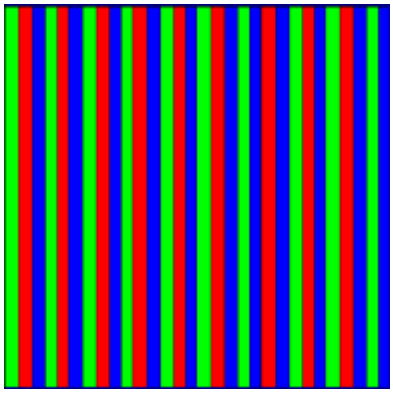

Figure 5.2.187 Compressed image of Vertical using JPEG-2000

CHAPTER 6
CONCLUSION

6.1.0 INTRODUCTION

The basic aim of the researcher is to optimize the compression ratio by retaining the quality of the resultant image. It is possible to use the optimization techniques at each of the stages of the compression. The work aims at optimizing all these stages of the compression method, and every stage of optimization is discussed in previous chapters and conclusions are elaborated.

In the research work the different algorithms are implemented and tested over the natural and synthetic images, and results are given. Based on the work the following concluding remarks are drawn.

6.1.1 SELECTION OF WAVELET

It is observed that the choice of mother wavelet used in the transformation depends on nature of the image. Haar wavelets, which are also known as db_1, give good results for synthetic images, and db_3, db_4, db_5, db_6 give good results for natural images. It is also observed that larger number of taps does not imply better peak signal to noise ratio and visual quality but the computational complexity is more in that case. A major disadvantage of Daubechies and Coiflet wavelets is their asymmetry, which can cause artifacts at borders of the wavelet sub-bands. Haar wavelet is the only wavelet, which is orthogonal, compactly supported and symmetric. For good visual quality, and more compression ratio, wavelet must support symmetry and compact properties. If both symmetry and compact support is required in wavelets, then one should relax the orthogonality condition and allow non-orthogonal wavelet functions. Bi-orthogonal wavelets are compactly supported and symmetric. It is observed that percentage of zeros in Bi-orthogonal wavelet is less by the amount of one to two percent as compared to the Daubechies wavelet. But the symmetry property present in Bi-orthogonal wavelets is responsible for good visual quality of an image. From comparative study of different wavelets, in still image compression techniques, it is concluded that the final choice of optimal wavelet depends on the subjective and objective image quality measures, and computational complexity. It is shown that the best of the known wavelets is Bior2.2 wavelet. It provides the best visual

image quality for different image contents with comparable percentage of zeros and it has low computational complexity.

6.1.2 WAVELET PACKETS

It is observed that for most of natural images, the percentage of zeros of wavelet packets is more than wavelet, by 0.0437 to 2.6366 percent. This change is significant for the high frequency images and insignificant for low frequency images. For the synthetic images, percentage of zeros is less by 0.003 to 1.2372. There is a negligible change in peak signal to noise ratio. The wavelet packets tree preserves the high frequency components, those are lost in wavelet decomposition, and therefore, researcher strongly recommends the wavelet packets decomposition for image compression, even though the changes in percentage of zeros is not significant in few natural and synthetic images[110].

6.1.3 SELCTION OF BEST BASIS

In wavelet packets tree, number of sub-bands are more, for J level decomposition the number of sub-bands are 4^J, and hence it takes more time for the decomposition. To reduce the time complexity of wavelet packets decomposition, there is a need to select the sub-bands, which include significant information in compact form. The Threshold entropy, Log entropy and Shannon entropy are used as the cost functions to select the best basis. In an efficient image compression process, it is desired that the time complexity should be minimum, and the developed algorithm should not be human dependant. For example in an algorithm of selection of best basis based on Threshold entropy, the human interaction is required for selection of threshold value. As a threshold value changes the structure of a tree also changes, and there is no assurance of visual quality of an image, the important information may be lost in the process [113]. Hence even though the selection of best basis based on Threshold entropy method is simple with less time complexity, it cannot be preferred because of its human dependency. The wavelet packets best tree based on Log entropy and wavelet packets best tree based on Shannon entropy, do not have human dependency, but their time complexity is more [112,110]. Researcher strongly recommends, the wavelet packets best tree based on energy contain. In proposed method there is no human dependency, and its time complexity is also less. It is observed that for most of natural images, percentage of zeros of proposed method is more than percentage of zeros of wavelet packets best tree based on threshold entropy and wavelet packets best tree

based on log entropy by 0.0418 to 1.4332 percent and 0.0898 to 3.6417 with good visual quality. The percentage of zeros of proposed method is same as percentage of zeros of wavelet packets best tree based on Shannon entropy. By considering time complexity, human dependency, peak signal to noise ratio and percentage of zeros, researcher strongly recommends the wavelet packets best tree based on energy contain [111].

6.1.4 THRESHOLD

The high compression ratio is achieved by using the thresholding to the wavelet packets coefficients. The advantages of wavelet packets can be gained by proper selection of thresholds. In image compression the selection of threshold plays the crucial role. In the proposed algorithm threshold is adaptive, and the adaptive threshold is calculated on the basis of nature of the image. The statistical properties of the sub-images of different orientations are usually different, and thus different thresholds should be adaptive to each sub-image. The threshold is calculated for each resolution and orientation, taking into account the different statistical properties of each sub-image, in order to prevent the major structures from being smoothened.

For high value of threshold, most of the coefficients are zero, and it results in high compression, but visual quality of image is poor, and the peak signal to noise ratio is very low. For low value of threshold the visual quality of signal is good, peak signal to noise ratio is high, but compression ratio is low. The basic aim of the research is to improve the compression ratio with maintaining the quality of image, by exploiting the advantages of wavelet packets tree. For fixed global threshold the result is good for one image but for same value of threshold the result for other images may be poor. Therefore selection of threshold is important in image compression.

To obtain good visual quality of the image, human perception is main factor to select the threshold. Human eye is less sensitive to high frequency signal and more sensitive to low frequency signal. Hence most of the researchers suggest the low value of threshold for high frequency spectrum and high value of threshold for low frequency spectrum. But these thresholds can work well, if image has maximum low frequency components, and less value of high frequency components. The result for the image, which includes more high frequency spectrum distributed all over the image, is poor. The goal to select variable threshold is to achieve the good visual picture quality at low bit rate. In

order to benefit from variable threshold, proper model for determining the threshold, based on perceptual value of the human eye must be employed.

Thus the technique of evaluating adaptive threshold is recommended, which is based on mother wavelet, energy concentrated in sub-bands, and level of decomposition. The algorithm is developed, implemented, and tested over the natural and synthetic images [109]. In algorithm the variable P is used to provide the flexibility to the user in terms of visual quality, and compression ratio. By considering the constraints of human visual system, the value of P chosen for higher-level decomposition is more and is lower for low-level decomposition.

The human visual system is more sensitive to low frequency components, and less sensitive to high frequency components. Therefore for high frequency sub-bands the threshold value should be more to neglect the high frequency components. But it is observed that if the energy contain of high frequency component is low in a sub-band, then the above observation holds true. But if the energy of high frequency component in a sub-band is more, then one cannot neglect the high frequency components. And hence in threshold calculation researcher has considered the energy contain of a sub-band and the median of the sub-band. To conclude, the recommended threshold is adaptive, which is based on nature of the image, and type of wavelet used. The threshold is calculated for the Y, Cr and Cb of color images separately for different value of P and it is observed that as a value of P increases, the value of thresholds decrease. For example for the image Mandrill, the value of threshold of Y component, for the value of P = 10, changes from 1.6730 to 169.2168, for the value of P = 20, it changes from 14.0137 to 239.2168.

6.1.5 ENCODING

After the process of thresholding, most of the components are adjusted to zero values, and encoder further compresses the coefficients of wavelet packets tree to give better overall compression. An encoding process removes the redundancies in the form of repetitive bit patterns in the output of thresholding. The most commonly used entropy encoders are Huffman encoder, and Arithmetic encoder, and simple Run-Length Encoder. The researcher suggests the modified technique for the encoding. After the thresholding, repetitions of the coefficients of a wavelet packets tree can be a eliminated by using suggested ***enhanced Run-Length Encoding,*** and then for the bit coding well known Huffman coding or Arithmetic coding methods are used.

In simple RLE, some data sets can be highly compressed, whereas other data sets can actually grow larger due to the encoding. This problem of an existing run-length encoding technique is eliminated up to the certain extent by using ***enhanced Run-Length Encoding*** technique. Although this method overcomes the problem of RLE, it introduces little error that is not much noticeable. As the flexibility is already extended to the user about required quality of resultant image verses compression ratio by selecting the value of P, the effect of error introduced by ***enhanced RLE*** technique is compensated and hence, the enhanced RLE technique is strongly recommended.

6.2.0 CONCLUDING REMARKS

The final algorithm of image compression using wavelet packet best tree based on energy contain with adaptive threshold and enhanced RLE is implemented, and tested over the set of natural and synthetic images and concluding remarks based on results are discussed.

Aishwarya is widely used natural image, which does not contain large amount of high frequency or oscillating patterns. It is 24-bit RGB colored bitmap image. The original size of the image is 640×480 (file size is 900KB). The result shows that the arithmetic encoding gives better performance than Huffman encoding for the proposed algorithm. The proposed compression algorithm using arithmetic encoding gives compression ratio in the range of 19:1 to 53:1, and for Huffman encoding from 17:1 to 50:1, as the value of P changes from 5 to 60. The peak signal to noise ratio varies from 80.0646 dB to 64.8412 dB.

Cheetah is widely used natural image, which has maximum low frequency components and few high frequency components. It is 24-bit RGB bitmap image. The original size of the image is 640×480 (file size is 900KB). The result shows that the arithmetic encoding gives the better performance than Huffman encoding for the proposed algorithm. The proposed compression algorithm using arithmetic encoding gives compression ratio in the range of 11:1 to 42:1, and for Huffman encoding from 9:1 to 39:1, as the value of P changes from 5 to 60. The peak signal to noise ratio varies from 79.1685 dB to 59.1732 dB.

Lena is widely used natural image, which has maximum low frequency components and few high frequency components. It is 24-bit RGB bitmap image. It contains the maximum value for luminance (Y) and negligible values of Cr and Cb in YCrCb color model, and hence it is observed that the compression ratio is high as compared to the other

colored images. The original size of the image is 640×480 (file size is 900KB). The result shows that the arithmetic encoding gives the better performance than Huffman encoding for the proposed algorithm. The proposed compression algorithm using arithmetic encoding gives compression ratio in the range of 24:1 to 75:1, and for Huffman encoding from 20:1 to 67:1, as the value of P changes from 5 to 60. The peak signal to noise ratio varies from 85.6561 dB to 66.7228 dB.

Barbara is popular choice from the class of natural test images that exhibits large amount of high frequency and oscillating patterns. It is 24-bit RGB bitmap image. The original size of the image is 501×511 (file size is 764 KB). The result shows that the arithmetic encoding gives the better performance than Huffman encoding for the proposed algorithm. The proposed compression algorithm using arithmetic encoding gives compression ratio in the range of 7:1 to 37:1, and for Huffman encoding from 6:1 to 34:1, as the value of P changes from 5 to 60. The peak signal to noise ratio varies from 71.921 dB to 51.9716 dB.

Mandrill image is another image that is quite difficult to compress significantly. The texture of the Mandrill image has a large amount of high frequency contents, and spread over most of the image. It is 24-bit colored RGB bitmap image. The original size of the image is 512×512 (file size is 768 KB). The result shows that the arithmetic encoding gives the better performance than Huffman encoding for the proposed algorithm. The proposed compression algorithm using arithmetic encoding gives compression ratio in the range of 4:1 to 21:1, and for Huffman encoding from 4:1 to 19:1, as the value of P changes from 5 to 60. The peak signal to noise ratio varies from 62.1245 dB to 46.1098 dB.

Bird is another natural image, which has very bright colors. It is 24-bit RGB colored bitmap image. The original size of the image is 640×480 (file size is 900KB). The result shows that the arithmetic encoding gives the better performance than Huffman encoding for the proposed algorithm. The proposed compression algorithm using arithmetic encoding gives compression ratio in the range of 11:1 to 39:1, and for Huffman encoding from 9:1 to 35:1, as the value of P changes from 5 to 60. The peak signal to noise ratio varies from 75.417 dB to 57.2633 dB.

Rose is another natural image, which has maximum red and green basic colors, and surrounded by water drops textures. It is 24-bit RGB colored bitmap image. The original size of the image is 640×480 (file size is 900KB). The result shows that the arithmetic encoding gives the better performance than Huffman encoding for the proposed algorithm.

The proposed compression algorithm using arithmetic encoding gives compression ratio in the range of 4:1 to 20:1, and for Huffman encoding from 4:1 to 18:1, as the value of P changes from 5 to 60. The peak signal to noise ratio varies from 65.134 dB to 46.7576 dB.

Donkey is another natural image, which is mainly a smooth image with slight oscillating pattern observed at the fur on the neck. It is 24-bit RGB colored bitmap image. The original size of the image is 600×440 (file size is 773KB). The result shows that the arithmetic encoding gives the better performance than Huffman encoding for the proposed algorithm. The proposed compression algorithm using arithmetic encoding gives compression ratio in the range of 7:1 to 35:1, and for Huffman encoding from 6:1 to 35:1, as the value of P changes from 5 to 60. The peak signal to noise ratio varies from 72.2084 dB to 50.6168 dB.

Butterfly is synthetic image, which has prominent color patches distributed all over the image. It is 24-bit RGB colored bitmap image. The original size of the image is 452×290 (file size is 384KB). The result shows that the arithmetic encoding gives the better performance than Huffman encoding for the proposed algorithm. The proposed compression algorithm using arithmetic encoding gives compression ratio in the range of 6:1 to 30:1, and for Huffman encoding from 5:1 to 26:1, as the value of P changes from 5 to 60. The peak signal to noise ratio varies from 77.4233 dB to 46.5698 dB.

Horizontal is synthetic image, which has colored horizontal geometric bars with alternating red, green and blue colors, constructed using paint applications. It is 24-bit RGB colored bitmap image. The original size of the image is 571×377 (file size is 631KB). The result shows that the arithmetic encoding gives the better performance than Huffman encoding for the proposed algorithm. The proposed compression algorithm using arithmetic encoding gives compression ratio in the range of 6:1 to 12:1, and for Huffman encoding from 4:1 to 10:1, as the value of P changes from 5 to 60. The peak signal to noise ratio varies from 76.2735 dB to 47.7637 dB.

Vertical is synthetic image, which has colored vertical geometric bars with alternating green, red, and blue colors, constructed using paint applications. It is 24-bit RGB colored bitmap image. The original size of the image is 620×377 (file size is 684KB). The result shows that the arithmetic encoding gives the better performance than Huffman encoding for the proposed algorithm. The proposed compression algorithm using arithmetic encoding gives compression ratio in the range of 14:1 to 46:1, and for Huffman encoding

from 12:1 to 42:1, as the value of P changes from 5 to 60. The peak signal to noise ratio varies from 77.3835 dB to 49.5102 dB.

- The results show that the compression ratio is good for low frequency (smooth) images, and it is observed that it is very high for gray images. For high frequency images such as Mandrill, Barbara, the compression ratio is good, and the quality of the images is also retained. These results are compared with JPEG-2000 application, and it is found that the results obtained by using the proposed algorithm are better.
- The results are taken only for limited values of P in the range of 5 to 60 only; it is possible for few images that the value of P may be taken more than 60 or less than 5 with comparable results.
- The results obtained using implemented algorithm with arithmetic encoding, and Huffman encoding are compared, and it is concluded that for the implemented algorithm arithmetic encoding gives better results than Huffman encoding.
- It is observed that if the background of the image is mono-color then the distortion takes place for high compression ratio. This distortion is mostly observed at the backgrounds. For example in the synthetic image Butterfly, it is observed for P = 50 and P = 60.

6.3.0 FUTURE SCOPE

The wavelet packet best tree based on energy contain with adaptive thresholding and enhanced RLE techniques for image compression, presented in this thesis produced the best results for natural as well synthetic images, low as well as high frequency images. Nonetheless, there is always a room for improvement. The following list includes a number of possible future topics for study:

- In this thesis, the standard basis functions of wavelet are used for transformation but it may be possible to use the segment of the image as a basis function for transformation.
- It is important to note that adaptive threshold technique is discussed, and used in this thesis. The algorithm used for calculation of thresholds for Y, Cr, and Cb components is same. It may be possible to develop the different algorithms for calculation of thresholds for Y, Cr, and Cb components by considering their importance.

- In this work lossy RLE technique is discussed and implemented. The algorithm used for calculation of lossy factor for the Y, Cr, and Cb components is same. It may be possible to develop the different algorithms for calculation of lossy factor for Y, Cr, and Cb components by considering their importance.
- The wavelet packet best tree based on energy content with adaptive thresholding and enhanced RLE has produced good compression ratio with good quality of still image. Future research will apply this method to video sequences. It would be a natural extension to attempt wavelet packet based video compression.
- The work can be further extended such that, it may become possible for the parallelization of the technique for the parallel computer architectures to achieve good speed.

REFERENCES

[1] Subhasis Saha, "Image Compression- from DCT To Wavelet: A Review," ACM Crossroads Student Magazine, Vol.6, No.3, Spring 2000.

[2] Andrew B. Watson, "Image Compression Using the Discrete Cosine Transform," NASA Ames Research Center, Mathematical Journal, Vol.4, Issue 1, pp 81-88, 1994.

[3] "Video Compression- An Introduction" Array Microsystems Inc., White Paper, 1997.

[4] Sergio D. Servetto, Kannan Ramchandran, Michael T. Orchard, " Image Coding Based on A Morphological Representation of Wavelet Data," IEEE Transaction On Image Processing, Vol.8, No.9, pp.1161-1174, 1999.

[5] M. K. Mandal, S. Panchnathan, T. Aboulnasr, "Choice of Wavelets For Image Compression (Book Title: Information Theory & Application)," Lecture Notes In Computer Science, Vol.1133, pp.239-249, 1995.

[6] Andrew B. Watson, "Image Compression Using the Discrete Cosine Transform," NASA Ames Research Center, Mathematical Journal, Vol.4, Issue 1, pp. 81-88, 1994.

[7] Wayne E. Bretl, Mark Fimoff, "MPEG2 Tutorial Introduction & Contents: Video Compression Basics- Lossy Coding," 1999.

[8] M. M. Reid, R.J. Millar, N. D. Black, " Second-Generation Image Coding; An Overview," ACM Computing Surveys, Vol.29, No.1, March 1997.

[9] Aleks Jakulin, "Baseline JPEG And JPEG2000 Artifacts Illustrated," Visicron, 2002.

[10] S. Lawson, J. Zhu, "Image Compression Using Wavelets And JPEG2000: A Tutorial," Electronics & Communication Engineering Journal, Vol.14, No.3, pp. 112-121, June 2002.

[11] A. K. Jain, "Fundamentals of Digital Image Processing" Pearson Education, ISBN 81-297-0083-2, First Indian reprint 2003.

[12] MATLAB Documentation Reference Manual " Wavelet Toolbox 6.5".

[13] Rafael C. Gonzalez, Richard E. Woods," Digital Image Processing", Pearson Education, ISBN 81-7808-629-8, First Indian reprint 2002.

[14] C. Wayne Brown and Barry J. Shepherd, " Graphics File Formats", reference and guide, ISBN-884777-00-7, Printed in the United State of America.

[15] Martin Bernas " Image Quality Evaluation" VIPromCom-2002, 4th EURISP-IEEE Region 8th International Symposium on video/Image Processing and Multimedia Communication, 16-19 June 2002, Zadar, Croatia.

[16] Marta Mrak, Sonja Grigic and Mislav Grigic "Picture Quality Measure in Image Compression System", EUROCON-2003Slovenia, IEEE 2003.

[17] Sonja Grigic, Mislav Grigic, and Marta Mrak "Reliability of Objective Picture Quality Measure", Journal of Electrical Engineering, Vol. 55, No. 1-2, 2004.

[18] Zhou Wang, Alan C. Bovik, and Ligang Lu " Wavelet Based Foveated Image Quality Measurment for Region of Interest Image Coding" 2001 IEEE

[19] Zhou Wang, Alan C. Bovik, Haqmid Rahim Sheikh and Eero P. Simonelli " Image Quality Assessment: From Error Visibility to Structural Similarity" IEEE Transactions on image Processing Vol. 13. No. 4. April-2004.

[20] Niranjan Damera Venkata, Thomos D., Kite, Willson S Geisler, Brain L. Evans " Image Quality Assessment Based on a Degradation Model" IEEE transactions on Image Processing Vol. 9 No. 4. April-2000.

[21] Marta Mrak, Sonja Gregic, Mislav Grgic, "Picture Quality Measures In Image Compression Systems," EUROCON 2003, Vol.1, pp. 233-236, Sept. 2003

[22] Sonja Grgic, Mislav Grgic, "Performance Analysis of Image Compression Using Wavelets," IEEE Int. Symposium On Industrial Electronics, Vol.48, No.3, pp. 682-695, June 2001.

[23] Mark Nelson, Jea-Loup Gailly "The Data Compression Book", M & T Books, ISBN-1-55851-434-1, Printed in the USA 1996.

[24] Debra A.Lelewer, Danial S. Hirschberg, "Data Compression," ACM Computing Surveys, Vol.19, No.3, Sept.1987.

[25] Feng G.C. And Jiang J (2003): "Image Segmentation In Compressed Domain" Journal Of Electronic Imaging, Vol .12, No.3, SPIE, pp390-397.

[26] David Jeff Jackson, Sidney Joel Hannah, "Comparative Analysis Of Image Compression Techniques," System Theory, pp.513-517, Mar.1993

[27] Lena Chang, Ching-Min Cheng, Ting-Chung Chen, "An Efficient Adaptive KLT For Multispectral Image Compression," Southwest Symposium On Image Analysis & Interpretation, Vol.00, pp. 252-258, Apr.2000

[28] Gokturk S B, Tomasi C, Girod B, Beaulieu CF, "Medical Image Compression Based on Region of Interest, With Application to Colon CT Images", In 23rd Annual International Conference of The IEEE Engineering In Medicine And Biology Society, Istanbul, Turkey, 2001.

[29] Jeffery C. Wenes, Hung_Ta Pai, Alan C.Bewik, “Fast Lossless Image Compression,” Image Analysis & Interpretation, pp. 145-148, Apr. 1996.

[30] Weinberger M. J., Seroussi G., Sapiro G., “The LOCO-I Lossless Image Compression Algorithm: Principles and Standardization into JPEG-LS,” IEEE Transactions on Image Processing, Vol. 9, No.8, pp.1309-1324, Aug. 2000

[31] Ramos, Marcia G.; Hemami, Sheila S., “Edge-Adaptive JPEG Image Compression,” Proc. SPIE On Visual Communications And Image Processing, Vol. 2727, pp. 1082-1093, Feb.1996

[32] Hororshi Konodo, Yuriko Oishi, “Digital Image Compression Using Directional Sub-Block DCT,” Int. Conf. on Communication Technology, Vol.1, pp.985-992, 2000.

[33] Mitchell A. Gonier, Wasfy B. Mikhael, Venkatesh Krishnan, Arun Ramaswamy, “Region Based Variable Quantization For JPEG Image Compression,” Proc. 43rd IEEE Midwest Symposium On Circuits And Systems, Vol.2, pp. 604-607, Aug. 2000

[34] G. F. Fahmy, J. Bhalod, S. Panchanathan, “A joint Compression and Indexing Technique in Wavelet compressed Domain,” IEEE Int. Conf. on Multimedia & Expo (ICME), Vol. 00, pp. 64, 200

[35] E. Yeung, “Image Compression Using Wavelets,” CCECE’97, Vol.1, pp. 241-244, May 1997.

[36] Sonja Grgic, Kresimir Kers, Mislav Grgic, “Image Compression Using avelets”, IEEE, Vol. No. 48, No. 3, pp. no. 682 – 695, June 2001.

[37] Tao Yu, Anthony Tung-Shuen Ho, Siu-Chung Tam, Siong-Chai Tan, Lian-Teck Yap, “A Novel Hybrid Bi-Orthogonal Wavelets/ADPCM Algorithm For Very Low Bit Rate Satellite Image Compression,” IEEE, Vol. 4,pp. 2051-2053, 1999.

[38] C. Chrysafis and A.Ortega, "Line-Based, Reduced Memory, Wavelet Image Compression," IEEE Trans. Image Processing, Vol. 9, No. 3, pp. 378-389, Mar.2000

[39] Y. Li, C. Moloney, “SAR Image Compression Using Wavelet Transform And Soft-Thresholding,” CCECE’97, Vol.1, pp.387-390, May 1997

[40] V. N. Ramaswamy, K.R. Namuduri, N. Rangnathan, “Lossless Image Compression Using Wavelet Decomposition,” IEEE Proc. Of ICPR, Vol.3, No.3, pp. 924-928, 1996

[41] Julien Reichel,Gloria Menegaz, Marcus J. Nadenau, Murat Kunt, " Integer Wavelet Transform For Embedded Lossy To Lossless Image Compression," IEEE Transactions On Image Processing, Vol.10, No.3, pp. 383-392, Mar.2001

[42] C. Chrysafis, A. Ortega, "Efficient Context-Based Entropy Coding For Lossy Wavelet Image Compression," Data Compression Conference, pp. 241-250, Mar. 1997

[43] Jiaming Li, Jesse S. Jin, "An Image Coding Method Of High Compression Rate And Clarity Preserving," Australian New Zealand Conf. On Intelligent Information Systems, pp. 151-154, Nov. 1996

[44] Maria Grazia Albansi, "Wavelets and Human Visual Perception in Image Compression," Int. Conference on Pattern Recognition, (Vienna, 25-30 Agosto 1996), pp. 859-863.

[45] Dorota Biela-Wirasazka, " Two-Stage Approach To Image Compression Using Wavelet And Piecewise-Linear Transforms," Int. Conf. On Mathematical Methods In Electromagnetic Theory, Vol.1, pp. 438-441, 1998

[46] A. P. Began, L. R. Iyer, A. E. Bell, V. R. Maher, M. A. Ross, "Design and Evaluation of Perceptual Masks o Wavelet Image Compression", DSP workshop program, Session3: Image Processing, Oct 2002

[47] Olivier Rioul, "On The Choice Of Wavelet Filters For Still Image Compression," IEEE Transactions On Image Processing, Vol.5, pp.550-553, April 1993

[48] S. Phimoltares, K. Chamnogthai, C. Lursinsap, "Hybrid Binary Image Compression," IEEE Southwest Symposiums On Image Analysis And Interpretation, Vol.2, pp. 801-812, Aug. 1999

[49] Amir Averbuch, Danny Lazar, Moshe Israen, "Image Compression Using Wavelet Transform And Multiresolution Decomposition," IEEE Transactions On Image Processing, Vol.5, No.1, pp.4-15, Jan. 1996

[50] Surya Peramraju, Sunanda Mitra, "Efficient Image Coding Using Multiresolution Wavelet Transform And Vector Quantization," Image Analysis and Interpretation, pp. 134-140, Apr. 1996

[51] Mohamad A. El-Sharkawy, Christian A. White, Harry Gundrum, "Subband Image Compression Using Wavelet Transform And Vector Quantization," IEEE 39th Midwest Symposium On Circuits And Systems, Vol.2, pp. 659-662, Aug. 1996

[52] Olga Kosheleva, Vladdik Kreinovich, "On The Optimal Choice Of Quality Metric In Image Compression," IEEE Southwest Symposiums On Image Analysis And Interpretation, Vol.8, No.4, pp. 268-273, 2004

[53] Armando J. Pinho, "On The Impact of Histogram Sparseness On Some Lossless Image Compression Techniques," Proc. Of The IEEE Int. Conf. On Image Processing, ICIP 2001, Vol. 3, pp.442-445, Oct.2001

[54] Armando J. Pinho, Antonio J.R. Nevws, "Improvement Of The Lossless Compression Of Images With Quasi-Sparse Histograms," Signal Processing XI- Theories And Applications, Proc. Of The 11th European Signal Processing Conf., Vol.2, pp.467-470, Sept.2002

[55] Ferreira Paulo, Pinho Armando, "Histogram Packing, Total Variation, And Lossless Image Compression," Proc. of EUSIPCO-2002, Paper 375, pp. 498-501,Sept. 2002

[56] Jinwen Tian, Su Kang, Jian Lin, Qian Gao, "A Novel Image Compression Encoding," Image Compression Of Signal Processing, 1996, Vol.2, pp.982-985, Oct. 1996

[57] Mirosolav Galabou, "Fractal Image Compression," ACM Library, pp. 320-326, 2003

[58] I. Andreopoulos, Y. A. Karayannis, T. Stouraitis, "A Hybrid Image Compression Algorithm Based On Fractal Coding And Wavelet Transform," IEEE Int. Symposium On Circuits & Systems, May 2000

[59] Davis G. M., "A Wavelet-Based Analysis Of Fractal Image Compression," IEEE Transactions On Image Processing, Vol. 7, No.2, pp.141-154, Feb 1998

[60] Vania Cordeiro Da Silva, Joao Marques De Carvalho, "Image Compression Via TRITREE Decomposition"

[61] Axel van de Walle, "Merging Fractal Image Compression And Wavelet Transform Methods," Fractals, 5 (Supplementary Issue): 3-15, April 1997

[62] Sunanda Mitra, Rodney Long, Surya Permmaraju, Richard Muyshondt, George Thomal, "Color Image Coding Using Wavelet Pyramid Coders," Image Analysis & Interpretation, pp. 129-134, Apr. 1996

[63] Armando Manduca, Amir Said, "Wavelet Compression Of Medical Images With Set Portioning In Hierarchical Trees," Proc. SPIE, Vol.2707, pp.192-200, Apr. 1996

[64] Fredrick W. Wheeler, William A. Pearlman, "Low-Memory Packetized SPHIT Image Compression," Proc. Of 33rd Asilomar Conference On Signals, Systems and Computer, Oct./Nov. 1999

[65] Jerome M Shapiro, " Embedded Image Coding Using Zerotrees of Wavelet Coefficients", IEEE transactions on signal processing, vol 41, No. 12, Dec 1993

[66] Jayshree Karlekar, P. G. Poonacha, U. B. Desai, " Image Compression using Zerotree and Multistage Vector Quantization"

[67] David Taubman, "High Performance Scalable Image Compression With EBCOT," IEEE Transactions On Image Processing, Vol. 9, No. 7, pp. 1158-1170, Jul 2000

[68] Jon K. Rogers, Pamela C.Cosman, " Wavelet Zerotree Image Compression With Packetization," IEEE Signal Processing Letters, Dec.1998

[69] Jon K. Rogers, Pamela C. Cosman, "Robust Wavelet Zerotree Image Compression With Fixed-Length Packetization". Vol.8, Session 9, pp. 418-427, Mar. 1998.

[70] Zixiang Xiong, Kannan Ramchandran, Michael T. Orchard, "Joint Optimization Of Scalar And Tree-Structured Quantization Of Wavelet Image Decomposition," Proc. 27th Ann. Asilomar Conf. Signal System Comp., Vol. 2, (Pacific Grove, CA), pp. 891-895, Nov. 1993

[71] Marcus J. Nadenau, Julien Reichel, Murat Kunt, "Wavelet-Based Color Image Compression: Exploiting The Contrast Sensitivity Function," IEEE Transactions On Image Processing, Vol.12, No.1, pp.58-70, Jan.2003

[72] Lakshmi R. Iyer, Amy E. Bell, "Improving Image Compression Performance With Balanced Multiwavelets," Proc. Of 35th Asilomar Conference On Signals, Systems & Computers, pp. 773-777, Nov. 2001

[73] S. Rout, A. E. Bell, "Color Image Compression: Multiwavelets Vs. Scalar Wavelets," IEEE International Conference on Acoustics Speech & Signal Processing, Virginia Tech, Vol.4, pp. 3501-3504, May 2002

[74] Deepti Gupta, Shital Mutha, "Image Compression Using Wavelet Packet," IEEE, Vol.3, pp. 922-926, Oct. 2003

[75] A. Majid Awan, Nasir M. Rajpoot, S. Afaq Husain, "Stack-Run Adaptive Wavelet Image Compression"

[76] Francois G. Meyar, Amir Averbuch, Jan-Olvo Stromberg, Ronald R. Coifman, "Fast Wavelet Packet Image Compression," IEEE Transaction On Image Processing, Vol.9, No.5, pp. 563-572, May 2000

[77] Francois G. Meyer, Amir Z. Averbuch, Jan-Olov Stromberg, " Fast Adaptive Wavelet Packet Image Compression," IEEE Transactions On Image Processing, Vol.9, No.5, pp. 792-800, May 2000

[78] G Hong, G Hall, T J Terrell, " Joint Entropy And Multiband Prediction For Lossless Compression," Image Processing And Its Applications Conference (IEE), Publication: 410, pp. 603-607, Jul. 1995

[79] Andreas Uhl, "Wavelet Packet Best Basis Selection On Moderate Parallel MIMD Architectures[1]," Parallel Computing, Vol.22, No.1, pp. 149-158, Jan. 1996

[80] Michel B. Martin, Amy E. Bell, "New Image Compression Techniques Using Multiwavelets And Multiwavelet Packets," IEEE Transactions On Image Processing, Vol.10, No.4, pp. 500-510, Apr. 2001

[81] Agostino Abbate, Casimer M. DeCusatis, Pankaj K. Das, "Wavelets and Subbands fundamentals and applications", ISBN 0-8176-4136-X printed at Birkhauser Boston.

[82] Michael L. Hilton, Bjorn D. Jawerth, Ayan Sengupta, "Compressing Still And Moving Images With Wavelets," Multimedia Systems, Vol.2, No.3, pp. 218-277, 1994.

[83] Stephane Mallat, "A Wavelet Tour of Signal Processing", Second Edition, Elsevier publication, ISBN 0-12-466606-X, printed at USA.

[84] Eugene Belogy, Yang Wang, "Arbitrarily Smooth Orthogonal Nonseparable Wavelets In R^2," SIAM J. MATH. ANAL., Vol.30, No.3 pp.678-697, May 1999.

[85] Ronald A. Devore, Bradley J. Lucier, "Fast Wavelet Techniques For Near-Optimal Image Processing," IEEE Military Communications Conference Record, pp. 1129-1135, Oct. 1992.

[86] Sonja Gergic, Kresimir Kers, Mislav Grgic, "Image Compression Using Wavelets," ISIE99, Vol.48, No.3, pp. 682-695, June 2001.

[87] Rajan Bose, "Information Theory Coding and Cryptography", Tata McGraw Hill publication, ISBN 0-07-048297-7, 2002.

[88] Simon Haykin, "Communication System", 4th Edition, John Wiley & Sons, Inc. publication, ISBN 9971-51-305-6, 2001.

[89] Luc Vandendrope, Benoit Maison Fabrice Labeau, “An Adaptive Transform Approach For Image Compression,” IEEE Digital Signal Processing Workshop, pp.41-44, Jan.1997.

[90] Jose Oliver, Manuel Perez Malumbres, “Fast And Efficient Spatial Scalable Image Compression Using Wavelet Lower Trees,” Proceedings Of The Data Compression Conference, pp. 133-142, Mar. 2003.

[91] Roger L. Claypoole, Jr, Geoffery M. Davis, Wim Sweldens, Richard G. Baraniuk, “Nonlinear Wavelet Transforms For Image Coding Via Lifting,” 31st Asilomar Conference On Signals, Systems & Computers, Vol.1, pp.662-667.

[92] Jung-Hua Wang, Ker-Jiang Gou, “Image Compression Using Wavelet Transform And Self-Development Neural Network,” IEEE International Conference On Systems, Man, And Cybernetics, Vol. 4, pp.4104-4108, 1998.

[93] M. Frydrych, P.J. Toivanen, “Arithmetic Coding With Sliding Window For Controlpoint Based Image Compression,” Image Processing And Its Applications Conference No.465, pp. 601-604, July 1999.

[94] R Fraile, S. Maybank, "Image Compression For Trajectory Refinement", In PETS 2000, IEEE Workshop Proceedings, pps 46-49 (2000).

[95] Mike Liddle, Alistair Moffat, “Length-Restricted Coding Using Modified Probability Distributions,” IEEE, Vol.11, pp. 117-124, 2001.

[96] Luc Vandendrope, Benoit Maison Fabrice Labeau,” An Adaptive Transform Approach For Image Compression,” IEEE Digital Signal Processing Workshop, pp.41-44, Jan.1997.

[97] K. S. Prashant, V. John Mathews, Peter Hahn, “A New Model of Perceptual Threshold Function In Image Compression Systems,” Data Compression Conference, pp. 371-380, Mar.1995.

[98] Todd Hinck, Allyn E. Hubbard, “ Image Edge Enhancement, Dynamic Compression and Noise suppression using Analog Circuit Processing,” 17th Conference on Advanced Research in VLSI, Arvlsi, Vol. 00, pp.113-125, 1997.

[99] James A. Storer, “Lossless Image Compression Using Generalized LZI-Type Methods,” Data Compression Conference,” pp. 290-299, Mar/Apr. 1996.

[100] Martin Boliek, Michael J. Gormish, Edward L. Schwartz, Alexander Keith, “ Next Generation Image Compression And Manipulation Using CREW”, Int. Conf. On Image Processing, Santa Barbara, CA, October 1997.

[101] Ephraim Feig, Heidi Peterson, Viresh Patankar, “Image Compression Using Spatial Prediction,” Acoustic, Speech & Signal Procesing, Vol.4, pp. 2339-2342, May 1995.

[102] H.J. Grosse, M.R. Varley, T.J. Terrell, Y.K. Chan, “Sub-Block Classification Using A Neural Network For Adaptive Zigzag Recording On JPEG-Like Image Compression Scheme,” Neural & Fuzzy Systems, pp. 9.1-9.4, May 1997.

[103] Clark N. Taylor, Sujit Dey, "Adaptive Image Compression For Wireless Multimedia Communication", ICC 2001 - IEEE International Conference On Communications, No. 1, June 2001, pp. 1925-1929.

[104] Gregory W. Cook, Edward J. Delp, “The Use of High Performance Computing In JPEG Image Compression,” IEEE Transactions On Image Processing, pp.846-851, Oct./Nov. 1993.

(Continued)

LIST OF PUBLICATIONS

[105] G. K. Kharate, Dr. A. A. Ghatol and Dr. P. P. Rege, "Image Processing", Presented at *State level IEEE conference on Signal Processing and Parallel Computing*, Alandi, Pune (MH), India, July 2003.

[106] G. K. Kharate, Dr. A. A. Ghatol and Dr. P. P. Rege, "Image Processing", Presented at *National Conference on Recent Advance in Mechanical Engineering* (RAME2004)at, Nashik (MH), India, January 2004.

[107] G. K. Kharate, Dr. A. A. Ghatol and Dr. P. P. Rege, "Multi Wavelet Image Compression", Presented at *National level conference on Multimedia Technology and Applications*, Karunya Institute of Technology and Science, deemed University, Karunya Nagar, Coimbatore (T.N.), India, July 2004.

[108] G. K. Kharate, Dr. A. A. Ghatol and Dr. P. P. Rege, "Wavelets and Human Visual Perception Image Compression", Presented at *National level Seminar on Applied Computing & Communication Technology*, Rajkot, (Rajsthan), India, June 2005.

[109] G. K. Kharate, Dr. A. A. Ghatol and Dr. P. P. Rege, "Image Compression on Adaptive Thresholding", Presented at *the 5th IASTED International conference Visualization, Image and Image Processing*, Benodrom, Spain, September 2005.

[110] G. K. Kharate, Dr. A. A. Ghatol and Dr. P. P. Rege, "Image compression using wavelet packet tree", Published at *ICGST International Journal on Graphics, Vision and Image Processing GVIP-2005* Cairo, Egypt, Vol-5, Issue-7, July 2005.

[111] G. K. Kharate, Dr. A. A. Ghatol and Dr. P. P. Rege, "Intelligent Image Compression Algorithm Using Wavelet Packet", Presented at *International Conference (INCRUIS 2006),* Perunduri Erode, Tamilnadu, India, January 2006.

[112] G. K. Kharate, Dr. A. A. Ghatol and Dr. P. P. Rege, "Image Compression Using Wavelet Packet Tree based on log Entropy", Presented at *International Conference on Systemics, Cybernetics and Informatics ICSCI-2006*, Hydrabad, (A.P), India, January 2006.

[113] G. K. Kharate, Dr. A. A. Ghatol and Dr. P. P. Rege, "Image Compression Using Wavelet Packet Tree Based on Threshold Entropy", Presented at *the Third IASTED International Conference on Signal Processing, Pattern*

Recognition and Applications, SPPRA 2006, Innsbruck, Austria, February 2006.

[114] G. K. Kharate, Dr. A. A. Ghatol and Dr. P. P. Rege, "Image Compression Algorithm Using Wavelet Packet Tree on Human Perception", *International Congress of imaging science, ICIS'06*, Rochester, New York, USA, May 7-12, 2006.

[115] G. K. Kharate, Dr. A. A. Ghatol and Dr. P. P. Rege, "Selection of Mother Wavelet For Image Compression on Basis of Image", National Journal CSI (under review)